UNIVERSITA' DEGLI STUDI DI MILANO

PhD Course in Molecular and Cellular Biology

XXXVIII Cycle

Department of Biosciences

Targeting α-synuclein aggregation and inflammation in Parkinson's disease: the role of Poly-γ-Glutamic Acid

Tesi redatta con il contributo finanziario dell'Unione europea - Next Generation EU e iBiotech Ltd

Claudia Novello
Matr. R13953
ORCID n. 0009-0007-6658-7595

PhD Thesis

Tutor: Prof. Graziella Cappelletti

PhD coordinator: Prof. Stefano Ricagno

Academic Year: 2024-2025

Table of contents

Abbreviations

ALP: autophagy-lysosomal pathway

APC: antigen presenting cells

BAMs: border-associated macrophages

BBB: blood-brain barrier

BDNF: brain-Derived Neurotrophic Factor

BCA: bicinchoninic acid

BSA: bovine serum albumin

C1q: Complement Component Subunit 1q

CD: cluster of differentiation

CNS: Central nervous system

COX-2: cyclooxygenase-2

CSF: cerebral spinal fluid

CXCL10: C-X-C motif chemokine ligand 10

ER: endoplasmic reticulum

FITC: Fluorescein-5-isothiocyanate

GAPDH: Glyceraldehyde 3-phosphate dehydrogenase

GBA: glucocerebrosidase

GFAP: glial fibrillary acidic protein

HLA-DR: Leukocyte Antigen – DR isotype

hrs: hours

IL: interleukine

LAMP1 lysosome-associated membrane protein 1

LB: Lewy bodies

LC3: microtubule-associated protein 1A/1B-light chain 3

LN: Lewy neurite

LPS: lipopolysaccharide

LRRK2: Leucine-rich repeat kinase 2

MAO-B: monoamine oxidase-B

MFI: mean fluorescence intensity

min: minutes

MW: molecular weight

NAC: non amyloid component

NGF: nerve growth factor

NO: nitric oxide

PBS: phosphate buffered saline

PD: Parkinson's disease

PFFs: pre-formed fibrils

PLA; proximity ligation assay

PMA: Phorbol 12-Myristate 13-Acetate

PNS: peripheral nervous system

RNS: reactive nitrogen species

ROS: reactive oxygen species

RT-QuIC: real-time quaking-induced conversion

SNpc: *substantia nigra pars compacta*

TBS: Tris-buffered saline

TBS-T: Tris-buffered saline-Tween 20

TEM: transmission electron microscopy

TLR4: toll-like receptor 4

TNF-α: Tumour Necrosis Factor alpha

TNF-β: Tumour Necrosis Factor beta

UPS: ubiquitin-proteasome system

wt: wild-type

γ-PGA: Poly- γ-glutamic-acid

Abstract

Parkinson's disease (PD) is a complex multifactorial neurodegenerative disorder affecting more than 10 million people worldwide. As a synucleinopathy, PD is characterized by the pathological accumulation of misfolded and aggregated α-synuclein in both the central and peripheral nervous system. In this context, many efforts have been made to counteract α-synuclein aggregation, propagation, and associated inflammatory responses, which are key features of the disease. However, despite the tremendous effort and research investment, no disease-modifying therapies are currently available, and symptomatic approaches remain the standard cure for the treatment of PD.

In this work we aimed to evaluate the therapeutic potential of commercially available poly-γ-glutamic acid (γ-PGA) polymers, a natural, non-toxic and non-immunogenic biopolymer, in different *in vitro* models of PD, focusing on its properties as anti-inflammatory agent and modulator of aggregation. Indeed γ-PGA has gained significant interest in biomedicine due to its antioxidant, anti-inflammatory, and neuroprotective effects, providing evidence for its beneficial value in neurodegenerative disorders.

To investigate these biological properties, we selected complementary *in vitro* models that recapitulate different aspects of PD pathogenesis. Primary murine astrocytes were employed for their central role in α-synuclein clearance and neuroinflammation, given their involvement in the interplay between protein aggregation and immune responses in the central nervous system. Macrophages were selected to assess peripheral immune cell activation, which is strongly implicated in PD pathogenesis. Finally, neuronal *in vitro* model and cell free system assay were employed to assess the specific effect of γ-PGA in interfering with α-synuclein aggregation.

Using primary murine astrocytes exposed to α-synuclein preformed fibrils (PFFs) we demonstrated that γ-PGA restored cell viability, reduced astrocyte inflammation, and decreased α-synuclein pathology burden. These effects were associated with the reduced internalization of aggregates and the direct interference with α-synuclein aggregation, as confirmed by cell-free system assays. In addition, we examined the impact of α-synuclein aggregates on macrophage immune response, focusing on their polarization. Using an *in vitro* model of macrophages, we observed that PFFs induced a mixed M1/M2 phenotype without affecting cytotoxicity and ROS production, and that γ-PGA administration attenuated this polarization, suggesting a modulatory role in α-synuclein-induced immune response. Finally, in a neuronal *in vitro* model, γ-PGA polymers significantly reduced the burden of early-stage α-synuclein aggregates supporting its direct anti-aggregation capacity.

Overall, this work provides *in vitro* proof-of-concept evidence that γ-PGA can modulate α-synuclein aggregation and aggregate-induced inflammatory response, highlighting its potential as a safe and effective therapeutic strategy for PD. Interestingly, given its additional role as a prebiotic able to modulate the gut microbiome, and the emerging evidence that dysbiosis is linked to PD, future research that explores γ-PGA effects on the gut-brain axis and focuses on inflammation and microbiota modulation in the gut, as well as α-synuclein propagation and neuronal function in PD pathogenesis, holds promise.

Aim of the project

PD is a progressive complex multisystemic neurodegenerative disorder characterized by progressive motor and non-motor impairments, linked to both neuronal loss and pathological protein aggregation. (Balestrino & Schapira, 2020; Spillantini et al., 1997). Current therapies aim to alleviate the motor symptoms only providing a temporary relief without halting or reversing the neurodegenerative process. Thus, developing new disease-modifying strategies targeting the pathophysiology remains a critical priority. In this context, α-synuclein aggregation, propagation and associated inflammatory responses are key features in neuronal dysfunction that involve many cell types and contribute to disease progression (Marogianni et al., 2020; Mehra et al., 2019).

This thesis investigates a novel biopolymer, poly-γ-glutamic acid (γ-PGA), as a potential therapeutic strategy for PD. γ-PGA is a biodegradable, non-toxic, and non-immunogenic biopolymer whose interest in biomedicine has seen recent development. Among its peculiar features, γ-PGA has demonstrated anti-inflammatory and antioxidative properties and has been shown to alleviate neuronal cell death and memory deficits (Ahn et al., 2018; Jeong et al., 2021; Lee et al., 2020; T. Zhang et al., 2021), providing evidence of its potential therapeutic value in neurodegenerative diseases.

On this basis, we aim to explore the therapeutic potential of commercially available γ-PGA polymers in PD, evaluating their effect on α-synuclein aggregation, clearance, and aggregate-induced inflammatory responses in different *in vitro* models of PD. Specially, we aim to:

- **investigate the biological effect of γ-PGA on a PD cellular model of murine primary astrocytes**, a cell type involved in the clearance of extracellular aggregated α-synuclein and neuroinflammation. In this cell model, we aim to evaluate the restoration of cell viability, the extent of α-synuclein pathology burden, the autophagy-lysosomal pathway involvement and cytokine release.
- **unravel the direct effects of α-synuclein fibrils on a cell model of macrophages and assess the modulatory role of γ-PGA** in terms of cytotoxicity, ROS production, and polarization toward pro-inflammatory (M1) or anti-inflammatory (M2) profile.
- **explored γ-PGA ability as an α-synuclein anti-aggregation compound** by performing both cell-free system and *in vitro* assays.

The results obtained from this study will provide *in vitro* evidence for the use of γ-PGA as a safe and effective therapeutic approach for the treatment of PD. By analyzing its role in α-synuclein aggregation, clearance, and inflammation, we aim to discover new mechanisms through which γ-

PGA may exert neuroprotective effects, laying the groundwork for future preclinical studies. Moreover, data obtained from the *in vitro* study on macrophage cell model will help elucidate the direct effect of α-synuclein misfolding and accumulation on their immune response.

1

Chapter 1: Introduction

1.1 Parkinson's disease and α-synuclein

1.1.1 Epidemiology, aetiology, and clinical manifestation

Parkinson's disease (PD) is the second most common neurodegenerative disorder and the most frequent movement disorder of the central nervous system. The estimated global prevalence of PD ranges from 1 to 2 per 1,000 in the general population, affecting about 1% of individuals over the age of 60 years. Its prevalence increases with age, peaking around 80 years, and it is expected to increase mirroring the demographic shift toward aging population (Ben-Shlomo et al., 2024). Nevertheless, some cases manifest before the age of 40. These fall into the category of early-onset PD, which includes young-onset PD (onset between ages 21 and 40) and juvenile parkinsonism (onset before the age of 21) (Thomsen & Rodnitzky, 2010). Notably, the incidence of PD is higher in men than in women by a ratio of 1.4:1. This difference might be due to greater exposure of men to risk factors or to the potential neuroprotective effect of female hormones as women appear to have lower risk at all ages. However, the underlying reasons remain uncertain, and this topic is still controversial (Ben-Shlomo et al., 2024).

Geographical and ethnic differences in PD prevalence have also been documented. Hight rates are generally reported in industrialized countries, probably due to differences in life expectancy, environmental exposure and diagnostic capabilities (Ben-Shlomo et al., 2024). Furthermore, PD is less common in black and Asian population compared to white population (Ben-Joseph et al., 2020).

Overall, PD is generally characterized by a slow progression, and its disease duration after diagnosis can extend up to 20 years.

Until date, the aetiology of the disease remains not entirely clear. Although age is considered as one of the major risk factors for its developing, other factors, such as environmental exposures, genetic mutations and racial predisposition, may also contribute to its onset (Tysnes & Storstein, 2017). At first, PD was thought to be primarily caused by environmental factors. This idea originated from the discovery that intravenous injection of 1-methyl-4-phenyl-1,2,3,6-tetrahydropyridine (MPTP) toxin induces the selective degeneration of the dopaminergic neurons of *substantia nigra*, leading to parkinsonian symptoms. Since then, epidemiological studies have identified different environmental factors associated with the risk of developing the disease, including pesticide exposure, prior head injury, rural living, β-blocker use, agricultural occupation, and diet. On the contrary, factors such as tobacco smoking, coffee and tea drinking, anti-inflammatory drug use and physical exercise have been associated with lower risk of PD (Ascherio & Schwarzschild, 2016; Ben-Shlomo et al., 2024). However, most cases of PD result from the combination of environmental exposure and genetic susceptibility and are classified as sporadic or idiopathic PD. Nevertheless, genetic mutations contribute to the onset of "familial" or "genetic" PD which account for

approximately 10-15% of PD total cases. The first gene associated with familial PD was the *SNCA* gene, first discovered in 1997 (Goedert et al., 2017). Later, other mutations in gene such as *LRRK2*, *VPS35*, *EIF4G1*, *DNAJC13*, and *CHCHD2* have been associated with the autosomal-dominant forms of familial PD with later onset. Conversely, mutations in *Parkin*, *PINK1*, and *DJ-1* have been associated with autosomal recessive forms of PD which is more frequently linked with early onset (Day & Mullin, 2021). Moreover, genome-wide association studies (GWASs) have also identified genetic variants with a variable penetrance. Among these, the stronger association has been detected in the glucocerebrosidase (*GBA*) gene, that encodes for β-glucocerebrosidase, a lysosomal hydrolase, whose homozygote deficiency is responsible for Gaucher's disease (Sidransky & Lopez, 2012).

Clinically, PD is diagnosed upon the onset of its cardinal motor symptoms, according to the UK Parkinson's disease Society Brain Bank clinical diagnostic criteria, which include rest tremor, muscular Rigidity, Akinesia (namely bradykinesia), and Postural instability. Nonetheless, due to the heterogeneity of clinical manifestation, and its overlapping with other neurodegenerative disorders or secondary parkinsonism, diagnosis can be prone to misclassification. Indeed, the define diagnosis occurs after *post-mortem* examination through histopathological evidence. Despite PD is primarily known as a movement disorder, growing evidence highlights the presence of several non-motor symptoms that define a pre-motor or prodromal phase, which can precede motor manifestations by up to 20 years (Poewe et al., 2017) (**Figure 1.1**). Non-motor symptoms include constipation, rapid eye movement sleep behaviour disorder, depression, orthostatic hypotension, hyposmia, anxiety and somnolence. Other non-motor symptoms such as pain, fatigue, urinary symptoms and dementia, arise as the disease progresses, worsening the patient's clinical picture and highlighting PD as a multisystemic disorder in which the peripheral nervous system (PNS) is also involved (Postuma & Berg, 2019). It is becoming evident that, during this phase, the pathogenic processes underlying PD have already begun, and by the time of diagnosis, the disease is already at a quite advanced stage. Therefore, in the last years, PD research focuses on finding biomarkers to diagnose the pathology during the prodromal phase, and to monitor the disease progression. This would offer the possibility to study the early stages of the disease, enhancing our understanding of its progression and provide a potential window during which disease-modifying therapies, could be administered to prevent or delay the onset and progression of PD. In this sense, various biomarkers are being investigated, including imaging biomarkers such as DAT-SPECT and PET scans, biochemical biomarkers found in cerebrospinal fluid and blood (like α-synuclein, lysosomal and inflammatory markers) (Kwon et al., 2022), as well as genetic biomarkers associated with familial forms of PD.

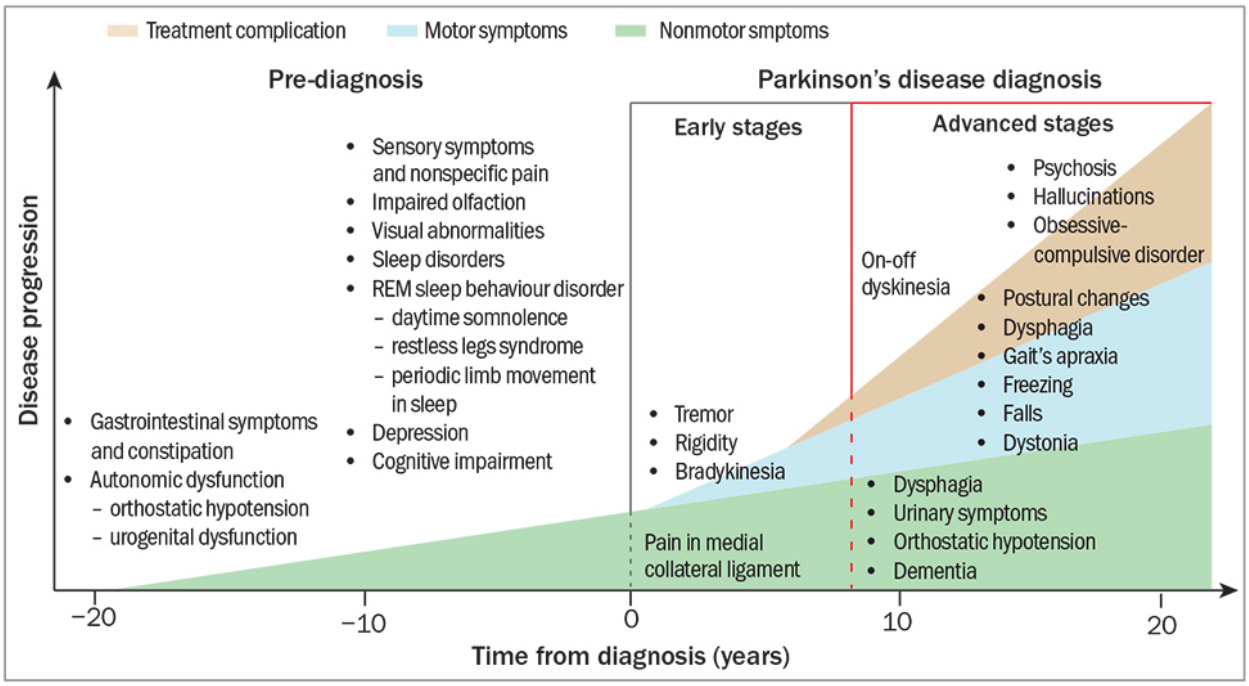

Figure 1.1. Clinical symptoms and progression of Parkinson's disease*. Schematic representation of symptomatology progression during different stages of PD. Clinical diagnosis occurs with the onset of the motor symptoms. However, this is preceded by a prodromal phase characterized by non-motor symptoms such as constipation, rapid eye movement sleep behaviour disorder (RBD), depression and hyposmia. Progressive disability is given by increasing severity of both motor and non-motor symptoms. Image from (Rowe, 2023)*

Regarding the imaging biomarkers, DAT-SPECT can be a useful tool for distinguishing or confirming diagnosis in PD and other parkinsonism, characterised by loss of striatal dopaminergic neurons and synapses (Tinaz et al., 2018). However, these imaging techniques are weak in predicting PD progression due to slow disease progression, plateau of dopaminergic loss that usually occurs within 5 years after diagnosis, age, and medication effect (Zarkali et al., 2024).

Detection of α-synuclein in the fluid of PD patient is one of the promising approaches for distinguishing patients from healthy controls. Total α-synuclein can be measured in body fluids, but levels are heterogeneous and can overlap between patients and controls. More recently, seed amplification assays (SAA), that include the real time quaking induced conversion (RT-QuIC) assay and the protein misfolding cyclic amplification assay, are promising in detecting pathological α-synuclein prone to aggregate in the CSF. For instance, in a study of 172 patients, SAA showed an 88% sensitivity and a 96.3 % specificity in distinguishing PD patients from healthy controls (Siderowf et al., 2023). However, obtaining CSF is quite invasive, and other biological samples, including, skin biopsies, nasal mucosa, submandibular glands, saliva and colonic biopsies, are currently considered for SAA (Yamashita et al., 2023).

Another biomarker that can be found in the CSF and serum is the glial fibrillary acidic protein (GFAP), an intermediate filament expressed by astrocytes, the major cell type in the CNS (Yamashita et al., 2023). In the presence of injury, astrocytes release GFAP in the CSF and serum; therefore, high levels of GFAP indicate astrocytic damage, inflammation and possible neurodegeneration. However, this biomarker does not allow for distinguishing PD patients from individual with other neurodegenerative disorders, that also present high levels of GFAP in the CSF (Ishiki et al., 2016; Oeckl et al., 2018).

Among the approaches with strong potential for preventive diagnosis, there is the quantification of proteins released from brain-derived extracellular vesicles (EVs) (Yamashita et al., 2023). EVs can cross the blood-brain barrier (BBB) and transfer neuronal cell content to the periphery trough blood. In a recent study, neuronal EVs derived from 275 PD patients, and 144 controls were isolated and analysed to measure protein levels including α-synuclein and the chaperon clusterin (Jiang et al., 2020). Both proteins were found increased in the EVs derived from PD patients compared with controls.

Lastly, special attention is currently paid to skin biopsies as potential diagnostic site of α-synuclein pathology. A major advantage is represented by the simple and easy way to obtain and perform them with a relatively high rate of accurate results (Peng et al., 2023). To date, different studies have demonstrated the presence of pathological α-synuclein within the autonomic nerve structures of the skin. Indeed, both phosphorylated α-synuclein and oligomeric α-synuclein have been detected in the skin and have been used to successfully distinguish patients from healthy controls (Donadio, 2019; Gibbons et al., 2024; Mazzetti, Contaldi, et al., 2024; Mazzetti et al., 2020). However, other effort needs to be made to distinguish between the different subtypes of synucleinopathies.

Unfortunately, there are currently no therapies available that can prevent or slow down the progression of PD. Patients receive symptomatic treatment aimed at alleviating both motor and non-motor symptoms, thereby improving the quality of life. The cardinal motor symptoms are due to the loss of dopaminergic neurons of the *substantia nigra pars compacta* (SNpc). This degeneration alters basal ganglia circuits, resulting in downstream inhibition of the cerebral cortex, and impaired movement. Consequently, current treatments aim to restore dopamine levels in the brain (Galvan & Wichmann, 2008). Orally administration of levodopa is the major treatment options chose soon after diagnosis, administrated in combination with dopamine agonists and/or monoamine oxidase-B (MAO-B) inhibitors. However, long-term treatment is associated with motor fluctuations and dyskinesias (Lewitt, 2015). Treatment with levodopa-carbidopa enteral suspension can help individuals with medication-resistant-tremor. Non-pharmacological approaches are also available.

Among these, an appropriate exercise regimen and rehabilitative therapies, such as physical, occupational, and speech therapies, are highly recommended. For selected patients, deep brain stimulation targeting the subthalamic nucleus or the internal segment of the globus pallidus may be recommended to improve motor symptoms (Armstrong & Okun, 2020). Currently, various disease-modifying therapies, including pharmacological treatments, immunotherapy, gene therapy, as well as cell therapy, are under investigation (Yaribash et al., 2025). Targets such as α-synuclein, *LRRK2* and *GBA* genes, inflammation, lysosomal calcium, mitochondrial function, calcium homeostasis, insulin resistance, and iron metabolism (Vijiaratnam et al., 2021), are among those currently being explored.

1.1.2 Pathophysiology of PD: a focus on α-synuclein pathology

Beside the loss of the dopaminergic neurons in the SNpc, the other pathological hallmark of PD is the presence of intraneuronal inclusion known as Lewy body (LB) and Lewy neurites (LN), respectively found in the cell body or processes of neurons, throughout the CNS. Although many proteins have been identified as part of these inclusions, misfolded and aggregated α-synuclein is the main component of LB and LN, leading to the classification of PD as a synucleinopathy (Goedert et al., 2017; Spillantini et al., 1997). The central role of this protein in PD pathogenesis is further supported by the identification, in PD-affected families, of missense mutation and copy number variations (duplication and triplication) in the *SNCA* gene, encoding α-synuclein (Goedert et al., 2017).

α-Synuclein is a small protein of 140 amino acid (aa) residues (Polymeropoulos, 1997). Structurally, α-synuclein consists of three domains: *i*) a basic N-terminal domain (1-60 aa); *ii*) a hydrophobic "non amyloid component (NAC) domain (61-95 aa); and *iii*) a C-terminal domain (96-140 aa) (Bendor et al., 2013; Fan et al., 2021). The N-terminal region is responsible for interacting with lipid membranes, forming an amphipathic α -helix secondary structure (**Figure 1.2, A, B**). Additionally, this region also contains almost all PD-related missense mutations (**Figure 1.2, A**).

The central NAC domain is a hydrophobic region in which residues 71-82 exhibit a strong propensity to form cross β-sheets, a feature essential for α-synuclein aggregation. Finally, the C-terminal tail of the protein is responsible for mediating the interaction with different cellular elements such as other proteins, ligands, metal ion, and α-synuclein itself (Mehra et al., 2019). Furthermore, due to the presence of many charged aa residues, the C-terminal tail is subjected to various post-translational modifications, among which phosphorylation at Serine 129 (Ser129-p) is the most studied in PD pathology (Xu et al., 2015).

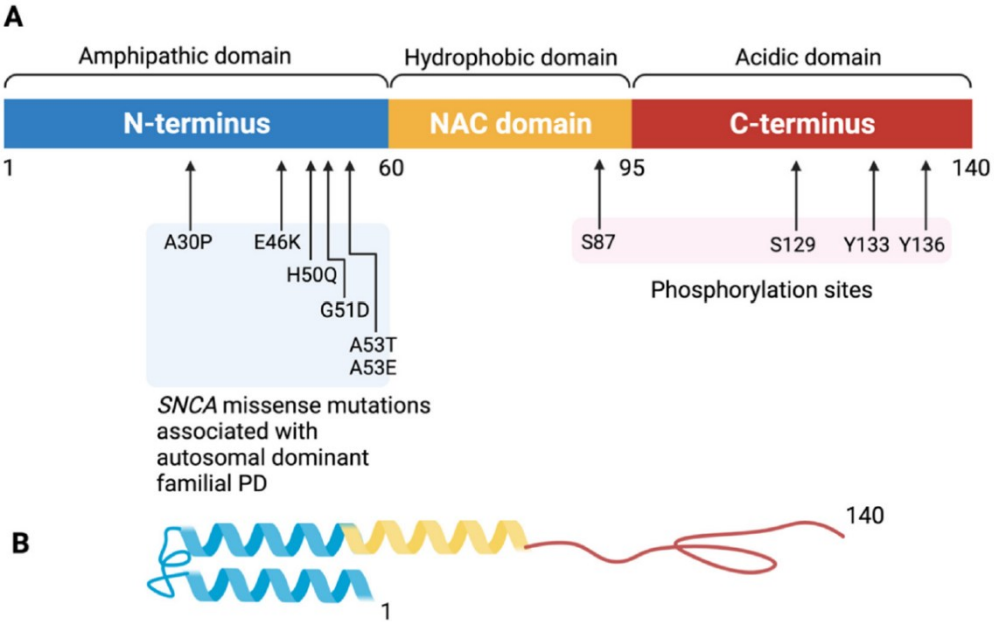

Figure 1.2. The structure or α-synuclein protein. ***A)*** *α-synuclein protein is composed by three domains: a basic N-terminal domain, a central hydrophobic NAC domain, and an acidic C-terminal domain.* ***B*** *shows the folded structure of the α-synuclein monomer. Image from (Fan et al., 2021).*

Although the exact physiological function of α-synuclein remains unclear, its localization at presynaptic terminal, both in the CNS and PNS, and association with synaptic vesicles suggest a role in modulating neurotransmission, as well as synaptic function and plasticity. Indeed, α-synuclein promotes the SNARE-complex assembly, the synaptic vesicle membrane fusion, and the release of the neurotransmitter, including dopamine (Burré, 2015; Burré et al., 2018). Furthermore, several evidence report the presence of α-synuclein within mitochondria, suggesting a role of the protein in mitochondrial function, the fusion/fission machinery, and the interaction between mitochondria and endoplasmic reticulum at mitochondria-associated membranes (Basellini et al., 2023; Guardia-Laguarta et al., 2014; Parihar et al., 2008). α-Synuclein accumulation is currently used as marker for disease staging. Indeed, LB and LN, are not only present in the SNpc but in various brain regions. According to this observation, Braak and colleagues proposed a six-staging scheme of α-synuclein pathology in PD, in which the disease propagates in a time-dependent, ascending manner through connected areas that show vulnerability to the pathology (Braak et al., 2003). Based on this staging, α-synuclein accumulation first appears in the olfactory bulb and/or the dorsal motor nucleus of the vagus nerve, then spread through the lower brainstem and midbrain, eventually reaching the neocortex (Braak et al., 2003). Recent evidence shows that α-synuclein inclusions first start in the enteric nervous system and spread, retrogradely, via the vagus nerve, to CNS, suggesting that the pathology could start in the periphery. This "body-first" hypothesis is supported by multiple evidence:

i) the detection of LB pathology in gastrointestinal nerve fibres prior to PD diagnosis (Stokholm et al., 2016); *ii*) *in vivo* injections with pathological seeds (pre-formed fibrils or pathological α-synuclein isolated from transgenic mice) in the intestinal walls of animal models has been found to induce α-synuclein pathology and neurodegeneration, far from the injection site (Holmqvist et al., 2014); *iii*) truncal vagotomy can prevent gut to brain spread, neurodegeneration and behavioural deficits in a novel gut-to-brain α-synuclein transmission mouse model (Kim et al., 2019).

However, other studies suggest that PD does not necessarily originate in the enteric nervous system in all cases. Autopsy studies have shown that a minority of individuals with LB pathology lack pathological inclusions in the dorsal motor nucleus of the vagus (Parkkinen et al., 2008), showing a limbic-predominant distribution of α-synuclein accumulation with less inclusions in the brainstem (Raunio et al., 2019). Based on this, it is widely accepted that PD comprises two subtypes: a body-first (bottom-up propagation) and a brain-first (top-down propagation) form (Horsager et al., 2020).

1.1.3 Molecular mechanisms involved in PD

The pathogenesis of PD is extremely complex. The coexistence of various motor and non-motor clinical symptoms, the involvement of multiple anatomical structures within the CNS, both dopaminergic and non-dopaminergic, as well as the involvement of the PNS, define PD as a multisystem disorder. Moreover, the combination of diverse factors (genetic, environmental, etc.) required to trigger the pathogenesis, has made the identification of a single unifying mechanism with a clear causal link to PD onset and neurodegeneration particularly challenging. Nowadays, several cellular pathways are thought to be altered in PD patients, including protein homeostasis (with particular emphasis to α-synuclein and its aggregation), the autophagy-lysosomal pathway (ALP), the ubiquitin-proteasome system (UPS), mitochondrial function, metabolic and oxidative stress, inflammation, axonal transport and microtubule dynamics (Basellini et al., 2023). Importantly, these mechanisms are not independent but rather interconnected. For instance, mitochondrial dysfunction and oxidative stress can exacerbate protein aggregation while failure of ALP and UPS systems further promotes α-synuclein accumulation. Moreover, microtubule dysfunction has been linked to PD pathogenesis (L. Pellegrini et al., 2017). *Post-mortem* analyses of PD human brain have revealed that LBs contain many cytoskeletal proteins, such as tubulin, MAPs, and neurofilament (Moors et al., 2021). The role of microtubule in PD pathogenesis is further supported by the involvement of acetylated α-tubulin in α-synuclein oligomerization and LB formation (Calogero et al., 2023; Mazzetti, Giampietro, et al., 2024) and by numerous *in vitro* and *in vivo* evidence of α-synuclein and tubulin interaction (Alim et al., 2004; Cartelli et al., 2016; Zhou et al., 2010).

For the sake of brevity and relevance to the present research activity, the following discussion will focus on α-synuclein aggregation and clearance, as well as on inflammation and their involvement in PD.

1.1.4 α-Synuclein aggregation, propagation, clearance, and biological impact

Physiologically, α-synuclein is a soluble, unstructured, and monomeric protein that exists in equilibrium with its amphipathic α-helix secondary structure, when bounded to lipid membranes (Burré et al., 2018) (**Figure 1.3**). In addition, a soluble and stable tetrameric form of endogenous α-synuclein, with an approximate molecular weight of 58 kDa has been described in neuronal and red blood cells (Bartels et al., 2011).

However, under pathological conditions, α-synuclein is prone to aggregate, first in small oligomers and protofibrils, then in β-sheet-rich conformation fibrils, eventually incorporated in highly ordered structures such as LB and LN found in PD patients (**Figure 1.3**) (Du et al., 2020).

In detail, monomeric α-synuclein can self-aggregate leading to the formation of dimers stabilized by hydrophobic interactions or covalent crosslinking. Subsequent nucleation events promote the recruitment of additional soluble α-synuclein monomers, which interact through hydrophobic patches located in the amino acid region between residues 71 and 82, ultimately giving rise to oligomers (Mor et al., 2016).

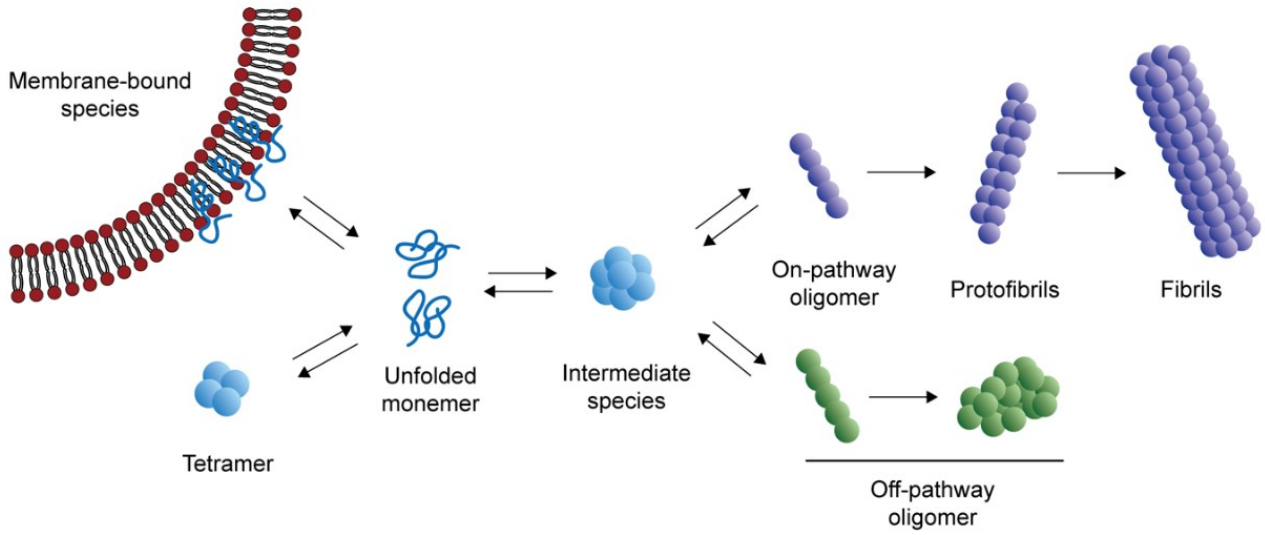

Figure 1.3. α-Synuclein aggregation process. *Physiologically, α-synuclein exists as unfolded monomers in a dynamic equilibrium with a tetrameric conformation. Under certain conditions the monomers aggregate to form oligomers, including "on-pathway" oligomers, prone to form protofibril and fibrils, and "off pathway" oligomers, that cannot form amyloid fibrils. Image from Du et al., 2020.*

Unlike fibrils, whose structure has been elucidated at the atomic level by cryo-electron microscopy, α-synuclein oligomer structure is still debated. Most likely, a metastable α-synuclein

oligomeric species exists, consisting of a mostly disordered spherical assembly of 11 monomers. Moreover, evidence exist that oligomers present a slightly elongated cylindrical structure with a cavity in the middle (Giehm et al., 2011).

This intermediate state is thought to a crucial step in the early stages of α-synuclein aggregation, as a structural rearrangement can lead to the formation of oligomers with distinct chemical, structural, and toxic properties. Two types of oligomers have been described: *i*) "on pathway oligomers" assume a quaternary structure and are converted in compact protofibrils and fibrils; *ii*) off-pathway species remain soluble, form amorphous aggregates that do not assemble into fibrils (Du et al., 2020) (**Figure 1.3**).

Nevertheless, effort need to be made to reveal the exact nature and structure of oligomers, and which type plays a critical role in PD pathogenesis.

In vitro studies have shown that fibrils may also form through secondary nucleation, in which fragmentation of existing fibrils increases the number of elongation sites. This process facilitates the formation of additional oligomers through interactions between soluble monomers and the fibril surface (Ghosh et al., 2017).

Regarding toxicity, whether α-synuclein oligomers or fibrils represent the more toxic species remains a matter of debate. Different mechanisms of α-synuclein oligomers toxicity have been reported. First, oligomers with a β-sheet core can insert into the lipid bilayer, disrupt the membrane, increasing cellular permeability and influx of ions from the extracellular space (Fusco et al., 2017). Multiple evidence also shows that α-synuclein oligomers induce mitochondrial dysfunction through mitochondrial complex impairment and lipid peroxidation, which in turn facilitates the opening of the mitochondrial permeability transition pore. This can lead to mitochondrial swelling, increased level of reactive oxygen species (ROS), and, ultimately, cell death (Ludtmann et al., 2018). α-Synuclein oligomers also induce endoplasmic reticulum (ER) stress (Colla et al., 2012) and synaptic impairment via inhibition of the SNARE complex formation, thereby reducing dopamine release (Choi et al., 2013).

Similarly, fibrillar α-synuclein aggregates have been proposed to contribute to PD pathology and exert toxicity by impairing cellular ion homeostasis and compromising the integrity and function of cytosolic organelles, including mitochondria, the ER, and the Golgi apparatus (Flavin et al., 2017).

Moreover, both oligomers and fibrils impair the UPS and ALP pathways, leading to loss of proteostasis (Du et al., 2020).

Notably, α-synuclein aggregates exert prion-like properties, as misfolded species can act as seeds that induce the assembly of soluble monomeric α-synuclein into higher molecular weight aggregates (Brundin & Melki, 2017). In this sense, α-synuclein fibrils are thought to be more efficient

as seeds than oligomers, likely due to their ordered β-sheet structure, which provides a stable template for monomer recruitment and elongation (Alam et al., 2019).

Current evidence also suggests that α-synuclein aggregates may also be transmitted from cell to cell, contributing to disease progression (Valdinocci et al., 2017). Several studies in cellular models support the idea that such transfer could occur through different pathways, including tunneling nanotubes, endocytosis, and exosomes (Abounit et al., 2016; Bieri et al., 2018; Mao et al., 2016). Moreover, it is known that α-synuclein aggregates can also be secreted from neurons during stress or their degeneration, resulting in an increased concentration of these species in the extracellular environment.

In this sense, the clearance of misfolded α-synuclein aggregates plays a crucial role in PD progression. Physiologically, natively unfolded α-synuclein is mostly degraded by the UPS (Kumar et al., 2018), responsible for the recycling of soluble cellular proteins with a short half-life. However, under pathological and stress conditions, when α-synuclein aggregates into oligomers and fibrils, the ALP, plays a critical role in clearing these larger, insoluble species (Ho, 2025). In PD pathology, key proteins of the macroautophagic pathway, such as Beclin-1 and LC3II, which are involved in the recognition and formation of autophagosomes, are described to be increased in SNpc of PD patients (Miki et al., 2016). Consistently, an increased number of autophagosomes and reduced levels of lysosomal markers have been observed in *post-mortem* PD human brain, suggesting deregulation of these pathways in the presence of α-synuclein pathology (Dehay et al., 2010; Nechushtai et al., 2023). Astrocytes, in addition to microglia, are integral to this process, contributing to the uptake and degradation of extracellular aggregated α-synuclein species released from neurons, by internalizing and degrading them through the endo-lysosomal pathway, thus playing a protective role for neurons (Booth et al., 2017; Lindström et al., 2017; Loria et al., 2017). Indeed, astrocytes with α-synuclein-positive inclusions have been detected in *post-mortem* PD brains (Braak et al., 2007). Several might be the mechanisms involved in extracellular α-synuclein internalization by astrocytes, ranging from receptor-mediated phagocytosis to a mechanosensitive process (Giusti et al., 2024). However, this initial protective role becomes markedly compromised in the later stages of the pathology, resulting in astrocyte dysfunction and disruption of neuron–glia crosstalk. Astrocyte clearance capacity is limited as excessive uptake of α-synuclein aggregates can overwhelm these cells, leading to an impaired phagocytic activity, accumulation of engulfed material that results in cellular toxicity (**Figure 1.4**) (Giusti et al., 2024; Raj et al., 2024). Besides impairing local homeostasis, this dysfunction may also lead to accumulation of extracellular aggregates that facilitate the intracellular accumulation and propagation of pathogenic α-synuclein species, thereby exacerbating PD pathology.

Lastly, aggregated α-synuclein has been demonstrated to induce neuronal and glial inflammation (Du et al., 2020; Giusti et al., 2024), creating a feed-forward loop that accelerates disease progression. The role of inflammation in PD, along with the specific cell types involved, will be addressed in the following section.

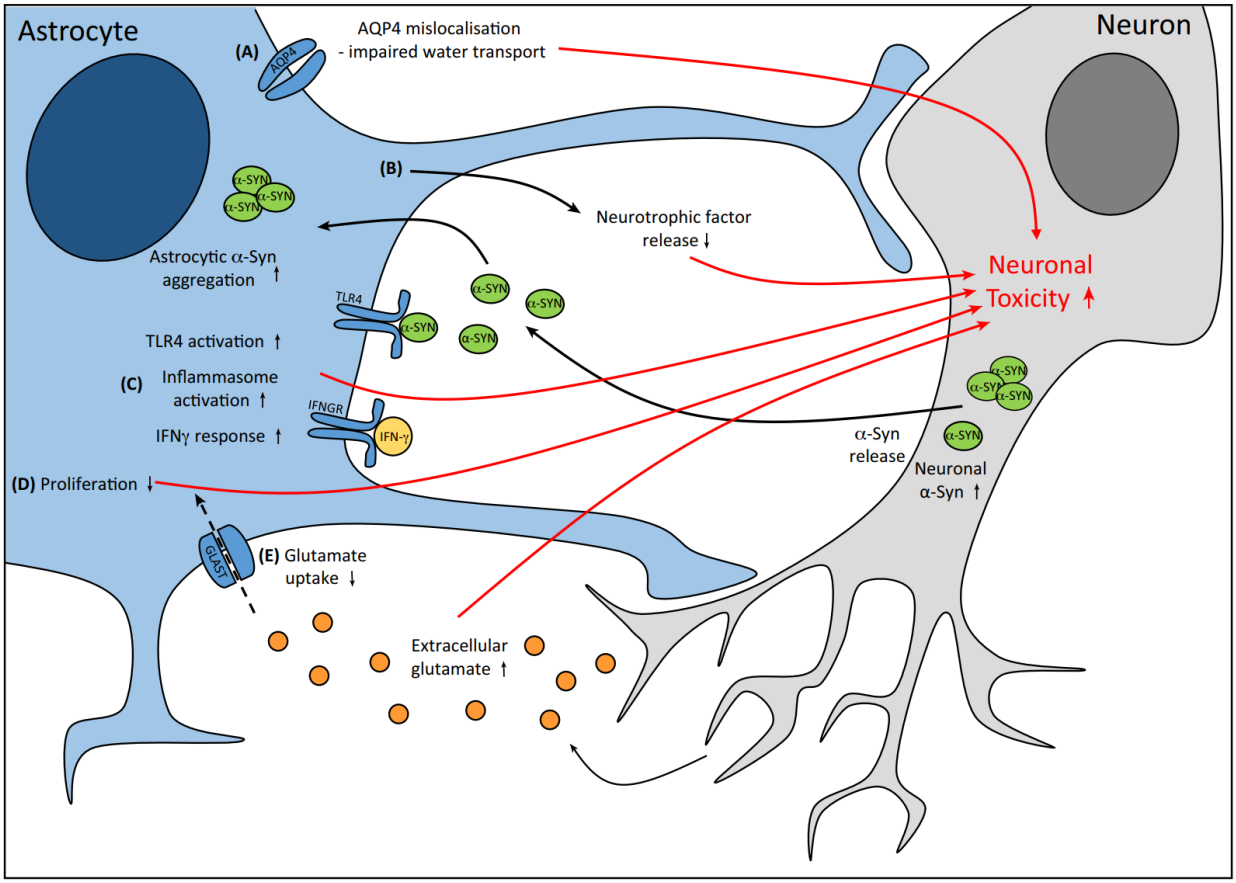

Figure 1.4. Astrocyte's role in α-synuclein aggregate clearance, inflammation, and cellular toxicity. *Astrocytes are involved in the uptake and degradation of extracellular aggregated* α-synuclein. *Excessive uptake results in dysfunctional astrocytes, activation of inflammatory pathways and neuronal toxicity. Image from Booth et al., 2017*

1.1.5 Inflammation in PD

Various evidence in human samples and from animal models support the involvement of inflammation in the pathogenesis of PD (Tansey et al., 2022). Although the exact mechanism triggering this response is still under investigation, the ongoing neuronal cell death and accumulation of misfolded, aggregated α-synuclein are most likely key players (Pajares et al., 2020). Both central and peripheral inflammation are reported in PD patients and contribute to a chronic inflammatory response that exacerbate neurodegeneration (Tansey et al., 2022).

Inflammation in the CNS

In the CNS, astrocytes and microglia play a key role in inflammatory processes. Astrocytes are the most abundant cell type in the CNS; they participate in the maintenance of the BBB, contribute to synaptogenesis and synaptic function, and support neuronal survival by realising trophic factors, such as brain-derived neurotrophic factor (BDNF) and nerve growth factor (NGF) (Sofroniew & Vinters, 2010). Moreover, astrocytes are also key regulators of innate and adaptive immune response, and their response might be beneficial or detrimental depending on the kind of stimuli they encounter (Colombo & Farina, 2016). Astrocytes involvement in PD inflammation is supported by the strong astrogliosis reported in the SNpc of PD *post-mortem* human brains and in animal models (Braak et al., 2007; Gu et al., 2010). Indeed, under pathological conditions, and in response to external stimuli and altered microglial states, astrocytes can acquire a reactive phenotype with morphological and gene expression alterations (Fisher & Liddelow, 2024; Liddelow et al., 2017). Reactive astrocytes can be distinguished in two types: A1 neurotoxic reactive astrocytes, and A2 neuroprotective reactive astrocytes (Patani et al., 2023). Upon stress stimuli, reactive A1 astrocytes release pro-inflammatory cytokines and chemokines, including Interleukin 1 beta (IL-1β), IL-6, Complement Component Subunit 1q (C1q), Tumour Necrosis Factor alpha (TNF-α) and CXCL10, leading to glial reactivity and neuronal dysfunction (Liddelow & Barres, 2017). Moreover, in A1 astrocytes, the classical complement pathway is activated, ultimately leading to complement C3 protein activation, one of the most upregulated gene in these cells (Chi et al., 2025; Lawrence et al., 2023). In contrast, A2 astrocytes upregulates neurotrophic factors that can promote neuronal survival and tissue repair, and release anti-inflammatory cytokines such as IL-4 and Tumour Necrosis Factor beta (TNF-β) (Colombo & Farina, 2016). Their polarization is closely associated to ischemic injuries.

Regarding PD, reactive A1 astrocytes, marked with C3 protein, have been detected in *post-mortem* human brain tissue (Liddelow et al., 2017). Indeed, multiple evidence show that high concentration of α-synuclein aggregates in the extracellular environment activate a TLR4-dependent inflammatory pathway that swiches astrocytes to the A1 reactive type, leading to pro-inflammatory molecules release and pathology progression (Booth et al., 2017; Giusti et al., 2024; Hindeya Gebreyesus & Gebrehiwot Gebremichael, 2020) (**Figure1.4**). Moreover, intracellular inclusion of α-synuclein in astrocytes may affect their homeostasis, as previously discussed, impairing BBB permeability. This can lead to infiltration of blood immune cells such as CD4+ and CD8+ lymphocytes and induce neuronal loss (Pajares et al., 2020).

Astrocytes polarization towards A1 phenotype can also be induced by activated microglia. *In vitro* studies showed that cultured medium from LPS-treated microglia, containing Il-1α, TNF-α and C1q cytokines, is sufficient to induceA1 astrocyte conversion (Liddelow et al., 2017) (**Figure 1.5**).

In the CNS, microglia are responsible for the main active immune defence and physiologically, they mediate synaptic pruning and remodelling, which are crucial for brain connectivity. Upon inflammatory stimuli, microglia functional polarized towards a pro-inflammatory or cytoprotective phenotype (Joe et al., 2018). Microgliosis has been described in *post-mortem* PD patients (Ho, 2019), where activated microglia engulf apoptotic and cell debris, release pro-inflammatory molecules and ROS that contributes to increase chronic neuroinflammation.

As with astrocytes, microglia activation can be mediated by the extensive presence of aggregated α-synuclein in the extracellular environment (Su et al., 2008; W. Zhang et al., 2005), and this activated state is further stimulated by factors released by A1 astrocytes.

Thus, the overall picture of inflammation in the CNS is extremely complex. Activated astrocytes and microglia contribute to chronic inflammation driven both by extracellular accumulation of aggregated α-synuclein as well as by cell damage-associated molecular patterns released by dying neurons, establishing a feed-forward loop that exacerbates PD progression (**Figure 1.5**).

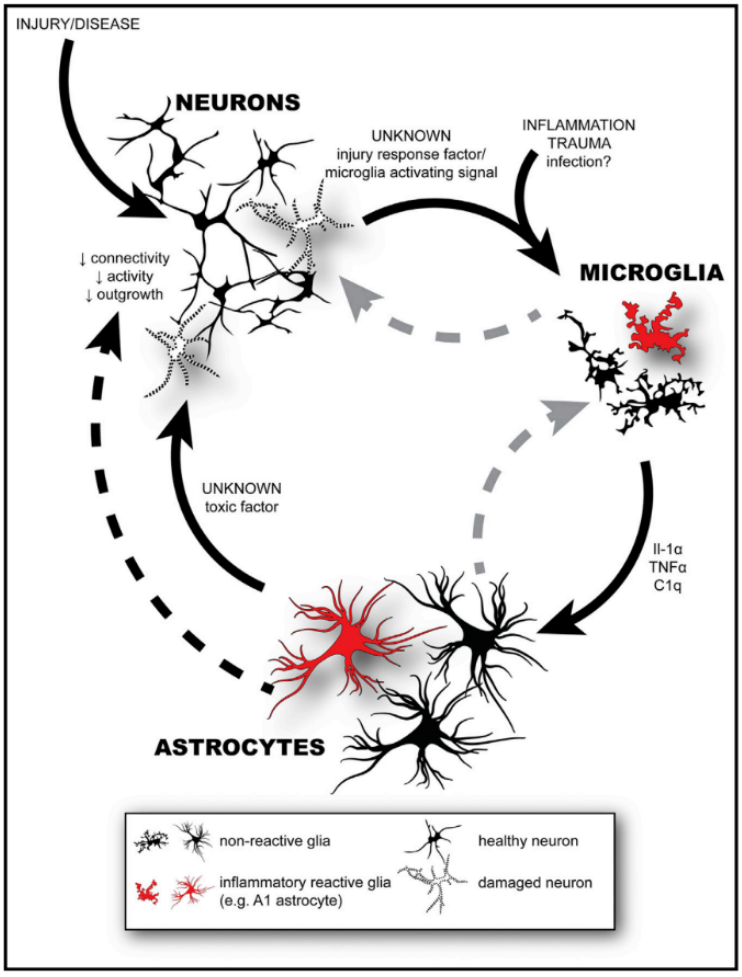

Figure 1.5. Astrocytes and microglia involvement in inflammation. *External stimuli, such as aggregated α-synuclein, trigger microglia and astrocytes activation. Activated microglia release pro-inflammatory molecules that contributes to A1 neurotoxic phenotype conversion in astrocytes. Astrocytes, in turn, release toxic factors that further damage neurons and sustain microglial activation. Image from Liddelow & Barres., 2017.*

Inflammation in the PNS: the role of macrophages

The involvement of peripheral inflammation in PD pathology is now well established. In PD patients, elevated inflammatory markers (C-reactive protein (CRP) and various cytokines) have been detected in the blood and CSF, along with chronic inflammation in the gastrointestinal tract (Houser & Tansey, 2017; Zimmermann & Brockmann, 2022). Notably, several studies support the idea that gut inflammation and dysbiosis can contribute to α-synuclein misfolding and aggregation in the enteric nervous system, that may spread via the vague nerve to the lower brainstem. This concept is now known as gut-brain axis hypothesis (Morais et al., 2021).

In the periphery, macrophages play a key role in the initiation, maintenance, and resolution of inflammatory processes. According to the environment, inactivated macrophages can polarize towards two different phenotypes with different functions and transcriptional profiles: M1 and M2 macrophages (Martinez et al., 2008) (**Figure 1.6**).

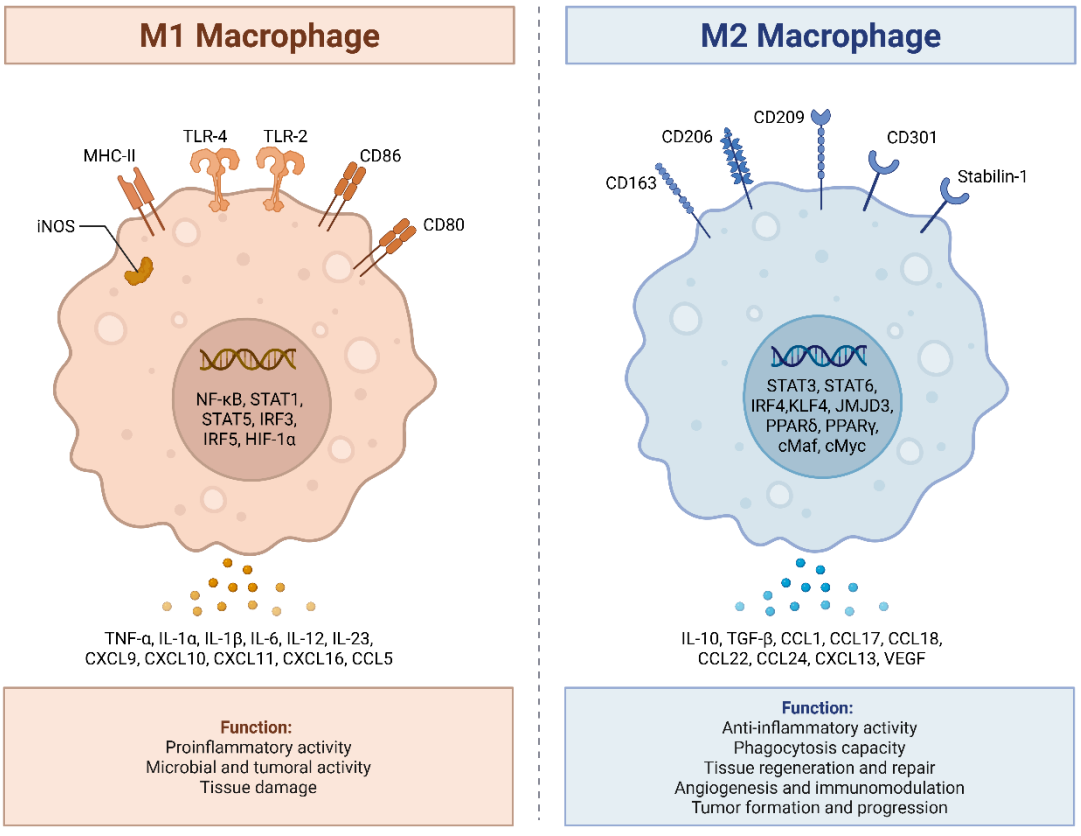

Figure 1.6 M1 and M2 macrophage polarization. *M1 macrophages, induced by pro-inflammatory signals such as IFN-γ and LPS, express surface markers including MHC-II, TLR-2, TLR-4, CD80, and CD86. They secrete pro-inflammatory cytokines (TNF-α, IL-1β, IL-6, IL-12, IL-23) and chemokines (CXCL9, CXCL10, CXCL11, CCL5). M2 macrophages are induced by anti-inflammatory signals, such as IL-4, IL-10 and IL-13, and express CD206, CD209, CD163, CD301 and Stabilin-1 surface markers. They secrete anti-inflammatory molecules such as IL-10, TGF-β, CCL17, CCL18, CCL22 and CCL24. Image modified from Briorender.com template.*

M1 macrophages have strong anti-microbial activity being primarily responsible for removal of pathogens during infection. These cells can be activated by Interferon-γ or bacterial LPS, release nitric oxide (NO), reactive nitrogen species (RNS), ROS and pro-inflammatory cytokines, including TNF-α, IL-1α, IL-1β, IL-6, IL-12, IL-23, and cyclooxygenase-2 (COX-2), thereby impairing tissue regeneration (Shapouri-Moghaddam et al., 2018). Once activated, M1 macrophages express T helper cells 1 attracting chemokines, such as CXCL9, CXCL10 CXCL11 and CXCL16, and upregulates membrane antigen presenting and co-stimulatory molecules such as MHC class I and II, TLRs, CD80 and CD86 molecules (**Figure 1.6**). This process leads to T cells recruitment and activation, initiating an adaptive immune response (Shapouri-Moghaddam et al., 2018).

On the contrary, although M2 macrophages can function as antigen presenting cells (APC), they express low levels of MHC class I/II and co-stimulatory molecules and are primary involved in inhibiting chronic inflammation through regulatory mechanisms (Helm et al., 2014). Indeed, these cells, activated by IL-4, IL-13 and IL-10 cytokines, release anti-inflammatory cytokine such as IL-10, IL-4, TGF-β, and IL-1Ra (Shrivastava & Shukla, 2019). Functionally, M2 macrophages possess high phagocytic activity and express scavenger receptors on their surface, including CD163, CD206, Stabilin-1, CD301 and CD209 (Yunna et al., 2020) (**Figure 1.6**). Furthermore, activated M2 macrophages recruits T helper 2 cells, regulatory T cells, and granulocytes through secretion of the CCL17, CCL18, CCL22, CCL24 and CXCL13 chemokines (Shapouri-Moghaddam et al., 2018).

Regarding PD, GWAS studies have highlighted the human leukocyte antigen-DR (HLA-DR) locus, an MHC class II molecule, as a risk factor for developing the disease, thus supporting the APC role in PD inflammation (Ahmed et al., 2012; Hamza et al., 2010). Indeed, local antigen presentation via MHCII expression has been shown to contribute to the loss of dopaminergic neurons in the SNpc (Williams et al., 2018). Moreover, in a *in vivo* study on a rodent model of PD, border-associated macrophages (BAMs), which are physiologically found in the CNS's borer region, have been shown to mediated CD4+ T cells recruitment in the brain parenchyma. This process was associated with BAMs upregulation of MHCII molecules (Frosch et al., 2023; Schonhoff et al., 2022).

Thus, so far, evidence points out M1 macrophages with APC activity as primarily involved in PD susceptibility and progression. Nevertheless, *in vivo*, macrophages do not exhibit exclusively M1 or M2 phenotype but can display an intermediate activation state or mixed activation (Moehle & West, 2014; Vogel et al., 2013). In other chronic neuroinflammatory disorders, such as multiple sclerosis, a mixed activation of both M1 and M2 macrophages has been described (Z. Zhang et al., 2011). Similarly, this might occur in PD; however, the mechanisms by which macrophages are affected by α-synuclein aggregates, including their polarization toward M1 and/or M2 phenotype and their involvement in PD pathology, remain questioned.

1.2 Poly-γ-Glutamic Acid

Poly-γ-glutamic acid (γ-PGA) is a natural, non-toxic, non-immunogenic, biodegradable, edible and environmentally friendly biopolymer. This polymer is composed of D- and/or L-glutamic acid monomers that are coupled to each other via amide bonds between α or γ-carboxylic groups (Nair et al., 2023) (**Figure 1.7**). γ-PGA exhibits five distinct structural forms: α-helix, β-sheet, random coil, helix-to-random coil transition, and enveloped aggregate. It is mainly produced by *Bacillus* species such as *Bacillus anthracis*, where it was first discovered, *B. subtilis*, *B. licheniformis, B. amyloliquefaciens*, *B. velezensis*, and others (Sirisansaneeyakul et al., 2017). *B. subtilis* and *B. licheniformis* are high potential microbial sources of γ-PGA. The biosynthesis of the polymer is entirely dependent on the microenvironment and the specific organism that produces it. The physiological function of γ-PGA is not fully understood and is thought to be influenced by the organism's environment. Some organisms may synthesize γ-PGA to evade antibodies and antimicrobial peptides, while others might utilize it as a nutrient source during periods of starvation (Luo et al., 2016; Sirisansaneeyakul et al., 2017). Indeed, γ-PGA can enhance biofilm formation and aid in the absorption of essential nutrients from the environment (Yan et al., 2015).

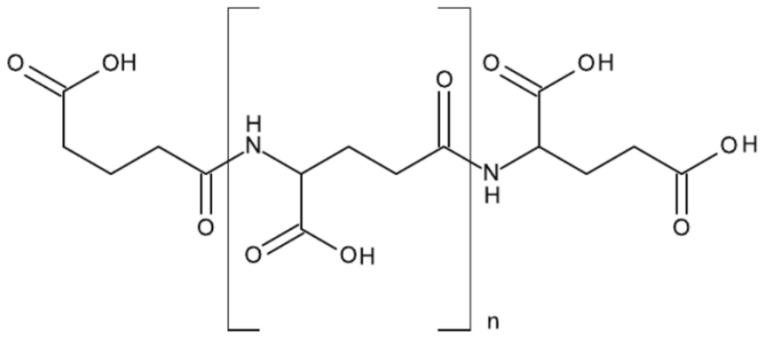

Figure 1.7: The chemical structure of γ-PGA. *Image from Balogun-Agbaje et al., 2021.*

1.1.1 The functional properties of γ-PGA

The molecular structure of γ-PGA is influenced by its molecular composition. Depending on its stereochemistry, γ-PGA can be divided into three types: the homopolymer of D-glutamic acid (D-γ-PGA), the homopolymer of L-glutamic acid (L-γ-PGA), and the copolymer of D- and L-glutamic acid (DL-γ-PGA) (Nair et al., 2023). The biological functions and applications of γ-PGA mainly depend on its molecular weight (MW). γ-PGA with a MW exceeding 1,000 kDa has high viscosity and can be used as a thickener or biomaterial. In contrast, γ-PGA with a MW below 400 kDa is preferred for certain medical applications (L. Wang et al., 2022). The MW of the polymer can be

influenced by both the genetic of the microorganism, as well as the conditions of the fermentation environment. For instance, deletion of the gene encoding for γ-PGA hydrolases can influence the MW of the polymer (Kimura et al., 2004). Nevertheless, the MW of γ-PGA can be affected by modulating growth medium of the strain producers. Parameters such as concentration of dissolved oxygen, working volume, and the concentration of sodium chloride can be crucial. Indeed, since γ-PGA is produced by organisms upon stress stimuli, as the concentrations of osmotically disruptive compounds become more toxic, the cell responds by increasing the production of higher MW γ-PGA (Parati et al., 2022; Shimizu et al., 2007). Moreover, it has been demonstrated that γ-PGA polymers decrease in MW during the fermentation procedure. This could be attributed to the increased synthesis of degradative enzymes as the fermentation proceeds. (Ogunleye et al., 2015). All of this can result in MW polydispersity, meaning that the MW of the γ-PGA produced it is not uniform but falls within a specific range (Parati et al., 2022).

Like other polymers, the behaviour of γ-PGA can be influenced by both its chemical properties and its physical arrangement in solution. The γ-peptidic bond structure of γ-PGA results in a high availability of carboxylic groups (L. L. Wang et al., 2017). Chemically, this abundance allows for significant intramolecular associations and a strong affinity for cations (Parati et al., 2022). Generally, solubility increases with rising pH due to the enhanced ionization of -COOH groups. This ionization disrupts the hydrogen bonding between the -COOH group of the γ-peptide bond and the $-NH_2$ group of a second γ-peptide monomer, leading to an increased molecular extension of the γ-PGA chains (L. L. Wang et al., 2017).

1.1.2 γ-PGA biomedical applications

The growing industrial interest in γ-PGA is mainly due to the polymer's versatility. γ-PGA has been used in food, cosmetics, agriculture, and wastewater industries, but due to is non-toxic and non-immunogenic properties, γ-PGA has gained relevance in biomedical applications (Ogunleye et al., 2015).

Indeed, low MW γ-PGA has shown great promise as a drug delivery platform and as an effective carrier for gene therapy (Balogun-Agbaje et al., 2021). Its carboxylic side groups provide attachment points for therapeutic agents, allowing for the creation of conjugated or encapsulated nanoparticles. For instance, γ-PGA has been tested in cancer therapy as γ-PGA-based molecules enter the tumor site and gradually release the drug as the polymer biodegrades. This system can improve the active drug concentration in the target site while limiting the exposure in normal tissue and systemic toxicity (Cai et al., 2023; L. Wang et al., 2022). Additionally, the ability of γ-PGA as carrier has also been tested in vaccine development, where it showed excellent adjuvant properties,

improving antigen uptake and inducing stronger cellular immune response (Mohammadzadeh et al., 2023; Yang et al., 2022).

γ-PGA also showed good antioxidant and cytoprotective properties as it is able to prevent hydroxyl radical formation by chelating iron, thus inhibiting hydroxyl radical generation in concentration-dependent manner. Additionally, the polymer can also scavenge hydrogen peroxide, another contributor to oxidative damage (Lee et al., 2020). These scavenging activities are likely due to the ability of amino and hydroxyl groups to donate electrons to ROS (Lee et al., 2020). All together, these properties make γ-PGA highly effective in protecting against oxidative cell damage.

Emerging evidence also showed that γ-PGA exert anti-inflammatory properties. A study on bone marrow-derived macrophages reported the polymer's ability to reduce inflammasome activation and its immune-modulating properties through enhancing antigen uptake by APC cells and promoting cytokine production (Ahn et al., 2018). Moreover, an *in vivo* study on colitis mouse model showed γ-PGA ability to reduce leukocyte recruitment in the inflamed colon, thus reducing inflammation and attenuating the symptoms (Davaatseren et al., 2013).

γ-PGA is also known to be a powerful prebiotic agent (Jin et al., 2017). High MW γ-PGA, with its viscous properties, can stabilize gut microorganisms, while low MW γ-PGA that reaches the colon acts as a prebiotic, promoting the growth of species associated with a healthy microbiome (Jin et al., 2017). Moreover, a recent study in mice also showed γ-PGA ability to ameliorate slow transit constipation by modulating aquaporins and gut microbiota (X. Wang et al., 2025). For instance, γ-PGA is commonly consumed in the Asian continent and is a major part of Japanese food culture as fermented sticky *natto,* soybeans fermented with *B. subtilis* natto (Bhat et al., 2013). Interestingly, age dependent relative PD incidence rate is significantly lower in Japan when compared with Europe (Kanaya et al., 2021).

A study conducted on male gerbils, in which stroke symptoms were induced by carotid artery occlusion, demonstrated that γ-PGA has anti-inflammatory properties and reduces neuronal cell death, by potentially enhancing the gut-brain axis, increasing blood flow, and improving β-cell functions (T. Zhang et al., 2021).

Therefore, given its anti-inflammatory, antioxidant, and neuroprotective properties, γ-PGA could be a promising candidate for a potential preventive strategy against PD, in which inflammation, dysbiosis, and the presence of α-synuclein in the gut during the prodromal phase of the disease are key elements of the pathology.

2

Chapter 2: γ-PGA alleviates cytotoxicity and inflammation induced by pre-formed fibrils of α-synuclein in murine primary astrocytes

2.1 Introduction

Astrocytes are involved in the clearance of extracellular aggregated α-synuclein species released from neurons by internalizing and degrading them through the endo-lysosomal pathway, thus playing a protective role for neurons. However, their capacity is limited, and excessive uptake can overwhelm astrocytes, leading to cellular toxicity (Giusti et al., 2024). Moreover, high concentrations of α-synuclein in the extracellular environment activate the innate immune-dependent inflammatory pathway that induces the acquisition by astrocytes of a reactive inflammatory phenotype (A1 type). This feature could contribute to the progression of the pathology as astrocytes lose the ability to promote neuronal survival, synaptogenesis, outgrowth, and phagocytosis, and release pro-inflammatory molecules that trigger neuronal cell death (Liddelow et al., 2017; Patani et al., 2023). Thus, approaches that can regulate extracellular α-synuclein aggregates and act on neuroinflammation might be beneficial. Here we aim to explore the biological effect of γ-PGA, produced through fermentation from generally recognized as safe (GRAS) organism *Bacillus subtilis* Natto, in murine primary astrocytes exposed to α-synuclein pre-formed fibrils (PFFs), a recognized cellular model used to recapitulate astrocyte pathological hallmarks in PD (Chou et al., 2021; Filippini et al., 2021). This work was published in the *International Journal of Biological Macromolecules* in June 2025 and can be found attached in Appendix II: published paper (Novello et al., 2025).

2.2 Results

2.2.1 γ-PGA rescues α-synuclein PFF induced cytotoxicity on murine primary astrocytes

γ-PGA is a well-characterized, non-toxic, and non-immunogenic biomacromolecule (Li et al., 2022) but its effect on murine primary astrocytes has yet to be investigated. Thus, to examine the potential cytotoxic effects of γ-PGA on astrocytes, cells were incubated with increasing concentrations of γ-PGA for 24 hrs and viability was evaluated using MTT assay. As expected, we observed that γ-PGA had no cytotoxic effect on primary astrocytes at any of the tested concentrations (0.275, 2.75, and 27.5 μM). Surprisingly, we observed a dose-dependent increase in cell viability, with the 27.5 μM concentration significantly improving primary astrocytes viability compared to the control and the 0.275 μM concentration (**Figure 2.1, A**). Therefore, 27.5 μM concentration was selected to test the protective or recovery effect of γ-PGA on PFF-treated primary astrocytes, a widely used model to recapitulate the pathological features of astrocytes in PD (Chou et al., 2021; Filippini et al., 2021). For this purpose, we used a treatment approach of either adding γ-PGA before (PRE treatment) or after (POST treatment) PFF administration. As expected, the addition of PFFs to astrocytes decreased cell survival, that was significantly rescued following POST treatment with γ-PGA (**Figure 2.1, B**).

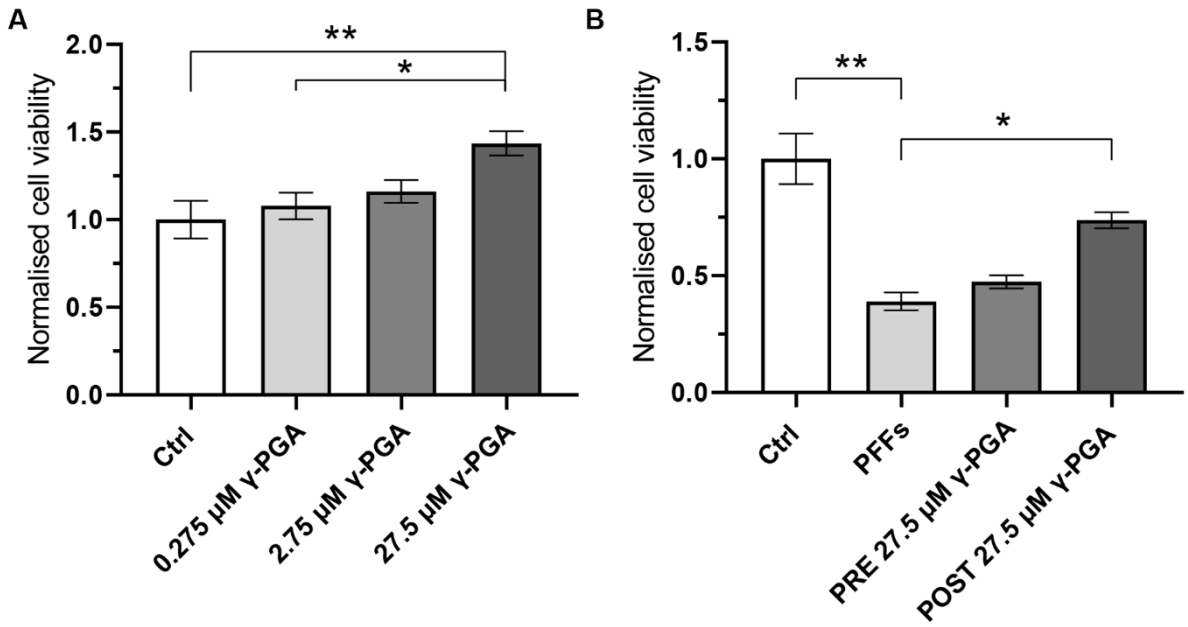

Figure 2.1. γ-PGA rescues α-synuclein PFF-induced toxicity in primary astrocytes. *A) Cell viability of primary astrocytes treated with increasing concentrations of γ-PGA (0.275, 2.75, 27.5 µM). Data are expressed as mean ± SEM, normalized to control and analyzed by ordinary one-way ANOVA with Tukey's post hoc test (n = 5).* ***B****) Cell viability of primary astrocytes treated with α-synuclein PFFs alone and in co-treatment with γ-PGA added before (PRE) or after PFFs (POST). Data are expressed as mean ± SEM, normalized to control and analyzed by Kruskal-Wallis test with Dunn's correction (n = 5), **p < 0.01, *p < 0.05.*

2.2.2 γ-PGA impacts on the distribution of α-synuclein PFFs in primary astrocyte culture

We explored whether the impact of γ-PGA on astrocyte viability could be attributed to its capacity to modulate or interfere with α-synuclein PFFs. Hence, with the same experimental design, we initially analyzed the total area of α-synuclein PFFs by immunofluorescence and using an antibody against total α-synuclein (**Figure 2.2**). By adding γ-PGA either before or after PFFs, the extent of α-synuclein aggregates was reduced compared to PFF treatment alone (**Figure 2.2, A, B, C**). Notably, the PRE treatment significantly decreased the total area of PFFs compared to PFF treatment alone (**Figure 2.2, D**). To further assess how γ-PGA distributes relative to α-synuclein PFFs in astrocytes cell culture, we labeled γ-PGA with FITC and investigated its localization by means of immunofluorescence assay. We observed that when astrocytes were treated with γ-PGA only, γ-PGA distributed mainly inside the cells (**Figure 2.3, A**, white arrowheads), as shown by the orthogonal view of the image (**Figure 2.3, A', A"**), and by 3D reconstruction with arivis Vision4D® 3.6.0 software (Figure 3B, B'; white arrowheads; video: https://ars.els-cdn.com/content/image/1-s2.0-S0141813025058581-mmc1.mp4). When astrocytes were treated with α-synuclein PFFs only, we also observed their intra and extracellular distribution (Figure 3B, white arrowheads and arrow, respectively). Z-axis orthogonal projections of confocal multiplane images revealed the

internalization of α-synuclein PFFs within astrocytes (**Figure 2.3, C-C"**), further confirmed by the 3D reconstruction with arivis Vision4D® 3.6.0 software (**Figure 2.3, D'**, white arrowheads; video: https://ars.els-cdn.com/content/image/1-s2.0-S0141813025058581-mmc2.mp4). Lastly, when γ-PGA was co-administered with α-synuclein PFFs to primary astrocytes, we observed that γ-PGA colocalized with α-synuclein PFFs in both PRE treatment (**Figure 2.3, E, F**, video: https://ars.els-cdn.com/content/image/1-s2.0-S0141813025058581-mmc3.mp4) and POST treatment (data not shown). Moreover, upon observing their arrangement relative to the cell, γ-PGA clearly localized between α-synuclein PFFs and S100β-labelled astrocytes, as shown in the orthogonal projection (**Figure 2.3, E, E"**) and 3D reconstruction (**Figure 2.3, F'**).

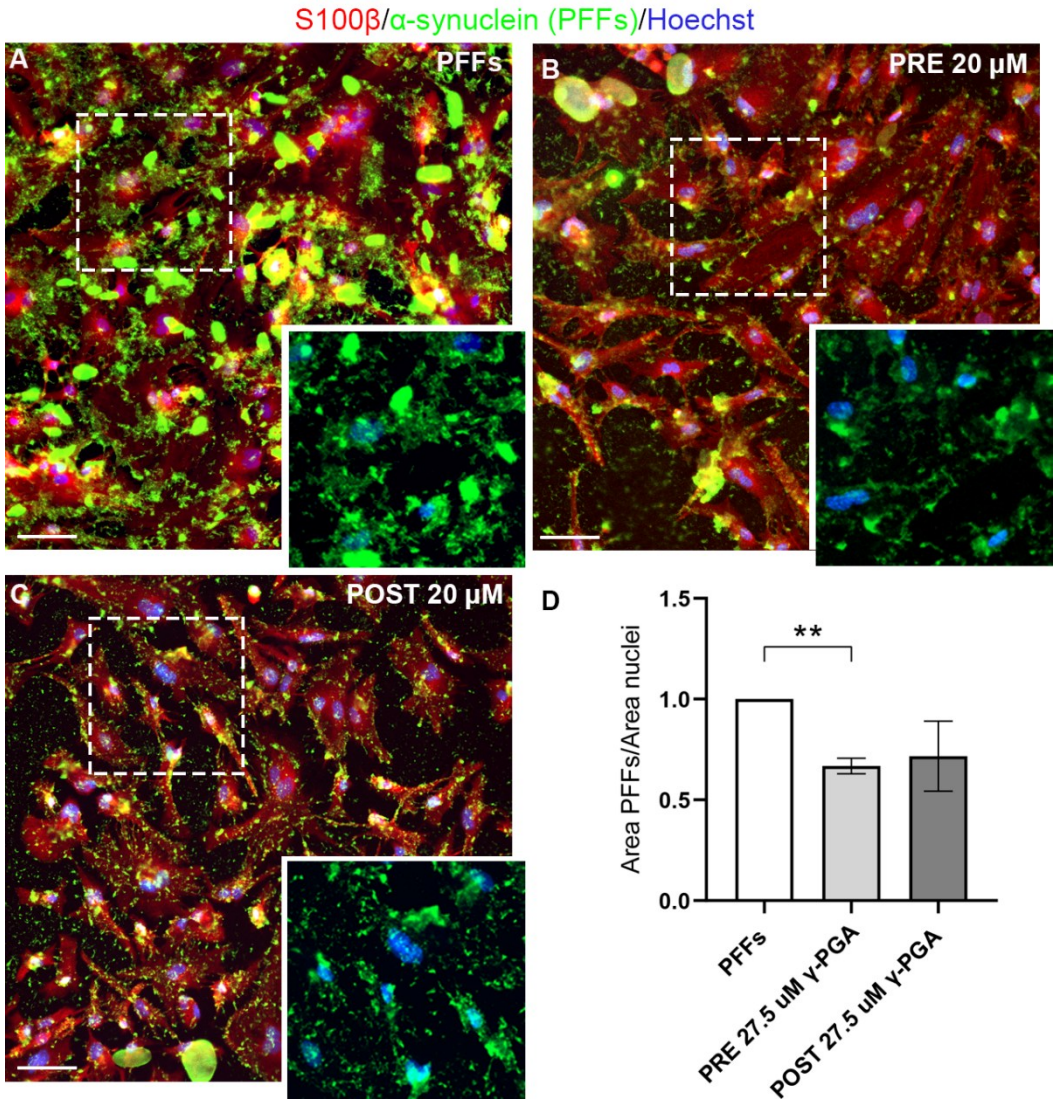

Figure 2.2. γ-PGA limits the extent of α-synuclein PFFs in primary astrocytes. *Spinning disk confocal microscopy images showing α-synuclein PFF distribution in primary astrocytes, labeled with S100β (**A**) and treated with γ-PGA before (**B**) or after (**C**) the addition of PFFs. Nuclei were counterstained with Hoechst. Scale bar, 50 µm (**D**). The graph shows the total area of PFFs normalized on the area of nuclei. Data are expressed as fold change of control ± SEM and analyzed by One sample t-test (n = 4), **p < 0.01.*

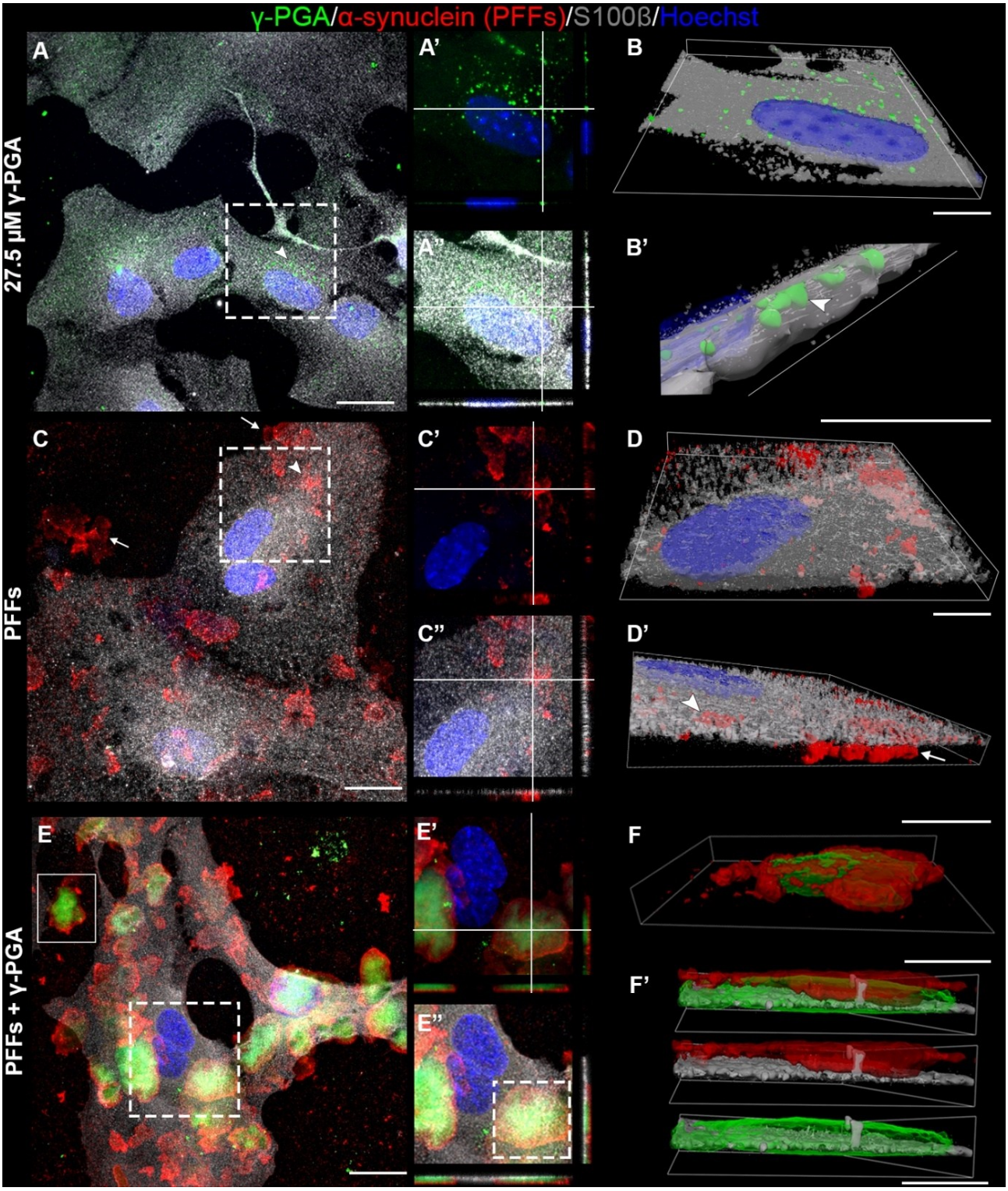

Figure 2.3. The interplay between γ-PGA and α-synuclein PFFs in primary astrocytes. *A) Spinning disk confocal images showing the distribution of γ-PGA in murine primary astrocytes.* ***A'*** *and* ***A"*** *show the magnification of the dashed rectangle in A and the orthogonal projections that represent the XZ (bottom) and YZ (right) planes and highlight the presence of γ-PGA inside the cell.* ***B*** *and* ***B'*** *show the top and side view of the 3D reconstructions obtained with arivis Vision4D® 3.6.0 software*

*of A". **C)** Spinning disk confocal images showing α-synuclein PFF distribution in astrocytes. **C'** and **C"** show the magnification of the dashed rectangle in C and the Z-axis projection. **D** and **D'** show the top and side view of the 3D reconstructions obtained with arivis Vision4D® 3.6.0 software of C. **E)** Representative spinning disk confocal image of PRE treatment with γ-PGA of primary astrocytes. **E'** and **E"** show the magnification of the dashed rectangle in E and orthogonal view showing the distribution of γ-PGA relative to α-synuclein PFFs. **F** represents the 3D reconstruction by arivis Vision4D® 3.6.0 software of the rectangle in E showing γ-PGA and α-synuclein PFFs colocalization in the extracellular environment. **F'** illustrates the lateral view of 3D reconstruction of the dashed rectangle in E"; the split channels highlight the disposition of γ-PGA and α-synuclein PFFs when compared to S100β labeled astrocytes. Nuclei were counterstained with Hoechst. White arrows and white arrowheads in A, B', C and D' show the intracellular and extracellular localization, respectively, of either γ-PGA or PFFs. **A, A', A", C, C', C", E, E', E"**: scale bar, 20 µm. **B, B', D, D', F, F'**: scale bar, 5 µm.*

2.2.3 γ-PGA limits the internalization of α-synuclein PFF by primary astrocytes

The amount of α-synuclein PFFs within astrocytes is a key factor, which affects their ability to clear it, whereby excessive accumulation could impair the protein's degradation pathway (Giusti et al., 2024). Thus, we explored whether γ-PGA could have any impact on the internalization of PFFs by astrocytes. To evaluate this hypothesis, we labelled α-synuclein PFFs with a pH-sensitive dye (pHrodo-PFFs) that becomes fluorescent when the pH of the surrounding environment increases in acidity, such as late endosomes and lysosomes. We noted that fluorescence area and intensity of pHrodo-PFFs were significantly lower following both γ-PGA treatments (**Figure 2.4, B, C**) compared to pHrodo-PFFs alone (**Figure 2.4, A**). Notably, γ-PGA PRE-treatment was the most effective in reducing α-synuclein PFF internalization (**Figure 2.4, D**).

In parallel, we explored whether γ-PGA may affect the degradation of PFFs by analyzing the autophagic and lysosomal pathways involved in their clearance (Gao et al., 2019; Pantazopoulou et al., 2021). To assess the effect of γ-PGA treatment on autophagy, we examined LC3 and p62 levels by Western blotting. Treatment with α-synuclein PFFs led to a significant increase of LC3-II/LC3-I ratio (**Figure 2.4, E, F**) and accumulation of p62 (**Figure 2.4, E, G**), suggesting an impairment in the autophagic flux. Although no differences were observed with PRE-treatment of γ-PGA, POST treatment resulted in a mild decrease in p62 levels (**Figure 2.4, E, G**). With respect to the lysosomal pathway, we employed LAMP1 as a marker of autophagy-related lysosomal organelles (Cheng et al., 2018), and found an increase in LAMP1 fluorescence area and intensity with PFF treatment, that was not altered by γ-PGA treatment (**Figure 2.5**). These results suggest that γ-PGA mainly exerts its effect by limiting PFF internalization in primary astrocytes.

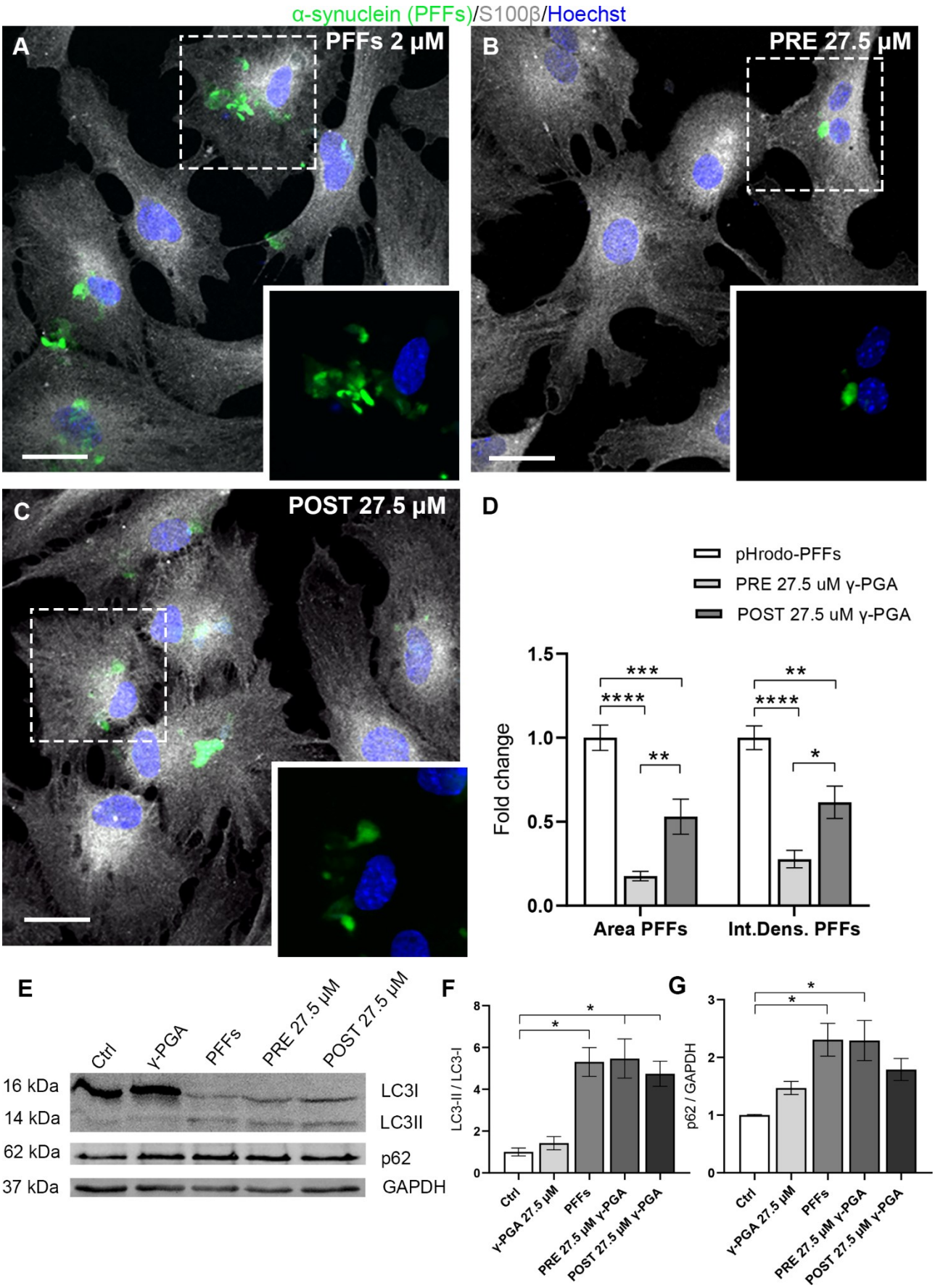
α-synuclein (PFFs)/S100β/Hoechst
A
PFFs 2 µM
B
PRE 27.5 µM
C
POST 27.5 µM
D
pHrodo-PFFs
PRE 27.5 uM γ-PGA
POST 27.5 uM γ-PGA
Fold change
1.5
1.0
0.5
0.0
***
****
**
**
****
*
Area PFFs
Int.Dens. PFFs
E
Ctrl
γ-PGA
PFFs
PRE 27.5 µM
POST 27.5 µM
16 kDa
14 kDa
62 kDa
37 kDa
LC3I
LC3II
p62
GAPDH
F
LC3-II / LC3-I
G
p62 / GAPDH
Ctrl
γ-PGA 27.5 µM
PFFs
PRE 27.5 µM γ-PGA
POST 27.5 µM γ-PGA

***Figure 2.4**. **γ-PGA administration decreases PFF internalization by primary astrocytes**. Maximum intensity Z-projection confocal images of primary astrocytes labeled with S100β and treated with pHrodo-PFFs (**A**) and with γ-PGA added before (**B**) or after (**C**) PFFs. Nuclei were counterstained using Hoechst. Scale bar, 20 µm. **D**) The graph shows the area covered by pHrodo-PFF and pHrodo-PFFs fluorescence intensity (Integrated Density) both normalized on the area of nuclei. **E**) Representative immunoblots for LC3 (LC3I, 16 kDa; LC3II, 14 kDa), p62 (62 kDa) and GAPDH (37 kDa). **G**) and **H**) graphs show LC3-II/LC3-I ratio and quantification of p62 normalized over GAPDH. Data are reported as mean ± SEM, normalized to control and analyzed by ordinary one-way ANOVA with Tukey's post hoc test (n = 4), *p < 0.05, **p < 0.01, ***p < 0.001, ****p < 0.0001.*

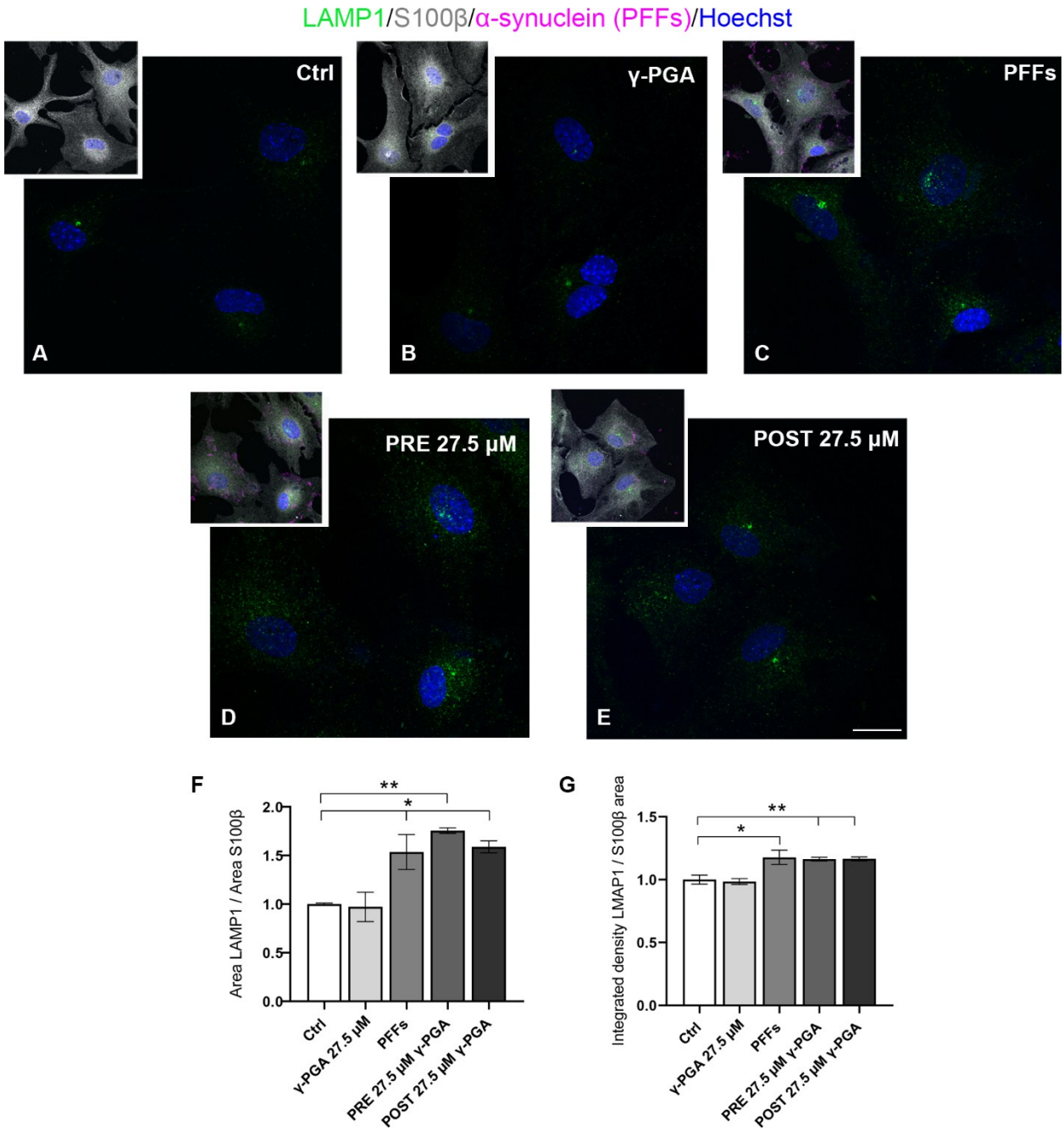

Figure 2.5. Lysosome evaluation in primary astrocytes treated with PFF and γ-PGA. *Representative staining of primary astrocytes labeled for LAMP1 (green signal), α-synuclein (pink signal), S100β (grey signal), and nuclei (blue signal).* ***A****) control cells,* ***B****) cells treated with 27.5 µM γ-PGA,* ***C****) cells treated with 2 µM PFFs,* ***D****) PRE treatment, and* ***E****) POST treatment. Scale bar, 20 µm. The graphs show the area (****F****) and the fluorescence intensity (Integrated density) (****G****) of LAMP1 signal normalized on the area of S100β. Data are reported as fold change of control, expressed as mean ± SEM and analysed by ordinary one-way ANOVA with Tukey's post hoc test (n = 3), **p < 0.01, *p < 0.05.*

2.2.4 γ-PGA prevents and recovers PFF-induced inflammation in primary astrocytes

It is widely recognised that astrocytes play a key role in the inflammatory response during PD pathogenesis (Booth et al., 2017). Several studies have shown that α-synuclein aggregates can activate the astrocytic inflammatory response inducing the acquisition of a reactive phenotype that exacerbates the pathological condition (Chou et al., 2021; Hindeya Gebreyesus & Gebrehiwot Gebremichael, 2020). Thus, given the anti-inflammatory properties of γ-PGA (Ahn et al., 2018; Jeong et al., 2021), we tested whether this biomacromolecule could prevent or alleviate astrocyte inflammation induced by α-synuclein PFFs. Immunofluorescence assay was employed to evaluate Complement C3 protein, a marker of A1 reactive astrocytes (Liddelow et al., 2017) (**Figure 2.6, Figure 2.7**). As expected, γ-PGA alone had no effect on C3 protein in terms of both fluorescence area and intensity (**Figure 2.6**) whereas treatment with α-synuclein PFFs increased C3 deposition compared to the control (**Figure 2.7, A, B**). Both PRE and POST treatment with γ-PGA significantly reduced fluorescence area and intensity of C3 staining compared to PFFs (**Figure 2.7, C, D, E, F**). Notably, we did not observe any significant difference in γ-PGA anti-inflammatory properties between PRE and POST treatment **(Figure 2.7, E, F**).

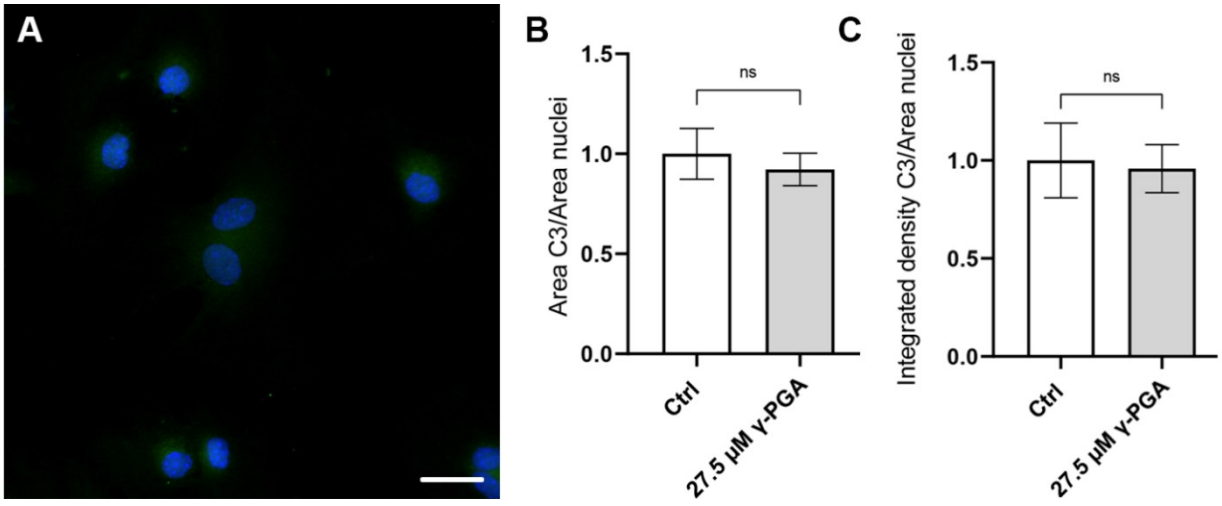

***Figure 2.6. γ-PGA at 27.5 µM administration does not affect inflammation in primary astrocytes**. **A)** Representative staining of complement C3 inflammation (green signal) of control cells (Ctrl) or treated with 27.5 µM γ-PGA. Scale bar, 20 µm. The graphs show the area (**B**) and the fluorescence intensity (Integrated density) (**C**) of C3 normalized on the area of nuclei (blue signal). Data are reported as fold change of control, express as mean ± SEM and analysed by Student t test; ns, not significant.*

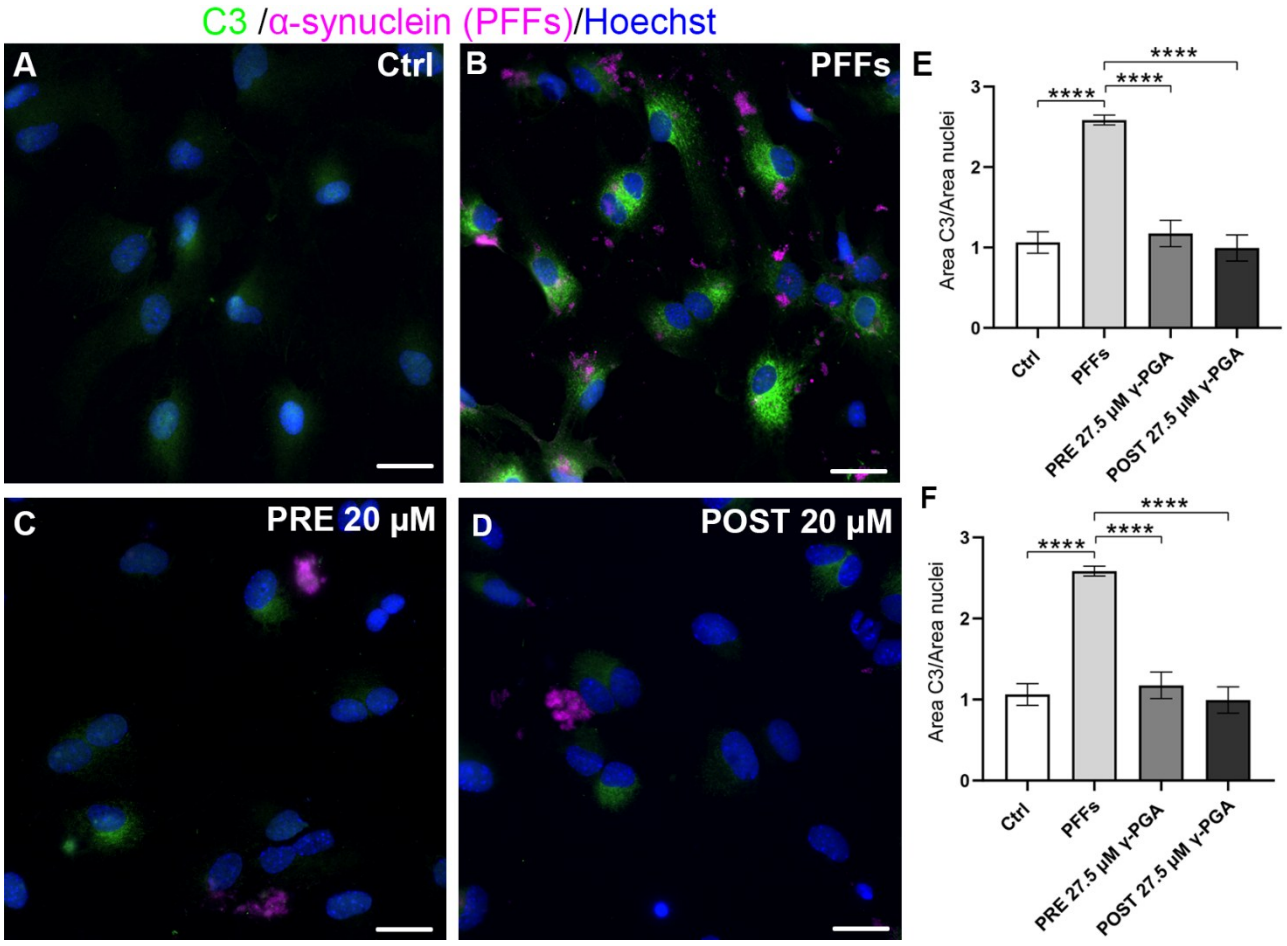

Figure 2.7. γ-PGA administration decreases complement C3-induced inflammation in primary astrocytes. *Representative confocal images showing complement C3 staining in primary astrocytes in control condition (**A**), treated with PFFs (**B**) and with γ-PGA added before (**C**) or after (**D**) the addition of PFFs. Nuclei were counterstained using Hoechst. Scale bar, 20 µm. The Graphs show area (**E**) and fluorescence intensity (Integrated density) (**F**) of C3 protein. Data are reported as mean ± SEM and analyzed by ordinary one-way ANOVA with Tukey's post hoc test (n = 4), *p < 0.05, **p < 0.01, ***p < 0.001, ****p < 0.0001. normalized on the area of nuclei.*

To further investigate the inflammatory response, we measured the levels of pro-inflammatory cytokines released by treated astrocytes, including TNF-α, IL-1β, IL-6, and the chemokine CXCL10, which have previously been reported to be elevated in PFF treated astrocytes (Chou et al., 2021; Raj et al., 2024). In both control and γ-PGA-treated astrocytes, we detected very low levels of CXCL10 and IL-1β release (**Figure 2.8, A, B**), while no detectable levels of TNF-α and IL-6 were observed (**Figure 2.8, C, D**). As expected, PFF treatment led to a significant increase in the release of CXCL10, IL-1β and TNF-α, which was significantly attenuated following POST treatment with γ-PGA (**Figure 2.8, A, B, C**). Moreover, no differences were found between control and POST treatment. Regarding

IL-6, γ-PGA POST treatment showed a trend toward reduced release in PFF treated cells (**Figure 2.8, D**). Collectively, these findings support the role of γ-PGA in attenuating the inflammatory response induced by α-synuclein PFFs.

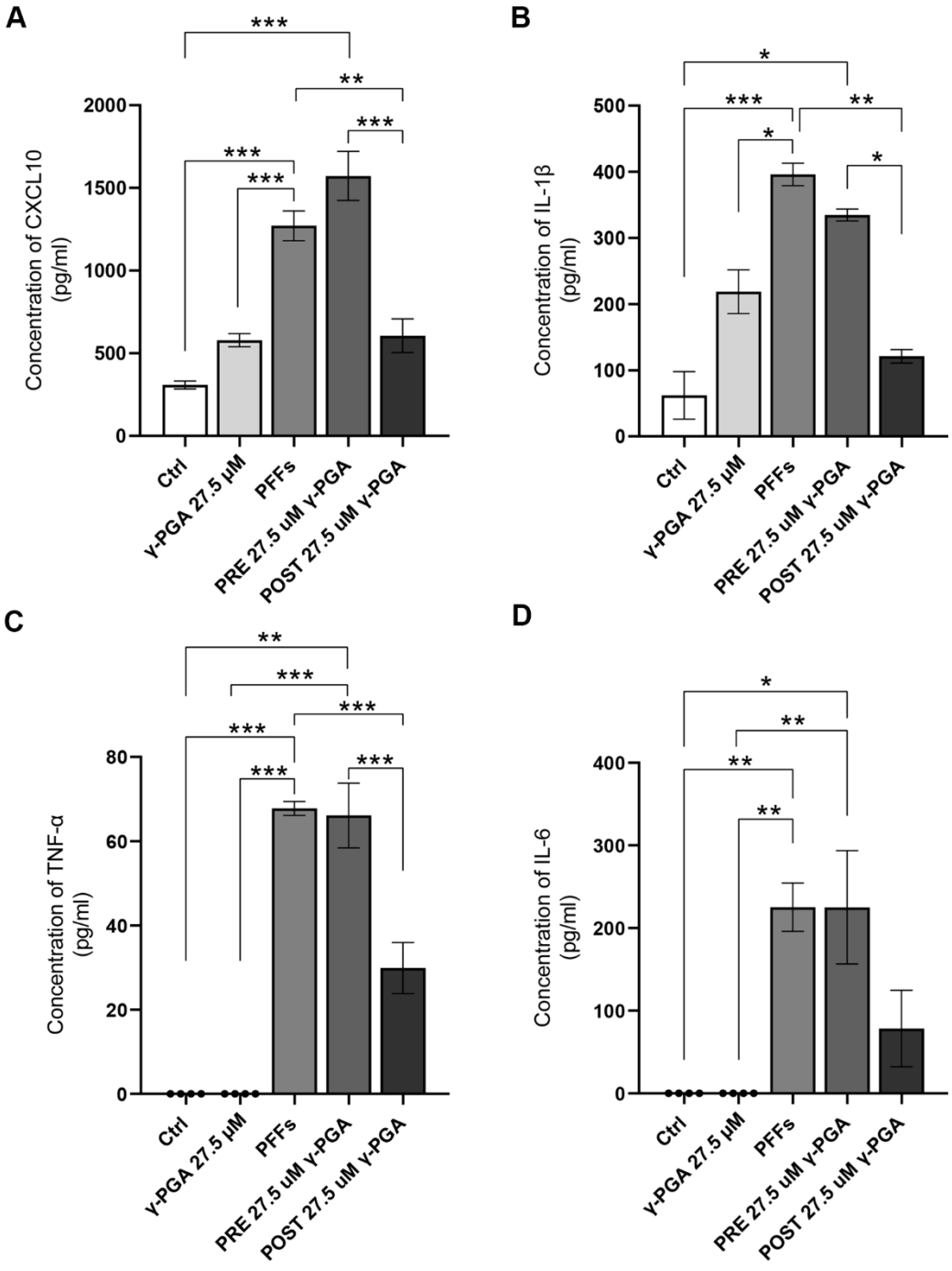

Figure 2.8 γ-PGA decreases cytokine release in primary astrocytes treated with PFFs. *Graphs **A**, **B**, **C** and **D** show ELISA quantification of CXCL10, IL-1β, TNF-α, and IL-6, respectively, released by primary astrocytes alone or in the presence of γ-PGA, PFFs or the combination of the two following PRE and POST treatment. Data are reported as mean ± SEM and analyzed by ordinary one-way ANOVA with Tukey's post hoc test (n = 4), *p < 0.05, **p < 0.01, ***p < 0.001.*

2.3 Discussion

This study explored, for the first time, the biological effect of γ-PGA in a PD model of astrocytes. γ-PGA can be synthesised naturally by *Bacillus subtilis* during the fermentation of Natto beans. These traditional soybean fermented foods are highly consumed in Japan where, interestingly, the relative PD incidence rate is reported to be significantly lower than in Europe (Kanaya et al., 2021). Given the properties of γ-PGA, we investigated its biological effect on murine primary astrocytes treated with α-synuclein PFFs as a model of PD for the study of cytotoxicity, neuroinflammation, and protein clearance. Indeed, astrocytes play a crucial role in PD pathogenesis by regulating both the clearance of extracellular aggregated α-synuclein and the modulation of neuroinflammatory responses (Colombo & Farina, 2016; Giusti et al., 2024). We chose two types of treatment by either administering γ-PGA before or after α-synuclein PFFs to explore its protective or rescue effect on murine primary astrocytes. The major finding of our study is that γ-PGA reverses the cytotoxic effects of α-synuclein PFFs, acts on the ability of astrocytes to internalize them and decreases cellular inflammation, as summarized by the proposed model in **Figure 2.9.**

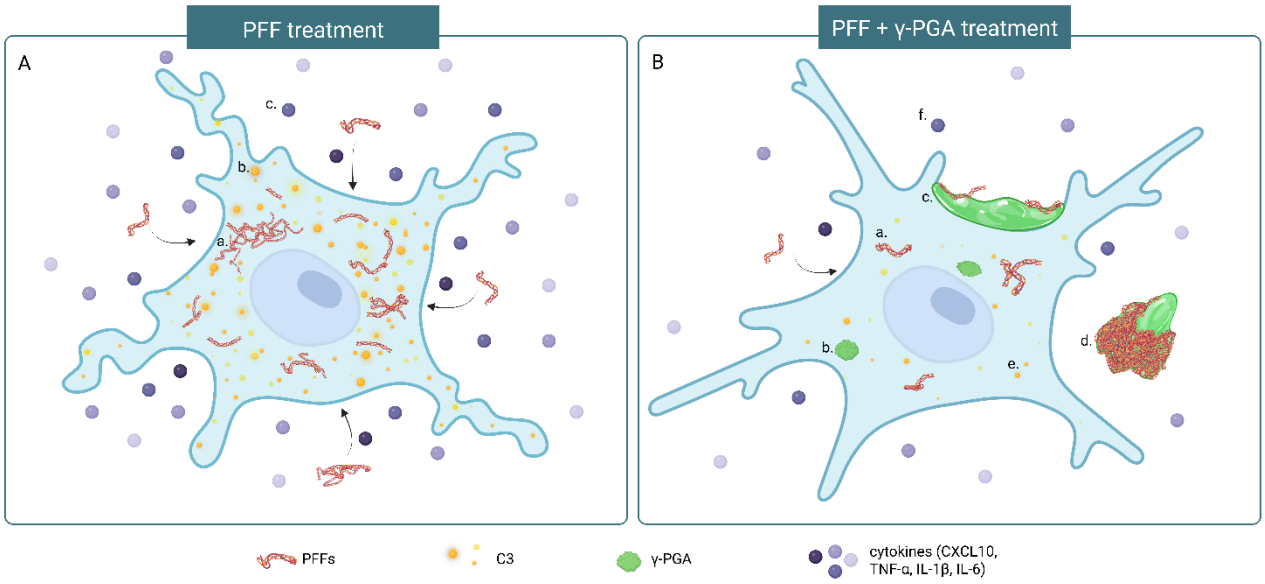

Figure 2.9. Schematic illustration of γ-PGA effect on PFF-treated primary astrocytes. *A) In primary astrocytes that are treated with PFFs, the fibrils are internalized by the cell (**a**), and an inflammatory response is observed, as shown by C3 staining (**b**), and by the release of pro-inflammatory cytokines (**c**); this results in cell toxicity. **B**) In primary astrocytes co-treated with γ-PGA, a reduction in PFF internalization is observed (**a**). γ-PGA localizes inside the cell (**b**), on its surface (**c**), and colocalizes with PFFs in the extracellular space (**d**). A decrease in C3 inflammation and pro-inflammatory cytokines release is also observed (**e**, **f**), leading to reduced cellular toxicity. Created in BioRender. Cappelletti, G. (2025) https://BioRender.com/bbanupg.*

Emerging research has demonstrated the non-toxic and excellent safety profile of γ-PGA in diverse experimental settings (Lee et al., 2020; Parati et al., 2022). Here, we tested whether γ-PGA could affect primary murine astrocyte survival and reported that, it increased cell viability in a dose-dependent manner. In the context of α-synuclein PFFs, multiple evidence suggests that aggregated α-synuclein species induce toxicity (Alam et al., 2019). However, the mechanisms are still debated. Some studies hypothesize that the interaction of aggregated α-synuclein with cellular membranes induces their disruption, activation of inflammatory pathways, autophagic and lysosomal processes, and cell death through apoptosis (Chou et al., 2021; Guiney et al., 2020). We report that α-synuclein PFFs decrease astrocyte viability and that γ-PGA, can counteract PFFs-induced toxicity, suggesting that the polymer may have cell-protective effects. Our results could be explained in two possible ways. First, cell protection could be due to the potent antioxidant properties of γ-PGA that can act as ion chelator, free radical scavenger, and inhibitor of lipid peroxidation (Lee et al., 2020). Indeed, we demonstrated, for the first time, that γ-PGA is readily internalized by astrocytes, with diffuse, punctate cytoplasmatic localization. Secondly, γ-PGA may exert a direct buffering effect on α-synuclein PFFs thereby reducing their toxicity.

In addition, we showed that the two proteins colocalize in both extracellular and intracellular environments, and that both POST and PRE treatments with γ-PGA are effective in reducing α-synuclein PFF burden. This might suggest that γ-PGA may, at least to some extent, disrupt α-synuclein aggregates or, alternatively, reduce their interaction with astrocytes, potentially affecting their internalization. Indeed, the internalization of extracellular α-synuclein aggregates by astrocytes is a key aspect in neurodegenerative processes, as astrocytes are known to be actively involved in their clearance (Filippini et al., 2019, 2021; Giusti et al., 2024). Nevertheless, the amount of α-synuclein uptake is critical for astrocyte homeostasis as excessive accumulation could overwhelm protein degradation processes leading to cellular stress (Filippini et al., 2019; Giusti et al., 2024). Several mechanisms may be involved in the entry of PFFs into the cells, such as direct membrane penetration (Dieriks et al., 2017), caveolae-mediated (Madeira et al., 2011) and clathrin-dependent endocytosis (Rodriguez et al., 2018). In addition, one study showed that PFF uptake by astrocytes could be mediated by dynamin-mediated endocytosis as dynamin facilitates the budding of endocytic vesicles from the plasma membrane (Filippini et al., 2021).

Here, we found that γ-PGA has a marked inhibitory effect on astrocytes ability to internalize α-synuclein PFFs (**Figure 2.9, B, (a)**). Interestingly, the PRE treatment reduced both the size and the intensity of internalized α-synuclein PFFs to a greater extent, compared to POST treatment. In respect to the mechanisms by which γ-PGA limits α-synuclein PFFs internalization, we propose two hypotheses. Firstly, γ-PGA could compete for cellular uptake pathways employed by α-

synuclein aggregates. This hypothesis is supported by our findings on both the presence of γ-PGA within astrocytes (**Figure 2.9, B, (b)**), and its localization between the cell and α-synuclein PFFs **Figure 2.9, B, (c)**). The second hypothesis builds upon our results on the colocalization of the two molecules, suggesting that γ-PGA may have a buffering effect and retain PFFs, preventing their internalization (**Figure 2.9, B, (d)**). Moreover, we investigated the lysosomal and autophagic pathway which is responsible for clearing cytosolic aggregated proteins such as fibrillar α-synuclein (Pantazopoulou et al., 2021). We observed that γ-PGA treatment alone led to a mild non-significant increase of p62 levels, which is not indicative of autophagic flux impairment as LC3-II/LC3-I ratio remained unchanged compared to the control. This suggest that the basal autophagic machinery is functional and that the slight increase in p62 might be attributed to biological variability or at least to a potential and transient delay of the autophagic flux resulting from the uptake and turnover of the polymer by the endolysosomal system. Conversely, we observed that treatment with PFFs impairs autophagy-lysosome pathways, as suggested by the increase of LC3-II/LC3-I ratio, the accumulation of p62, and the increase of LAMP1-labeled lysosomes, as previously demonstrated (Gao et al., 2019; Pantazopoulou et al., 2021). Interestingly, POST treatment with γ-PGA led to a mild decrease of p62 accumulation, which might suggest a partial role in modulating PFF-impaired autophagy. However, our results support the hypothesis that γ-PGA primarily exerts its effect by limiting PFF internalization in astrocytes. Despite we also observed a reduction in the overall extent of extracellular aggregates, further studies are required to better investigate the buffering capacity of γ-PGA in limiting α-synuclein spreading and its effect on neurons.

A relevant feature of astrocytes is that they are active players in neuroinflammation, and their response may be beneficial or detrimental, depending on the kind of stimuli they encounter (Colombo & Farina, 2016). Previous studies have demonstrated that extracellular α-synuclein aggregates, such as α-synuclein fibrils, induce innate immune pathway activation such as Toll-like receptor 4-mediated pathways, causing inflammatory responses in astrocytes (Rannikko et al., 2015). However, although it is still debated whether adult astrocytes express TLR4 *in vivo* (Gregersen et al., 2021; Liddelow et al., 2017; Zhang et al., 2016), it has been stated that innate Complement component 3 (C3) is one of the most distinctive and highly upregulated genes in neurotoxic and pro-inflammatory astrocytes, namely A1 astrocytes (Lawrence et al., 2023; Liddelow et al., 2017). Indeed, *in situ* hybridization and qPCR assays for C3 on *post-mortem* human brain of PD patients have revealed that $C3^+$ astrocytes abundance is significantly increased compared to controls (Liddelow et al., 2017). Therefore, we investigated the effect of γ-PGA on α-synuclein PFF-induced inflammation of astrocytes by evaluating C3 as an inflammatory

marker. Our results suggest, in accordance with what has been previously shown (Ma et al., 2021), that α-synuclein PFFs increases C3 deposition in astrocytes (**Figure 2.9, B (e)**) and that γ-PGA can both prevent and recover astrocytes inflammation. Given that C3 expression in α-synuclein PFF-treated astrocytes has been reported to induce neuronal cell death (Ma et al., 2021), a molecule capable of mitigating complement activation in astrocytes holds significant promise as a therapeutic strategy for PD. Moreover, we observed a pro-inflammatory profile in α-synuclein PFF-treated astrocytes, characterized by increased release of TNFα, IL-1β, IL-6 and CXCL10 (**Figure 2.9, A, (c)**). High levels of TNF-α, IL-1β and IL-6 can promote glial reactivity, contribute to chronic inflammation and neuronal dysfunction, while CXCL10 can lead to sustained neuroinflammation and immune cell infiltration, ultimately disrupting neural homeostasis (Fisher & Liddelow, 2024). In our study, we found that POST treatment with γ-PGA led to a mild decrease in IL-6 release, while significantly reduced TNF-α, IL-1β and CXCL10 levels (**Figure 2.9, B, (f)**). Thus, even though the PRE treatment may provide a greater reduction in α-synuclein PFF internalization, our results on the autophagic pathway and on astrocyte inflammation indicate POST treatment as the most promising therapeutic strategy. This is essential for any therapeutic strategies targeting PD, where inflammation is already ongoing and aggregate of α-synuclein already exist and need to be effectively "inactivated" or removed.

3

Chapter 3: The effect of PFFs and γ-PGA on M1 and M2 macrophage polarization

3.1 Introduction

Peripheral inflammation involvement in PD pathogenesis is now well documented (Pajares et al., 2020). In PD patients, the presence of gut inflammation and elevated inflammatory cytokines in the blood and CSF have been detected, whereas immune cell infiltration into the brain has been described in PD animal models (Earls et al., 2019; Houser & Tansey, 2017; Zimmermann & Brockmann, 2022). However, the mechanism that initiates the inflammatory response in the periphery and how immune cells are recruited in the brain parenchyma, is still controversial.

In this picture, macrophages play a pivotal role as coordinator of the immune response upon exogenous stimuli and pathological conditions. Macrophages can be polarized toward a pro-inflammatory M1 profile, promoting the activation of the adaptive immune response, and an anti-inflammatory and regulatory M2 phenotype, which modulates and promotes tissue regeneration (Helm et al., 2014). Despite an activation of M1 macrophages has been described in PD animal models (Frosch et al., 2023; Schonhoff et al., 2022) there is a lack of studies on the involvement of α-synuclein aggregate accumulation in macrophage polarization. Thereby, in the present work, we aim to address the effect of α-synuclein PFFs on M1/M2 macrophage polarization and how γ-PGA may influence this process. Particularly, γ-PGA polymer chosen for this study was the commercially available YRSPEC γ-PGA, as described in section 6.2. This work was carried out at iBiotech LTD and the University of Wolverhampton (UK) during my international PhD research

3.2 Results

3.2.1 Macrophage model establishment

To establish a macrophage cell model, THP-1 cells were treated with phorbol 12-myristate 13-acetate (PMA) as described in section 6.3.2. After PMA treatment, cells were analyzed through flow cytometry to confirm their differentiation into macrophages, which are adherent cells showing higher dimension and complexity. To investigate the effect of PMA treatment in THP1-cells, a gate strategy was applied on forward scatter (FSC) and side scatter (SSC) parameters to identify the main cell population (**Figure 3.1, A, A′**). PMA treatment induced morphological changes in THP-1 cells as evidenced by the increased FSC and SSC values, indicating an increase in cell size and granularity (Figure 3.1, A′) compared to the DMSO-treated control (**Figure 3.1, A**). To further characterize macrophage differentiation, cells were analyzed for the expression of CD68 and CD14 markers. Indeed, CD68 is a pan-macrophage marker, associated with lysosomal membranes in mature macrophages, while CD14 is GPI-linked receptor for LPS, widely used as a marker for early differentiation from monocytes to macrophages (Liu et al., 2023). As illustrated in **Figure 3.1,** the flow cytometry dot plots (**Figure 3.1, B**) and histogram overlays (**Figure 3.1, C**) show a shift in

CD68 fluorescence intensity in PMA-treated cells, which was also confirmed by a significant increase in mean fluorescence intensity (MFI) (**Figure 3.1, D**).

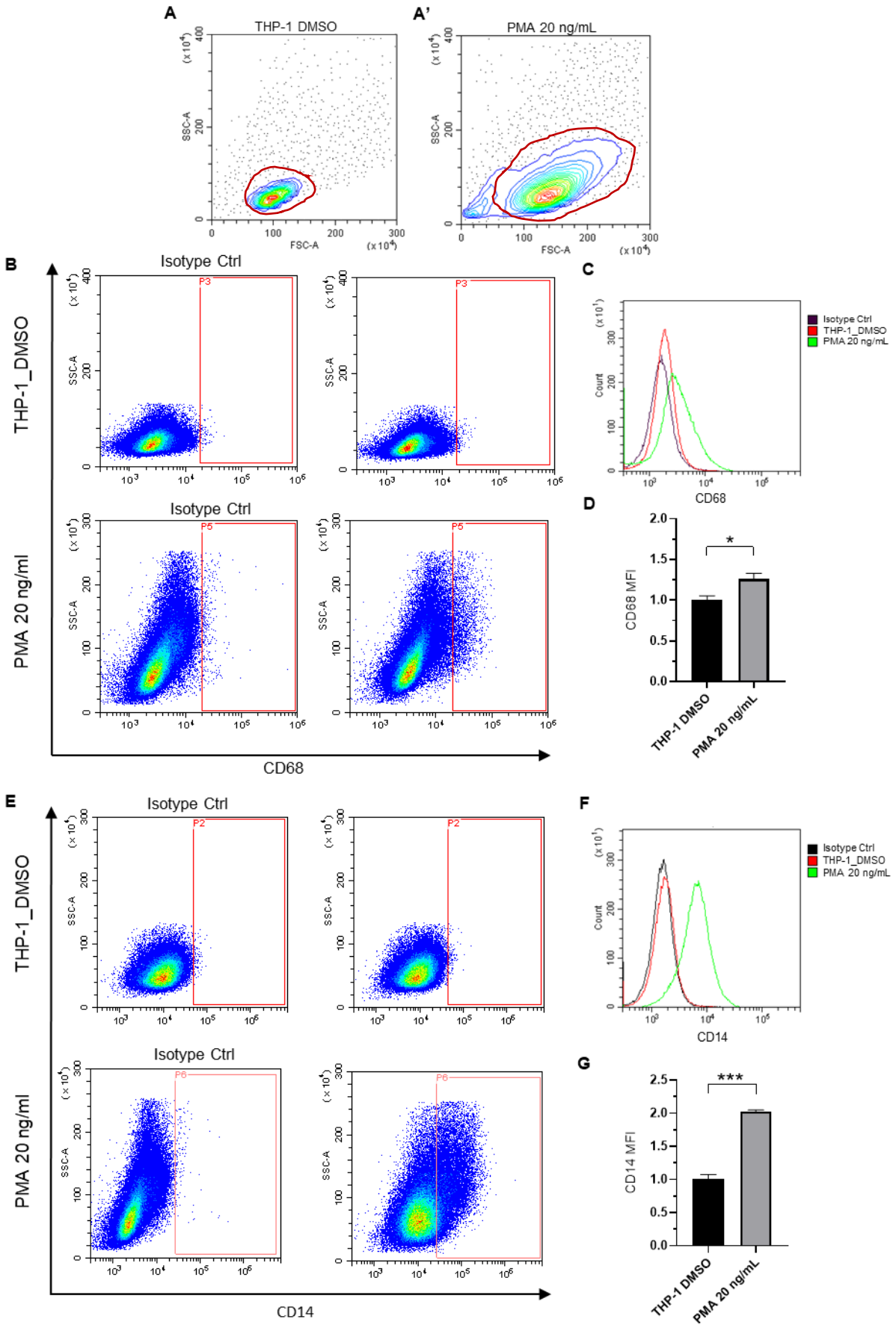

Figure 3.1. Differentiation of THP-1 cells into macrophages*. **A, A')** Density dot plot showing differences in morphology between undifferentiated (THP-1_DMSO) **(A)** and differentiated (PMA 20 ng/ml) **(A')** THP-1 cells. Cells were initially gated (red circle) using Forward scatter Area (FSCA) vs Side Scatter Area (SSC-A) and then examined for macrophage marker expression. **Panel B**: Flow cytometry dot plots showing CD68 expression. Upper panels represent THP-1_DMSO control cells stained with isotype control (left) and anti-CD68 (right). Lower panels show PMA-treated cells stained with isotype control (left) and anti-CD68 (right). Positive populations are outlined by red gates made on the Isotype control (background fluorescence). **C)** Histogram comparing CD68 mean fluorescence intensity (MFI) in isotype ctrl (black), DMSO-treated (red), and PMA-treated (green) cells. **D)** The graph shows the MFI of CD68. A statistically significant increase (*$p < 0.05$) in CD68 expression is observed in PMA-treated cells compared to DMSO-treated control. **Panel E:** Dot plots showing CD14 expression in THP-1 cells. Upper panels show DMSO-treated cells stained with isotype control (left) and anti-CD14 (right); lower panels show PMA-treated cells. **F)** Histogram comparing CD14 MFI in isotype control (black), DMSO (red), and PMA-treated cells (green). **G)** The graph shows the mean fluorescence intensity of CD14. PMA treatment results in a highly significant increase (***$p < 0.001$) in CD14 expression compared to undifferentiated cells. Data are reported as mean ± S.E.M., normalized to control and analysed by Student t-test (n=3). MFI = mean fluorescence intensity.*

Similarly, we examined CD14 expression, a well-established marker of monocyte to macrophage differentiation. Flow cytometry dot plots (**Figure 3.1, E**) and histograms (**Figure 3.1, F**) revealed a marked upregulation of CD14 following PMA treatment. Quantification of MFI showed a statistically significant increase in CD14 expression by PMA-treated cells compared to DMSO control (**Figure 3.1, G**).

Next, we examined whether PMA differentiated THP-1 cells could be considered as M_0 macrophages. To do so, we tested the expression of M1 and M2 markers of macrophages using flow cytometry. As M1 marker we employed CD86 and CD80, co-stimulatory membrane molecules involved in T cells activation and maturation (Yunna et al., 2020). As shown in **Figure 3.2**, PMA treated THP-1 cells exhibit comparable MFI levels of CD86 (**Figure 3.2, A, C, D)**, compared to THP-1 cells treated with DMSO (**Figure 3.2, A, B, D).** The same pattern was also observed with CD80 marker (**Figure 3.2, E-H**). Moreover, we used HLA-DR as marker of APC cells, which is highly express in M1 rather than in M2 macrophages. Flow cytometry analysis showed that PMA treated cells do not express higher levels of HLA-DR, in terms of MFI, compared to control (**Figure 3.3**).

Next, we employed CD163 and CD206 molecules as markers of M2 phenotype. Indeed, these are scavenger's receptor involved in the phagocytosis function of M2 macrophages. No differences were found in the MFI of PMA treated compared with DMSO treated THP-1 cells for both CD163 (**Figure 3.4, A-D**) and CD206 (**Figure 3.4, E-H**). Thus, these results confirm that THP-1 cells differentiate into M_0 macrophages under our experimental conditions.

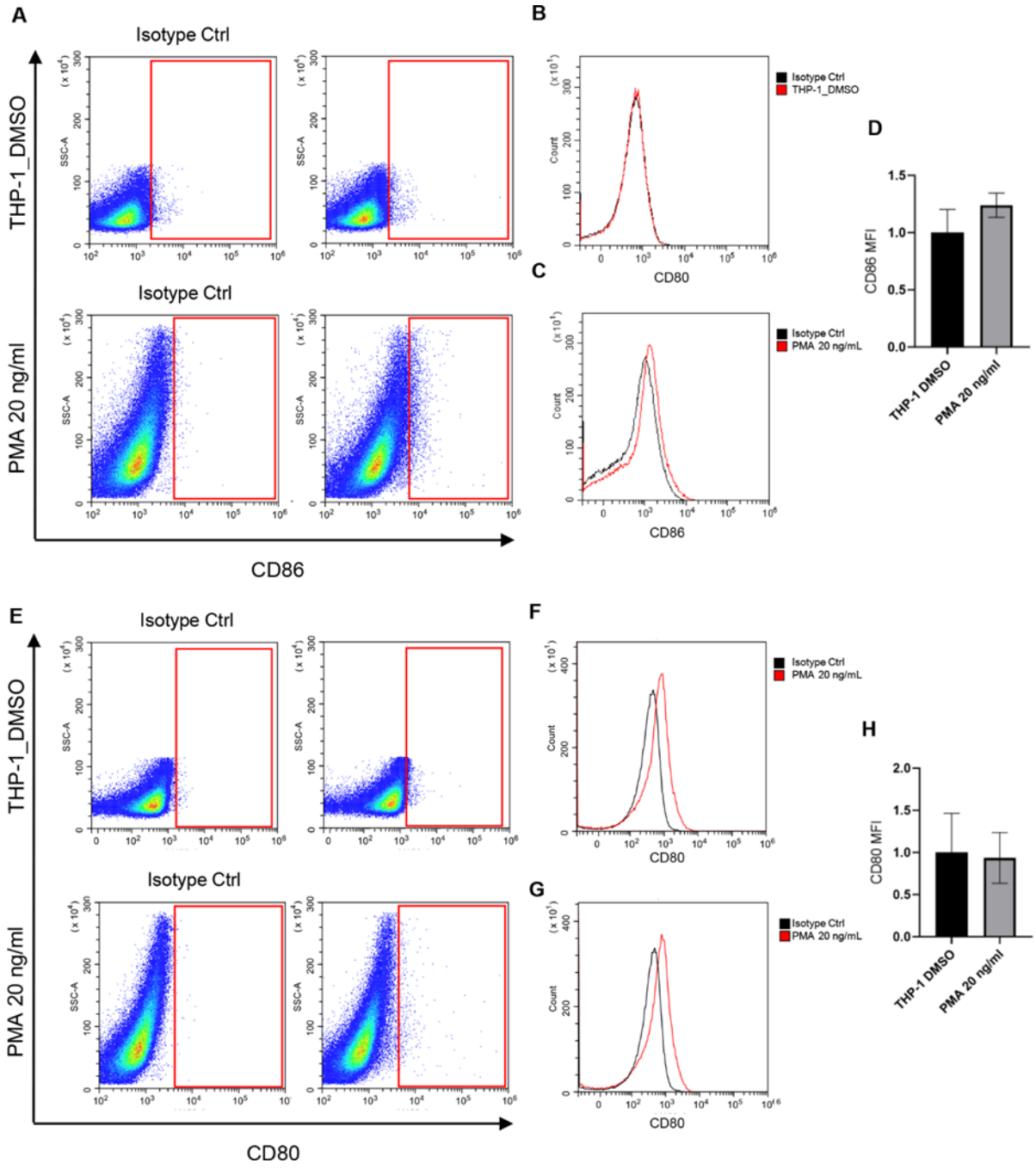

Figure 3.2. M1 marker expression in undifferentiated and differentiated THP-1 cells. *(**A**, **E**) Representative flow cytometry dot plots showing the expression of CD86 (**A**) and CD80 (**E**) in untreated (THP-1_DMSO) and PMA-treated (20 ng/mL) cells. Positive populations are outlined in red gates made on Isotype control. (**B**, **C**, **F**, **G**) Histograms showing the fluorescence intensity distribution for CD86 (**B**, **C**) and CD80 (**F**, **G**), comparing Isotype control (black) with treated cells (red). (**D**, **H**) Graphs show the mean fluorescence intensity (MFI) of CD86 (D) and C80 (H). Data are shown as mean ± SEM, normalized to control (THP-1 DMSO) and analyzsed by Student t test (n=3).*

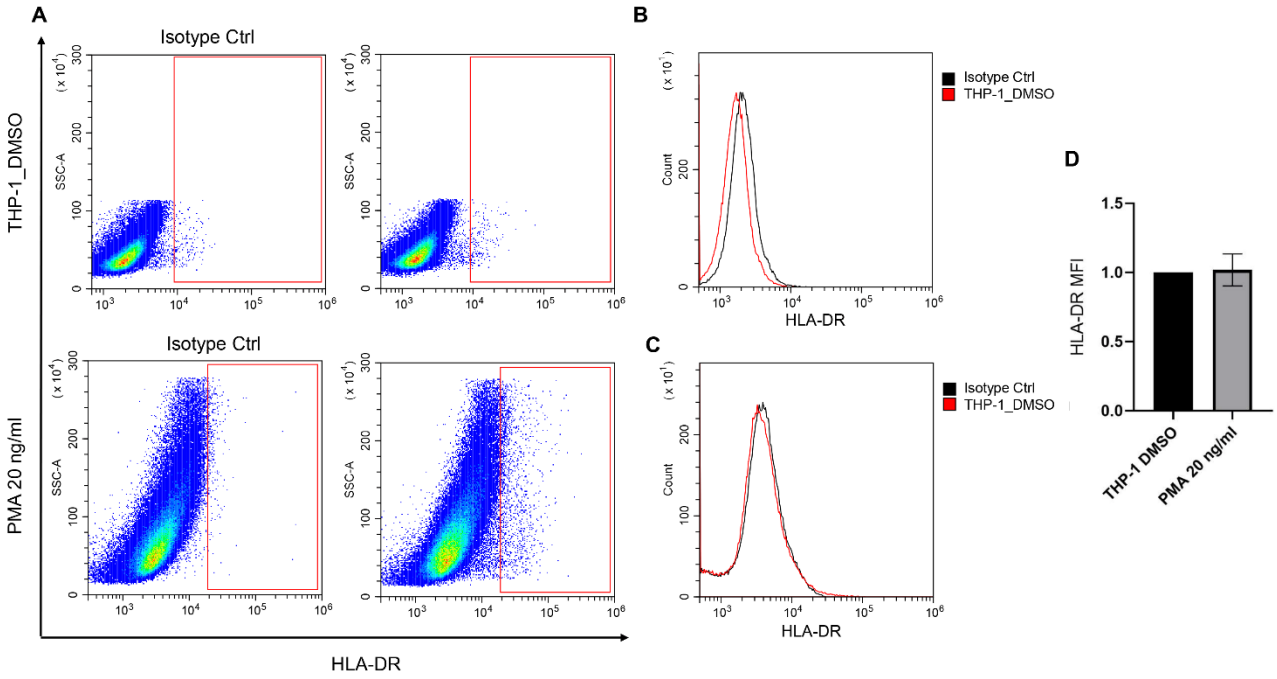

Figure 3.3 HLA-DR expression in undifferentiated and differentiated THP-1 cells. A) *Dot plots showing the expression of HLA-DR assessed by flow cytometry in untreated (THP-1_DMSO) and PMA-treated (20 ng/mL) cells. Positive populations are outlined by the red gates made on Isotype Ctrl.* ***B*** *and* ***C*** *represent histograms showing the fluorescence intensity distribution for HLA-DR in THP-1 cells and macrophages.* ***D****) The Graph shows the mean fluorescence intensity (MFI) of HLA-DR. Data are shown as mean ± SEM, normalized to control (THP-1_DMSO) and analzsed by One sample t-test (n=3).*

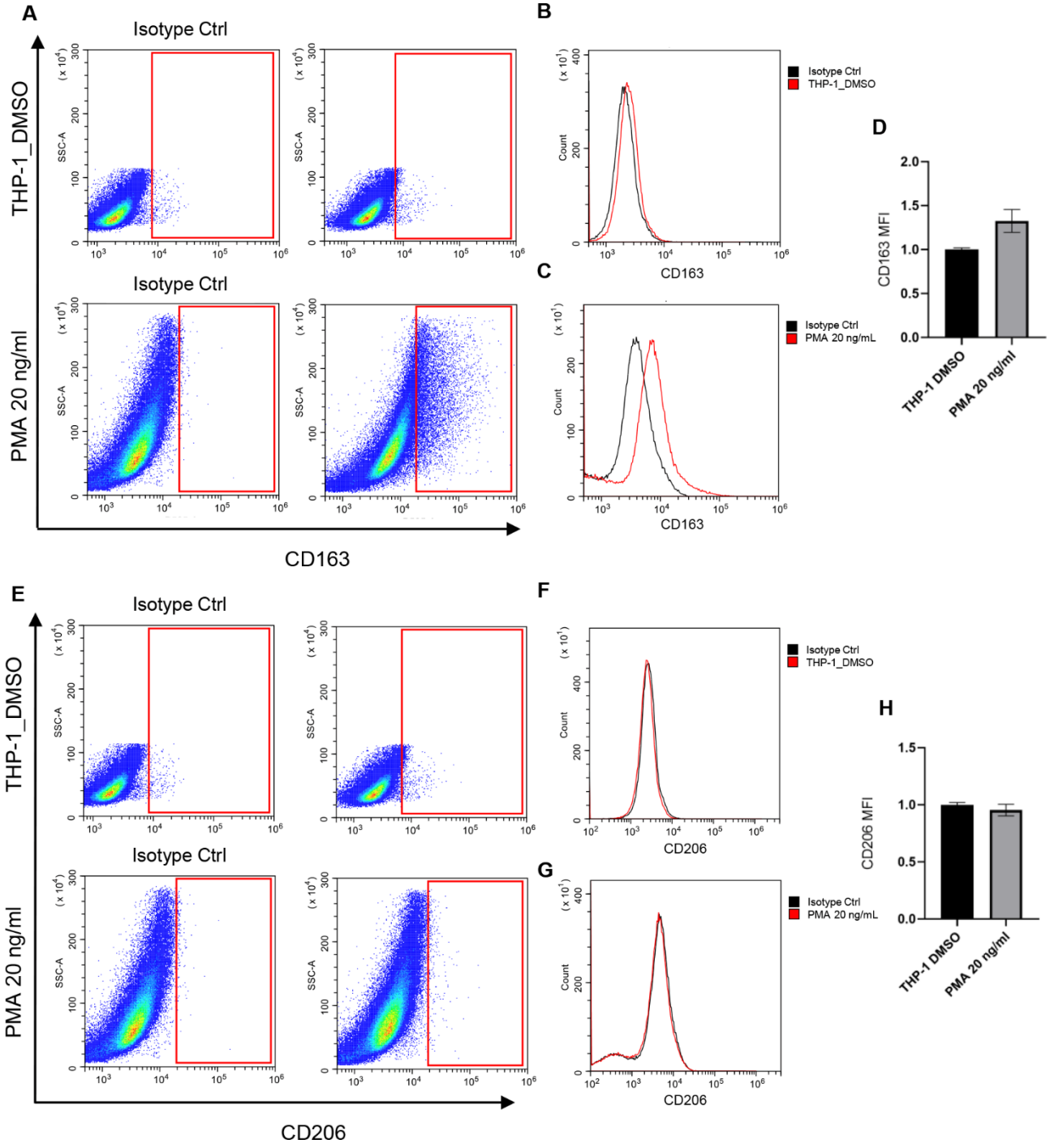

Figure 3.4. M2 marker expression in undifferentiated and differentiated THP-1 cells. *(**A, E**) Dot plots showing the expression of CD163 (**A**) and CD206 (**E**) assessed by flow cytometry in untreated (THP-1_DMSO) and PMA-treated (20 ng/mL) cells. Positive populations are outlined in red gates made on Isotype control. (**B**, **C**, **F**, **G**) Histograms showing the fluorescence intensity distribution for CD163 (**B**, **C**) and CD206 (**F**, **G**), comparing isotype control (black) with treated cells (red). (**D**, **H**) Graphs show the mean fluorescence intensity (MFI) of CD163 (D) and CD206 (H). Data are shown as mean ± SEM, normalized to control (THP-1 DMSO) and analyzed by Student t test (n=3).*

3.2.2 α-synuclein PFFs affect macrophage polarization

The direct effect of α-synuclein aggregates on macrophages has never been investigated. Thus, we employed α-synuclein PFFs and assessed their effect on cell viability. Interestingly, PFFs at all tested concentrations (0.1, 1, and 2 μM), did not induced cell toxicity upon 24 hrs of treatment (**Figure 3.5**).

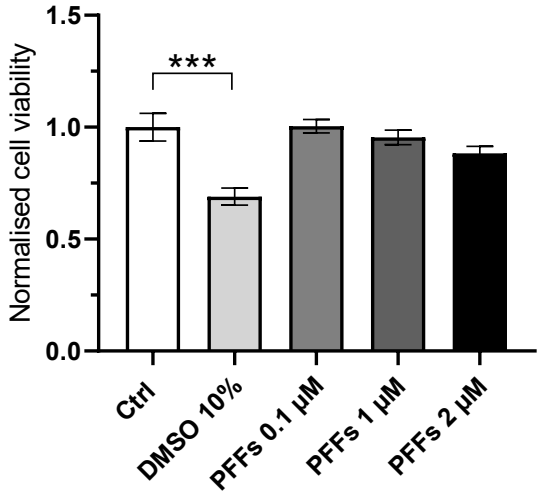

Figure 3.5. PFF effect on macrophage viability. *Cell viability of macrophages treated with increasing concentrations of PFFs. Data are expressed as mean ± SEM, normalized to control and analyzed by ordinary one-way ANOVA with Tukey's post hoc test (n = 5), ***p < 0.001. 10% DMSO was used as a positive control.*

Given this results, α-synuclein PFF involvement in macrophage polarization was evaluated at all previously tested concentrations. As shown in **Figure 3.6**, flow cytometry analysis revealed that PFF treatment significantly increased the percentage of CD86-positive cells, but not CD86 MFI, at 1 and 2 μM concentration compared with control and 0.1 μM of PFFs (**Figure 3.6, A-C**). No differences were observed between 0.1 μM PFF and control. A similar trend was also observed for CD80 marker (**Figure 3.6, D-F**), where treatment of PFF at 1 and 2 μM concentration effectively increased CD80 percentage of positive cells (**Figure 3.6, F**). Consistently with the results for CD86 and CD80 markers, a comparable effect was also observed for HLA-DR expression (**Figure 3.7**): PFF treatment at 1 and 2 μM significantly increased the percentage of HLA-DR-positive cells, but not the MFI, when compared with control and 0.1 μM of PFFs (**Figure 3,7, A, B, C**).

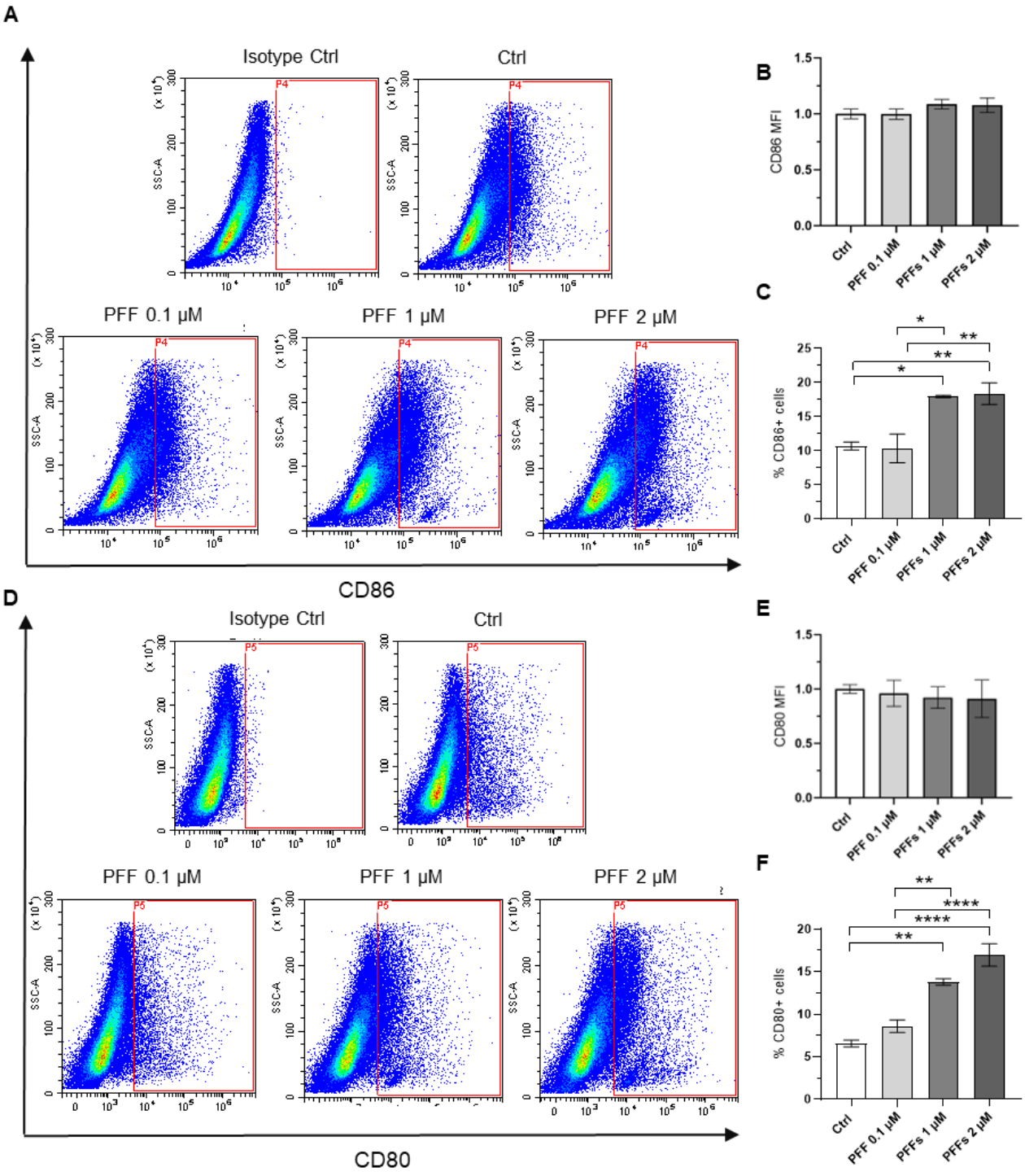

Figure 3.6. α-synuclein PFF effect on M1 marker expression in macrophages. A, D) *Representative flow cytometry dot plot showing the expression of CD86 (**A**) and CD80 (**D**) in macrophages treated with increasing concentration of PFFs (0.1 µM, 1 µM, and 2 µM) compared to control. Positive populations are outlined in red gates. **B**, **E**) Graphs show mean fluorescence intensity (MFI) for CD86 and CD80, respectively. **C**, **F**) Graphs show the percentage of positive cells for CD86 and CD80, respectively. Data are shown as mean ± SEM, normalized to control and analyzsed by Ordinary one-way ANOVA with Tukey's post hoc test (n=3). *p < 0.05, **p < 0.01, ***p < 0.001, ****p < 0.0001.*

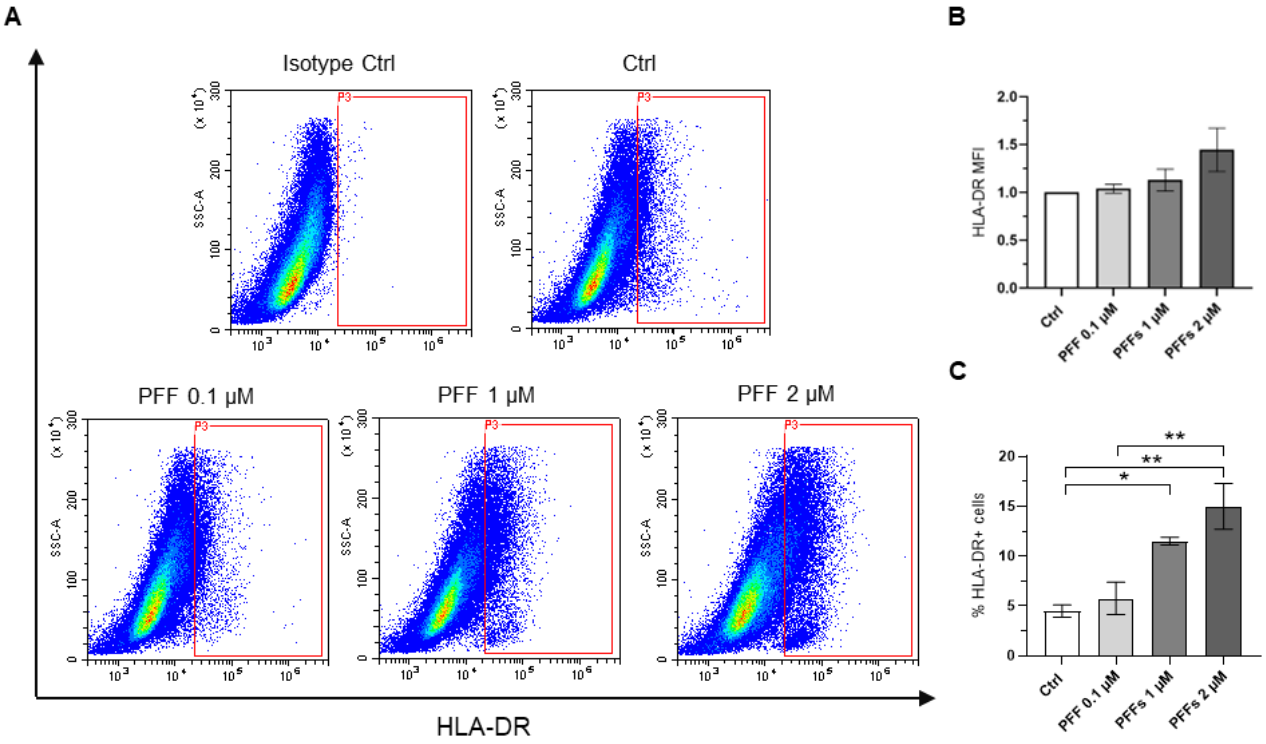

Figure 3.7. α-synuclein PFF effect on HLA-DR expression in macrophages. *A) Representative flow cytometry dot plot showing the expression of HLA-DR in macrophages treated with increasing concentration of PFFs (0.1 µM, 1 µM, and 2 µM) compared to control. Positive populations are outlined in red gates. B) Quantification of HLA-DR mean fluorescence intensity (MFI). Data are shown as mean ± SEM, normalized to control and analysed by One sample t-test (n=3).* ***C****) Quantification of percentage of HLA-DR positive cells. Data are shown as mean ± SEM, normalized to control and analzsed by Ordinary one-way ANOVA with Tukey's post hoc test (n=3). *p < 0.05, **p < 0.01.*

Regarding the effect on α-synuclein on macrophage M2 phenotype, we investigated CD163 and CD206 expression (**Figure 3.8**). No differences were observed in either CD163 MFI or percentage of positive cells at any of the tested PFF concentration compared with control (**Figure 3.8, A-C**). For CD206 marker, PFF treatment at 2 µM induced a significant increase in the percentage of CD206-positive cells, whereas no changes were observed in MFI values or at lower concentrations (**Figure 3.8, D-F**).

These results support a role for α-synuclein PFFs in the polarization of macrophages. This effect seems to be concentration-dependent, as treatment with PFF at 1 µM predominantly shape macrophage polarization towards M1 phenotype, whereas treatment with PFF at 2 µM induced a mixed M1/M2 phenotype of macrophages. Nevertheless, α-synuclein PFFs primarily promote M1 polarization, as indicated by the lack of CD163 upregulation, despite the increase in CD206 expression.

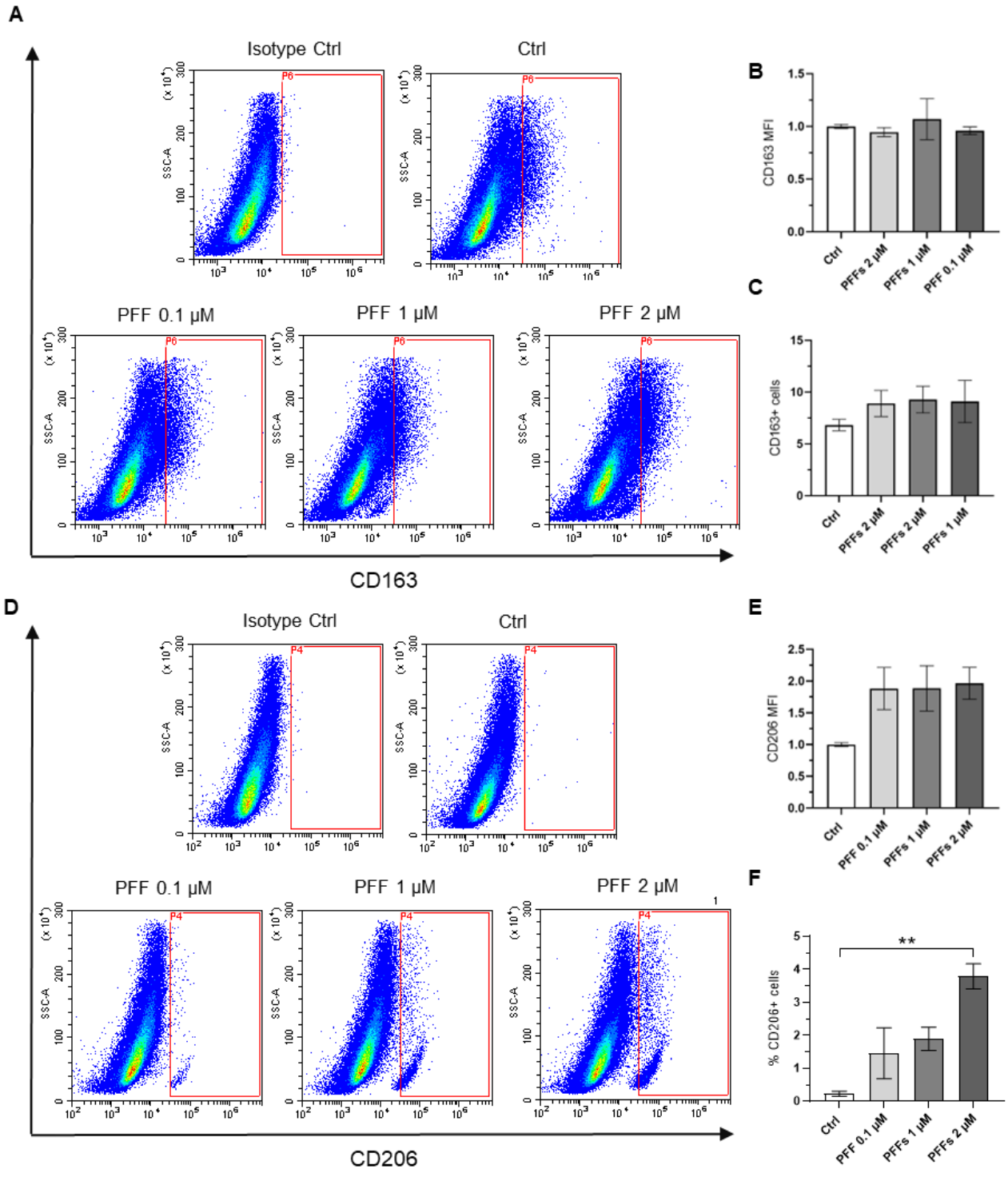

Figure 3.8. α-synuclein PFF effect on M2 marker expression in macrophages. A, D) *Representative flow cytometry dot plot showing the expression of CD163 (**A**) and CD206 (**D**) in macrophages treated with increasing concentration of PFFs (0.1 µM, 1 µM, and 2 µM) compared to control. Positive populations are outlined in red gates. **B**, **E**) Graphs show mean fluorescence intensity (MFI) for CD163 and CD206, respectively. **C**, **F**) Graphs show the percentage of positive cells for CD163 and CD206, respectively. Data are shown as mean ± SEM, normalized to control and analyzsed by Ordinary one-way ANOVA with Tukey's post hoc test (n=3). **p < 0.01.*

3.2.3 γ-PGA modulates macrophage polarization induced by α-synuclein PFFs

In this study, YRSPEC γ-PGA was employed to assess its potential role in modulating macrophage polarization induced by α-synuclein PFFs. First, YRSPEC γ-PGA of initial 440 kDa was hydrolysed to reduce the MW, as described in section 6.2.2, and polymers of 100 kDa and 280 kDa were selected. Then, γ-PGA cytotoxicity was evaluated by MTT test, and we observed that none of the tested concentrations resulted in cellular toxicity (**Figure 3.9**). The highest concentration chosen for the 280 kDa γ-PGA polymer was 20 µM as higher concentration were not suitable with this cytotoxicity test. Moreover, 20 µM treatment resulted in a mild increase in macrophage viability (**Figure 3.9, B).**

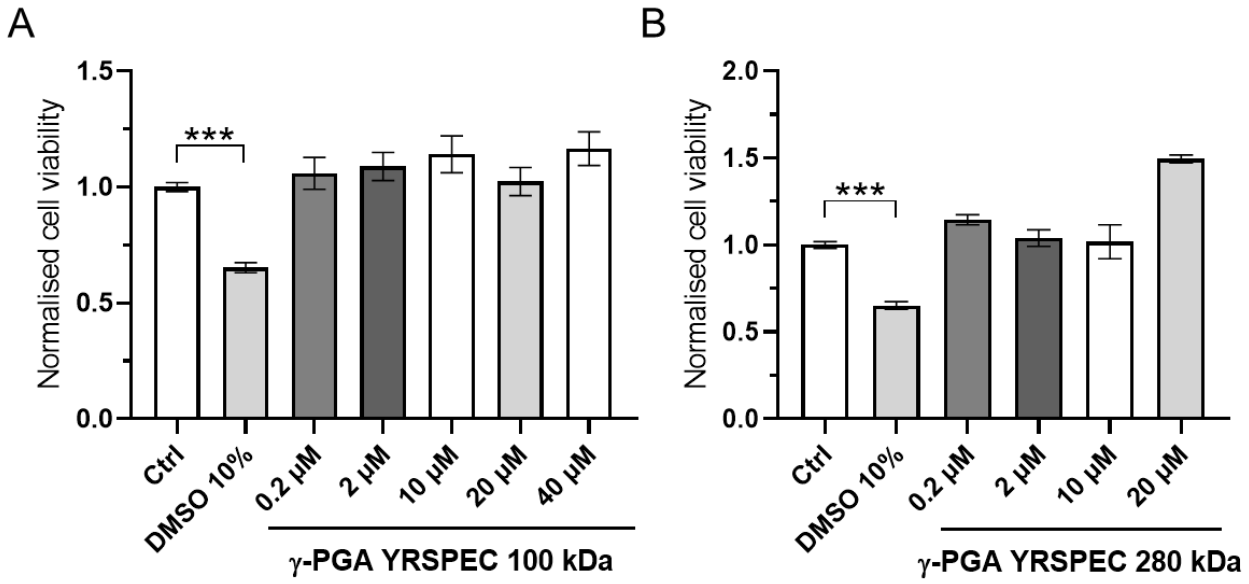

Figure 3.9. γ-PGA effect on macrophage viability. A) *Cell viability of macrophages treated with increasing concentrations of 100 kDa YRSPEC γ-PGA (0.2, 2, 20, and 40 µM). Data are expressed as mean ± SEM, normalized to control and analyzed by ordinary one-way ANOVA with Tukey's post hoc test (n = 3).* ***B)*** *Cell viability of macrophages treated with increasing concentrations of 280 kDa YRSPEC γ-PGA (0.2, 2, and 20 µM). Data are expressed as mean ± SEM, normalized to control and analyzed by Kruskal-Wallis test with Dunn's (n = 3), 10% DMSO was used as a positive control. ***p < 0.001.*

Given these results, we decided to use 20 and 40 µM of γ-PGA at 100 kDa and 20 µM of γ-PGA at 280 kDa for co-treatment with PFFs at 2 µM, following PRE and POST treatment, as described in section 6.3.4.

Treatments with 100 kDa γ-PGA polymer

For the analyses of 100 kDa γ-PGA, we tested 20 µM and 40 µM concentrations following PRE and POST treatment with α-synuclein PFFs to explore their immunomodulatory effect on

surface marker expression of M1 and M2 macrophages. Both MFI and percentage of positive cells were evaluated with flow cytometry for CD86, CD80, HLA-DR and CD206. All the corresponding scatter plots for the data presented in the following figures are provided in Appendix I (Figure I.1-Figure I.4).

No significant differences were observed between the 20 µM γ-PGA treatment alone and the control group for any of the surface markers analyzed (**Figure 3.10**), while α-synuclein PFF stimulation alone significantly increased the expression of M1 markers CD86, CD80, and HLA-DR and M2 marker CD206, both in terms of MFI (**Figure 3.10, A–D**) and percentage of positive cells (**Figure 3.10, A'–D'**), compared with control.

PRE treatment with 20 µM γ-PGA did not showed any differences in terms of MFI for all markers (**Figure 3.10, A–D)**. However, it resulted in a mild decrease, although not statistically significant, in the percentage of $CD86^+$, $CD80^+$, and $HLA\text{-}DR^+$ cells compared with PFF treatment (**Figure 3.10, A'–C').** However, the levels remained significantly higher than control.

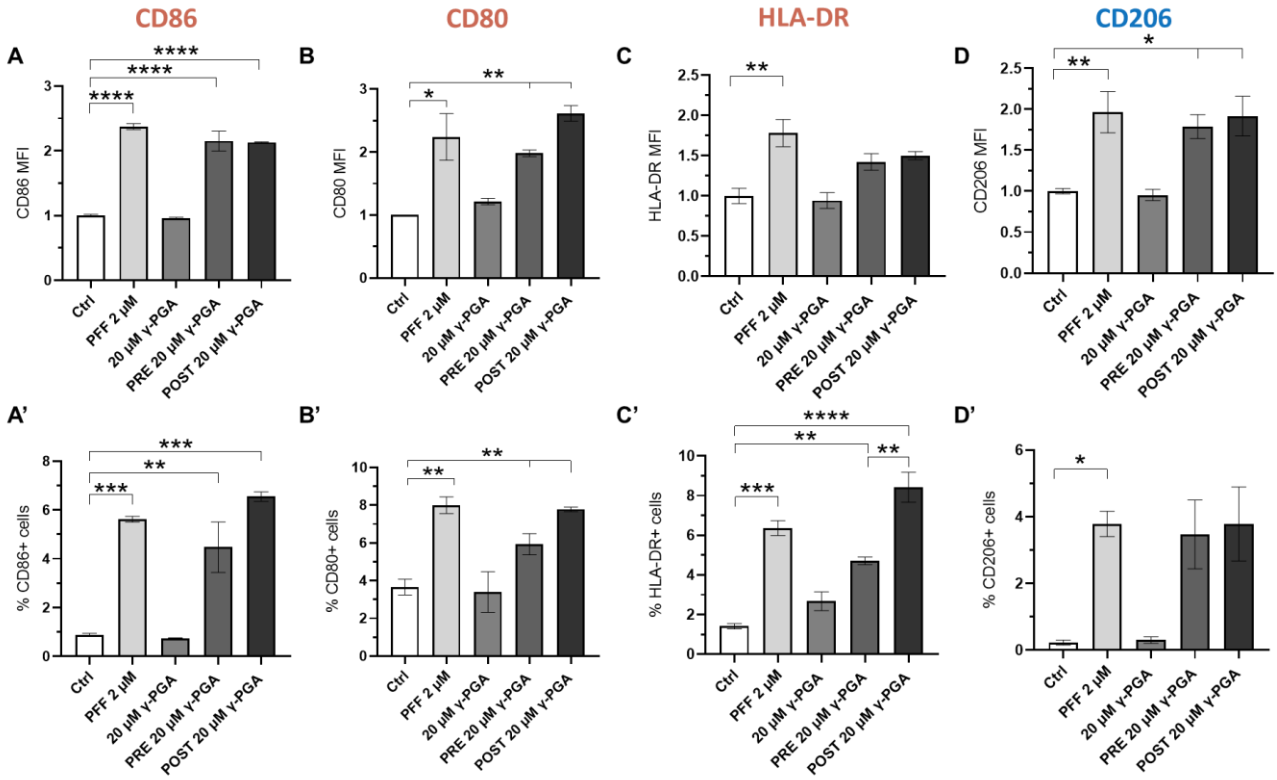

Figure 3.10. 100 kDa γ-PGA (20 µM) effect on M1 and M2 markers in PFF-treated macrophages. *Flow cytometry analyses of surface marker expression in macrophages treated with α-synuclein PFFs, in co-treatment with 100 kDa γ-PGA at 20 µM. The graphs represent the MFI (**A-D**) and percentage of positive cells (**A'-D'**) for CD86, CD80, HLA-DR and CD206. Dare are expressed as mean ± SEM, normalized to control and analyzed either by ordinary one-way ANOVA with Tukey's post hoc test (n = 3) (**A**, **A'**, **B'**, **C**, **C'**, **D**, **D'**) or One sample t test (n = 3) (**B**) *p < 0.05, **p < 0.01, ***p < 0.001, ****p < 0.0001.*

POST-treatment with 20 µM γ-PGA did not produce any significant changes in the expression of CD86, CD80, and CD206, when compared to PFF treatment alone. This was consistent for both MFI (**Figure 3.10, A, B, D**) and percentage of positive cells (**Figure 3.10, A', B', D'**).

Regarding HLA-DR, POST treatment with 20 µM γ-PGA led to a mild increase in the percentage of HLA-DR$^+$ cells compared with PFF treatment, and a significant increase compared with PRE-treatment, while no changes were observed in the MFI (**Figure 3.10, C, C'**). Thus, a more focused analysis was conducted for identifying and gating the population of cells activated by α-synuclein PFFs (R1) based on HLA-DR expression (**Figure 3.11, B–D**). This allows the evaluation of HLA-DR expression specifically within this activated subpopulation. Within this R1 gate, no significant changes were observed in either MFI (**Figure 3.11, E**) or the percentage of HLA-DR$^+$ cells (**Figure 3.11, F**) following γ-PGA POST treatment compared to PFFs alone. However, a mild decrease in HLA-DR$^+$ cells was observed with PGA PRE treatment (**Figure 3.11, F**).

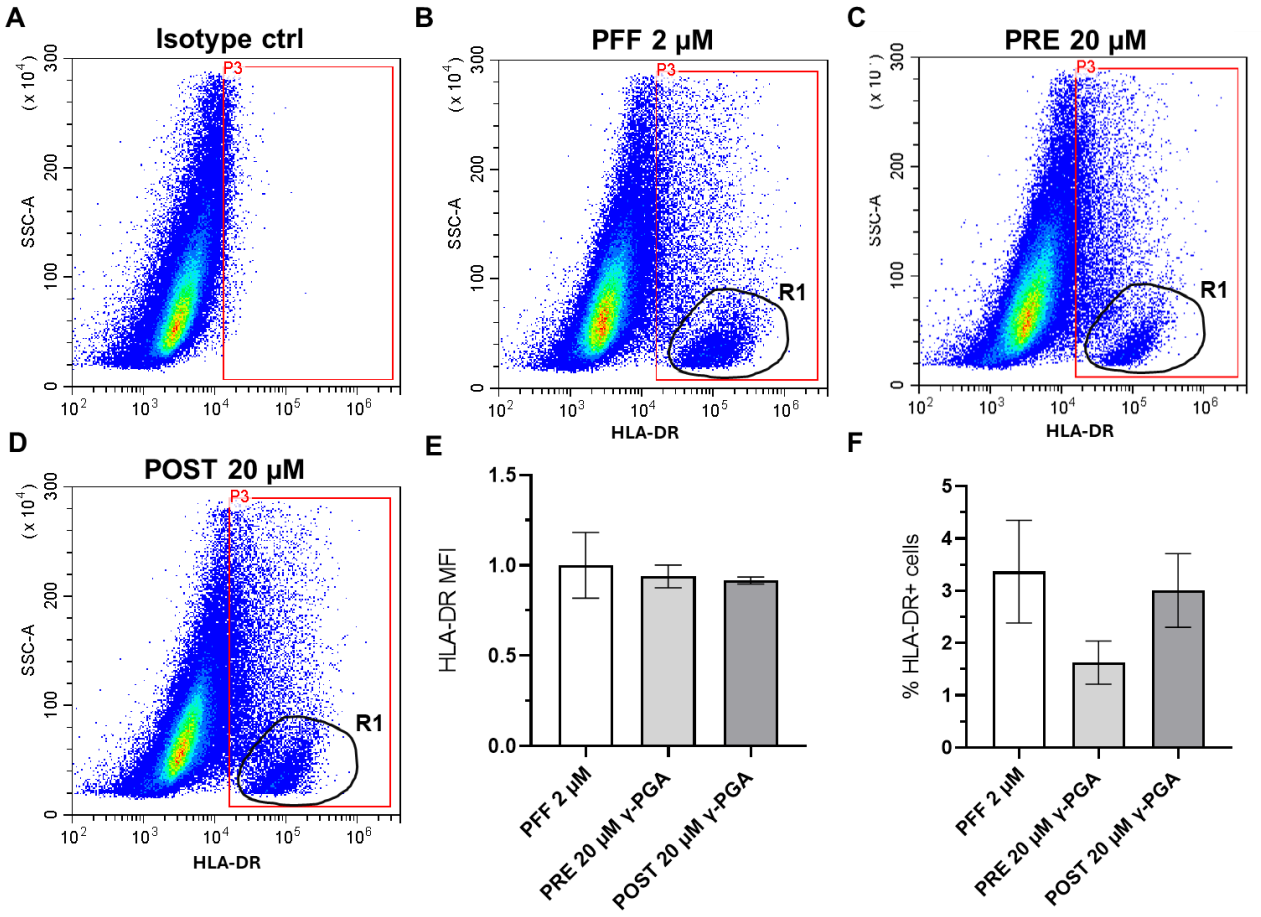

Figure 3.11. 100 kDa γ-PGA (20 µM) effect on HLA-DR marker in PFF-activated macrophages (R1 region). *Representative flow cytometry dot plot showing HLA-DR expression in macrophages treated with PFFs alone and in co-treatment with 100 kDa γ-PGA at 20 µM. Red gates (based on Isotype control) indicate HLA-DR$^+$ cells, and R1 represent the positive population activated by PFF treatment. Graphs show the mean ± SEM of HLA-DR MFI (**E**) and percentage of positive cells (**F**) in R1, normalized to PFF treatment. Statistical analysis was performed using Ordinary one-way ANOVA with Tukey's post hoc test (n=3).*

Overall, these data indicate that treatment with 100 kDa γ-PGA at 20 µM was not sufficient to reverse or attenuate the phenotype induced by α-synuclein PFFs.

100 kDa γ-PGA at 40 µM was also tested. Flow cytometry analysis of CD86 revealed that PRE treatment with γ-PGA statistically reduced the percentage of positive cells but not to levels observed with control group (**Figure 3.12, A'**). No differences were observed with POST treatment (**Figure 3.12, A, A'**).

Regarding CD80, no differences were found in either MFI or percentage of positive cells with PRE and POST γ-PGA treatment (**Figure 3.12, B, B'**). However, analysing the population of cells activated by α-synuclein PFFs in R1 (**Figure 3.13, A-D**), a significant reduction in the $CD80^+$ cells was observed with γ-PGA PRE treatment compared with PFF administration alone, while POST treatment only led to a mild decrease (**Figure 3.13, F)**. No differences were observed in CD80 MFI in all treated group (**Figure 3.13, E).**

As for HLA-DR expression, PRE treatment with γ-PGA resulted in a decreased MFI compared with PFF administration (**Figure 3.12, C**). In terms of the percentage of $HLA\text{-}DR^+$ cells,

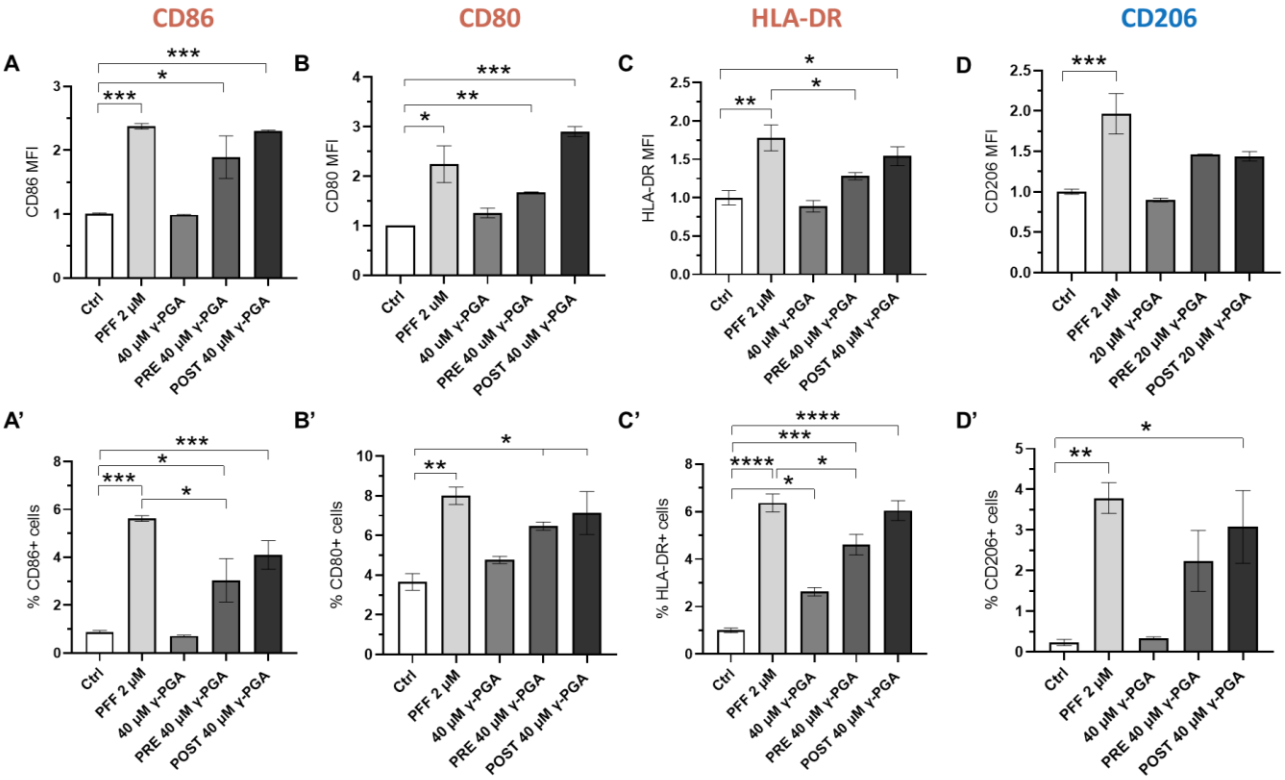

Figure 3.12. 100 kDa γ-PGA (40 µM) effect on M1 and M2 markers in PFF-treated macrophages. *Flow cytometry analyses of surface marker expression in macrophages treated with α-synuclein PFFs and in co-treatment with 100 kDa γ-PGA at 40 µM. The graphs represent the MFI (**A-D**) and percentage of positive cells (**A'-D'**) for CD86, CD80, HLA-DR, and CD206. Dare are expressed as mean ± SEM, normalized to control and analyzed either by ordinary one-way ANOVA with Tukey's post hoc test (n = 3) (**A**, **A'**, **B'**, **C**, **C'**, **D**, **D'**) or One sample t test (n = 3) (**B**) *p < 0.05, **p < 0.01, ***p < 0.001, ****p < 0.0001.*

γ-PGA alone induced an increased compared with control, while PRE treatment reduced the PFF-induced upregulation, but not to control levels (**Figure 3.12 C'**).

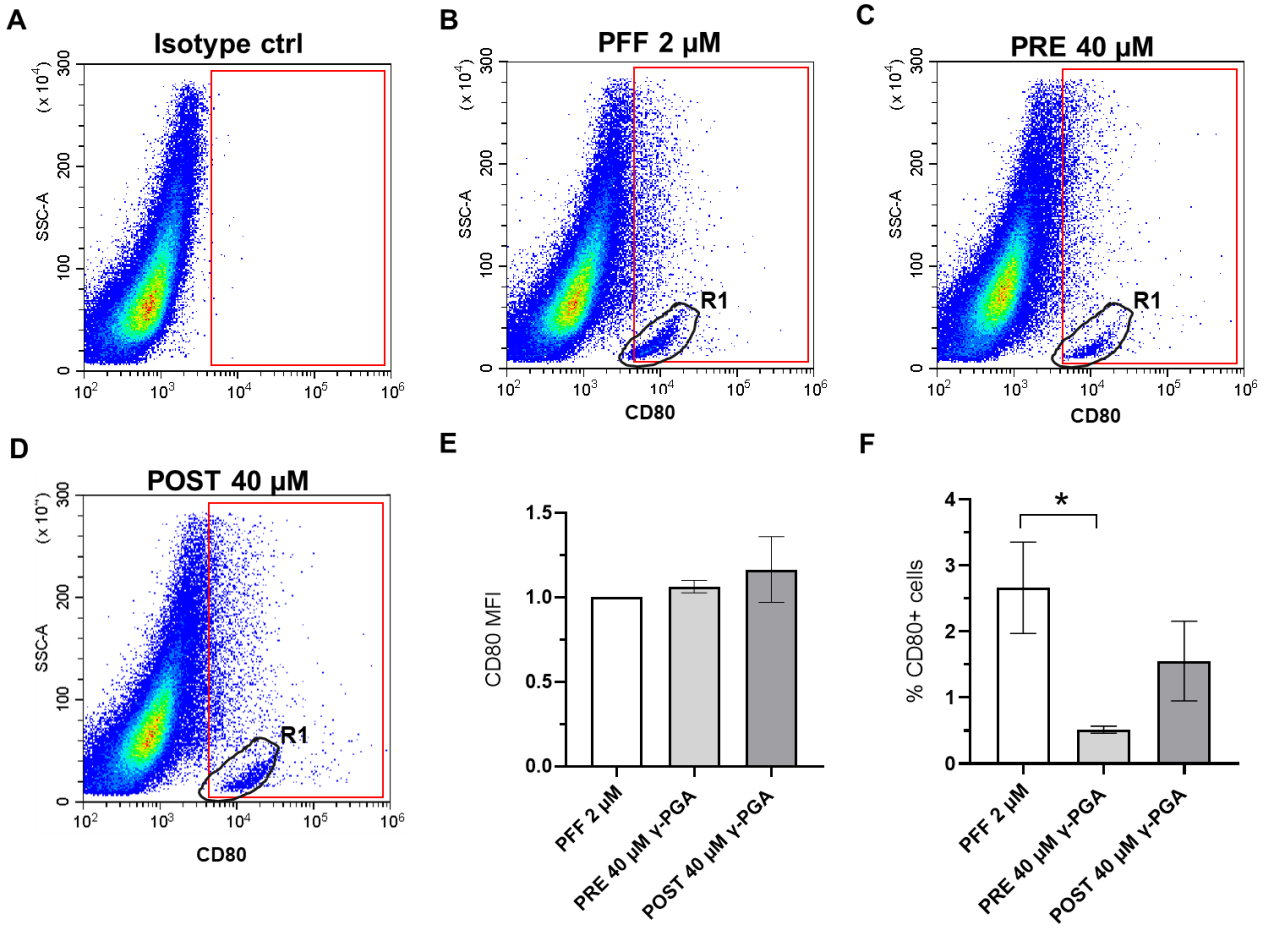

Figure 3.13. 100 kDa γ-PGA (40 µM) effect on CD80 marker in PFF-activated macrophages (R1 region). *Representative flow cytometry dot plot showing CD80 expression in macrophages treated with PFFs alone and in co-treatment with 100 kDa γ-PGA at 40 µM. Red gates (based on Isotype control) indicate CD80⁺ cells, and R1 represent the positive population activated by PFF treatment. Graphs show the mean ± SEM of CD80 MFI (**E**) and percentage of positive cells (**F**) in R1, normalized to PFF treatment. Statistical analysis was performed using One sample t test (E) and Ordinary one-way ANOVA with Tukey's post hoc test (F) (n=3), *p < 0.05.*

Similarly, PRE and POST treatment with γ-PGA had no effect on CD206 expression compared with PFF, as no differences were observed in either MFI or percentage of positive cells (**Figure 3.12, D, D'**). However, the analyses within R1 gate (**Figure 3.14, A-D**), showed a significant reduction in CD206⁺ cells with γ-PGA PRE treatment compared with PFF treatment alone (**Figure 3.14, F**). No differences were observed with POST treatment (**Figure 3.14, E).**

These results suggest that 100 kDa γ-PGA at 40 µM effectively modulates PFF-induced polarization of macrophages.

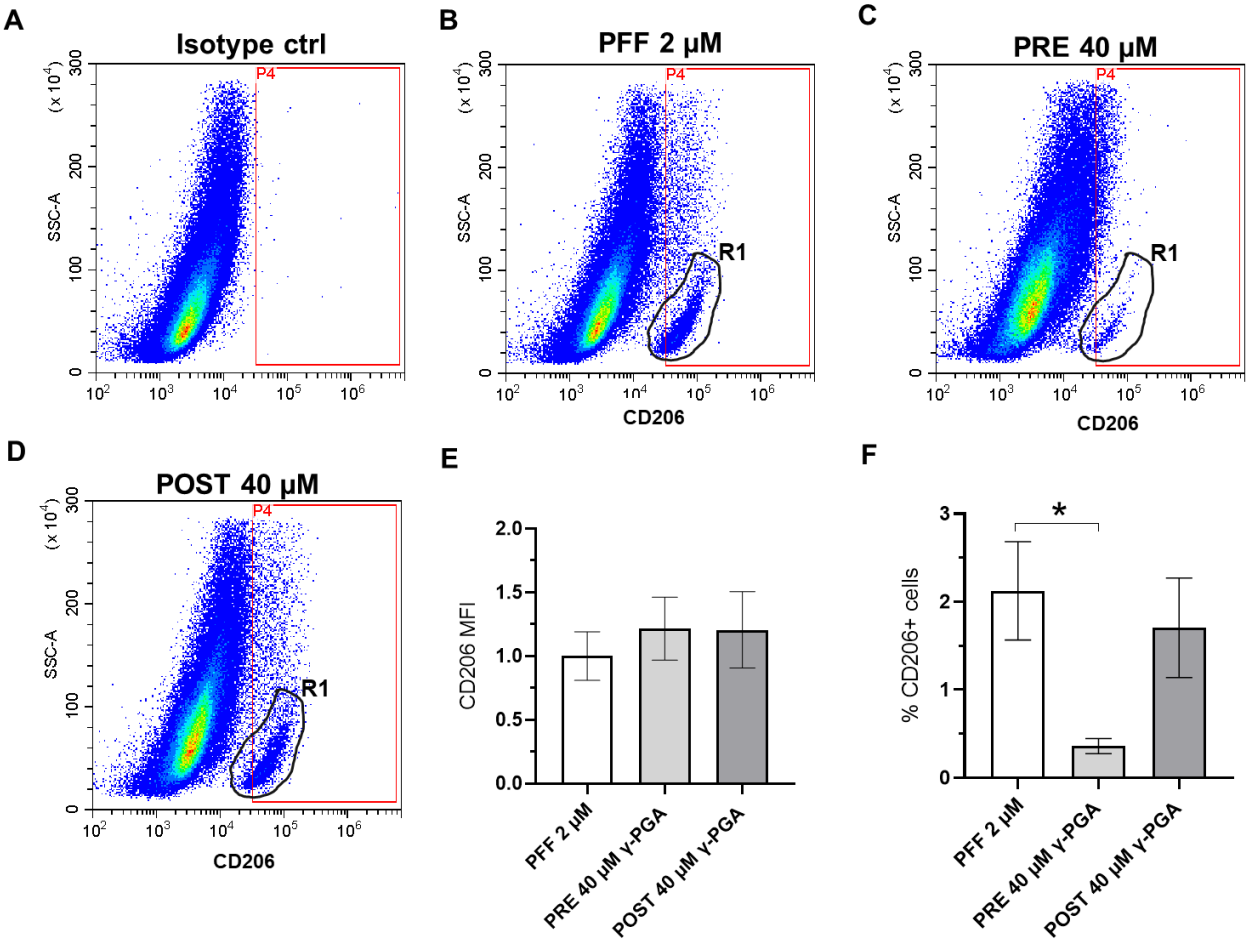

Figure 3.14. 100 kDa γ-PGA (40 µM) effect on CD206 marker in PFF-activated macrophages (R1 region). *Representative flow cytometry dot plot showing CD206 expression in macrophages treated with PFFs alone and in co-treatment with 40 µM 100 kDa γ-PGA. Red gates (based on Isotype control) indicate CD206$^+$ cells, and R1 represent the positive population activated by PFF treatment. Graphs show the mean ± SEM of CD206 MFI (**E**) and percentage of positive cells (**F**) in R1, normalized to PFF treatment. Statistical analysis was performed using Ordinary one-way ANOVA with Tukey's post hoc test (n=3), *p < 0.05.*

Treatments with 280 kDa γ-PGA polymer

γ-PGA of 280 kDa was also tested for its ability to exert a modulatory effect on PFF-induced macrophage polarization. In this case, a concentration of 20 µM was selected based on previously obtained cytotoxic data (**Figure 3.9**).

Flow cytometry analysis of CD86 marker showed that both PRE and POST treatment with γ-PGA of 280 kDa significantly reduced the MFI compared to PFF treatment alone (**Figure 3.15, A**) but were not effective on the percentage of positive cells (**Figure 3.15, A'**). This might suggest that the polymer does not affect the number of cells expressing CD86 but rather modulates the level of

CD86 expression per cell. However, the treatment was not effective in reversing the phenotype back to control levels.

No differences were observed on either CD80 MFI or percentage of positive cells before or after γ-PGA administration (**Figure 3.15, B, B'**).

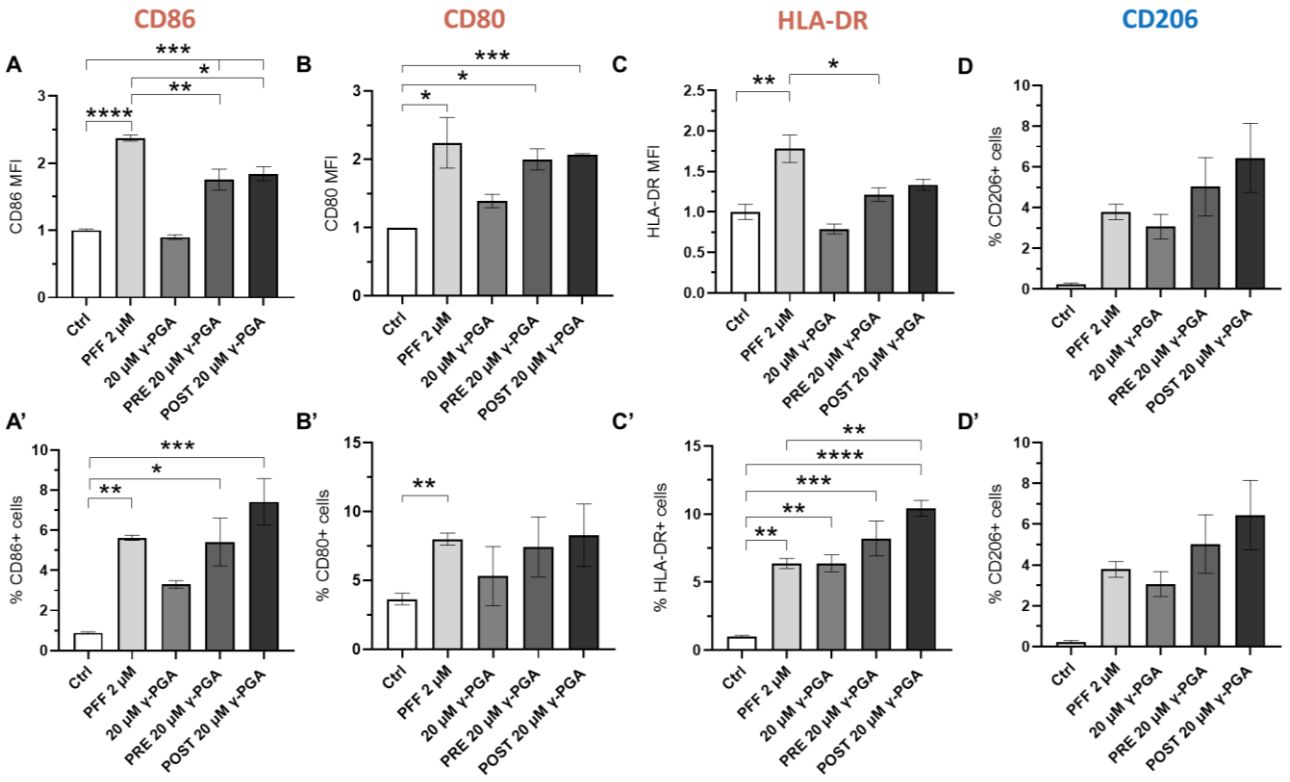

Figure 3.15. 280 kDa γ-PGA effect on M1 and M2 markers in PFF-treated macrophages. *Flow cytometry analyses of surface marker expression in macrophages treated with α-synuclein PFFs alone and in co-treatment with 280 kDa γ-PGA at 20 µM. The graphs represent the MFI (**A-D**) and percentage of positive cells (**A'-D'**) for CD86, CD80, HLA-DR, and CD206. Dare expressed as mean ± SEM, normalized to control and analyzed either by ordinary one-way ANOVA with Tukey's post hoc test (n = 3) (**A**, **A'**, **B'**, **C**, **C'**, **D**, **D'**) or One sample t test (n = 3) (**B**) *p < 0.05, **p < 0.01, ***p < 0.001, ****p < 0.0001.*

By focusing the analyses on the population of cells specifically activated by α-synuclein PFFs in R1 (**Figure 3.16, A-D**), a significant decrease in the percentage of $CD80^{+}$ cells and a significant increase in the MFI were observed with γ-PGA PRE treatment compared with PFFs (**Figure 3.16, E, F**).

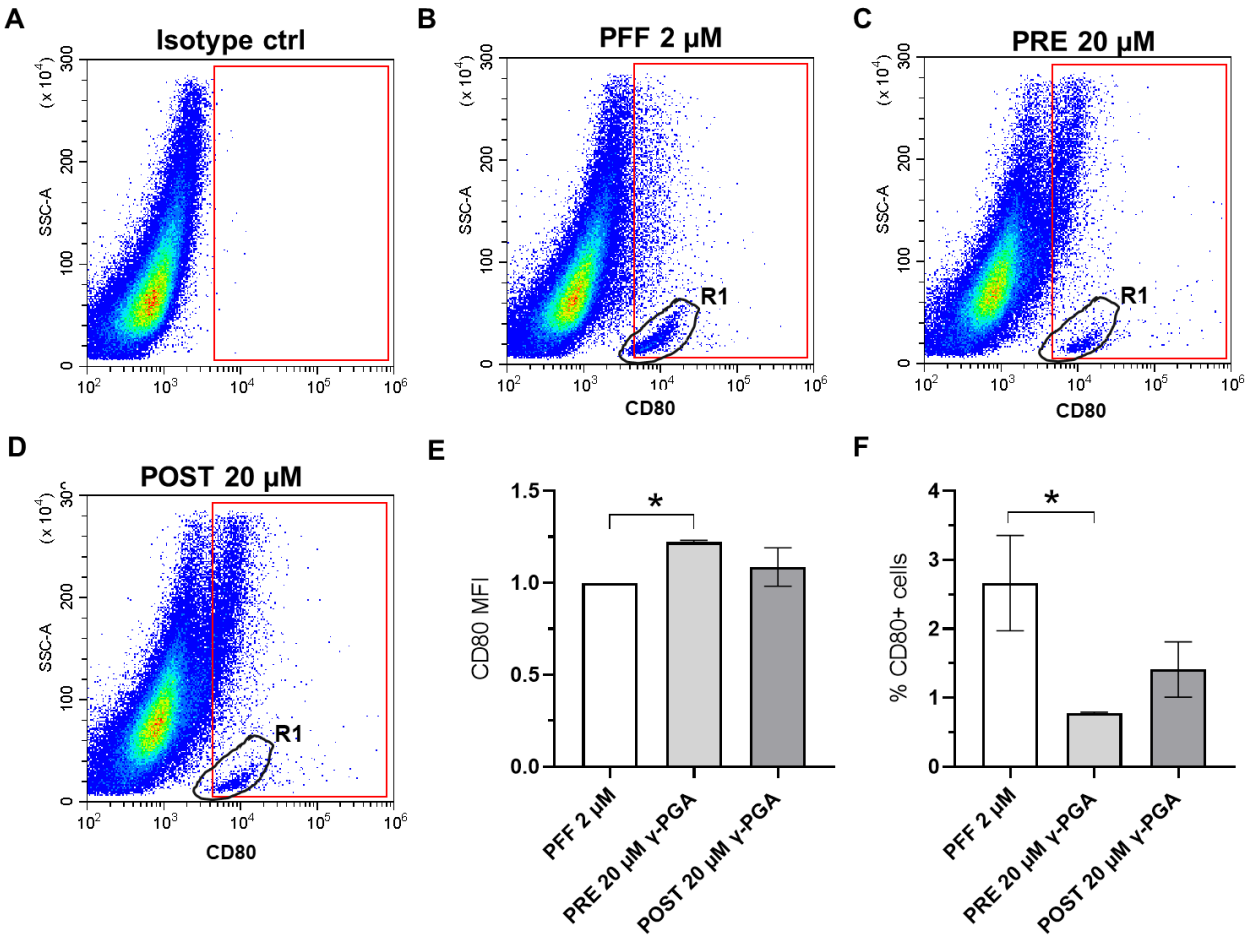

Figure 3.16. 280 kDa γ-PGA effect on CD80 marker in PFF-activated macrophages (R1 region). *Representative flow cytometry dot plot showing CD80 expression in macrophages treated with PFFs alone and in co-treatment with 280 kDa γ-PGA at 20 µM. Red gates (based on Isotype control) indicate CD80$^+$ cells, and R1 represent the positive population activated by PFF treatment. Graphs show the mean ± SEM of CD80 MFI (**E**) and percentage of positive cells (**F**) in R1, normalized to PFF treatment. Statistical analysis was performed using Ordinary one-way ANOVA with Tukey's post hoc test (n=3), *p < 0.05.*

Regarding HLA-DR, PRE treatment decreased the MFI compared to PFF administration alone (**Figure 3.15, C**); however, a different patter was observed in the percentage of positive cells. In this case, γ-PGA administration alone increased the percentage of HLA-DR$^+$ cells at the same levels of PFFs (**Figure 3.15, C'**). Moreover, POST treatment with γ-PGA induced an increase in HLA-DR$^+$ cells compared with PFFs.

A similar trend to HLA-DR was also observed for CD206 MFI and percentage of positive cells, but no statistical significance was observed due to biological variability (**Figure 3.15, D, D'**).

Thus, the analysis of HLA-DR and CD206 MFI and percentage of positive cells, was also carried out considering the PFF-activated cells in R1 (**Figure 3.17** and **Figure 3.18**). No differences were observed in the HLA-DR MFI (**Figure 3.17, E**). However, a significant reduction in the percentage of HLA-DR$^+$ cells was detected with PRE treatment with γ-PGA, along with a slight decrease following POST treatment (**Figure 3.17, F**). A similar trend was also observed for CD206 (**Figure 3.18**).

This might suggest that γ-PGA at 280 kDa have a modulatory effect on cells specifically activated by PFFs.

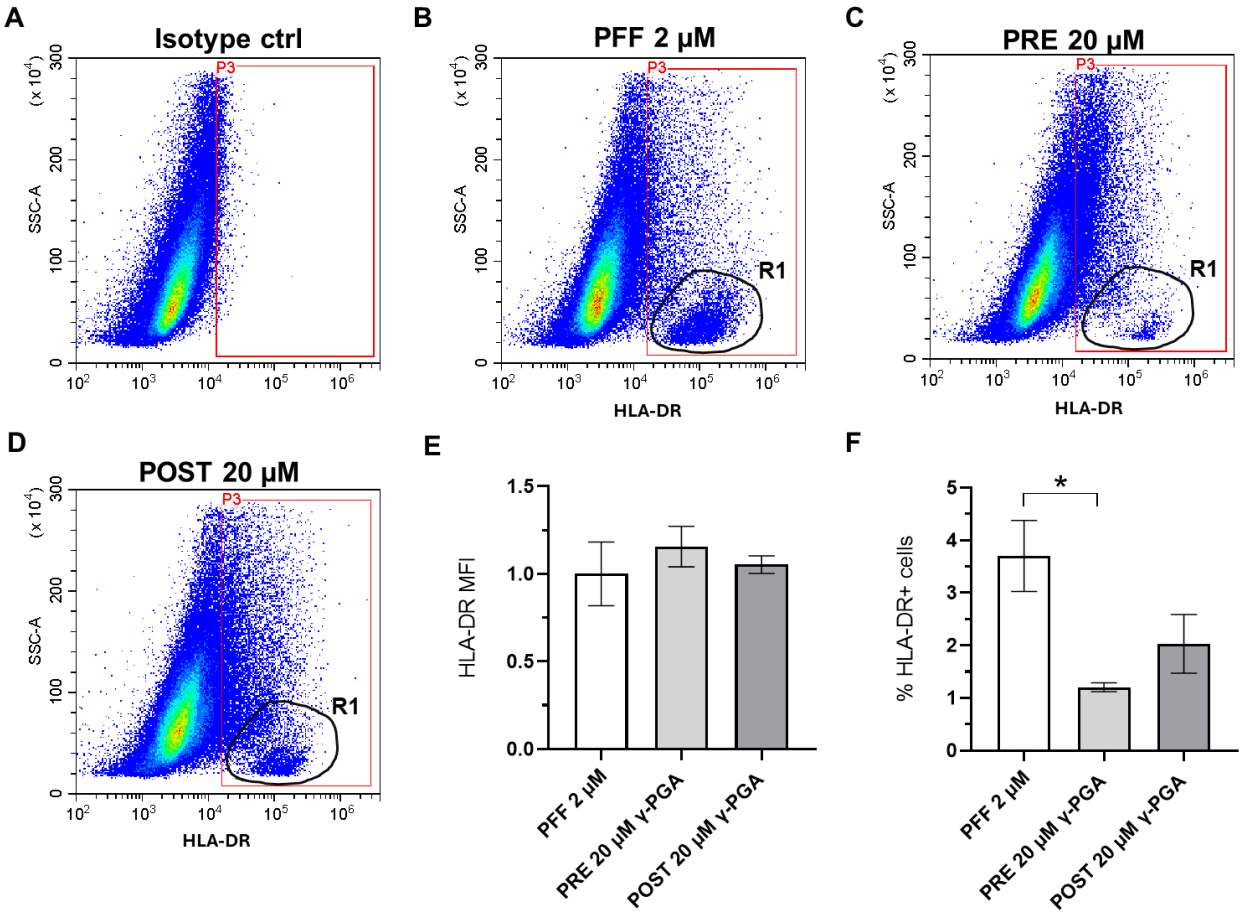

Figure 3.17. 280 kDa γ-PGA effect on HLA-DR marker in PFF-activated macrophages (R1 region). *Representative flow cytometry dot plot showing HLA-DR expression in macrophages treated with PFFs alone and in co-treatment with 280 kDa γ-PGA at 20 µM. Red gates (based on Isotype control) indicate HLA-DR$^+$ cells, and R1 represent the positive population activated by PFF treatment. Graphs show the mean ± SEM of HLA-DR MFI (**E**) and percentage of positive cells (**F**) in R1, normalized to PFF treatment. Statistical analysis was performed using Ordinary one-way ANOVA with Tukey's post hoc test (n=3), *p < 0.05.*

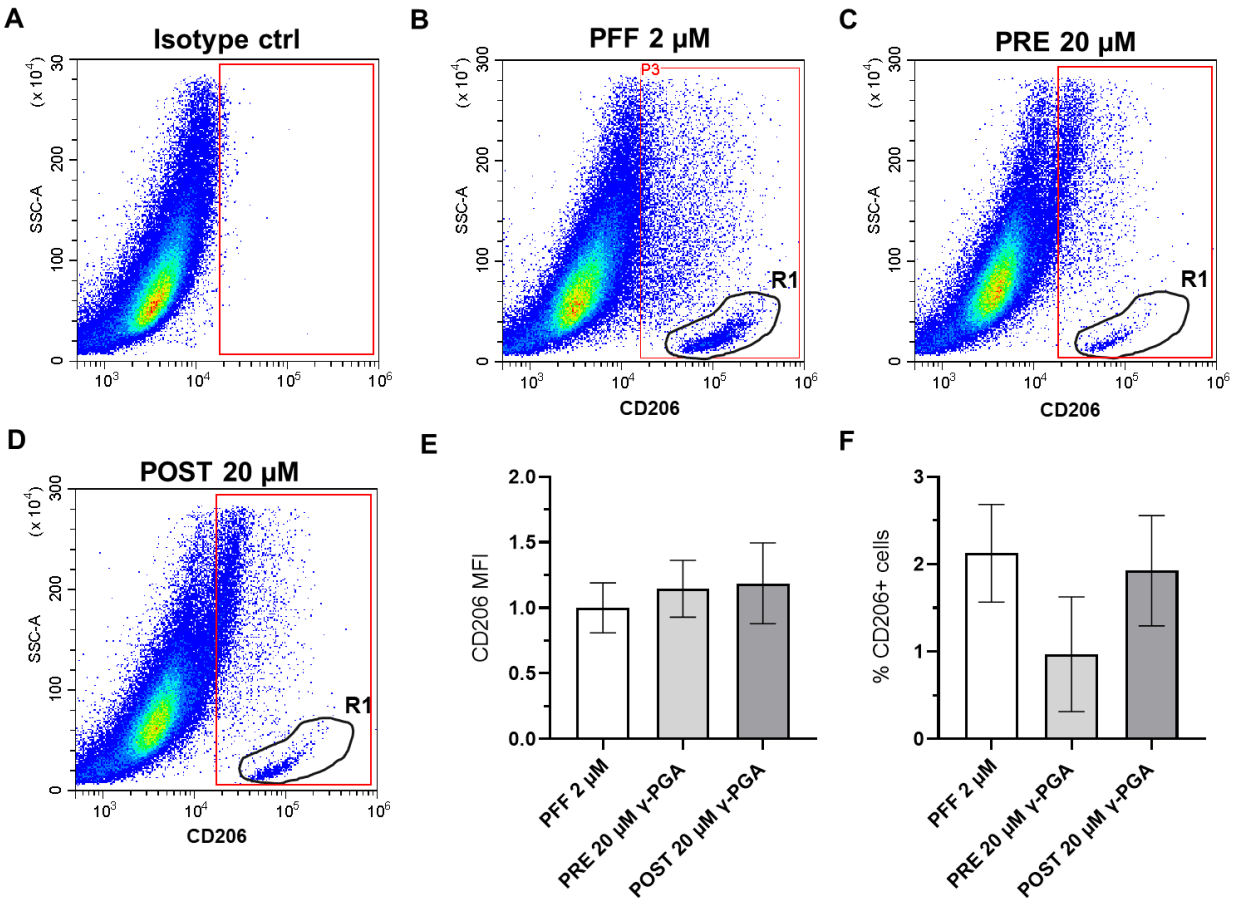

Figure 3.18. 280 kDa γ-PGA effect on CD206 marker in PFF-activated macrophages (R1 region). *Representative flow cytometry dot plot showing CD206 expression in macrophages treated with PFFs alone and in co-treatment with 280 kDa γ-PGA at 20 µM. Red gates (based on Isotype control) indicate CD206⁺ cells, and R1 represent the positive population activated by PFF treatment. Graphs show the mean ± SEM of CD206 MFI (**E**) and percentage of positive cells (**F**) in R1, normalized to PFF treatment. Statistical analysis was performed using Ordinary one-way ANOVA with Tukey's post hoc test (n=3).*

Lastly, the effect of both α-synuclein PFFs and γ-PGA on oxidative stress was evaluated by measuring ROS generation in macrophages. Indeed, ROS have a major role in regulating gene expression and signalling pathways, control macrophage polarization and cytokines release. High concentration and prolongated exposure to ROS can induce DNA, protein and lipid damage, leading to cellular oxidative stress and inflammation (Canton et al., 2021; Martínez-Reyes & Chandel, 2020).

In our experimental condition, neither 2 μM PFFs or γ-PGA at 100 kDa (20 and 40 μM) and 280 kDa (20 μM), induced ROS production compared with control (**Figure 3.19**). ROS inducer and ROS inhibitor were used as positive and negative controls, as described in section 6.9.

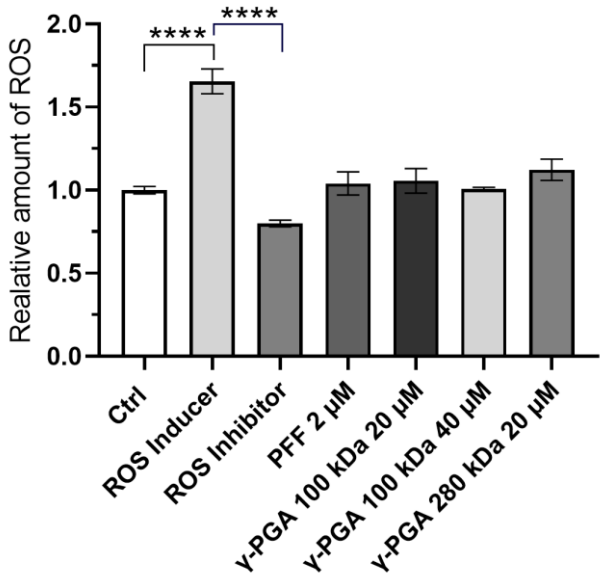

Figure 3.19. Reactive oxygen species (ROS) production in PFF and γ-PGA treated macrophages. *Cellular ROS generation in macrophages treated with 2 μM PFFs, 100 kDa, and 280 kDa γ-PGA. ROS inducer (Pyocyanin) and ROS inhibitor (NAC (N-acetyl-l-cysteine) were used as positive and negative controls, respectively. Data, representing the normalised fluorescence intensity, are analyzsed by ordinary one-way ANOVA with Tukey's post hoc test (n = 4), ****p < 0.0001.*

3.3 Discussion

This study explored the biological effect of α-synuclein aggregates and γ-PGA polymers on macrophage polarization towards either pro-inflammatory M1 or anti-inflammatory M2 profile. Indeed, although in PD current data suggest an involvement of M1-type macrophages, little is known about the biological effects of α-synuclein aggregates on this cell type.

For this reason, we investigated the effect of PFFs on a cell model of macrophages in terms of cytotoxicity, expression of M1 and M2 surface markers, and ROS production. In parallel, we tested the potential modulatory effect of a commercially available γ-PGA (YRSPEC), used at two different molecular weights in co-treatment with PFFs, and applied either as a preventive strategy (PRE treatment) and recovery approach (POST treatment).

The major finding of this study is that α-synuclein PFFs exert a concentration-dependent effect on macrophage polarization. Indeed, flow cytometry analysis revealed that PFFs treatment both at 1 μM and 2 μM increases the percentage of CD86, CD80, and HLA-DR positive cells, which are markers of pro-inflammatory M1 macrophage phenotype. CD86 and CD80 co-stimulatory molecules, together with HLA-DR that plays a crucial role in antigen presentation, are necessary for a full T cell activation (Shapouri-Moghaddam et al., 2018). These findings are in accordance with what has been previously reported in PD pathology. For instance, an upregulation of MHCII has been described *in vivo* both in microglia and in border-associated macrophages (BAMs) (Harms et al., 2017; Schonhoff et al., 2022). In fact, α-synuclein fibril injections in the rat SNpc were shown to promote antigen presentation and activation of microglia, along with peripheral immune cell infiltration (Harms et al., 2017). A study in α-synuclein overexpressing mouse model showed that BAMs play a crucial role in mediating α-synuclein-induced neuroinflammation by acting as antigen presenting cells and by recruiting T cells into the brain parenchyma (Schonhoff et al., 2022). Further analyses in PD human brain highlighted a higher percentage of $CD3^+$ T cells adjacent to $CD68^+$ BAMs compared with healthy controls (Schonhoff et al., 2022). Moreover, Ozono and colleagues reported that, in HEK293T cells that stably overexpress α-synuclein, HLA-DR molecules capture and transport structurally abnormal α-synuclein to the cell surface (Ozono et al., 2023).

Lastly, an *in vitro* study on THP-1 cell-derived macrophages showed that the prolongated exposure to monomeric α-synuclein induces a pro-inflammatory profile characterized by release of pro-inflammatory cytokines and impaired autophagy (Limanaqi et al., 2024).

Regarding M2 markers, only the exposure to the higher concentration of α-synuclein PFF (2 μM) increased the percentage of $CD206^+$ cells compared to control, with no differences in CD163 expression. This might suggest that treatment with PFF at 2 μM induce a mixed phenotype of M1/M2 macrophages or a non-canonical macrophage activation. Nevertheless, α-synuclein PFFs primarily

promote M1 polarization, as indicated by the upregulation of CD206 marker but not CD163, suggesting a context-dependent adaptation rather than a full activation to the classical M2 profile. However, other possibilities might be considered. For instance, the selective induction of CD206, in the absence of CD163, may also represent an adaptive response aimed at enhancing aggregate clearance. For instance, CD206 receptor is associated to the clearance of endogenous molecules through endocytosis, and the modulation of phagocytosis (Gantzel et al., 2021). This might suggest a macrophage activation towards phagocytosis or aggregate recognition rather than to inflammation resolution.

Although we did not observe any significant effect on CD163 following PFF administration, it is worth mentioning that current data point out an involvement of CD163 in PD pathology. Soluble CD163 has been found increased in the CSF and blood of PD patients compared with healthy control (Nissen et al., 2021). Moreover, it has been proposed as a potential biomarker of cognition decline in PD, as its increase is detectable in the late stage of the disease, directly correlates with PD biomarker such as α-synuclein accumulation, and inversely correlates with patients' cognitive scores (Nissen et al., 2021). In a rat model of PD, α-synuclein nigrostriatal PFF injection recruited peripheral $CD163^+$ macrophages prior to neurodegeneration (Harms et al., 2017). Furthermore, transcriptional profiling of peripheral monocyte from PD patients showed that CD163 transcripts were low in the early stage of PD but increased progressively as the disease advanced, while CD206 expression was already elevated in the early phases of the disease (Thome et al., 2025).

Lastly, no effects were observed in cytotoxicity and ROS production at any of the tested concentrations of PFFs. Altogether, this pattern is consistent with a mixed or transitional phenotype that might be oriented toward antigen presentation and aggregate clearance rather than classical M1 cytotoxic macrophages or M2 anti-inflammatory one. The lack of ROS production and cytotoxic effects further supports the idea that *in vitro* PFF administration induces functionally primed but non-destructive immune activation.

The second part of this study aimed to explore the immunomodulatory effect of YRSPEC γ-PGA on M1 and M2 macrophage expression. In detail, 100 kDa and 280 kDa γ-PGA were tested in co-treatment with α-synuclein PFFs following PRE and POST treatment. We observed that only PRE treatment with 100 kDa γ-PGA polymer at 40 μM significantly reduced the percentage of CD86, CD80, HLA-DR, and CD206 positive cells compared with PFF treatment alone, suggesting an attenuation of PFF-induced activation.

The higher molecular weight γ-PGA (280 kDa) directly increased the percentage of $HLA\text{-}DR^+$ and $CD206^+$ compared to control, thus suggesting a possible activation of antigen presentation and clearance-related mechanisms. The absence of cell toxicity and ROS production following γ-PGA

suggests macrophage activation without cytotoxicity. Interestingly, 280 kDa γ-PGA administrated as PRE treatment with PFFs reduced the percentage of $CD80^+$ cells and the percentage of PFF-induced $HLA\text{-}DR^+$ and $CD206^+$ cells. This suggests that γ-PGA may have a protective or modulatory effect on PFF-activated population, thus interfering with the phenotype specifically triggered by α-synuclein PFFs.

The mechanisms underlying the effect of γ-PGA in modulating PFF-activated macrophages can be multiples and further studies are required to elucidate the molecular pathways that may be involved.

Overall, we acknowledge that this is a preliminary study, and it is not devoid of limitations. First, although PMA-differentiated THP-1 cells are extensively used to study macrophage responses, they do not fully recapitulate the complexity and the heterogeneity of primary human macrophages. Therefore, further studies in a more physiologically relevant system, such as peripheral blood mononuclear cells (PBMC) or tissue resident macrophages, are required to confirm our findings.

Moreover, further investigation is needed to fully elucidate macrophage response to α-synuclein PFFs in terms of cytokines release and co-expression of M1/M2 marker to investigate a possible phenotype overlapping as M1 and M2 cells are not static but highly plastic immune cells. Additionally, it would be relevant to investigate the biological effect of other aggregated species, such as α-synuclein oligomers, which are key players in α-synuclein pathology propagation.

4

Chapter 4: γ-PGA as a novel α-synuclein anti-aggregation compound

4.1 Introduction

The modulation of α-synuclein aggregation has emerged as a promising therapeutic approach for the treatment of PD. In recent years, a wide range of anti-aggregation agents have been investigated for their potential to inhibit α-synuclein aggregation and mitigate its associated pathology (Oliveri, 2019; Singh et al., 2017). Among these, dietary natural compounds have attracted significant attention. In this study, we tested for the first time the activity of Natto and YRSPEC γ-PGA at different molecular weights as modulators of α-synuclein aggregation both in cell-free system and *in vitro*. This work was partially conducted in collaboration with the Fabio Moda's group at Carlo Besta Neurological Institute (Milan, Italy).

4.2 Results

4.2.1 Natto γ-PGA affects α-synuclein aggregation in a cell-free system

To investigate whether Natto γ-PGA interferes with α-synuclein aggregation *per se*, we performed RT-QuIC studies, in collaboration with Carlo Besta Neurological Institute, and showed the biopolymer's capacity to delay the aggregation of α-synuclein in a dose-dependent manner (**Figure 4.1, A**).

In particular, the green curve shows the aggregation kinetics of recombinant α-synuclein in the absence of γ-PGA. The pink, blue and red curves refer to the experimental conditions with increasing concentrations of Natto γ-PGA at 2.75 μM, 27.5 μM, and 275 μM, respectively. Remarkably, the 27.5 μM and the 275 μM concentrations were the most effective in inhibiting the aggregation of α-synuclein. Notably, at the concentration of 275 μM, aggregation did not occur even after 40 hrs. The grey curves in the graph refer to γ-PGA alone (at the different concentrations tested: 2.75 μM, 27.5 μM, and 275 μM) and none of them show any propensity to undergo self-assembly (**Figure 4.1, A**).

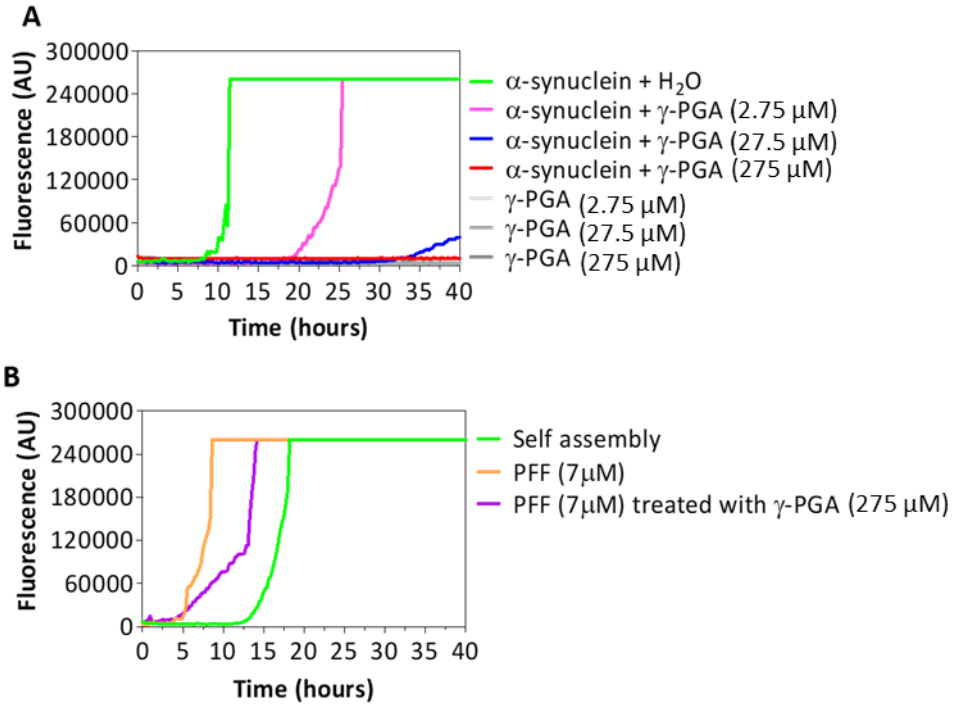

Figure 4.1. Natto γ-PGA affects α-synuclein aggregation in a cell-free system*. A) Aggregation kinetics of monomeric α-synuclein supplemented with different concentrations of γ-PGA: 2.75 μM (pink curve), 27.5 μM (blue curve), and 275 μM (red curve). The gray lines refer to γ-PGA alone (2.75, 27.5, and 275 μM). B) Aggregation kinetics of monomeric α-synuclein in the presence of PFFs (orange curve) and PFFs incubated with 275 μM γ-PGA (purple curve) The graphs show the average fluorescence intensity of the four replicates for each curve plotted against time.*

Samples collected following incubation with 27.5 μM γ-PGA were analyzed by transmission electron microscopy to better characterize the effect of the polymer on the presence and the ultrastructure of α-synuclein aggregates. Following γ-PGA incubation with monomeric recombinant α-synuclein, no fibrils were observed, while oligomer-like structures were detected (**Figure 4.2**). This strengthens the role of γ-PGA in interfering with α-synuclein aggregation.

The highest concentration of γ-PGA (275 μM) was used to treat PFFs before testing their ability to trigger the aggregation of α-synuclein (**Figure 4.1, B**). Both treated and untreated PFFs (purple and orange curves, respectively) were able to accelerate the aggregation kinetics of α-synuclein (green curve). Interestingly, a trend toward attenuation of PFF effect is observed when preincubated with γ-PGA.

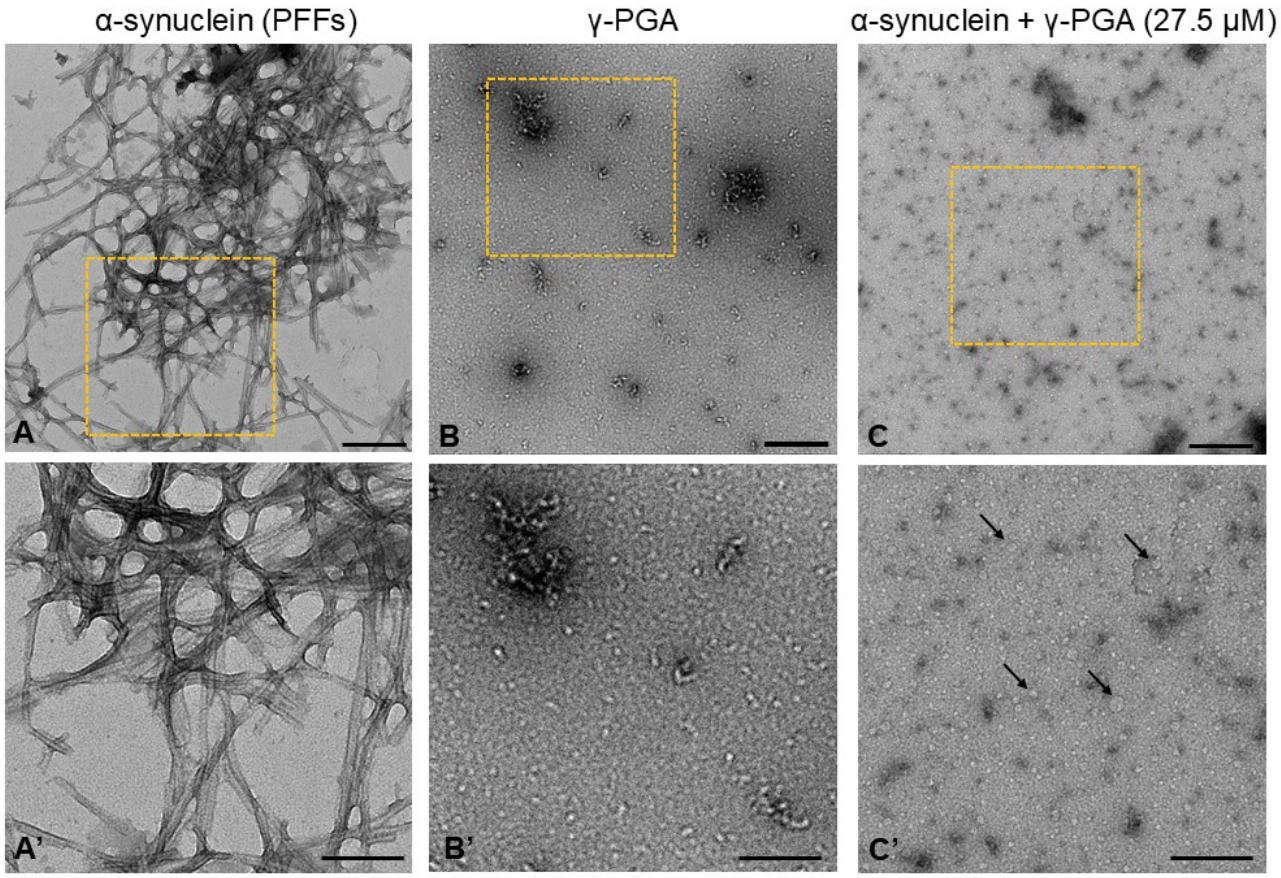

Figure 4.2. Electron microscopy analyses of α-synuclein and Natto γ-PGA samples collected at the end of RT-QuIC aggregation assay following an incubation of 40 hrs. ***A*** *and* ***A'*** *show α-synuclein fibrils (PFFs) formed after monomeric α-synuclein aggregation.* ***B*** *and* ***B'*** *show the sample of γ-PGA.* ***C*** *and* ***C'*** *show the sample obtained following the incubation of α-synuclein with 27.5 μM γ-PGA. Black arrows in C' highlight the presence of oligomer-like structures. A', B', and C' represent 1.5× magnification of the orange dashed rectangles. A, B and C: scale bar, 200 nm; A', B' and C': scale bar, 100 nm.*

4.2.2 γ-PGA administration significantly decreases oligomeric α-synuclein pathology in vitro

The ability of γ-PGA to interfere with α-synuclein aggregation was further tested *in vitro*. Specially, we used *SNCA*-stably transfected SK-N-SH cells (Syn^+), a neuroblastoma cell line widely used as cellular model in PD research, as they can be differentiated into dopaminergic-like neurons upon treatment with retinoic acid. In these cells overexpressing α-synuclein, the presence of oligomers has been previously reported (Calogero et al., 2023; Basellini et al., 2025). In detail, proximity ligation assay (PLA) was used to identify α-synuclein early aggregates as it enables the detection of two proteins that are in close spatial proximity (< 40 nm), indicative of oligomeric or aggregated states (Roberts et al., 2015; Mazzetti et al., 2020). Differentiated Syn^+ SK-N-SH cells displayed an increased amount of α-synuclein aggregates compared to Naïve cells, evaluated as Area of PLA puncta per cell (**Figure 4.3, A, B, D**). Interestingly, administration of 27.5 μM Natto γ-PGA for 24 hrs resulted in

50.7% decrease in the extent of aggregates compared to Syn^{+}, with levels not significantly different from those observed in Naïve cells (**Figure 4.3, D**).

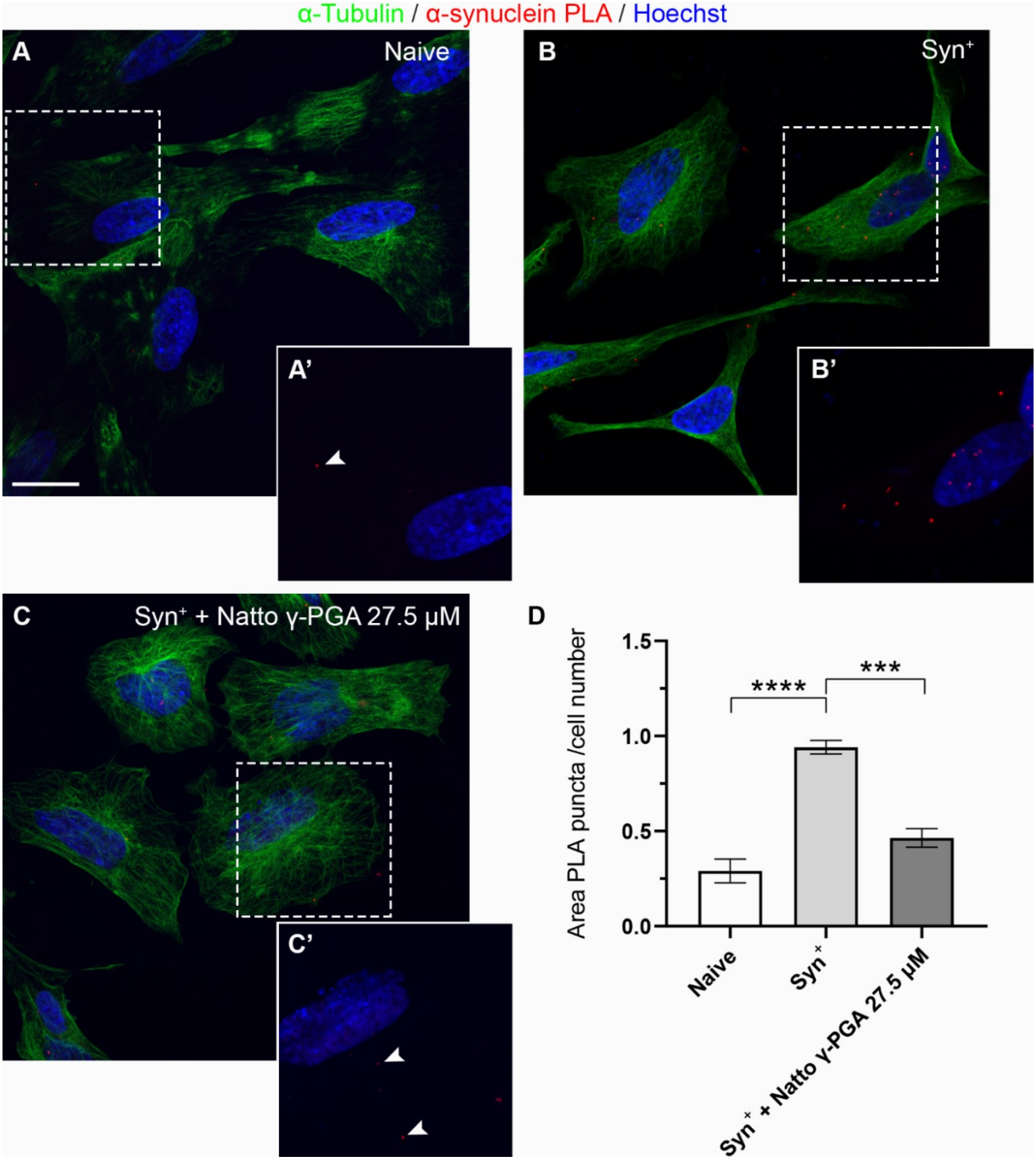

Figure 4.3. Effect of Natto γ-PGA on early α-synuclein pathology in cells. A, A') *Naïve SK-N-SH cells show little positivity to α-synuclein oligomers (PLA signal, withe arrowheads in A'). **B, B')** α-Synuclein overexpressing SK-N-SH cells (Syn^{+}) naturally display an extensive amount of early-type α-synuclein oligomers. **C, C')** The extent of α-synuclein oligomers significantly decreases after administration of Natto γ-PGA at 27.5 μM. scale bar: 20 μm. Insets show 1.5× magnification of selected areas from the original images (white dashed squares). D) The graph shows the Area of PLA puncta normalized on the number of cells. Data are shown as mean ± SEM and analyzed by One-way ANOVA with Tukey's post hoc test (n=3). ***p < 0.001, ****p < 0.0001.*

YRSPEC γ-PGA of two different molecular weights (118 kDa and 70 kDa) was also tested for its activity to reduce α-synuclein aggregates in Syn^+ SK-N-SH cells. First, we investigated the effect of the two polymers on cell viability and observed that γ-PGA at both molecular weights did not affect cell viability at the tested concentrations (**Figure 4.4**).

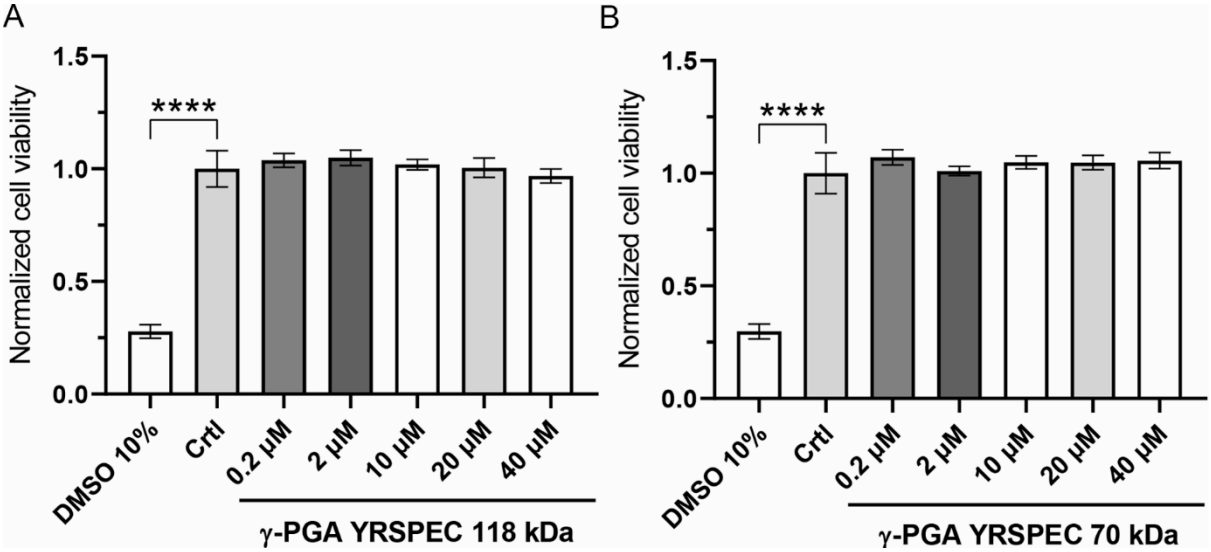

Figure 4.4. YRSPEC γ-PGA effect on cell viability of differentiated Syn⁺ SK-N-SH cells. *A) Cell viability of Syn⁺ SK-N-SH cells treated with increasing concentrations of 118 kDa YRSPEC γ-PGA (0.2, 2, 20, and 40 µM). Data are expressed as mean ± SEM, normalized to control and analyzed by Kruskal-Wallis test with Dunn's (n = 3).* ***B)*** *Cell viability of Syn+ SK-N-SH cells treated with increasing concentrations of 70 kDa YRSPEC γ-PGA (0.2, 2, 20, and 40 µM). Data are expressed as mean ± SEM, normalized to control and analyzed by ordinary one-way ANOVA with Tukey's post hoc test (n = 3). ***p < 0.001. 10% DMSO was used as a positive control*

Then, we quantified PLA staining in cells treated with YRSPEC γ-PGA polymers. Both 20 µM and 40 µM γ-PGA of 118 kDa significantly reduced the Area of PLA puncta per cell compared to untreated Syn^+ SK-N-SH cells (**Figure 4.5, A-D, G**). Notably, the higher concentration restored the extent of α-synuclein pathology to levels comparable to the Naïve phenotype (**Figure 4.5, D, G)**. A similar effect was also observed for γ-PGA of 70 kDa (**Figure 4.5, E, F)**, where both 20 µM and 40 µM concentration decreased the extent of α-synuclein compared with Syn^+ cells, and showed no significant differences compared with Naïve cells (**Figure 4.5, H)**. Finally, comparisons between Natto and YRSPEC γ-PGA, as well as YRSPEC γ-PGA polymers of the two different molecular weights, revealed no significant differences in their ability to decrease the Area of PLA puncta per cell (**Figure 4.5, I**).

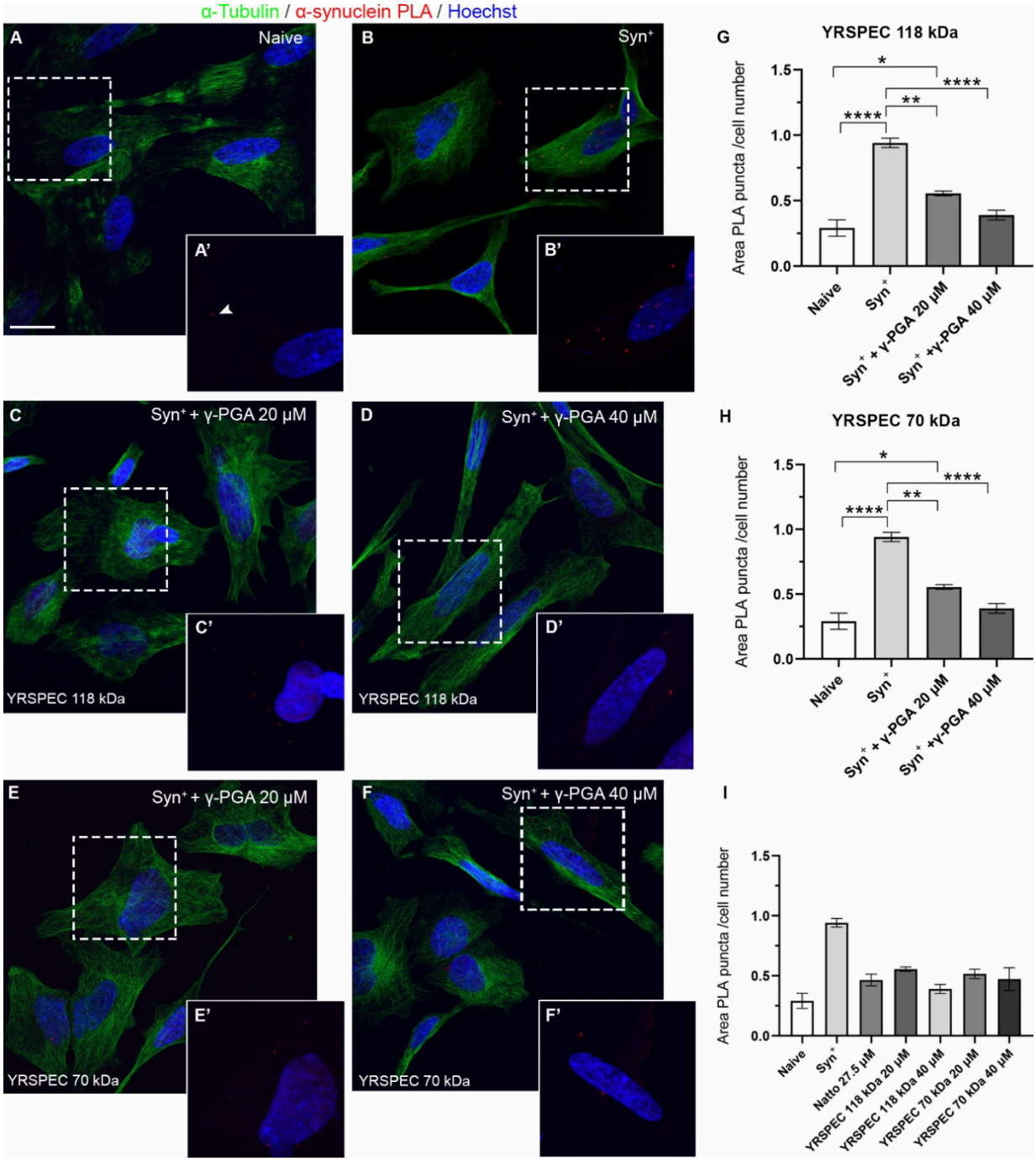

Figure 4.5. Effect of YRSPEC γ-PGA on early α-synuclein pathology in cells. A, A' *Naïve SK-N-SH cells show little positivity to α-synuclein oligomers (PLA signal, white arrowheads in A'). **B, B'**) α-Synuclein overexpressing SK-N-SH cells (Syn$^+$) exhibit a high level of early α-synuclein oligomers.* ***(C–F')*** *Treatment with YRSPEC affects early aggregates levels. Both 118 kDa (C, C' at 20 μM; D, D' at 40 μM) and 70 kDa (E, E' at 20 μM; F, F' at 40 μM) formulations significantly decrease the extent of α-synuclein oligomers. scale bar: 20 μm. Insets show 1.5× magnification of selected areas from the original images (white dashed squares).* ***G-H)*** *Graphs show the Area of PLA puncta normalized on the number of cells treated with YRSPEC γ-PGA 118 kDa (G) and 70 kDa (H). The graph in **I** shows the comparison between Natto and YRSPEC γ-PGA treatment in Syn$^+$ compared to Naïve SK-N-SH cells. Data are shown as mean ± SEM and analyzed by One-way ANOVA with Tukey's post hoc test (n=3). *p < 0.05, **p < 0.01, ***p < 0.001, ****p < 0.0001.*

4.3 Discussion

Current therapeutic strategies for PD treatment primarily aim to alleviate the motor symptoms by restoring the dopamine levels through the administration of levodopa or dopamine agonists. However, this strategy does not provide any disease-modifying effect and current research focuses on neuroprotective approaches in combination with symptomatic therapies. Among these, particular attention is paid to α-synuclein aggregation, a central event in the pathogenesis of PD and other synucleinopathies (Spillantini & Goedert, 2018). Different strategies to target α-synuclein might be pursued, including: *i*) inhibition of protein misfolding and thereby preventing the formation of toxic oligomeric and protofibrillar species, *ii*) conversion of toxic aggregates to non-toxic aggregates with different morphology, *iii*) acceleration of the fibril formation process so that α-synuclein might spend less time in the intermediate oligomeric state, which is considered the most toxic form, and *iv*) enhancement of α-synuclein clearance (Oliveri, 2019; Wong & Krainc, 2017).

Based on these considerations, several therapeutic strategies have emerged. First, gene silencing via RNAi and antisense oligonucleotides (ASOs) might directly target α-synuclein at the transcriptional level, before monomers aggregate into fibrils and propagate. In a mouse model of PD, local injection of ASOs against *SNCA* mRNA into the striatum, significantly reduced endogenous α-synuclein levels, preventing and inhibiting the spread of phosphorylated α-synuclein throughout the brain (Sano et al., 2024). However, a deeper understanding of native α-synuclein physiological role in synaptic plasticity is crucial for the implication of this strategy. Another promising approach is represented by small molecules directly targeting α-synuclein to prevent its misfolding or disrupt toxic oligomers (Staats et al., 2020). Moreover, small molecules have been developed to bind specific cell-surface receptors of α-synuclein, inhibiting α-synuclein recognition and internalization, thereby slowing its propagation (Chedid et al., 2022).

Current research also focuses on developing α-synuclein monoclonal antibodies and nanobodies that exclusively bind to extracellular oligomers and amyloid fibrils (Kuo et al., 2025). Both active and passive immunization entered clinical trials (Kuo et al., 2025); however, these are still in the early stages and significant work is required before they can be translated in effective treatments.

Alongside these synthetic approaches, a wide range of natural anti-aggregation agents have been investigated, due to their safety, antioxidant and anti-inflammatory properties (Oliveri, 2019; Singh et al., 2017). For instance, different natural products, such as polyphenols, alkaloids and terpenes, have shown ability to interfere with amyloid formation (Ardah et al., 2016; Freyssin et al., 2018; Gupta & Sashidhara, 2023; Pogačnik et al., 2020). In this sense, we evaluated the ability γ-PGA to modulate α-synuclein aggregation both in a cell-free system and in an *in vitro* cellular model of PD.

In detail, we tested two different commercially available γ-PGA: Natto γ-PGA, and YRSPEC γ-PGA. Natto γ-PGA is a 193 kDa natural polymer that is found in Natto, a traditional Japanese fermented soybean food, and produced during fermentation by *Bacillus subtilis natto*. YRSPEC γ-PGA is a commercially available polymer of 440 kDa, purified by *Bacillus subtilis*, which molecular weight was reduced to 118 kDa and 70 kDa as described in Section 6.2.

First, we investigated Natto γ-PGA intrinsic capacity to influence α-synuclein aggregation *per se* by performing RT-QuIC studies. This *in vitro* assay indicated that γ-PGA could interfere with the aggregation process in a dose-dependent manner, with a trend towards attenuation of PFF assembly from monomeric human α-synuclein even when it was incubated with pre-formed aggregates. Moreover, incubation with γ-PGA seems to reduce the presence of fibrils, along with the appearance of small α-synuclein oligomer-like structure, suggesting that γ-PGA may influence α-synuclein aggregation in a cell-free system. Nevertheless, the polydispersity of α-synuclein PFFs must be considered when interpreting this type of *in vitro* assays, as the impact of γ-PGA could only involve specific subtypes of fibrils, size or morphology dependent.

Natto γ-PGA and YRSPEC γ-PGA anti-aggregation properties were also tested in an *in vitro* cellular model of PD. In detail, we employed α-synuclein stably overexpressing SK-N-SH (Syn^+) cells, which exhibit a higher extent of α-synuclein oligomers when compared to Naïve cells, to assess the effect of the polymers on early α-synuclein aggregates.

Our results showed that both γ-PGA polymers reduced α-synuclein burden in this neuronal cell model, restoring it to levels observed in Naïve cells. Given that Syn^+ cells already display oligomers prior to treatment, these findings suggest that γ-PGA may be capable of disrupting small aggregates, even after their formation. Moreover, no differences were observed between Natto and YRSPEC γ-PGA polymers, or between the two molecular weights of YRSPEC γ-PGA. This could suggest that the effect of the polymers on early α-synuclein aggregates might not be strictly dependent on the type of commercially source or molecular weights of γ-PGA. However, another aspect needs to be taken into consideration: γ-PGA is a polymer composed of both D and L-glutamic acid residues, but the ratio of D/L enantiomers in the samples still need to be characterized. A better understanding of the D/L enantiomers composition might be important as it could influence the polymer's structural properties. Further studies will be required to clarify the exact nature of the interaction between γ-PGA and α-synuclein species.

5

Chapter 5: Conclusions and future perspectives

The multicomponent aetiopathogenesis of PD makes it really challenging to point out a specific molecular mechanism that, if targeted, would result in a disease-modifying therapy. Among the altered molecular pathways in PD, the accumulation of misfolded and aggregated α-synuclein, as well as its propagation and inflammatory responses, are significant pathological features that contribute to neuronal dysfunction and disease progression, making α-synuclein an ideal target for developing disease-modifying strategies (Ben-Shlomo et al., 2024; Olanow & Kordower, 2017). Indeed, the current treatment approach available for PD patients mostly relies on symptomatic therapies, aimed at improving the motor symptoms through the administration of levodopa or dopamine agonists. However, these approaches are not resolutive and long-term administration can lead to medication-resistant-tremor and motor control fluctuations (Ben-Shlomo et al., 2024).

On this basis, the scope of this study was to investigate the modulatory effect of a natural polymer, γ-PGA, on α-synuclein aggregation and aggregate-induced cellular inflammation in *in vitro* models of PD. γ-PGA is a natural, non-toxic, non-immunogenic, biodegradable biopolymer composed of D- and/or L-glutamic acid monomers that are coupled to each other via amide bonds between α or γ-carboxylic groups (Nair et al., 2023). Recently, its interest in biomedicine has grown due to its antioxidant, anti-inflammatory, neuronal alleviation, and prebiotic properties (Jin et al., 2017; Lee et al., 2020; Nair et al., 2023; T. Zhang et al., 2021). In this work we tested the biological effect of two commercially available γ-PGA: Natto γ-PGA and YRSPEC γ-PGA. Natto γ-PGA is a biopolymer of 193 kDa that is synthesised naturally by *Bacillus subtilis* during the fermentation of Natto beans. These traditional soybean fermented foods are highly consumed in Japan where, interestingly, the relative PD incidence rate is reported to be significantly lower than in Europe (Kanaya et al., 2021). YRSPEC γ-PGA is a 440 kDa polymer whose MW has been reduced to lower MW species for biological reasons as described in chapter 6.2.2.

In chapter 2, we described the biological effects of Natto γ-PGA on a PFF treated astrocytes, an *in vitro* model that recapitulated PD pathology in this cell type. Indeed, astrocytes are key players in PD pathogenesis as they regulate the clearance of extracellular aggregated α-synuclein and modulate neuroinflammatory responses (Colombo & Farina, 2016; Giusti et al., 2024). However, high concentrations of extracellular aggregated α-synuclein can overwhelm astrocytes, and activate a detrimental immune response, leading to cellular toxicity and disease progression (Liddelow & Barres, 2017; Patani et al., 2023).

We reported that the treatment with γ-PGA successfully recovers astrocyte cytotoxicity and inflammation induced by PFFs (Novello et al., 2025). The possible molecular mechanisms underlying this effect are multiple, including the antioxidant properties of the polymers, its ability in interfering with aggregate internalization, as well as its direct effect on PFFs supported by the colocalization

analyses and the reduction in α-synuclein aggregate burden. This effect is also supported by our cell-free system and *in vitro* analyses of Natto γ-PGA on α-synuclein aggregation, described in chapter 4. In fact, Natto γ-PGA successfully inhibited α-synuclein aggregation and reduced α-synuclein oligomers pathology in a neuronal *in vitro* model. However, other studies are required to investigate the effect of the polymer on neuronal functions, with special attention to axonal transport dynamics and synaptic functionality. Moreover, another key aspect worth of investigation is the impact of the polymer on mechanisms involved in α-synuclein aggregate propagation in neurons and glia cells, focusing on tunneling nanotube-mediated transfer, endocytosis and exocytosis. This is essential as cell-to-cell transfer of α-synuclein aggregated species, including small oligomers and fibrils, is one of the key aspects of disease progression (Cascella et al., 2022).

In chapter 3 we investigated the biological effect of α-synuclein PFFs on macrophages focusing of macrophage polarization, and how YRSPEC γ-PGA might modulate this phenotype.

Macrophages are central coordinator of the immune response. Upon exogenous stimuli and pathological conditions, they polarize toward a pro-inflammatory M1 profile, which promote the activation of the adaptive immune response, and an anti-inflammatory and regulatory M2 phenotype, which modulates and promotes tissue regeneration (Helm et al., 2014).

As *in vitro* model we selected THP-1 cells, a cell line that is widely use as M_0 macrophage model upon differentiation with PMA. Our results suggest that PFFs administration functionally activate these cells towards a mixed M1/M2 phenotype without inducing cell toxicity and ROS production. Treatment with γ-PGA attenuated the PFF-induced phenotype, as reflected by a reduction in the expression of both M1 and M2 markers. The mechanism underlying the effect of γ-PGA in modulating PFF-activated macrophages can be multiples. Given the results obtained on astrocytes, we can speculate that YRSPEC γ-PGA might act similarly to Natto γ-PGA, exerting its protective role through different but potentially complementary mechanisms. These may include direct interplay with α-synuclein PFFs, thus preventing their recognition and uptake by macrophages, as well as the modulation of intracellular signalling pathways that drive macrophage polarization towards either the M1 or M2 phenotype. Furthermore, considering its antioxidant and immunomodulatory properties, YRSPEC γ-PGA may attenuate the response activated by PFFs, thereby reducing the risk of chronic inflammation reported in PD patients. We acknowledge that these are speculations, and future studies are required to elucidate the precise molecular pathways involved in γ-PGA-mediated modulation of macrophages. These include cytokines analyses and phagocytosis evaluation to fully elucidated macrophage phenotype in the presence of α-synuclein aggregated species such as fibrils and oligomers, and how γ-PGA might modulate these processes. Moreover, the possible co-expression of

M1/M2 marker needs to be investigated as these phenotypes may overlap since macrophages are highly plastic rather than static immune cells.

Lastly, in chapter 4, we tested Natto and YRSPEC γ-PGA as α-synuclein aggregation modulators confirming that both polymers efficiently diminished the early-stage aggregate of α-synuclein. This could suggest that the effect of the polymers on early α-synuclein aggregates might not be strictly dependent on the type of commercially source or molecular weights of γ-PGA. However, γ-PGA is a polymer composed of both D- and L-glutamic acid residues, and the ratio of D/L enantiomers in the samples still needs to be characterized. Thus, a deeper understanding of the D/L enantiomers composition is essential as it could influence the structural and functional properties of the polymer. Additional studies are required to explore the exact interaction of γ-PGA polymers with monomeric α-synuclein and α-synuclein aggregated species using tools such as computational modelling and protein-protein interaction assays, including dynamic light scattering, surface plasmon resonance and circular dichroism. These approaches will shed light on the affinity and kinetics of the interaction, as well as alteration of the α-synuclein secondary structure following incubation with γ-PGA.

In summary, this study provides consistent *in vitro* evidence that γ-PGA has excellent potential as a therapeutic agent for PD by targeting α-synuclein aggregation and modulating aggregate-induced inflammation. Despite the promising *in vitro* results, the molecular size of the γ-PGA polymers used in this study contributes to their scarce brain penetration, which represents a limitation for their therapeutic application in the CNS in PD pathology. However, our results on the aggregation properties of γ-PGA polymers of different molecular weights open promising possibilities for further investigation. Specifically, these findings support the rationale for exploring lower molecular weight γ-PGA derivatives, which could potentially exhibit enhanced BBB permeability while retaining their beneficial effects on α-synuclein aggregation. Alternatively, given the difficulty in achieving sufficient brain concentrations, γ-PGA may have a greater potential for therapeutic use in the periphery, where α-synuclein aggregate accumulation and inflammation are critical components of PD pathology. In this sense, the preliminary results obtained on the macrophage model are encouraging for their potential to modulate peripheral inflammation.

Importantly, γ-PGA is a well-characterized prebiotic that can increase the microbial species associated with a healthy microbiome (Jin et al., 2017). This property is particularly relevant considering the microbiota dysbiosis that is reported in PD pathology. Remarkably, increasing levels of gram-negative bacterial species (e.g., *Ralstonia*, *Lactobacillus*, *Bacteriodes* and *Akkermansia*) and enhanced LPS production, along with decreased gut microorganisms known to possess anti-inflammatory properties (e.g., *Roseburia* and members of the *Lachnospiraceae* family), have been

described (Wang et al., 2021; Romano et al., 2021). This is associated with high levels of gut inflammation, and intestinal accumulation of α-synuclein aggregates, key evidence of the gut-brain axis involvement in PD pathology (Houser & Tansey, 2017; Morais et al., 2021).

Thereby, future research should explore the polymer effects in PD gut models, by addressing inflammation, gut-barrier integrity and intestinal accumulation of α-synuclein. Examples include transgenic mouse model overexpressing human A53T mutated α-synuclein, which in the pre-symptomatic stage show constipation, colonic dysmotility and accumulation of α-synuclein inclusions in colonic neurons (C. Pellegrini et al., 2022), or intestinal α-synuclein PFF injection models for studying gut-to-brain propagation mechanisms (Chung et al., 2019; Kim et al., 2019).

Thus, γ-PGA dual biological activity as an anti-aggregation and anti-inflammatory polymer, along with its prebiotic activity, support the hypothesis that the polymer may be employed for a multi-target strategy. Additional investigations in neuronal and gut PD models, as well as extensive mechanistic studies, will be required to fully establish the therapeutic potential of γ-PGA and lay the groundwork for translational applications for the treatment of PD.

6

Chapter 6: Materials and Methods

6.1 α-Synuclein pre-formed fibrils (PFFs)

6.1.1 Human wt α-synuclein purification

Human α-synuclein was produced by *E. coli* and purified as previously described(Baden et al., 2023). In detail, E. coli strain DL21(BE3) competent for the production of human wt α-synuclein was streaked on LB medium with 1,5% agarose and ampicillin 100 μg/ml (AMP) to select the bacteria containing the construct for α-synuclein overexpression, and incubated overnight at 37°C. One of the colonies obtained was isolated and suspended in liquid LB agar + AMP, and incubated overnight, at 37°C, in shaking at 400 rpm. The following day, the pre-inoculation (1:50 dilution of the final volume) was transferred to LB medium containing AMP. The culture was then incubated with shaking at 37°C until it reached an optical density of 500 to 600 nm, as measured with a spectrophotometer at 600 nm. At this stage, a 1 ml aliquot of the non-induced culture was taken for later electrophoretic analysis, while the remaining culture was induced by adding 0.4 mM isopropyl-β-thiogalactopyranoside (IPTG) to initiate the expression of the α-synuclein gene. After 2 hours incubation at 37°C, in shaking, another 1 mL aliquot of the induced culture was recovered for the subsequent electrophoresis, while the rest of the culture was centrifuged at 1,960 g and 4°C for 10 minutes. The supernatant was discarded, while the pellet, containing the bacteria, was washed with 100 ml of DPBS, and centrifuged again. The pellet obtained was weighed and resuspended in HEPES1 buffer (1.1915 g HEPES, 1.864 g KCl, for 250 ml) to reach 25 mL/g. The solution was then incubated for 10 minutes, at 90°C, and an aliquot of the total extract obtained (1:1000 of the total volume) was retrieved, while the rest of it was ultracentrifuged at 40,000 g for 40 minutes. The supernatant, which constitutes the soluble fraction containing α-synuclein, was then stored at -80°C until the purification step. To purify α-synuclein from the soluble fraction, an ionic exchange chromatography was performed using two solutions: solution A (6.057 g Trizma for 1 l of solution, at 7.4 pH), used to balance the column, and solution B (3.0285 g Trizma, and 37.28 g KCl for 500 ml of solution, at pH 7.4), which contains a high percentage of salts and allows the elution of proteins from the column. Therefore, after filtering the soluble fraction, an aliquot was kept for further analysis, while the rest was loaded onto the column.

Then solution B was used for elution of the different fractions that were collected, and an aliquot (1:1000 of the final volume) was retrieved for each fraction. Based on the chromatogram obtained, to verify the correct expression of α-synuclein gene, the fraction of interest, along with all previously collected aliquots, were analysed through an electrophoretic run (**Figure 6.1**).

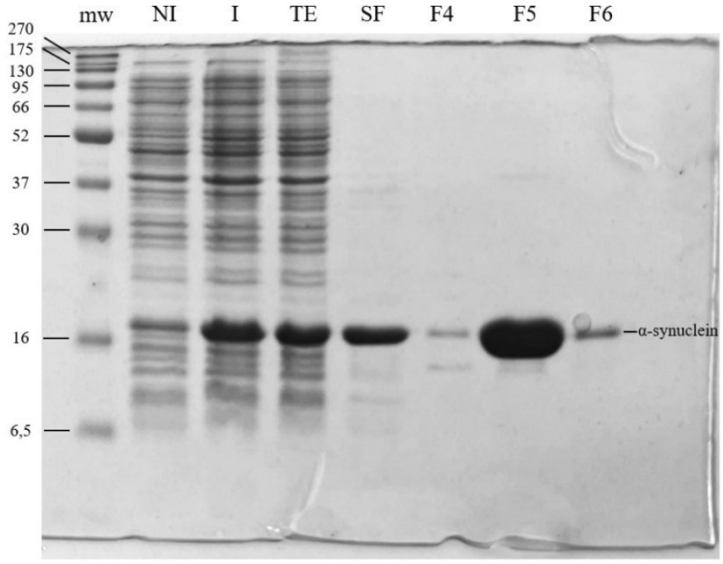

Figure 6.1 Electrophoretic run of aliquots retrieved during α-synuclein purification process: *mw = molecular weights ladder expressed in kDa, NI = not-induced, I = induced, TE = total extract, SF = soluble fraction, F4-6 = fractions obtained from the ionic exchange chromatography. Fraction 5 was selected for its highest α-synuclein protein content.*

In detail, the non-induced, induced, and total extract aliquots were centrifuged at 16,100 g, and the pellet obtained was resuspended with Sample Buffer 1X (SB = Tris 0.125 M, SDS 4%, glycerol 20%, bromophenol blue 0.002%). For the soluble fraction and the three fractions of interest (fractions four, five, and six), 1X SB and was added. Then, 5% of 2-mercaptoethanol was added to all samples, that were boiled for 3 minutes at 95°C. All samples were loaded on a vertical electrophoretic gel, composed of stacking gel (4% acrylamide) and running gel (15% acrylamide), and run in Running Buffer 1X (0.025MTris, 0.129Mglycine, 0.1% SDS at pH 8.3), first at 20 mA until the samples reached the running gel, then at 24 mA until the leading edge exited the gel. At this point, the gel was retrieved and stained with Coomassie blue for 20 minutes, then washed twice with a destaining solution containing 10% acetic acid and 25% ethanol. PD minitrap G25 GE columns were used to change the buffer of the fraction of interest. In particular, fraction five was loaded on the column, and the eluate was discarded, while α-synuclein was eluted using milliQ. The concentration of α-synuclein in the solution obtained was then measured with Nanodrop, and aliquoted to obtain 1 g or 0.5 g of protein. The aliquots obtained were therefore frozen at -20°C until lyophilization. After this, lyophilized α-synuclein was stored at -80°C.

6.1.2 PFF preparation

Lyophilized human wt α-synuclein was resuspended in sterile DPBS without $Ca^{2+}Mg^{2+}$ to reach a concentration of 5 mg/mL, and ultracentrifuged and ultracentrifuged at 220,000 *g* at 4°C for 45 min,

to remove contaminants or any amorphous aggregates. Then, the obtained supernatant was collected and the initial concentration of α-synuclein monomers obtained was measured at the Nanodrop, and total amount was calculated. To induce aggregation, solubilized α-synuclein monomers were placed in the thermomixer at 1000 rpm, at 37 °C. After 7 days, enriched-PFFs were isolated by the soluble part of the preparation by centrifugation at 16,100 g for 15 min. The supernatant obtained, containing both monomers and oligomers was then quantified using the bicinchoninic acid assay (BCA) assay following manufactory instruction. In this way, the amount of PFFs obtained was indirectly quantified, by measuring the amount of monomeric and oligomeric α-synuclein that remains in the supernatant and subtracting it to the total amount of α-synuclein before fibrillation, previously measured with Nanodrop. Then, PFFs were resuspended in sterile DPBS without $Ca^{2+}Mg^{2+}$ at the concentration of 5 mg/mL (500 µM) (Filippini et al., 2021a). A scheme of PFF preparation is illustrated in **Figure 6.2**

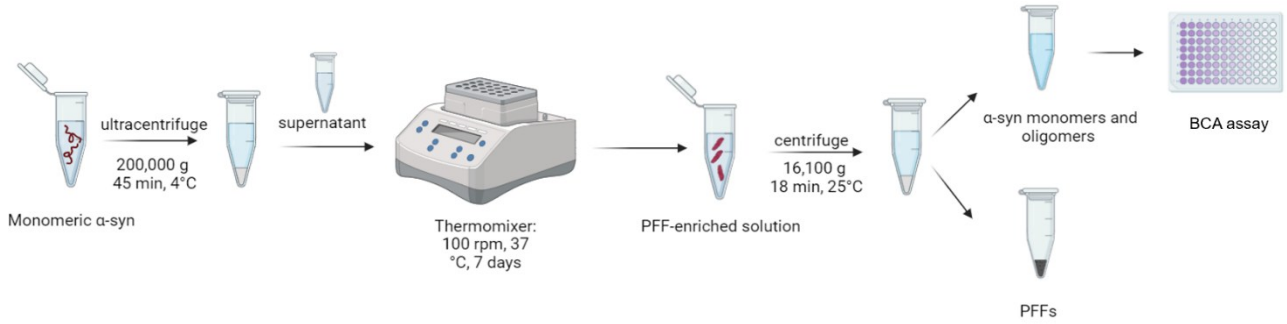

Figure 6.2 Schematic overview of PFF preparation. *Image created with Biorender.com*

6.1.3 Characterization of PFFs

Before proceeding with cell treatments, PFFs were characterized for both the presence of β-amyloid fibrils and their ultrastructure. The characterization was carried out by performing Thioflavin T assay (ThT) and transmission electron microscopy (TEM) analysis.

ThT assay

α-Synuclein PFF fibrillation was verified by ThT assay. ThT is a benzothiazole dye that enhances fluorescence when it binds to β-rich structures found in amyloid fibrils, such as PFFs (Filippini et al., 2021). When excited at 440 nm, it emits a signal at 482 nm, which is proportional to the concentration of PFFs. ThT assay was performed in a 96 well-plate; in detail, 10 µM α-synuclein PFFs and supernatant containing monomer were added to 25 µM of ThT in PBS to reach a final volume of 150 µL/well, mixed and incubated for 15 min at RT. 25 µM of ThT in PBS was used as a control measurement. All conditions were performed in triplicates. Fluorescence emission spectra were

recorded by EnSight Plate Reader (Perkin Elmer) spectrophotometer at 482 nm confirming the increased fluorescence of α-synuclein PFFs, containing amyloid-like fibrils, compared to monomers (**Figure 6.3, A**)

Transmission Electron Microscopy analysis

Transmission electron microscopy was carried out to observe the correct elongated ultrastructure of PFFs and the absence of bacterial contamination (**Figure 6.3, B**). In detail, 7 µL of 25 µM PFF protein sample was applied to glow discharged carbon formvar copper grids and allowed to air-dry. Then, negative staining was performed with 1% uranyl acetate, applied on the grids for 15 s. Electron microscopy images were captured using a Talos L120C microscopy at NOLIMITS facility, University of Milan.

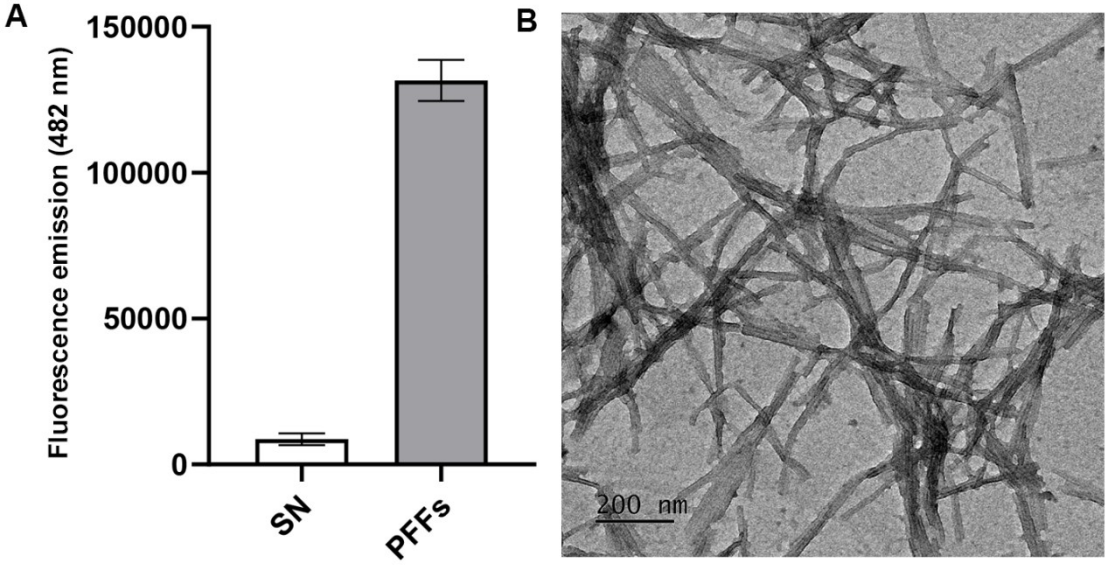

***Figure 6.3 Characterization of human α-synuclein PFFs**. (A) ThT assay performed on human α-synuclein PFFs shows high levels of ThT fluorescence signal compared to supernatant (SN) containing monomers. Data represents three independent PFF preparations. (**B**) Ultrastructure of human α-synuclein PFFs under the negative-stain transmission electron microscopy.*

6.1.4 PFFs conjugation to pH-rodoTM

PHrodo™ is a fluorescence dyes that shows little to no fluorescent signal at neutral pH and fluoresce brightly in the acidic environments of the cells, such as endosomes and lysosomes. Thus, it was conjugated to PFFs to enable the visualization of internalised PFFs as previously reported (Filippini et al., 2021).

PHrodo™ α-synuclein PFFs were generated by using pHrodo™ iFL Green Microscale Protein Labeling kit (Thermo Fisher Scientific, code number: P36015). In detail, α-synuclein PFFs, resuspended at a concentration of 1 mg/mL in PBSs with 100 mM sodium bicarbonate, were

incubated with pHrodo dissolved in 50 µL of DMSO for 90 min in the dark. pH Rodo α-synuclein PFFs, isolated by centrifugation at 16,100 g for 15 min, were washed with PBS twice to remove the un-conjugated pHrodo and resuspended in sterile PBS at the desire concentration (500 µM).

6.2 Poly-γ-glutamic acid

6.2.1 Natto γ-PGA

Lyophilized γ-PGA (Natto, Japan; Wako, 165-21364) of 193 kDa molecular weight was resuspended in sterile PBS to obtain a 2 mM stock solution. Then, the initial pH of 5.5 was adjusted to 7.4.

For the visualization in immunofluorescence, γ-PGA was conjugated with Fluorescein-5-isothiocyanate (FITC) (Merk, code number: 3326-32-7) as previously described (Khalil et al., 2018). In detail, γ-PGA was incubated with FITC with a 1:0.01 ratio in the dark at room temperature. After 90 min, the solution was eluted in a PD Spintrap^{TM} G-25 column using sterile PBS (Merk, code number: GE28-9180-04) to remove the unconjugated FITC. Then, FITC- γ-PGA was stored at -20°C until used.

6.2.2 YRSPEC γ-PGA

Lyophilized YRSPEC γ-PGA of 440 kDa molecular weight was purchased from YR Chemspec (China) (CAS No.25513-46-6; Batch Number: 211024-31). To reduce the initial molecular weight of the polymers, γ-PGA was dissolved in PBS at the concentration of 1mM. The stock solution was aliquoted in 1 mL Eppendorf tubes in equal volumes and subjected to gentle agitation (150 rpm) at 99 °C in a thermomixer. At pre-determined timepoint intervals, tubes were collected and placed at 4°C. Then, part of the γ-PGA obtained was analyzed to determine its MW (as described in section 6.2.4), while the remaining fraction was lyophilized and subsequently resuspended at 2 mM after MW determination. **Figure 6.4** illustrates the Hydrolytic degradation of commercial YRSPEC γ-PGA.

6.2.3 γ-PGA Molecular weight analysis

The analyses were conducted in collaboration with Barbara Mendrek at the Centre of Polymer and Carbon Materials, Polish Academy of Sciences.

The average molar mass and molar mass distributions of Natto and YRSPEC polymers were determined by gel permeation chromatography (GPC), using a differential refractive index detector (Δn-2010 RI WGE Dr. Bures, Berlin, Germany) in combination with a multiangle laser light

scattering detector (DAWN EOS, Wyatt Technologies, Santa Barbara, CA, USA). The chromatographic setup included a guard column (PSS SUPREMA 10 µm) followed by a series of analytical column: PSS SUPREMA Linear XL 10 µm and PSS SUPREMA Ultrahigh 10 µm (Polymer Standards Service, Mainz, Germany). A buffer containing 0.15M NaNO3, 0.01M EDTA, 0.02% NaN3, with pH = 6 adjusted using NaOH, was used as solvent with nominal flow rate of 0.5 mL/min. Measurements were done at 40 °C. ASTRA 4 software (Wyatt Technologies, Santa Barbara, CA, USA) was used to evaluate the results. All samples were filtered through the 0.45 µm PES syringe filters (Graphic Controls, DIA-Nielsen, Düren, Germany) before measurements. The refractive index increment of commercial γ-PGA was estimated in independent measurement in buffer using a differential refractive index detector. (SEC-3010 dn/dc WGE Dr. Bures, Berlin, Germany) and was equal 0.142 mL/g.

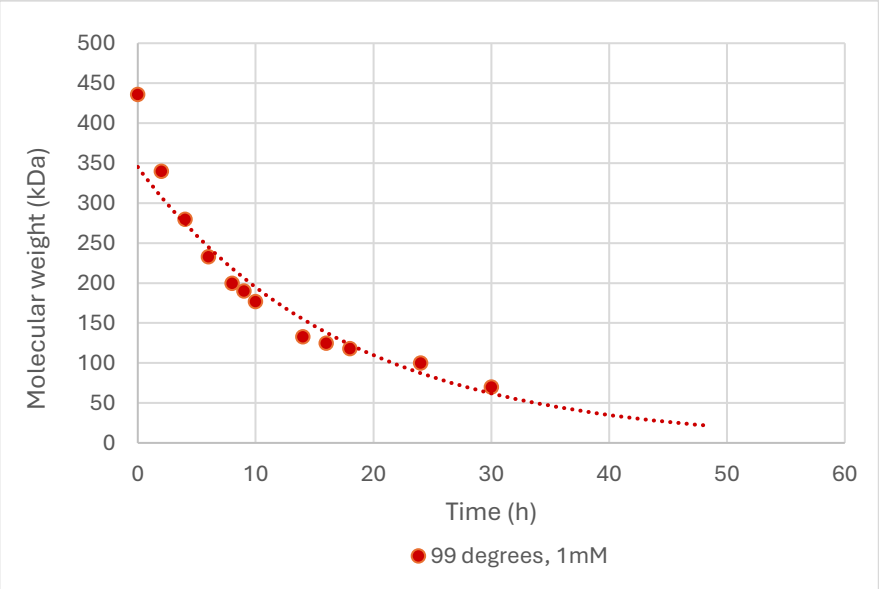

Time	MW (kDa)
0	440
2	340
4	280
6	233
8	200
9	190
10	177
15	133
16	125
18	118
24	100
30	70

Figure 6.4 Hydrolytic degradation of commercial YRSPEC γ-PGA. *γ-PGA of 440 kDa is placed in the thermomixer at 150 rpm, 99 °C. At different time point, γ-PGA samples were collected and analyzed with gel permeation chromatography. MW = molecular weights expressed in kDa.*

6.3 Cell culture

6.3.1 Primary cultures of mouse cortical astrocytes

Primary cultures of mouse astrocytes were derived from the spare cortex of postnatal Days 1–3 (P1-P3) C57BL/6J WT mice, as previously described (Boccazzi et al., 2014). Animal procedures were carried out in accordance with the guidelines of the care and use of laboratory animals established by Italian and European Directives (D. Lgs n° 2014/26, 2010/63/UE). Mice were anesthetized in ice for 10 min before their sacrifice, through decapitation. Heads were moved in a 10

cm Petri dish containing cold Dissection Buffer (DB: Hank Balanced Saline Solution, HBSS, to which was added 1% of Penicillin and Streptomycin antibiotic, Pen/Strep). The preparation was carried out under a horizontal fume hood and a stereomicroscope; skin and skull were removed with forceps starting from the cerebellum, the brain was extracted from the cavity and moved into a 6 cm Petri dish with cold DB to remove the cerebellum and the brain stem. Afterwards, the two hemispheres were separated along the midline fissure, and the meninges were peeled. Then, diencephalons, choroid plexus and hippocampus were removed. The obtained cortex was then transferred in tubes with cold DB. The remaining part of the procedure was then carried out under a vertical flow hood. The cortex, or pools of cortices (1 cortex for T25 flasks, and two cortices for T75 flasks), were placed in a 6-multiwell plate to mechanically break them into pieces using a scalpel and incubated for 15 min at 37 °C and 5% CO_2 with 2 mL of pre-warmed 0.05% trypsin-EDTA solution to enzymatically digest the tissues. Astrocyte Culture Medium (ACM = Dulbecco's Modified Eagle Medium, DMEM, with high glucose, to which is added 10% of Fetal Bovine Serum, FBS, and 1% Pen/Strep) was added to inhibit trypsin, and a homogeneous cell suspension was obtained by mechanical dissociation using a pipette. The suspension obtained was then centrifuged at 130 *g* at RT, first for 15 min, then for 5 min, and the pellet obtained was resuspended in 10 mL of ACM. The cell suspension was therefore seeded in an appropriate medium in T25 or T75 flasks, which were previously coated with poli-L-Lysine 10 µg/mL and maintained in culture at 37°C with 5% CO_2. The next day, the flasks were washed with Dulbecco's Phosphate Buffered Saline (DPBS) with $Ca^{2+}Mg^{2+}$ to remove any remaining tissue. The culture was kept until reaching confluence, changing 2/3 of the medium every 2 days to create a conditioned ACM medium.

Depending on the preparation, cells reached confluence after 7-10 days, after which the cells were shaken at 200 rpm for 2.5 hrs on an orbital shaker to remove microglia and oligodendrocytes, resulting in a pure astrocyte culture. A scheme of the process is illustrated in **Figure 6.5.**

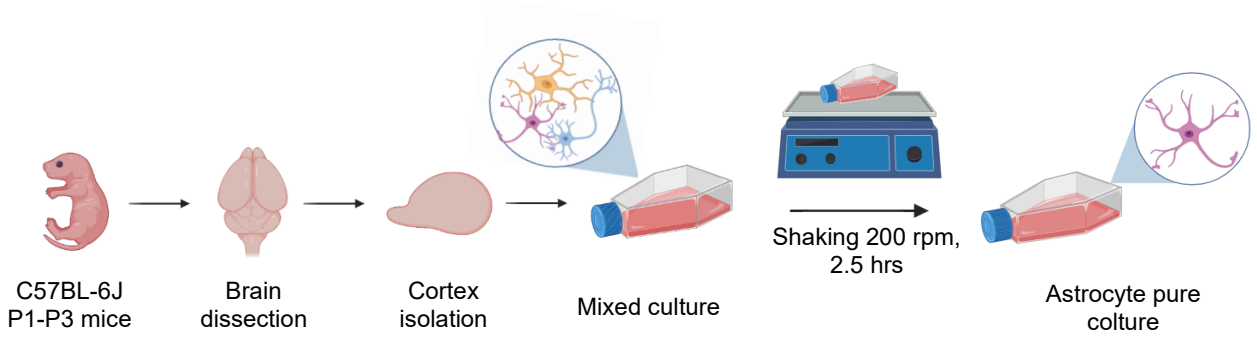

Figure 6.5 Overview of preparation of primary astrocytes from mouse cortex. *Image created with Biorender.com*

After shaking, primary astrocytes were plated for the following applications in ACM enriched with ROCK Inhibitor 1:500 (Ri = Y-27632 dihydrochloride (Merck, code number SCM075), a Rho-associated protein kinase inhibitor that prevents apoptosis.

6.3.2 Macrophage cell model

THP-1 cell line

THP-1 is a human leukemia monocytic cell line, which has been extensively used as a model to study monocyte/macrophage (Chanput et al., 2014). THP-1 cells (TIB-202, ATTC), which are floating cells, were maintained in T75 flasks with RPM1-1640 medium (Merk, code number: R7638), 10% FBS and 1% L-Glutamine–Pen/Strep (Merk, code number: G1146). Cells were subcultured 1:2 when the concentration reached 8 x10^5 cells/mL in the T75 flask. The medium was changed twice a week during subculture procedure.

THP-1 differentiation into macrophages

THP-1 cells were seeded at a density of 2,5 x10^4 cells/cm^2 and treated with phorbol 12-myristate 13-acetate (PMA) (Merck, code number: 524400**)** at 20 ng/ml concentration to induce their differentiation in M_0 macrophages. PMA was resuspended in DMSO at the concentration of 50 µg/ml and stored and -20 °C.

After 48h incubation, cells were washed with PBS twice to remove the excess of PMA and incubated for 24h with RPMI medium. This allows a rest period for complete differentiation before treatments. At this point, macrophages were treated with either PFFs or γ-PGA, or a combination of the two following PRE and POST treatment. A scheme of the process is illustrated in **Figure 6.6**.

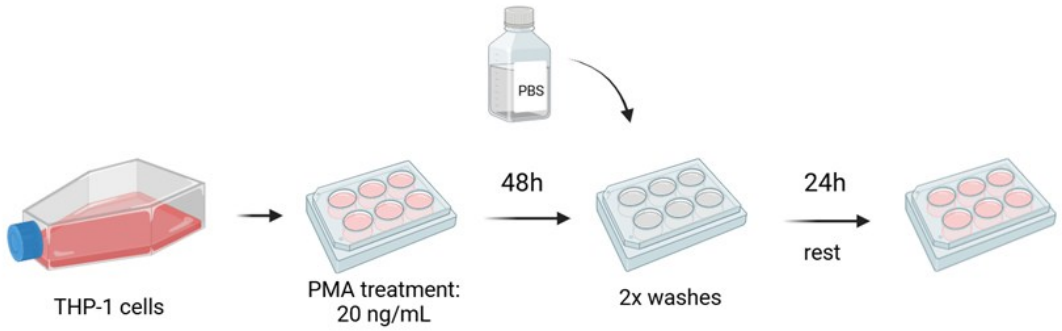

Figure 6.6 Schematic representation of THP-1 differentiation in macrophages. *Image created with Biorender.com*

6.3.3 Human neuroblastoma SK-N-SH cells

The human SK-N-SH cell line was established in 1970 from a bone marrow biopsy of a metastatic neuroblastoma in a 4-year-old female patient. These cells exhibit epithelial morphology and grow

adherently. Upon treatment with retinoic acid, they differentiate into a dopaminergic neuronal phenotype (Kovalevich & Langford, 2013).

Naïve SK-N-SH cells were cultured in complete medium composed of Dulbecco's modified Eagle's medium (DMEM) low glucose supplemented with 10% FBS, 1% L-glutamine, 1% penicillin/streptomycin, and 1% MEM Non-Essential Amino Acids Solution.

SNCA stable transfected SK-N-SH cells, gently provided by Arianna Bellucci (University of Brescia, Italy), were maintained in complete medium supplemented with 50 µg/mL Zeocin (Thermofisher, R25001) as selection antibody. Cells were maintained at 37°C in a 95% humidified incubator with 5% CO2. Medium was changed every 2 days.

SK-N-SH cells differentiation protocol

For differentiation, cells were seeded on 0.1 mg/mL Poly-L-Lysine coverslip glasses or well plate, at a density of $5x10^3$ cells/cm^2 and treated with 10 µM all-trans-retinoic acid (RA) for 6 days. RA was freshly supplemented daily. After 6 days of differentiation, cells were treated with γ-PGA (**Figure 6.7**) as described in section 4.3.4.

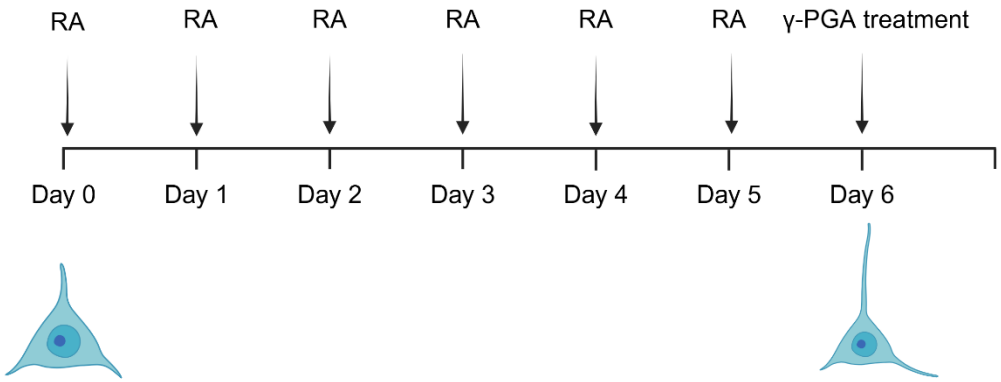

Figure 6.7 Schematic overview of SK-N-SH differentiation and treatment. *Image created with Biorender.com*

6.3.4 Cell treatments

Astrocytes were cultured onto poli-L-Lysine (10 µg/mL)-coated cover slips in a 24-well plate, in a poli-L-Lysine (10 µg/mL) coated 48-well plate or 6-well plate at a density of 2.1×10^4 cells/cm^2 for 24 hrs. THP-1 cells were differentiated in a 96-well plate and a 12-well plate while SK-N-SH cells were differentiated in a 96-well plate and onto poli-L-Lysine (10 µg/mL)-coated cover slips in a 24-well plate as previously described. Astrocytes and differentiated THP-1 cells were treated with 2 µM PFFs and γ-PGA at different concentrations in two experimental set up: *i)* the PRE treatment, in which γ-PGA is added before PFFs, and *ii)* the POST treatment, in which cells are first exposed to PFFs and then to γ-PGA. In both cases, PFF treatment was carried out for 18 hrs while γ-PGA is added 2 hrs

before or after PFFs. Syn^+ SK-N-SH cells were treated with γ-PGA at different concentrations and molecular weight for 24hrs.

6.4 Cell viability assay

3-(4,5-dimethylthiazol-2-yl)-2,5-diphenyl tetrazolium bromide (MTT) assay was performed to evaluate the cytotoxic the effect of γ-PGA and PFFs *in vitro*. Astrocytes were seeded in a poli-L-Lysine coated 48-well plate and cultured for 24 hrs. Then, cells were treated with PFF 2 μM, γ-PGA at different concentrations or a combination of the two following the PRE and POST treatment.

THP-1 and SK-N-SH cells were seeded in a 96-well plate, differentiated as previously described, and treated with either γ-PGA or PFF at different concentrations for 24 hrs.

At the end of the incubation period, cells were incubated with 0.5 mg/mL MTT solution (Merk, code number: M2128) for 3 hrs at 37°C. The formazan crystals that had formed were dissolved using a 0.1 M HCl, Triton X-100 in isopropanol solution. Then, the optical density (OD) was recorded at 570 nm using an Ensight plate reader (Perkin Elmer).

6.5 Immunofluorescence

Astrocytes were fixed with 4% paraformaldehyde for 10 min at RT and non-specific antigen were blocked with 1% BSA diluted in phosphate saline buffer 0.01 M (PBS) containing 0.3% Triton X-100 for 1 hr at RT. Primary antibodies were diluted in 1% BSA, 0.1% Triton X-100 in PBS; in detail, the following antibodies, incubated overnight at 4 ◦C, were used: mouse anti-α-synuclein 1:500 (Merck, code number: S5566), goat anti-Complement C3 1:500 (Life technologies, code number PA1-29715), chicken anti S100β 1:700 (Synaptic Systems, code number: 284006), and anti-LAMP1 1:500 (Abcam, code number ab24170). The following day, after three washes with PBS, cells were incubated for 45 min at RT with secondary antibodies diluted in 0.1 % BSA in PBS. The secondary antibodies used were: donkey anti-mouse Alexa 647 1:500 (Life technologies, code number: A32787), donkey anti-rabbit Alexa 488 (Life technologies, code number: A21206), donkey anti-goat Alexa 488 1:300, and donkey anti-chicken 568 1:300 (Jackson Immunoresearch, code numbers: 705-545-147, and 703-165-155, respectively). Later, after 3 washes with PBS, nuclei were stained using Hoechst 33342 1:5000 in PBS for 10 min at RT and coverslips were mounted using Mowiol®, DABCO®.

6.5.1 Image acquisition and 3D reconstruction

Images were acquired with a 20X objective, an oil-immersion 60X objective or a silicon-immersion 100X objective, using a Nikon spinning disk confocal microscope, equipped with CSI–W1 confocal

scanner unit, and a Nikon A1 laser scanning confocal microscope. Images were analysed using Fiji Software (ImageJ, USA).

For 3D visualization, images were imported into arivis Vision4D® 3.6.0 software (Zeiss Company). The region of interest (ROI) of 100X acquisitions was created using the "Transformation gallery > Crop" tool. The "Intensity threshold segmentation" pipeline was applied to reconstruct α-synuclein PFFs, S100β, and nuclei continuous staining. γ-PGA staining, which shows a pointy distribution, was reconstructed using "blob finder" pipeline.

6.6 Western blotting

Primary astrocytes, seeded in a 6-well plate, were lysed in Laemmli buffer. Equal amounts of protein (20 μg) were separated by SDS-PAGE and transferred overnight to a PVDF membrane (Immobilon®-P transfer membrane, Merck, code number IPFL00005). Membranes were blocked with 5 % BSA diluted in Tris-buffered saline (TBS: 20 mM Tris, 150 mM NaCl, pH 7.6) for 1 hr at RT and incubated overnight at 4 ◦C with the following primary antibodies diluted in TBS containing 0.1 % Tween-20 (TBST): LC3 1:1000 (SIGMA-Aldrich, code number: L8918), p62 1:2000 (SIGMA-Aldrich, code number P0067), GAPDH 1:5000 (SIGMA-Aldrich, code number: G8795). Then, membranes were washed with TBST for 3 times and incubated with secondary antibody donkey anti-rabbit Alexa 488 1:4000 (Invitrogen, code number A21206) for 1 hr at RT. After 3 washes, blots were visualized using iBright™ FL1500 (Life technologies) and band intensities were quantified using ImageJ software.

6.7 Enzyme linked immunosorbent assay (ELISA)

ELISA assay was performed in collaboration with Moira Paroni's group at the University of Milan (Department of Biosciences). For the quantification of cytokines released by astrocytes, supernatants of 200,000 cells were collected after 18 hrs of treatment as previously described, and analyzed for IL-6 (BioLegend, code number 431301), TNF-α (BioLegend, code number 430901), CXCL10 (BioTechne, code number DY466-05), and IL-1β (BioLegend, code number 432601) by ELISA according to the manufacturer's instructions. Then, ELISA plates were read on microplate reader (SAFAS MP96), and data were analyzed with Prism software.

6.8 Flow cytometry

Flow cytometry is a method for detecting and measuring the physical and chemical properties of a population of cells or particles. In this technique, a sample containing these cells or particles is

suspended in a fluid and introduced into the flow cytometer. As the sample passes through the instrument, individual cells or particles are illuminated by a laser, enabling the analysis of various parameters, including size, granularity, and fluorescence intensity. Flow cytometry was carried out to confirm THP-1 differentiation in M_0 macrophages and to characterized PMA primed-THP-1 cell population as M1 and M2 macrophages following PFF and γ-PGA treatments. Cells were plated in a 12-well plate at the density of 2.5 x 10^5/well. After PMA differentiation, cells were treated with PFFs and γ-PGA as described in section 6.3.4. At the end of the treatment, cells were washed twice in PBS with Ca^{2+}/Mg^{2+} and detached using a cell scraper. Afterwards, cells were centrifuged at 1,000 rpm for 5 min and incubated for 20 min in BSA 1% diluted in PBS to block non-specific antigens. Then, cells were centrifuges again, resuspended in BSA 1% diluted in PBS and primary antibodies (**Table 1**) and Isotype controls were incubated for 45 min. Subsequentially, cells were washed twice with PBS, fixed with 4% paraformaldehyde and analyzed using CytoFLEX flow cytometer. Analyses were performed using CytExpert software.

Antigen	*host*	*fluorophore*	*Code number*	*dilution*
CD68	mouse	FITC	BioLengend (333805)	5 µL/1 x 10^6 cells
CD14	mouse	PE	BD Pharmingen™(555398)	5 µL/1 x 10^6 cells
CD86	mouse	PerCP	Invitrogen (MA1-10297)	10 µL/1 x 10^6 cells
CD80	mouse	Brillanti Violet 785	BioLengend (305238)	5 µL/1 x 10^6 cells
HLA-DR	mouse	PE	Abcam (AB64676)	5 µL/1 x 10^6 cells
CD163	mouse	FITC	BioLengend (333618)	5 µL/1 x 10^6 cells
CD206	mouse	PE	Invitrogen (12-2069-42)	5 µL/1 x 10^6 cells

Table 1 Antibodies used for flow cytometry

6.9 Cellular Reactive Oxygen Species (ROS) assay

ROS assay is a high-sensitive technique that allows the detection of ROS in biological samples. ROS consists of various reactive molecules and free radicals that originate from molecular oxygen, leading to damage in DNA and RNA, as well as protein oxidation and lipid peroxidation. ROS assay was carried out to evaluate the impact of PFFs and γ-PGA on THP-1 cells oxidative stress using a fluorescence based commercial kit (Enzo Biochem, code number: ENZ-51010). In detail, increased fluorescence of the sample indicates increased ROS production.

TPH-1 cells were seeded in a 96 well plate and exposed to PMA for macrophages differentiation as described in section 6.3.2. After 48 hrs, cells were washed and let rest for 24 hrs. The day after,

macrophages were treated with PFFs and γ-PGA. At this point, freshly medium was added containing the 1mM ROS detection reagent and cells were incubated for 1h at 37°C in the dark. Positive and negative controls were also run. For positive control, cells were incubated with medium containing the ROS detection reagent and 300 μM ROS inducer (Pyocyanin) 30 min before reading the plate and maintained under these conditions until fluorescence measurement. For negative control, cells were pre-treated with 5 mM ROS inhibitor for 30 min, followed by incubation with the ROS detection reagent containing the ROS inducer (NAC (N-acetyl-l-cysteine).

Fluorescence emission spectra were recorded by an EnSight Plate Reader (Perkin Elmer) spectrophotometer at 520 nm upon excitation at 488 nm. Wells containing only medium with ROS detection reagent was read as background fluorescence reference.

6.10 Real-time quacking induced conversion assay (RT-QuIC)

RT-QuIC assay studies were performed to evaluate the potential effect of γ-PGA on α-synuclein aggregation. Indeed, RT-QuIC is an *in vitro* technique that relies on prion seed-induced misfolding and aggregation of a recombinant protein substrate, with the process accelerated by alternating cycles of shaking and resting in fluorescence plate readers (Schmitz et al., 2016). In detail, the recombinant prion protein, in this case α-synuclein, is incubated with ThT and silica beads at 42°C in constant shaking to induce aggregation. Aggregation is monitored by measuring ThT fluorescence, that binds to β-sheet structure of α-synuclein oligomers and fibrils and increases in fluorescence.

The experiments, carried out in collaboration with Fabio Moda's group at the Istituto Neurologico Carlo Besta, were performed in a black 384-well optical flat bottom plate (Thermo Scientific). Each well was filled with the reaction mix composed of 170 mM NaCl, 40 mM PBS pH 8, 10 μM Thioflavin-T (ThT), 7 μM α-synuclein with or without the presence of γ-PGA at three different concentrations (2 μM, 20 μM and 200 μM), reaching a final reaction volume of 50 μL. Two silica beads (0.8 mm) were added to each well to sustain α-synuclein aggregation. The capacity of γ-PGA to undergo self-assembly was evaluated.

Samples collected following incubation with 27.5 μM of γ-PGA, were analyzed by TEM as described in section 4.2.3.

Finally, 7 μM PFFs were pre-incubated with 200 μM γ-PGA for 2 h at 37°C to assess the effect of γ-PGA treated PFFs on α-synuclein aggregation compared to untreated PFFs. Every experimental condition was analyzed in quadruplicate to ensure reliability. The plates were inserted into a FLUOstar CLARIOSTAR microplate reader (BMG Labtech) and subjected to alternating cycles of shaking (1 min, 600 rpm, single orbital) and incubation (14 min at 42 °C). Fluorescence readings (480 nm) were taken every 15 min (30 flashes per well at 450 nm). The mean fluorescence values

obtained from the four replicates of each sample were plotted on a graph against time. A schematic overview of the process is represented in **figure 6.8.**

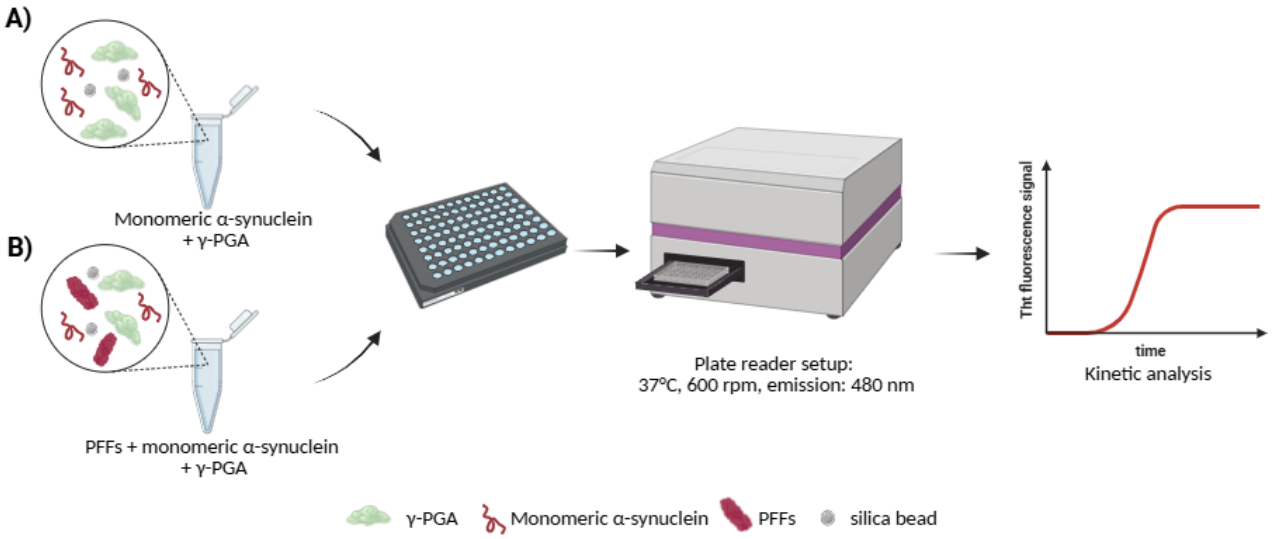

Figure 6.8 Schematic representation of RT-QuIC assay. *Image created with Biorender.com. γ-PGA is incubated together with recombinant monomeric α-synuclein and silica beads (**A**) or PFFs, monomeric α-synuclein and silica beads (**B**) to evaluate the potential effect of γ-PGA on α-synuclein aggregation. image created with Biorender.com*

6.11 Proximity ligation Assay (PLA)

PLA assay was performed to quantify the presence of α-synuclein oligomers in Naïve and α-synuclein overexpressing SK-N-SH (Syn^+) cells compared to γ-PGA treated Syn^+ cells. PLA experiments were conducted using the Duolink® *in-situ* PLA kit (Merck, St Louis, USA), according to the manufacturer's instructions.

Frist, the PLA MINUS and PLUS probes were conjugated to rabbit α-synuclein S3062 antibody as previously described (Mazzetti et al., 2020).

SK-N-SH were fixed with 4% paraformaldehyde and non-specific antigen were blocked with 1% BSA diluted in PBS and containing 0.1% Triton X-100 for 1 h at RT for cell permeabilization. Then, cells were incubated with Duolink® PLA PLUS and MINUS oligonucleotide probes conjugated to rabbit anti-α-synuclein 1:100 (Merck, SynS3062), and mouse anti-α-tubulin (Sigma-Aldrich, code number T6072, 1:1000) in PLA diluent, for 2 hrs at 37 °C. Afterwards, cells were shortly washed three times with PBS, and incubated with ligation solution containing Duolink® ligase (1:40) and Duolink® ligation solution (1:5) in milliQ H_2O for 1 h at 37°C. After ligation, cells were shortly washed and incubated with Duolink® polymerase (1:80), Duolink® green amplification reagent (1:5), and the secondary antibodies donkey anti-mouse Rhodamine Red™ 1:500 (Jackson Immunoresearch, code numbers 715-295-151) in milliQ H_2O for 2 hrs at 37°C. After two short

washes, nuclei were stained using Hoechst 33342 1:5000 in PBS for 10 min at RT and coverslips were mounted using Mowiol®, DABCO®. Images were collected using a Nikon spinning disk confocal microscope, equipped with CSI–W1 confocal scanner unit, using an oil-immersion 60X objective. Images were analysed using Fiji Software (ImageJ, USA). In detail, the Area of PLA puncta was analysed using the same threshold for each image and normalized on the number of cells.

6.12 Statistical analysis

Statistical analyses were conducted using GraphPad Prism 8 software (San Diego, CA, USA). All quantitative data are expressed as mean ± SEM and represent at least three independent sets of experiments. Data were tested for normal distribution by Shapiro-Wilk and D'Agostino-Pearson test. To compare two experimental groups, paired t-test was performed. Parametric or non-parametric One-way ANOVA was used for multiple comparison of data of more than two experimental groups.

To analyse the area covered by PFFs, and the MFI of HLADR and CD80 signal, data were normalised on control and analysed by One sample t. Significance was established at p value < 0.05.

References

Ahmed, I., Tamouza, R., Delord, M., Krishnamoorthy, R., Tzourio, C., Mulot, C., Nacfer, M., Lambert, J. C., Beaune, P., Laurent-Puig, P., Loriot, M. A., Charron, D., & Elbaz, A. (2012). Association between Parkinson's disease and the HLA-DRB1 locus. Movement Disorders, 27(9), 1104–1110. https://doi.org/10.1002/mds.25035

Ahn, H., Kang, S. G., Yoon, S. Il, Kim, P. H., Kim, D., & Lee, G. S. (2018). Poly-gamma-glutamic acid from Bacillus subtilis upregulates pro-inflammatory cytokines while inhibiting NLRP3, NLRC4 and AIM2 inflammasome activation. Cellular and Molecular Immunology, 15(2), 111–119. https://doi.org/10.1038/cmi.2016.13

Alam, P., Bousset, L., Melki, R., & Otzen, D. E. (2019). α-synuclein oligomers and fibrils: a spectrum of species, a spectrum of toxicities. Journal of Neurochemistry, 150(5), 522–534. https://doi.org/10.1111/JNC.14808

Alim, M. A., Ma, Q. L., Takeda, K., Aizawa, T., Matsubara, M., Nakamura, M., Asada, A., Saito, T., Kaji, H., Yoshii, M., Hisanaga, S., & Uéda, K. (2004). Demonstration of a role for α-synuclein as a functional microtubule-associated protein. Journal of Alzheimer's Disease, 6(4), 435–442. https://doi.org/10.3233/JAD-2004-6412

Ardah, M. T., Paleologou, K. E., Lv, G., Menon, S. A., Abul Khair, S. B., Lu, J. H., Safieh-Garabedian, B., Al-Hayani, A. A., Eliezer, D., Li, M., & El-Agnaf, O. M. A. (2016). Ginsenoside RB1 inhibits fibrillation and toxicity of alpha-synuclein and disaggregates preformed fibrils. Neurobiology of Disease, 74, 89. https://doi.org/10.1016/J.NBD.2014.11.007

Armstrong, M. J., & Okun, M. S. (2020). Diagnosis and Treatment of Parkinson Disease: A Review. JAMA - Journal of the American Medical Association, 323(6), 548–560. https://doi.org/10.1001/JAMA.2019.22360

Ascherio, A., & Schwarzschild, M. A. (2016). The epidemiology of Parkinson's disease: risk factors and prevention. The Lancet Neurology, 15(12), 1257–1272. https://doi.org/10.1016/S1474-4422(16)30230-7

Baden, P., Perez, M. J., Raji, H., Bertoli, F., Kalb, S., Illescas, M., Spanos, F., Giuliano, C., Calogero, A. M., Oldrati, M., Hebestreit, H., Cappelletti, G., Brockmann, K., Gasser, T., Schapira, A. H. V., Ugalde, C., & Deleidi, M. (2023). Glucocerebrosidase is imported into mitochondria and preserves complex I integrity and energy metabolism. Nature Communications, 14(1). https://doi.org/10.1038/s41467-023-37454-4

Balestrino, R., & Schapira, A. H. V. (2020). Parkinson disease. European Journal of Neurology, 27(1), 27–42. https://doi.org/10.1111/ENE.14108

Balogun-Agbaje, O. A., Odeniyi, O. A., & Odeniyi, M. A. (2021). Drug delivery applications of poly-γ-glutamic acid. Future Journal of Pharmaceutical Sciences, 7(1). https://doi.org/10.1186/s43094-021-00280-w

Basellini, M. J., Granadino-Roldán, J. M., Torres-Ortega, P. V., Simmini, G., Rubio-Martinez, J., Marin, S., Cappelletti, G., Cascante, M., & Cañuelo, A. (2025). Oleuropein Aglycone, an Olive Polyphenol, Influences Alpha-Synuclein Aggregation and Exerts Neuroprotective Effects in Different Parkinson's Disease Models. Molecular Neurobiology, 1–18. https://doi.org/10.1007/S12035-025-05208-6/TABLES/4

Basellini, M. J., Kothuis, J. M., Comincini, A., Pezzoli, G., Cappelletti, G., & Mazzetti, S. (2023). Pathological Pathways and Alpha-Synuclein in Parkinson's Disease: A View from the Periphery. In Frontiers in Bioscience - Landmark (Vol. 28, Issue 2). IMR Press Limited. https://doi.org/10.31083/j.fbl2802033

Bendor, J. T., Logan, T. P., & Edwards, R. H. (2013). The function of α-synuclein. Neuron, 79(6), 1044–1066. https://doi.org/10.1016/j.neuron.2013.09.004

Ben-Joseph, A., Marshall, C. R., Lees, A. J., & Noyce, A. J. (2020). Ethnic Variation in the Manifestation of Parkinson's Disease: A Narrative Review. Journal of Parkinson's Disease, 10(1), 31. https://doi.org/10.3233/JPD-191763

Ben-Shlomo, Y., Darweesh, S., Llibre-Guerra, J., Marras, C., San Luciano, M., & Tanner, C. (2024). The epidemiology of Parkinson's disease. The Lancet, 403(10423), 283–292. https://doi.org/10.1016/S0140-6736(23)01419-8

Bhat, A. R., Irorere, V. U., Bartlett, T., Hill, D., Kedia, G., Morris, M. R., Charalampopoulos, D., & Radecka, I. (2013). Bacillus subtilis natto: a non-toxic source of poly-γ-glutamic acid that could be used as a cryoprotectant for probiotic bacteria. AMB Express, 3(1), 1–9. https://doi.org/10.1186/2191-0855-3-36

Boccazzi, M., Rolando, C., Abbracchio, M. P., Buffo, A., & Ceruti, S. (2014). Purines regulate adult brain subventricular zone cell functions: Contribution of reactive astrocytes. GLIA, 62(3), 428–439. https://doi.org/10.1002/glia.22614

Booth, H. D. E., Hirst, W. D., & Wade-Martins, R. (2017). The Role of Astrocyte Dysfunction in Parkinson's Disease Pathogenesis. Trends in Neurosciences, 40(6), 358–370. https://doi.org/10.1016/j.tins.2017.04.001

Braak, H., Del Tredici, K., Rüb, U., De Vos, R. A. I., Jansen Steur, E. N. H., & Braak, E. (2003). Staging of brain pathology related to sporadic Parkinson's disease. Neurobiology of Aging, 24(2), 197–211. https://doi.org/10.1016/S0197-4580(02)00065-9

Braak, H., Sastre, M., & Del Tredici, K. (2007). Development of α-synuclein immunoreactive astrocytes in the forebrain parallels stages of intraneuronal pathology in sporadic Parkinson's disease. Acta Neuropathologica, 114(3), 231–241. https://doi.org/10.1007/S00401-007-0244-3/FIGURES/4

Brundin, P., & Melki, R. (2017). Prying into the Prion Hypothesis for Parkinson's Disease. The Journal of Neuroscience, 37(41), 9808–9818. https://doi.org/10.1523/JNEUROSCI.1788-16.2017

Cai, M., Han, Y., Zheng, X., Xue, B., Zhang, X., Mahmut, Z., Wang, Y., Dong, B., Zhang, C., Gao, D., & Sun, J. (2023). Synthesis of Poly-γ-Glutamic Acid and Its Application in Biomedical Materials. Materials, 17(1), 15. https://doi.org/10.3390/MA17010015

Calogero, A. M., Basellini, M. J., Isilgan, H. B., Longhena, F., Bellucci, A., Mazzetti, S., Rolando, C., Pezzoli, G., & Cappelletti, G. (2023). Acetylated α-Tubulin and α-Synuclein: Physiological Interplay and Contribution to α-Synuclein Oligomerization. International Journal of Molecular Sciences, 24(15). https://doi.org/10.3390/IJMS241512287

Canton, M., Sánchez-Rodríguez, R., Spera, I., Venegas, F. C., Favia, M., Viola, A., & Castegna, A. (2021). Reactive Oxygen Species in Macrophages: Sources and Targets. Frontiers in Immunology, 12. https://doi.org/10.3389/FIMMU.2021.734229

Cartelli, D., Aliverti, A., Barbiroli, A., Santambrogio, C., Ragg, E. M., Casagrande, F. V. M., Cantele, F., Beltramone, S., Marangon, J., De Gregorio, C., Pandini, V., Emanuele, M., Chieregatti, E., Pieraccini, S., Holmqvist, S., Bubacco, L., Roybon, L., Pezzoli, G., Grandori, R., … Cappelletti, G. (2016). α-Synuclein is a Novel Microtubule Dynamase. Scientific Reports, 6. https://doi.org/10.1038/srep33289

Cascella, R., Bigi, A., Cremades, N., & Cecchi, C. (2022). Effects of oligomer toxicity, fibril toxicity and fibril spreading in synucleinopathies. Cellular and Molecular Life Sciences, 79(3), 174. https://doi.org/10.1007/s00018-022-04166-9

Chanput, W., Mes, J. J., & Wichers, H. J. (2014). THP-1 cell line: An in vitro cell model for immune modulation approach. International Immunopharmacology, 23(1), 37–45. https://doi.org/10.1016/J.INTIMP.2014.08.002

Chedid, J., Labrador-Garrido, A., Zhong, S., Gao, J., Zhao, Y., Perera, G., Kim, W. S., Halliday, G. M., & Dzamko, N. (2022). A small molecule toll-like receptor antagonist rescues α-synuclein fibril pathology. The Journal of Biological Chemistry, 298(8). https://doi.org/10.1016/J.JBC.2022.102260

Cheng, X. T., Xie, Y. X., Zhou, B., Huang, N., Farfel-Becker, T., & Sheng, Z. H. (2018). Revisiting LAMP1 as a marker for degradative autophagy-lysosomal organelles in the nervous system. Autophagy, 14(8), 1472–1474. https://doi.org/10.1080/15548627.2018.1482147

Chi, X., Yin, S., Sun, Y., Kou, L., Zou, W., Wang, Y., Jin, Z., Wang, T., & Xia, Y. (2025). Astrocyte-neuron communication through the complement C3-C3aR pathway in Parkinson's disease. Brain, Behavior, and Immunity, 123, 229–243. https://doi.org/10.1016/J.BBI.2024.09.022

Choi, B. K., Choi, M. G., Kim, J. Y., Yang, Y., Lai, Y., Kweon, D. H., Lee, N. K., & Shin, Y. K. (2013). Large α-synuclein oligomers inhibit neuronal SNARE-mediated vesicle docking. Proceedings of the National Academy of Sciences of the United States of America, 110(10), 4087–4092. https://doi.org/10.1073/pnas.1218424110

Chou, T. W., Chang, N. P., Krishnagiri, M., Patel, A. P., Lindman, M., Angel, J. P., Kung, P. L., Atkins, C., & Daniels, B. P. (2021a). Fibrillar α-synuclein induces neurotoxic astrocyte activation via RIP kinase signaling and NF-κB. Cell Death & Disease 2021 12:8, 12(8), 1–11. https://doi.org/10.1038/s41419-021-04049-0

Chung, H. K., Ho, H. A., Pérez-Acuña, D., & Lee, S. J. (2019). Modeling α-Synuclein Propagation with Preformed Fibril Injections. Journal of Movement Disorders, 12(3), 139–151. https://doi.org/10.14802/JMD.19046

Colla, E., Jensen, P. H., Pletnikova, O., Troncoso, J. C., Glabe, C., & Lee, M. K. (2012). Accumulation of toxic α-synuclein oligomer within endoplasmic reticulum occurs in α-synucleinopathy in vivo. Journal of Neuroscience, 32(10), 3301–3305. https://doi.org/10.1523/JNEUROSCI.5368-11.2012

Colombo, E., & Farina, C. (2016). Astrocytes: Key Regulators of Neuroinflammation. Trends in Immunology, 37(9), 608–620. https://doi.org/10.1016/J.IT.2016.06.006

Davaatseren, M., Hwang, J. T., Park, J. H., Kim, M. S., Wang, S., & Sung, M. J. (2013). Poly-γ-Glutamic Acid Attenuates Angiogenesis and Inflammation in Experimental Colitis. Mediators of Inflammation, 2013(1), 982383. https://doi.org/10.1155/2013/982383

Day, J. O., & Mullin, S. (2021). The genetics of parkinson's disease and implications for clinical practice. Genes, 12(7). https://doi.org/10.3390/GENES12071006

Dehay, B., Bové, J., Rodríguez-Muela, N., Perier, C., Recasens, A., Boya, P., & Vila, M. (2010). Pathogenic lysosomal depletion in Parkinson's disease. Journal of Neuroscience, 30(37), 12535–12544. https://doi.org/10.1523/JNEUROSCI.1920-10.2010

Dieriks, B. V., Park, T. I. H., Fourie, C., Faull, R. L. M., Dragunow, M., & Curtis, M. A. (2017). α-synuclein transfer through tunneling nanotubes occurs in SH-SY5Y cells and primary brain pericytes from Parkinson's disease patients. Scientific Reports 2017 7:1, 7(1), 1–11. https://doi.org/10.1038/srep42984

Donadio, V. (2019). Skin nerve α-synuclein deposits in Parkinson's disease and other synucleinopathies: a review. Clinical Autonoic Research, 29(6), 577–585. https://doi.org/10.1007/S10286-018-0581-4

Du, X. Y., Xie, X. X., & Liu, R. T. (2020). The role of α-synuclein oligomers in parkinson's disease. In International Journal of Molecular Sciences (Vol. 21, Issue 22, pp. 1–17). MDPI AG. https://doi.org/10.3390/ijms21228645

Earls, R. H., Menees, K. B., Chung, J., Barber, J., Gutekunst, C. A., Hazim, M. G., & Lee, J. K. (2019). Intrastriatal injection of preformed alpha-synuclein fibrils alters central and peripheral immune cell profiles in non-transgenic mice. Journal of Neuroinflammation, 16(1). https://doi.org/10.1186/S12974-019-1636-8

Fan, T. S., Liu, S. C. H., & Wu, R. M. (2021). Alpha-synuclein and cognitive decline in parkinson disease. Life, 11(11). https://doi.org/10.3390/LIFE11111239

Filippini, A., Gennarelli, M., & Russo, I. (2019). α-Synuclein and Glia in Parkinson's Disease: A Beneficial or a Detrimental Duet for the Endo-Lysosomal System? Cellular and Molecular Neurobiology, 39(2), 161–168. https://doi.org/10.1007/S10571-019-00649-9

Filippini, A., Mutti, V., Faustini, G., Longhena, F., Ramazzina, I., Rizzi, F., Kaganovich, A., Roosen, D. A., Landeck, N., Duffy, M., Tessari, I., Bono, F., Fiorentini, C., Greggio, E., Bubacco, L., Bellucci, A., Missale, M., Cookson, M. R., Gennarelli, M., & Russo, I. (2021). Extracellular clusterin limits the uptake of α-synuclein fibrils by murine and human astrocytes. Glia, 69(3), 681. https://doi.org/10.1002/GLIA.23920

Fisher, T. M., & Liddelow, S. A. (2024). Emerging roles of astrocytes as immune effectors in the central nervous system. Trends in Immunology, 45(10), 824–836. https://doi.org/10.1016/J.IT.2024.08.008

Flavin, W. P., Bousset, L., Green, Z. C., Chu, Y., Skarpathiotis, S., Chaney, M. J., Kordower, J. H., Melki, R., & Campbell, E. M. (2017). Endocytic vesicle rupture is a conserved mechanism of cellular invasion by amyloid proteins. Acta Neuropathologica, 134(4), 629–653. https://doi.org/10.1007/S00401-017-1722-X

Freyssin, A., Page, G., Fauconneau, B., & Rioux Bilan, A. (2018). Natural polyphenols effects on protein aggregates in Alzheimer's and Parkinson's prion-like diseases. Neural Regeneration Research, 13(6), 955–961. https://doi.org/10.4103/1673-5374.233432

Frosch, M., Amann, L., & Prinz, M. (2023). CNS-associated macrophages shape the inflammatory response in a mouse model of Parkinson's disease Check for updates. https://doi.org/10.1038/s41467-023-39061-9

Fusco, G., Chen, S. W., Williamson, P. T. F., Cascella, R., Perni, M., Jarvis, J. A., Cecchi, C., Vendruscolo, M., Chiti, F., Cremades, N., Ying, L., Dobson, C. M., & Simone, A. De. (2017). Structural basis of membrane disruption and cellular toxicity by a-synuclein oligomers. Science, 358(6369), 1440–1443. https://doi.org/10.1126/science.aan6160

Galvan, A., & Wichmann, T. (2008). Pathophysiology of Parkinsonism. Clinical Neurophysiology, 119(7), 1459–1474. https://doi.org/10.1016/J.CLINPH.2008.03.017

Gantzel, R. H., Kjær, M. B., Laursen, T. L., Kazankov, K., George, J., Møller, H. J., & Grønbæk, H. (2021). Macrophage Activation Markers, Soluble CD163 and Mannose Receptor, in Liver Fibrosis. Frontiers in Medicine, 7. https://doi.org/10.3389/FMED.2020.615599

Gao, J., Perera, G., Bhadbhade, M., Halliday, G. M., & Dzamko, N. (2019). Autophagy activation promotes clearance of α-synuclein inclusions in fibril-seeded human neural cells. Journal of Biological Chemistry, 294(39), 14241–14256. https://doi.org/10.1074/jbc.RA119.008733

Gibbons, C. H., Levine, T., Adler, C., Bellaire, B., Wang, N., Stohl, J., Agarwal, P., Aldridge, G. M., Barboi, A., Evidente, V. G. H., Galasko, D., Geschwind, M. D., Gonzalez-Duarte, A., Gil, R., Gudesblatt, M., Isaacson, S. H., Kaufmann, H., Khemani, P., Kumar, R., … Freeman, R. (2024). Skin Biopsy Detection of Phosphorylated α-Synuclein in Patients with Synucleinopathies. JAMA, 331(15), 1298–1306. https://doi.org/10.1001/JAMA.2024.0792

Giusti, V., Kaur, G., Giusto, E., & Civiero, L. (2024). Brain clearance of protein aggregates: a close-up on astrocytes. In Molecular Neurodegeneration (Vol. 19, Issue 1). BioMed Central Ltd. https://doi.org/10.1186/s13024-024-00703-1

Goedert, M., Jakes, R., & Spillantini, M. G. (2017). The Synucleinopathies: Twenty Years On. Journal of Parkinson's Disease, 7(s1), S51–S69. https://doi.org/10.3233/JPD-179005

Gregersen, E., Betzer, C., Kim, W. S., Kovacs, G., Reimer, L., Halliday, G. M., Thiel, S., & Jensen, P. H. (2021). Alpha-synuclein activates the classical complement pathway and mediates complement-dependent cell toxicity. Journal of Neuroinflammation, 18(1). https://doi.org/10.1186/S12974-021-02225-9

Gu, X. L., Long, C. X., Sun, L., Xie, C., Lin, X., & Cai, H. (2010). Astrocytic expression of Parkinson's disease-related A53T -synuclein causes neurodegeneration in mice. Molecular Brain, 3(1), 1–16. https://doi.org/10.1186/1756-6606-3-12/figures/8

Guardia-Laguarta, C., Area-Gomez, E., Rub, C., Liu, Y., Magrane, J., Becker, D., Voos, W., Schon, E. A., & Przedborski, S. (2014). -Synuclein Is Localized to Mitochondria-Associated ER Membranes. Journal of Neuroscience, 34(1), 249–259. https://doi.org/10.1523/JNEUROSCI.2507-13.2014

Guiney, S. J., Adlard, P. A., Lei, P., Mawal, C. H., Bush, A. I., Finkelstein, D. I., & Ayton, S. (2020). Fibrillar α-synuclein toxicity depends on functional lysosomes. The Journal of Biological Chemistry, 295(51), 17497. https://doi.org/10.1074/JBC.RA120.013428

Gupta, J., & Sashidhara, K. V. (2023). Recent advances in natural products targeting α-synuclein aggregation or clearance in Parkinson's disease. European Journal of Medicinal Chemistry Reports, 9, 100114. https://doi.org/10.1016/J.EJMCR.2023.100114

Hamza, T. H., Zabetian, C. P., Tenesa, A., Laederach, A., Montimurro, J., Yearout, D., Kay, D. M., Doheny, K. F., Paschall, J., Pugh, E., Kusel, V. I., Collura, R., Roberts, J., Griffith, A., Samii, A., Scott, W. K., Nutt, J., Factor, S. A., & Payami, H. (2010). Common genetic variation in the HLA region is associated with late-onset sporadic Parkinson's disease. Nature Genetics, 42(9), 781. https://doi.org/10.1038/ng.642

Harms, A. S., Delic, V., Thome, A. D., Bryant, N., Liu, Z., Chandra, S., Jurkuvenaite, A., & West, A. B. (2017). α-Synuclein fibrils recruit peripheral immune cells in the rat brain prior to neurodegeneration. Acta Neuropathologica Communications, 5(1), 85. https://doi.org/10.1186/S40478-017-0494-9

Helm, O., Held-Feindt, J., Schäfer, H., & Sebens, S. (2014). M1 and M2: there is no "good" and "bad"—How macrophages promote malignancy-associated features in tumorigenesis. Oncoimmunology, 3(7), e946818. https://doi.org/10.4161/21624011.2014.946818

Hindeya Gebreyesus, H., & Gebrehiwot Gebremichael, T. (2020). The Potential Role of Astrocytes in Parkinson's Disease (PD). In Medical sciences (Basel, Switzerland) (Vol. 8, Issue 1). NLM (Medline). https://doi.org/10.3390/medsci8010007

Ho, M. S. (2019). Microglia in parkinson's disease. Advances in Experimental Medicine and Biology, 1175, 335–353. https://doi.org/10.1007/978-981-13-9913-8_13

Ho M. S. (2025). Clearance Pathways for α-Synuclein in Parkinson's Disease. Journal of neurochemistry, 169(6), e70124. https://doi.org/10.1111/jnc.70124

Holmqvist, S., Chutna, O., Bousset, L., Li, W., Björklund, T., Laurent, Z. W., & Li, R. M. J. (2014). Direct evidence of Parkinson pathology spread from the gastrointestinal tract to the brain in rats. https://doi.org/10.1007/s00401-014-1343-6

Horsager, J., Andersen, K. B., Knudsen, K., Skjærbæk, C., Fedorova, T. D., Okkels, N., Schaeffer, E., Bonkat, S. K., Geday, J., Otto, M., Sommerauer, M., Danielsen, E. H., Bech, E., Kraft, J., Munk, O. L., Hansen, S. D., Pavese, N., Göder, R., Brooks, D. J., Berg, D., … Borghammer, P.

(2020). Brain-first versus body-first Parkinson's disease: a multimodal imaging case-control study. Brain : a journal of neurology, 143(10), 3077–3088. https://doi.org/10.1093/brain/awaa238

Houser, M. C., & Tansey, M. G. (2017). The gut-brain axis: is intestinal in fl ammation a silent driver of Parkinson' s disease pathogenesis? November 2016. https://doi.org/10.1038/s41531-016-0002-0

Ishiki, A., Kamada, M., Kawamura, Y., Terao, C., Shimoda, F., Tomita, N., Arai, H., & Furukawa, K. (2016). Glial fibrillar acidic protein in the cerebrospinal fluid of Alzheimer's disease, dementia with Lewy bodies, and frontotemporal lobar degeneration. Journal of neurochemistry, 136(2), 258–261. https://doi.org/10.1111/jnc.13399

Jeong, D. Y., Ryu, M. S., Yang, H. J., & Park, S. (2021). γ-PGA-Rich Chungkookjang, short-term fermented soybeans: Prevents memory impairment by modulating brain insulin sensitivity, neuro-inflammation, and the gut–microbiome–brain axis. In Foods (Vol. 10, Issue 2). MDPI AG. https://doi.org/10.3390/foods10020221

Jiang, C., Hopfner, F., Katsikoudi, A., Hein, R., Catli, C., Evetts, S., Huang, Y., Wang, H., Ryder, J. W., Kuhlenbaeumer, G., Deuschl, G., Padovani, A., Berg, D., Borroni, B., Hu, M. T., Davis, J. J., & Tofaris, G. K. (2020). Serum neuronal exosomes predict and differentiate Parkinson's disease from atypical parkinsonism. Journal of neurology, neurosurgery, and psychiatry, 91(7), 720–729. https://doi.org/10.1136/jnnp-2019-322588

Jin, H. E., Choi, J. C., Lim, Y. T., & Sung, M. H. (2017). Prebiotic Effects of Poly-Gamma-Glutamate on Bacterial Flora in Murine Gut. Journal of microbiology and biotechnology, 27(2), 412–415. https://doi.org/10.4014/jmb.1611.11023

Joe, E.-H., Choi, D.-J., An, J., Eun, J.-H., Jou, I., & Park, S. (2018). Astrocytes, Microglia, and Parkinson's Disease. Experimental Neurobiology, 27(2), 77–87. https://doi.org/10.5607/en.2018.27.2.77

Kanaya, Y., Kume, K., Morino, H., Ohsawa, R., Kurashige, T., Kamada, M., Torii, T., Izumi, Y., Maruyama, H., & Kawakami, H. (2021). Analysis of genetic risk factors in Japanese patients with Parkinson's disease. Journal of Human Genetics 2021 66:10, 66(10), 957–964. https://doi.org/10.1038/S10038-021-00910-4

Khalil, I. R., Khechara, M. P., Kurusamy, S., Armesilla, A. L., Gupta, A., Mendrek, B., Khalaf, T., Scandola, M., Focarete, M. L., Kowalczuk, M., & Radecka, I. (2018). Poly-Gamma-Glutamic Acid (-PGA)-based encapsulation of adenovirus to evade neutralizing antibodies. Molecules, 23(10). https://doi.org/10.3390/molecules23102565

Kim, S., Kwon, S. H., Kam, T. I., Panicker, N., Karuppagounder, S. S., Lee, S., Lee, J. H., Kim, W. R., Kook, M., Foss, C. A., Shen, C., Lee, H., Kulkarni, S., Pasricha, P. J., Lee, G., Pomper, M. G., Dawson, V. L., Dawson, T. M., & Ko, H. S. (2019). Transneuronal Propagation of Pathologic α-Synuclein from the Gut to the Brain Models Parkinson's Disease. Neuron, 103(4), 627–641.e7. https://doi.org/10.1016/j.neuron.2019.05.035

Kimura, K., Tran, L. S., Uchida, I., & Itoh, Y. (2004). Characterization of Bacillus subtilis gamma-glutamyltransferase and its involvement in the degradation of capsule poly-gamma-glutamate. Microbiology (Reading, England), 150(Pt 12), 4115–4123. https://doi.org/10.1099/mic.0.27467-0

Kovalevich, J., & Langford, D. (2013). Considerations for the use of SH-SY5Y neuroblastoma cells in neurobiology. Methods in Molecular Biology, 1078, 9–21. https://doi.org/10.1007/978-1-62703-640-5_2

Kumar, V., Singh, D., Singh, B. K., Singh, S., Mittra, N., Jha, R. R., Patel, D. K., & Singh, C. (2018). Alpha-synuclein aggregation, Ubiquitin proteasome system impairment, and l-Dopa response in zinc-induced Parkinsonism: resemblance to sporadic Parkinson's disease. Molecular and Cellular Biochemistry, 444(1–2), 149–160. https://doi.org/10.1007/S11010-017-3239-Y

Kuo, G., Kumbhar, R., Blair, W., Dawson, V. L., Dawson, T. M., & Mao, X. (2025). Emerging targets of α-synuclein spreading in α-synucleinopathies: a review of mechanistic pathways and interventions. Molecular neurodegeneration, 20(1), 10. https://doi.org/10.1186/s13024-025-00797-1

Kwon, E. H., Tennagels, S., Gold, R., Gerwert, K., Beyer, L., & Tönges, L. (2022). Update on CSF Biomarkers in Parkinson's Disease. Biomolecules, 12(2), 329. https://doi.org/10.3390/biom12020329

Lawrence, J. M., Schardien, K., Wigdahl, B., & Nonnemacher, M. R. (2023). Roles of neuropathology-associated reactive astrocytes: a systematic review. Acta Neuropathologica Communications 2023 11:1, 11(1), 1–28. https://doi.org/10.1186/S40478-023-01526-9

Lee, J. M., Jang, W. J., Park, S. H., & Kong, I. S. (2020). Antioxidant and gastrointestinal cytoprotective effect of edible polypeptide poly-γ-glutamic acid. International Journal of Biological Macromolecules, 153, 616–624. https://doi.org/10.1016/j.ijbiomac.2020.03.050

LeWitt P. A. (2015). Levodopa therapy for Parkinson's disease: Pharmacokinetics and pharmacodynamics. Movement disorders : official journal of the Movement Disorder Society, 30(1), 64–72. https://doi.org/10.1002/mds.26082

Li, D., Hou, L., Gao, Y., Tian, Z., Fan, B., Wang, F., & Li, S. (2022). Recent Advances in Microbial Synthesis of Poly-γ-Glutamic Acid: A Review. In Foods (Vol. 11, Issue 5). MDPI. https://doi.org/10.3390/foods11050739

Liddelow, S. A., & Barres, B. A. (2017). Reactive Astrocytes: Production, Function, and Therapeutic Potential. Immunity, 46(6), 957–967. https://doi.org/10.1016/j.immuni.2017.06.006

Liddelow, S. A., Guttenplan, K. A., Clarke, L. E., Bennett, F. C., Bohlen, C. J., Schirmer, L., Bennett, M. L., Münch, A. E., Chung, W. S., Peterson, T. C., Wilton, D. K., Frouin, A., Napier, B. A., Panicker, N., Kumar, M., Buckwalter, M. S., Rowitch, D. H., Dawson, V. L., Dawson, T. M., … Barres, B. A. (2017). Neurotoxic reactive astrocytes are induced by activated microglia. Nature, 541(7638), 481–487. https://doi.org/10.1038/nature21029

Limanaqi, F., Zecchini, S., Ogno, P., Artusa, V., Fenizia, C., Saulle, I., Vanetti, C., Garziano, M., Strizzi, S., Trabattoni, D., Clerici, M., & Biasin, M. (2024). Alpha-synuclein shapes monocyte and macrophage cell biology and functions by bridging alterations of autophagy and inflammatory pathways. Frontiers in cell and developmental biology, 12, 1421360. https://doi.org/10.3389/fcell.2024.1421360

Lindström, V., Gustafsson, G., Sanders, L. H., Howlett, E. H., Sigvardson, J., Kasrayan, A., Ingelsson, M., Bergström, J., & Erlandsson, A. (2017). Extensive uptake of α-synuclein oligomers in astrocytes results in sustained intracellular deposits and mitochondrial damage. Molecular and Cellular Neuroscience, 82, 143–156. https://doi.org/10.1016/j.mcn.2017.04.009

Liu, T., Huang, T., Li, J., Li, A., Li, C., Huang, X., Li, D., Wang, S., & Liang, M. (2023). Optimization of differentiation and transcriptomic profile of THP-1 cells into macrophage by PMA. PloS one, 18(7), e0286056. https://doi.org/10.1371/journal.pone.0286056

Loria, F., Vargas, J. Y., Bousset, L., Syan, S., Salles, A., Melki, R., & Zurzolo, C. (2017). α-Synuclein transfer between neurons and astrocytes indicates that astrocytes play a role in degradation rather than in spreading. Acta Neuropathologica, 134(5), 789–808. https://doi.org/10.1007/S00401-017-1746-2

Ludtmann, M. H. R., Angelova, P. R., Horrocks, M. H., Choi, M. L., Rodrigues, M., Baev, A. Y., Berezhnov, A. V., Yao, Z., Little, D., Banushi, B., Al-Menhali, A. S., Ranasinghe, R. T., Whiten, D. R., Yapom, R., Dolt, K. S., Devine, M. J., Gissen, P., Kunath, T., Jaganjac, M., … Gandhi, S. (2018). α-synuclein oligomers interact with ATP synthase and open the permeability transition pore in Parkinson's disease. Nature Communications, 9(1). https://doi.org/10.1038/s41467-018-04422-2

Luo, Z., Guo, Y., Liu, J., Qiu, H., Zhao, M., Zou, W., & Li, S. (2016). Microbial synthesis of poly-γ-glutamic acid: current progress, challenges, and future perspectives. Biotechnology for biofuels, 9, 134. https://doi.org/10.1186/s13068-016-0537-7

Ma, S. X., Seo, B. A., Kim, D., Xiong, Y., Kwon, S. H., Brahmachari, S., Kim, S., Kam, T. I., Nirujogi, R. S., Kwon, S. H., Dawson, V. L., Dawson, T. M., Pandey, A., Na, C. H., & Ko, H. S. (2021). Complement and Coagulation Cascades are Potentially Involved in Dopaminergic Neurodegeneration in α-Synuclein-Based Mouse Models of Parkinson's Disease. Journal of proteome research, 20(7), 3428–3443. https://doi.org/10.1021/acs.jproteome.0c01002

Madeira, A., Yang, J., Zhang, X., Vikeved, E., Nilsson, A., Andrén, P. E., & Svenningsson, P. (2011). Caveolin-1 interacts with alpha-synuclein and mediates toxic actions of cellular alpha-synuclein overexpression. Neurochemistry international, 59(2), 280–289. https://doi.org/10.1016/j.neuint.2011.05.017

Marogianni, C., Sokratous, M., Dardiotis, E., Hadjigeorgiou, G. M., Bogdanos, D., & Xiromerisiou, G. (2020). Neurodegeneration and Inflammation-An Interesting Interplay in Parkinson's Disease. International journal of molecular sciences, 21(22), 8421. https://doi.org/10.3390/ijms21228421

Martinez, F. O., Sica, A., Mantovani, A., & Locati, M. (2008). Macrophage activation and polarization. Frontiers in Bioscience, 13(2), 453–461. https://doi.org/10.2741/2692

Martínez-Reyes, I., & Chandel, N. S. (2020). Mitochondrial TCA cycle metabolites control physiology and disease. Nature Communications, 11(1). https://doi.org/10.1038/S41467-019-13668-3

Mazzetti, S., Basellini, M. J., Ferri, V., Cassani, E., Cereda, E., Paolini, M., Calogero, A. M., Bolliri, C., De Leonardis, M., Sacilotto, G., Cilia, R., Cappelletti, G., & Pezzoli, G. (2020). α-Synuclein oligomers in skin biopsy of idiopathic and monozygotic twin patients with Parkinson's disease. Brain, 143(3), 920–931. https://doi.org/10.1093/brain/awaa008

Mazzetti, S., Contaldi, E., Basellini, M. J., Novello, C., Calogero, A. M., Straniero, L., Garrì, F., Ferri, V., Calandrella, D., Del Sorbo, F., Asselta, R., Cereda, E., Cappelletti, G., Isaias, I. U., & Pezzoli, G. (2024). Comparing GBA1-Parkinson's disease and idiopathic Parkinson's disease: α-Synuclein oligomers and synaptic density as biomarkers in the skin biopsy. Brain pathology (Zurich, Switzerland), 34(6), e13284. https://doi.org/10.1111/bpa.13284

Mazzetti, S., Giampietro, F., Calogero, A. M., Isilgan, H. B., Gagliardi, G., Rolando, C., Cantele, F., Ascagni, M., Bramerio, M., Giaccone, G., Isaias, I. U., Pezzoli, G., & Cappelletti, G. (2024). Linking acetylated α-Tubulin redistribution to α-Synuclein pathology in brain of Parkinson's disease patients. NPJ Parkinson's Disease, 10(1). https://doi.org/10.1038/S41531-023-00607-9

Mehra, S., Sahay, S., & Maji, S. K. (2019). α-Synuclein misfolding and aggregation: Implications in Parkinson's disease pathogenesis. In Biochimica et Biophysica Acta - Proteins and Proteomics (Vol. 1867, Issue 10, pp. 890–908). Elsevier B.V. https://doi.org/10.1016/j.bbapap.2019.03.001

Miki, Y., Tanji, K., Mori, F., Utsumi, J., Sasaki, H., Kakita, A., Takahashi, H., & Wakabayashi, K. (2016). Alteration of Upstream Autophagy-Related Proteins (ULK1, ULK2, Beclin1, VPS34 and AMBRA1) in Lewy Body Disease. Brain pathology (Zurich, Switzerland), 26(3), 359–370. https://doi.org/10.1111/bpa.12297

Moehle, M. S., & West, A. B. (2015). M1 and M2 immune activation in Parkinson's Disease: Foe and ally?. Neuroscience, 302, 59–73. https://doi.org/10.1016/j.neuroscience.2014.11.018

Mohammadzadeh, V., Rahiman, N., Cabral, H., Quader, S., Zirak, M. R., Taghavizadeh Yazdi, M. E., Jaafari, M. R., & Alavizadeh, S. H. (2023). Poly-γ-glutamic acid nanoparticles as adjuvant and antigen carrier system for cancer vaccination. Journal of Controlled Release, 362, 278–296. https://doi.org/10.1016/j.jconrel.2023.08.049

Moors, T. E., Maat, C. A., Niedieker, D., Mona, D., Petersen, D., Timmermans-Huisman, E., Kole, J., El-Mashtoly, S. F., Spycher, L., Zago, W., Barbour, R., Mundigl, O., Kaluza, K., Huber, S., Hug,

M. N., Kremer, T., Ritter, M., Dziadek, S., Geurts, J. J. G., … van de Berg, W. D. J. (2021). The subcellular arrangement of alpha-synuclein proteoforms in the Parkinson's disease brain as revealed by multicolor STED microscopy. Acta Neuropathologica, 142(3), 423–448. https://doi.org/10.1007/S00401-021-02329-9

Mor, D. E., Ugras, S. E., Daniels, M. J., & Ischiropoulos, H. (2016). Dynamic structural flexibility of α-synuclein. Neurobiology of Disease, 88, 66–74. https://doi.org/10.1016/J.NBD.2015.12.018

Morais, L. H., Schreiber, H. L., & Mazmanian, S. K. (2021). The gut microbiota–brain axis in behaviour and brain disorders. In Nature Reviews Microbiology (Vol. 19, Issue 4, pp. 241–255). Nature Research. https://doi.org/10.1038/s41579-020-00460-0

Nair, P., Navale, G. R., & Dharne, M. S. (2023). Poly-gamma-glutamic acid biopolymer: a sleeping giant with diverse applications and unique opportunities for commercialization. In Biomass Conversion and Biorefinery (Vol. 13, Issue 6, pp. 4555–4573). Springer Science and Business Media Deutschland GmbH. https://doi.org/10.1007/s13399-021-01467-0

Nechushtai, L., Frenkel, D., & Pinkas-Kramarski, R. (2023). Autophagy in Parkinson's Disease. Biomolecules, 13(10). https://doi.org/10.3390/BIOM13101435

Nissen, S. K., Ferreira, S. A., Nielsen, M. C., Schulte, C., Shrivastava, K., Hennig, D., Etzerodt, A., Graversen, J. H., Berg, D., Maetzler, W., Panhelainen, A., Møller, H. J., Brockmann, K., & Romero-Ramos, M. (2021). Soluble CD163 Changes Indicate Monocyte Association With Cognitive Deficits in Parkinson's Disease. Movement Disorders, 36(4), 963–976. https://doi.org/10.1002/MDS.28424

Novello, C., Parati, M., Mazzetti, S., Rampoldi, O., Isilgan, H. B., Basellini, M. J., De Luca, C. M. G., Ciullini, A., Dellarole, I. L., Fantin, A., Russo, I., Johnston, B. L., Paroni, M., Rolando, C., Moda, F., Pezzoli, G., Radecka, I. K., & Cappelletti, G. (2025). Poly-γ-glutamic acid alleviates cytotoxicity and inflammation induced by pre-formed fibrils of α-synuclein in murine primary astrocytes. International journal of biological macromolecules, 318(Pt 4), 145303. https://doi.org/10.1016/j.ijbiomac.2025.145303

Oeckl, P., Halbgebauer, S., Anderl-Straub, S., Steinacker, P., Hussa, A. M., Neugebauer, H., Von Arnim, C. A. F., Diehl-Schmid, J., Grimmer, T., Kornhuber, J., Lewczuk, P., Danek, A., Degeneration, L., Ludolph, A. C., & Otto, M. (2018). Glial Fibrillary Acidic Protein in Serum is Increased in Alzheimer's Disease and Correlates with Cognitive Impairment. Journal of Alzheimer's Disease, 67(2), 481–488. https://doi.org/10.3233/JAD-180325

Ogunleye, A., Bhat, A., Irorere, V. U., Hill, D., Williams, C., & Radecka, I. (2015). Poly-γ-glutamic acid: production, properties and applications. *Microbiology (Reading, England)*, *161*(Pt 1), 1–17. https://doi.org/10.1099/mic.0.081448-0

Olanow, C. W., & Kordower, J. H. (2017). Targeting α-Synuclein as a therapy for Parkinson's disease: The battle begins. Movement Disorders, 32(2), 203–207. https://doi.org/10.1002/mds.26935

Oliveri, V. (2019). Toward the discovery and development of effective modulators of α-synuclein amyloid aggregation. European Journal of Medicinal Chemistry, 167, 10–36. https://doi.org/10.1016/j.ejmech.2019.01.045

Ozono, T., Kimura, Y., Suenaga, T., Beck, G., Jinno, J., Aguirre, C., Ikenaka, K., Krainc, D., Mochizuki, H., & Arase, H. (2023). Extracellular transportation of α-synuclein by HLA class II molecules. Biochemical and biophysical research communications, 644, 25–33. https://doi.org/10.1016/j.bbrc.2022.12.082

Pajares, M., I Rojo, A., Manda, G., Boscá, L., & Cuadrado, A. (2020). Inflammation in Parkinson's Disease: Mechanisms and Therapeutic Implications. Cells, 9(7), 1687. https://doi.org/10.3390/CELLS9071687

Pantazopoulou, M., Brembati, V., Kanellidi, A., Bousset, L., Melki, R., & Stefanis, L. (2021). Distinct alpha-Synuclein species induced by seeding are selectively cleared by the Lysosome or the

Proteasome in neuronally differentiated SH-SY5Y cells. Journal of neurochemistry, 156(6), 880–896. https://doi.org/10.1111/jnc.15174

Parati, M., Khalil, I., Tchuenbou-Magaia, F., Adamus, G., Mendrek, B., Hill, R., & Radecka, I. (2022). Building a circular economy around poly(D/L-γ-glutamic acid)- a smart microbial biopolymer. Biotechnology advances, 61, 108049. https://doi.org/10.1016/j.biotechadv.2022.108049

Parihar, M. S., Parihar, A., Fujita, M., Hashimoto, M., & Ghafourifar, P. (2008). Mitochondrial association of alpha-synuclein causes oxidative stress. Cellular and Molecular Life Sciences, 65(7–8), 1272–1284. https://doi.org/10.1007/S00018-008-7589-1

Parkkinen, L., Pirttilä, T., & Alafuzoff, I. (2008). Applicability of current staging/categorization of α-synuclein pathology and their clinical relevance. Acta Neuropathologica, 115(4), 399–407. https://doi.org/10.1007/S00401-008-0346-6

Patani, R., Hardingham, G. E., & Liddelow, S. A. (2023). Functional roles of reactive astrocytes in neuroinflammation and neurodegeneration. Nature Reviews. Neurology, 19(7), 395–409. https://doi.org/10.1038/S41582-023-00822-1

Pellegrini, C., D'Antongiovanni, V., Miraglia, F., Rota, L., Benvenuti, L., Di Salvo, C., Testa, G., Capsoni, S., Carta, G., Antonioli, L., Cattaneo, A., Blandizzi, C., Colla, E., & Fornai, M. (2022). Enteric α-synuclein impairs intestinal epithelial barrier through caspase-1-inflammasome signaling in Parkinson's disease before brain pathology. Npj Parkinson's Disease, 8(1). https://doi.org/10.1038/s41531-021-00263-x

Pellegrini, L., Wetzel, A., Grannó, S., Heaton, G., & Harvey, K. (2017). Back to the tubule: microtubule dynamics in Parkinson's disease. Cellular and Molecular Life Sciences, 74, 409–434. https://doi.org/10.1007/s00018-016-2351-6

Peng, H., Chen, S., Wu, S., Shi, X., Ma, J., Yang, H., & Li, X. (2023). Alpha-synuclein in skin as a high-quality biomarker for Parkinson's disease. Journal of the Neurological Sciences, 451, 120730. https://doi.org/10.1016/J.JNS.2023.120730

Poewe, W., Seppi, K., Tanner, C. M., Halliday, G. M., Brundin, P., Volkmann, J., Schrag, A. E., & Lang, A. E. (2017). Parkinson disease. Nature reviews. Disease primers, 3, 17013. https://doi.org/10.1038/nrdp.2017.13

Pogačnik, L., Ota, A., & Ulrih, N. P. (2020). An Overview of Crucial Dietary Substances and Their Modes of Action for Prevention of Neurodegenerative Diseases. Cells 2020, Vol. 9, Page 576, 9(3), 576. https://doi.org/10.3390/CELLS9030576

Postuma, R. B., & Berg, D. (2019). Prodromal Parkinson's Disease: The Decade Past, the Decade to Come. Movement Disorders, 34(5), 665–675. https://doi.org/10.1002/MDS.27670

Raj, A., Banerjee, R., Holla, V., Kamble, N., Yadav, R., Pal, P. K., & Datta, I. (2024). Dysregulation of protein degradation and alteration of secretome in α-synuclein-exposed astrocytes: implications for dopaminergic neuronal dysfunction. Cell Communication and Signaling, 22(1). https://doi.org/10.1186/S12964-024-01928-9

Rannikko, E. H., Weber, S. S., & Kahle, P. J. (2015). Exogenous α-synuclein induces toll-like receptor 4 dependent inflammatory responses in astrocytes. BMC Neuroscience, 16(1). https://doi.org/10.1186/S12868-015-0192-0

Raunio, A., Kaivola, K., Tuimala, J., Kero, M., Oinas, M., Polvikoski, T., Paetau, A., Tienari, P. J., & Myllykangas, L. (2019). Lewy-related pathology exhibits two anatomically and genetically distinct progression patterns: a population-based study of Finns aged 85+. Acta Neuropathologica, 138(5), 771–782. https://doi.org/10.1007/S00401-019-02071-3

Roberts, R. F., Wade-Martins, R., & Alegre-Abarrategui, J. (2015). Direct visualization of alpha-synuclein oligomers reveals previously undetected pathology in Parkinson's disease brain. Brain : A Journal of Neurology, 138(Pt 6), 1642–1657. https://doi.org/10.1093/BRAIN/AWV040

Rodriguez, L., Marano, M. M., & Tandon, A. (2018). Import and export of misfolded α-synuclein. Frontiers in Neuroscience, 12(MAY), 358041. https://doi.org/10.3389/FNINS.2018.00344/BIBTEX

Romano, S., Savva, G. M., Bedarf, J. R., Charles, I. G., Hildebrand, F., & Narbad, A. (2021). Meta-analysis of the Parkinson's disease gut microbiome suggests alterations linked to intestinal inflammation. *NPJ Parkinson's disease*, *7*(1), 27. https://doi.org/10.1038/s41531-021-00156-z

Rowe, S. (2023). Towards the optimal care of Parkinson's disease – a guide for GPs. Medicine Today 2023; 24(8): 19-25.

Sano, T., Nagata, T., Ebihara, S., Yoshida-Tanaka, K., Nakamura, A., Sasaki, A., Shimozawa, A., Mochizuki, H., Uchihara, T., Hasegawa, M., & Yokota, T. (2024). Effects of local reduction of endogenous α-synuclein using antisense oligonucleotides on the fibril-induced propagation of pathology through the neural network in wild-type mice. Acta Neuropathologica Communications, 12(1). https://doi.org/10.1186/S40478-024-01766-3

Schmitz, M., Cramm, M., Llorens, F., Müller-Cramm, D., Collins, S., Atarashi, R., Satoh, K., Orrù, C. D., Groveman, B. R., Zafar, S., Schulz-Schaeffer, W. J., Caughey, B., & Zerr, I. (2016). The real-time quaking-induced conversion assay for detection of human prion disease and study of other protein misfolding diseases. Nature Protocols 2016 11:11, 11(11), 2233–2242. https://doi.org/10.1038/NPROT.2016.120

Schonhoff, A. M., Figge, D. A., Williams, G. P., Jurkuvenaite, A., Gallups, N. J., Childers, G. M., Webster, J. M., Standaert, D. G., Goldman, J. E., & Harms, A. S. (2022). Border-associated macrophages mediate the neuroinflammatory response in an alpha-synuclein model of Parkinson disease. https://doi.org/10.1038/s41467-023-39060-w

Shapouri-Moghaddam, A., Mohammadian, S., Vazini, H., Taghadosi, M., Esmaeili, S. A., Mardani, F., Seifi, B., Mohammadi, A., Afshari, J. T., & Sahebkar, A. (2018). Macrophage plasticity, polarization, and function in health and disease. Journal of Cellular Physiology, 233(9), 6425–6440. https://doi.org/10.1002/JCP.26429

Shimizu, K., Nakamura, H., & Ashiuchi, M. (2007). Salt-inducible bionylon polymer from Bacillus megaterium. Applied and Environmental Microbiology, 73(7), 2378–2379. https://doi.org/10.1128/AEM.02686-06/ASSET/E5768B0C-D455-4EF1-9216-9FC322D4108E/ASSETS/GRAPHIC/ZAM0070776480001.JPEG

Shrivastava, R., & Shukla, N. (2019). Attributes of alternatively activated (M2) macrophages. Life Sciences, 224, 222–231. https://doi.org/10.1016/J.LFS.2019.03.062

Siderowf, A., Concha-Marambio, L., Lafontant, D. E., Farris, C. M., Ma, Y., Urenia, P. A., Nguyen, H., Alcalay, R. N., Chahine, L. M., Foroud, T., Galasko, D., Kieburtz, K., Merchant, K., Mollenhauer, B., Poston, K. L., Seibyl, J., Simuni, T., Tanner, C. M., Weintraub, D., … Soto, C. (2023). Assessment of heterogeneity among participants in the Parkinson's Progression Markers Initiative cohort using α-synuclein seed amplification: a cross-sectional study. The Lancet Neurology, 22(5), 407–417. https://doi.org/10.1016/S1474-4422(23)00109-6

Sidransky, E., & Lopez, G. (2012). The link between the GBA gene and parkinsonism. The Lancet Neurology, 11(11), 986–998. https://doi.org/10.1016/S1474-4422(12)70190-4

Singh, S. K., Dutta, A., & Modi, G. (2017). α-Synuclein aggregation modulation: an emerging approach for the treatment of Parkinson's disease. Future Medicinal Chemistry, 9(10), 1039. https://doi.org/10.4155/FMC-2017-0016

Sirisansaneeyakul, S., Cao, M., Kongklom, N., Chuensangjun, C., Shi, Z., & Chisti, Y. (2017). Microbial production of poly-γ-glutamic acid. World Journal of Microbiology and Biotechnology, 33(9), 1–8. https://doi.org/10.1007/S11274-017-2338-Y/FIGURES/1

Sofroniew, M. V, & Vinters, H. V. (2010). Astrocytes: biology and pathology. Acta Neuropathologica, 119(1), 7–35. https://doi.org/10.1007/s00401-009-0619-8

Spillantini, M. G., & Goedert, M. (2018). Neurodegeneration and the ordered assembly of α-synuclein. Cell and Tissue Research, 373, 137–148. https://doi.org/10.1007/s00441-017-2706-9

Spillantini, M. G., Schmidt, M. L., Lee, V. M.-Y., Trojanowski, J. Q., Jakes, R., & Goedert, M. (1997). α-Synuclein in Lewy bodies. Nature, 388(6645), 839–840. https://doi.org/10.1038/42166

Staats, R., Michaels, T. C. T., Flagmeier, P., Chia, S., Horne, R. I., Habchi, J., Linse, S., Knowles, T. P. J., Dobson, C. M., & Vendruscolo, M. (2020). Screening of small molecules using the inhibition of oligomer formation in α-synuclein aggregation as a selection parameter. Communications Chemistry, 3(1), 1–9. https://doi.org/10.1038/S42004-020-00412-Y;TECHMETA

Stokholm, M. G., Danielsen, E. H., Hamilton-Dutoit, S. J., & Borghammer, P. (2016). Pathological α-synuclein in gastrointestinal tissues from prodromal Parkinson disease patients. Annals of Neurology, 79(6), 940–949. https://doi.org/10.1002/ANA.24648

Su, X., Maguire-Zeiss, K. A., Giuliano, R., Prifti, L., Venkatesh, K., & Federoff, H. J. (2008). Synuclein activates microglia in a model of Parkinson's disease. Neurobiology of Aging, 29(11), 1690–1701. https://doi.org/10.1016/J.NEUROBIOLAGING.2007.04.006

Tansey, M. G., Wallings, R. L., Houser, M. C., Herrick, M. K., Keating, C. E., & Joers, V. (2022). Inflammation and immune dysfunction in Parkinson disease. Nature Reviews Immunology 2022 22:11, 22(11), 657–673. https://doi.org/10.1038/s41577-022-00684-6

Thome, A. D., Wang, J., Atassi, F., Thonhoff, J. R., Faridar, A., Zhao, W., Beers, D. R., Lai, E. C., & Appel, S. H. (2025). Peripheral monocyte transcriptional signatures of inflammation and oxidative stress in Parkinson's disease. Frontiers in Immunology, 16, 1571074. https://doi.org/10.3389/FIMMU.2025.1571074/BIBTEX

Thomsen, T. R., & Rodnitzky, R. L. (2010). Juvenile parkinsonism: Epidemiology, diagnosis and treatment. CNS Drugs, 24(6), 467–477. https://doi.org/10.2165/11533130-000000000-00000

Tinaz, S., Chow, C., Kuo, P. H., Krupinski, E. A., Blumenfeld, H., Louis, E. D., & Zubal, G. (2018). Semiquantitative Analysis of Dopamine Transporter Scans in Patients with Parkinson Disease. Clinical Nuclear Medicine, 43(1), e1–e7. https://doi.org/10.1097/RLU.0000000000001885

Tysnes, O. B., & Storstein, A. (2017). Epidemiology of Parkinson's disease. In Journal of Neural Transmission (Vol. 124, Issue 8, pp. 901–905). Springer-Verlag Wien. https://doi.org/10.1007/s00702-017-1686-y

Vijiaratnam, N., Simuni, T., Bandmann, O., Morris, H. R., & Foltynie, T. (2021). Progress towards therapies for disease modification in Parkinson's disease. The Lancet Neurology, 20(7), 559–572. https://doi.org/10.1016/S1474-4422(21)00061-2

Vogel, D. Y. S., Vereyken, E. J. F., Glim, J. E., Heijnen, P. D. A. M., Moeton, M., van der Valk, P., Amor, S., Teunissen, C. E., van Horssen, J., & Dijkstra, C. D. (2013). Macrophages in inflammatory multiple sclerosis lesions have an intermediate activation status. Journal of Neuroinflammation, 10. https://doi.org/10.1186/1742-2094-10-35

Wang, L., Chen, S., & Yu, B. (2022). Poly-γ-glutamic acid: Recent achievements, diverse applications and future perspectives. In Trends in Food Science and Technology (Vol. 119, pp. 1–12). Elsevier Ltd. https://doi.org/10.1016/j.tifs.2021.11.009

Wang, L. L., Chen, J. T., Wang, L. F., Wu, S., Zhang, G. Z., Yu, H. Q., Ye, X. D., & Shi, Q. S. (2017). Conformations and molecular interactions of poly-γ-glutamic acid as a soluble microbial product in aqueous solutions. Scientific Reports 2017 7:1, 7(1), 1–11. https://doi.org/10.1038/S41598-017-13152-2

Wang, Q., Luo, Y., Ray Chaudhuri, K., Reynolds, R., Tan, E. K., & Pettersson, S. (2021). The role of gut dysbiosis in Parkinson's disease: Mechanistic insights and therapeutic options. In Brain (Vol. 144, Issue 9, pp. 2571–2593). Oxford University Press. https://doi.org/10.1093/brain/awab156

Wang, X., Zhou, J., Sun, Z., Jia, R., Huang, D., Tang, D., Xia, T., & Xiao, F. (2025). Poly-γ-glutamic acid alleviates slow transit constipation by regulating aquaporin and gut microbes. Scientific Reports, 15(1). https://doi.org/10.1038/S41598-025-92783-2

Williams, G. P., Schonhoff, A. M., Jurkuvenaite, A., Thome, A. D., Standaert, D. G., & Harms, A. S. (2018). Targeting of the class II transactivator attenuates inflammation and neurodegeneration in an alpha-synuclein model of Parkinson's disease. Journal of Neuroinflammation, 15(1), 1–14. https://doi.org/10.1186/S12974-018-1286-2/FIGURES/5

Wong, Y. C., & Krainc, D. (2017). α-synuclein toxicity in neurodegeneration: mechanism and therapeutic strategies. Nature Medicine, 23(2), 1–13. https://doi.org/10.1038/nm.4269

Yamashita, K. Y., Bhoopatiraju, S., Silverglate, B. D., & Grossberg, G. T. (2023). Biomarkers in Parkinson's disease: A state of the art review. Biomarkers in Neuropsychiatry, 9, 100074. https://doi.org/10.1016/J.BIONPS.2023.100074

Yan, S., Yao, H., Chen, Z., Zeng, S., Xi, X., Wang, Y., He, N., & Li, Q. (2015). Poly-γ-glutamic acid produced from Bacillus licheniformis CGMCC 2876 as a potential substitute for polyacrylamide in the sugarcane industry. Biotechnology Progress, 31(5), 1287–1294. https://doi.org/10.1002/BTPR.2118

Yang, J., Kim, J., Kwak, C., & Poo, H. (2022). Poly-γ-glutamic acid/Alum adjuvanted pH1N1 vaccine-immunized aged mice exhibit a significant increase in vaccine efficacy with a decrease in age-associated CD8+ T cell proportion in splenocytes. Immunity and Ageing, 19(1), 1–16. https://doi.org/10.1186/S12979-022-00282-Z/FIGURES/5

Yaribash, S., Mohammadi, K., & Sani, M. A. (2025). Alpha-Synuclein Pathophysiology in Neurodegenerative Disorders: A Review Focusing on Molecular Mechanisms and Treatment Advances in Parkinson's Disease. Cellular and Molecular Neurobiology 2025 45:1, 45(1), 1–16. https://doi.org/10.1007/S10571-025-01544-2

Yunna, C., Mengru, H., Lei, W., & Weidong, C. (2020). Macrophage M1/M2 polarization. European Journal of Pharmacology, 877. https://doi.org/10.1016/J.EJPHAR.2020.173090

Zarkali, A., Thomas, G. E. C., Zetterberg, H., & Weil, R. S. (2024). Neuroimaging and fluid biomarkers in Parkinson's disease in an era of targeted interventions. Nature Communications 2024 15:1, 15(1), 1–18. https://doi.org/10.1038/S41467-024-49949-9

Zhang, T., Ryu, M. S., Wu, X., Yang, H. J., Jeong, S. J., Seo, J. W., Jeong, D. Y., & Park, S. (2021). Alleviation of neuronal cell death and memory deficit with chungkookjang made with bacillus amyloliquefaciens and bacillus subtilis potentially through promoting gut–brain axis in artery-occluded gerbils. Foods, 10(11). https://doi.org/10.3390/foods10112697

Zhang, W., Wang, T., Pei, Z., Miller, D. S., Wu, X., Block, M. L., Wilson, B., Zhang, W., Zhou, Y., Hong, J.-S., & Zhang, J. (2005). Aggregated α-synuclein activates microglia: a process leading to disease progression in Parkinson's disease. The FASEB Journal, 19(6), 533–542. https://doi.org/10.1096/FJ.04-2751COM

Zhang, Y., Sloan, S. A., Clarke, L. E., Caneda, C., Plaza, C. A., Blumenthal, P. D., Vogel, H., Steinberg, G. K., Edwards, M. S. B., Li, G., Duncan, J. A., Cheshier, S. H., Shuer, L. M., Chang, E. F., Grant, G. A., Gephart, M. G. H., & Barres, B. A. (2016). Purification and Characterization of Progenitor and Mature Human Astrocytes Reveals Transcriptional and Functional Differences with Mouse. Neuron, 89(1), 37–53. https://doi.org/10.1016/J.NEURON.2015.11.013

Zhang, Z., Zhang, Z. Y., Schittenhelm, J., Wu, Y., Meyermann, R., & Schluesener, H. J. (2011). Parenchymal accumulation of CD163+ macrophages/microglia in multiple sclerosis brains. Journal of Neuroimmunology, 237(1–2), 73–79. https://doi.org/10.1016/j.jneuroim.2011.06.006

Zhou, R. M., Huang, Y. X., Li, X. L., Chen, C., Shi, Q., Wang, G. R., Tian, C., Wang, Z. Y., Jing, Y. Y., Gao, C., & Dong, X. P. (2010). Molecular interaction of α-synuclein with tubulin influences on

the polymerization of microtubule in vitro and structure of microtubule in cells. Molecular Biology Reports, 37(7), 3183–3192. https://doi.org/10.1007/S11033-009-9899-2

Zimmermann, M., & Brockmann, K. (2022). Blood and Cerebrospinal Fluid Biomarkers of Inflammation in Parkinson's Disease. Journal of Parkinson's Disease, 12(s1), S183–S200. https://doi.org/10.3233/JPD-223277

Appendix I: flow cytometry data

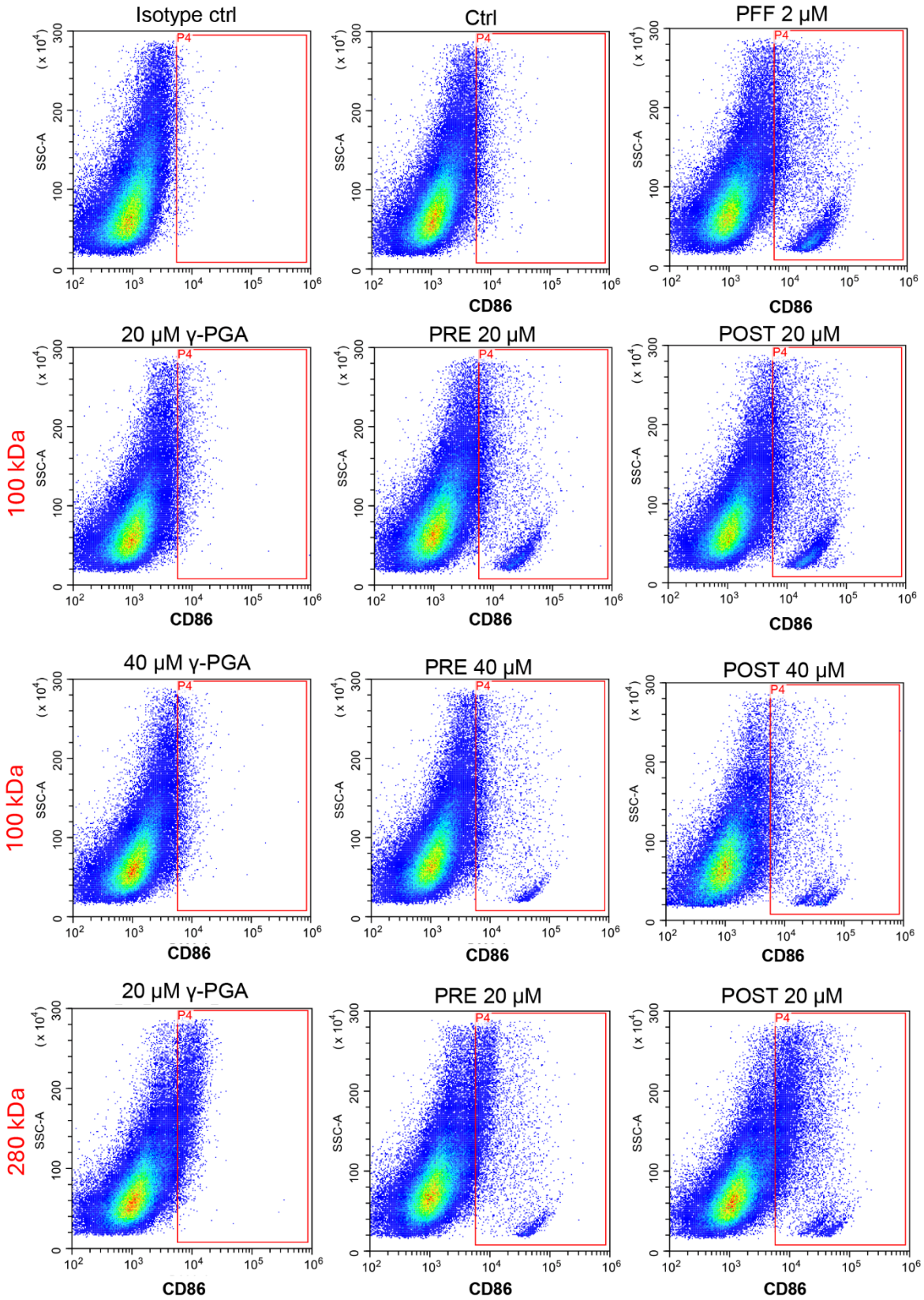

Figure I.1 CD86 marker expression in PFF and γ-PGA treated macrophages. *Representative flow cytometry dot plot showing the expression of CD86 in macrophages treated with PFFs, γ-PGA at 100 kDa and 280 kDa and in combination of PFFs and γ-PGA (PRE and POST treatment) compared to Ctrl. Positive populations are outlined in red gates made on the Isotype ctrl.*

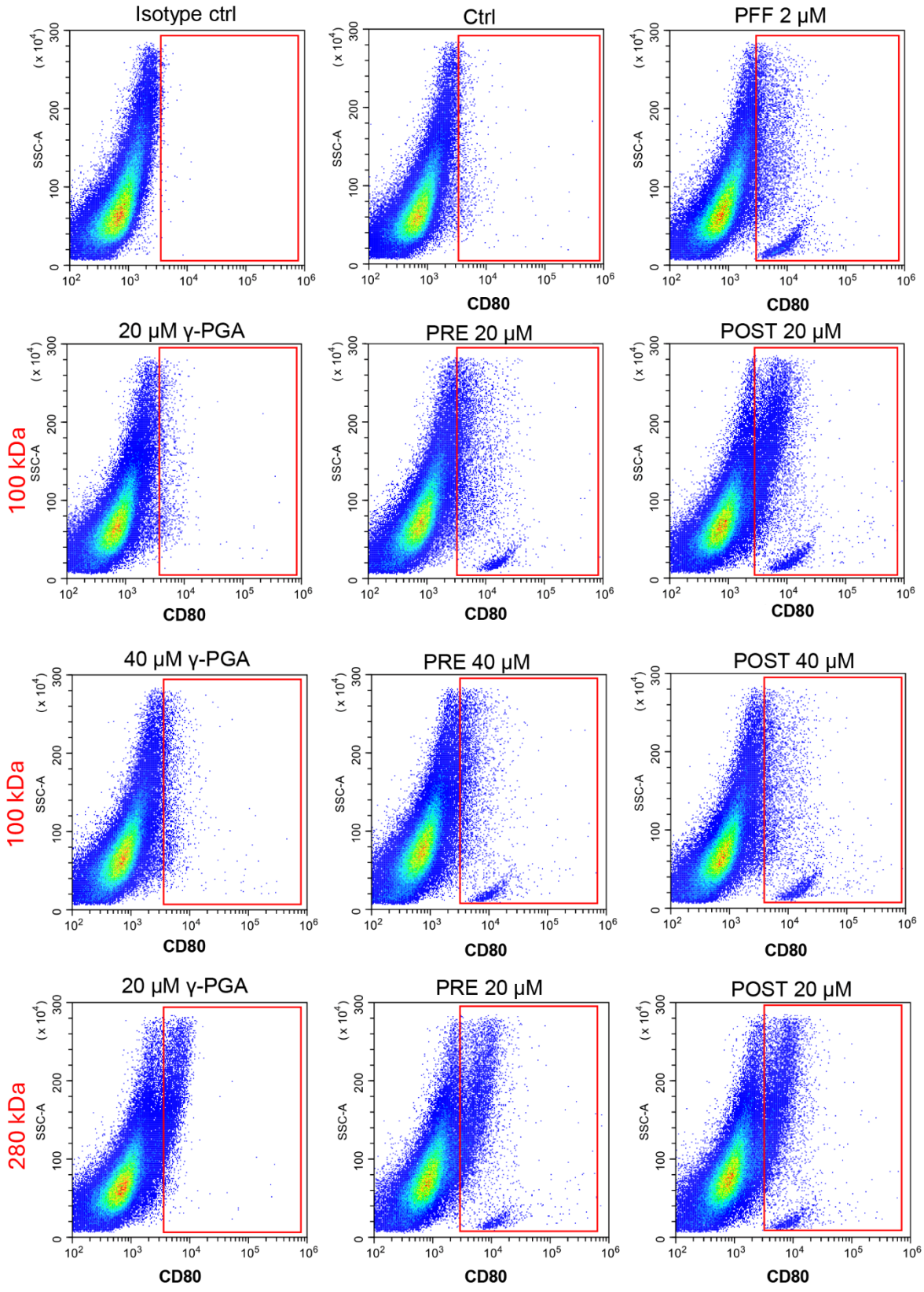

Figure I.2 CD80 marker expression in PFF and γ-PGA treated macrophages. *Representative flow cytometry dot plot showing the expression of CD86 in macrophages treated with PFFs, γ-PGA at 100 kDa and 280 kDa and in combination of PFFs and γ-PGA (PRE and POST treatment) compared to Ctrl. Positive populations are outlined in red gates made on the Isotype ctrl.*

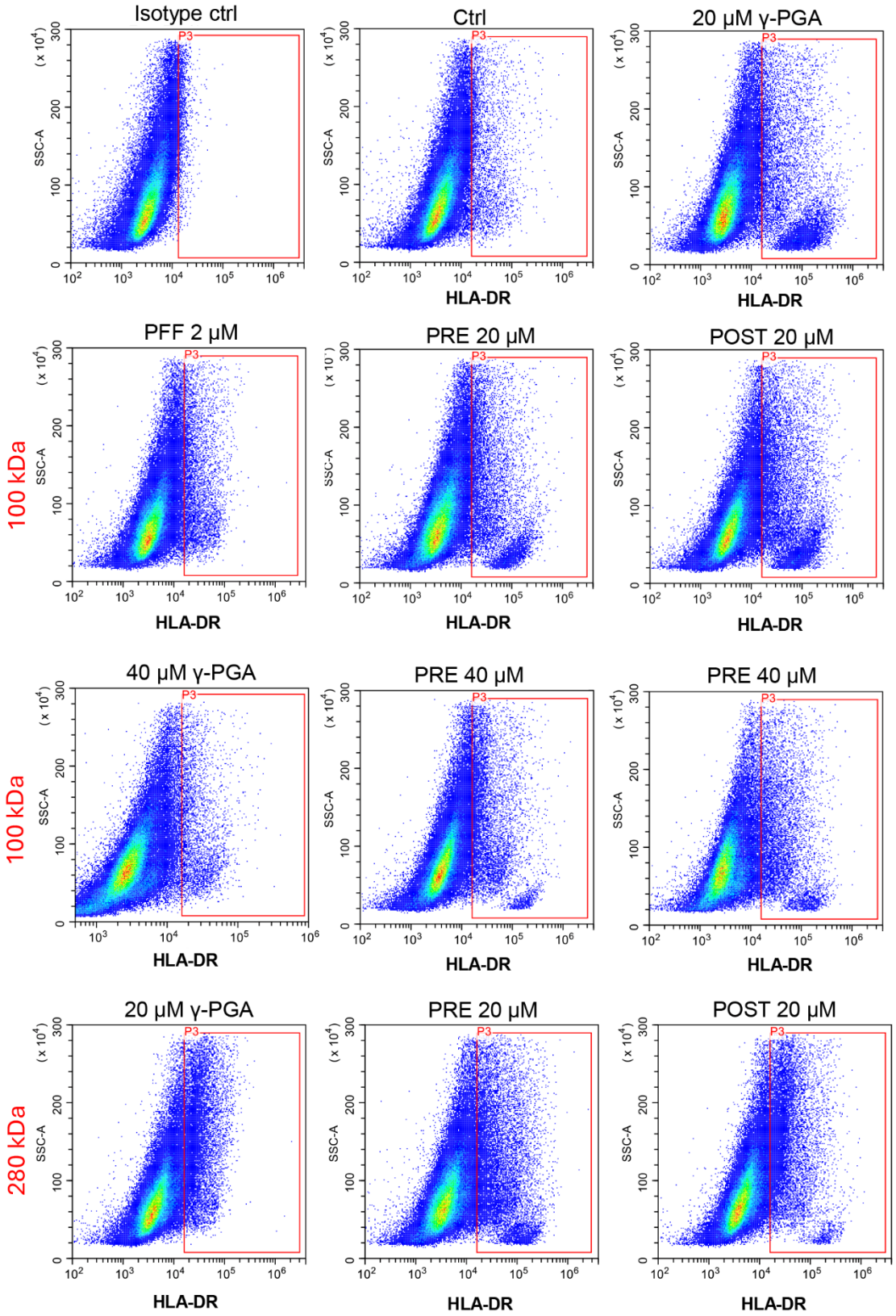

Figure I.3 HLA-DR marker expression in PFF and γ-PGA treated macrophages. *Representative flow cytometry dot plot showing the expression of CD86 in macrophages treated with PFFs, γ-PGA at 100 kDa and 280 kDa and in combination of PFFs and γ-PGA (PRE and POST treatment) compared to Ctrl. Positive populations are outlined in red gates made on the Isotype ctrl.*

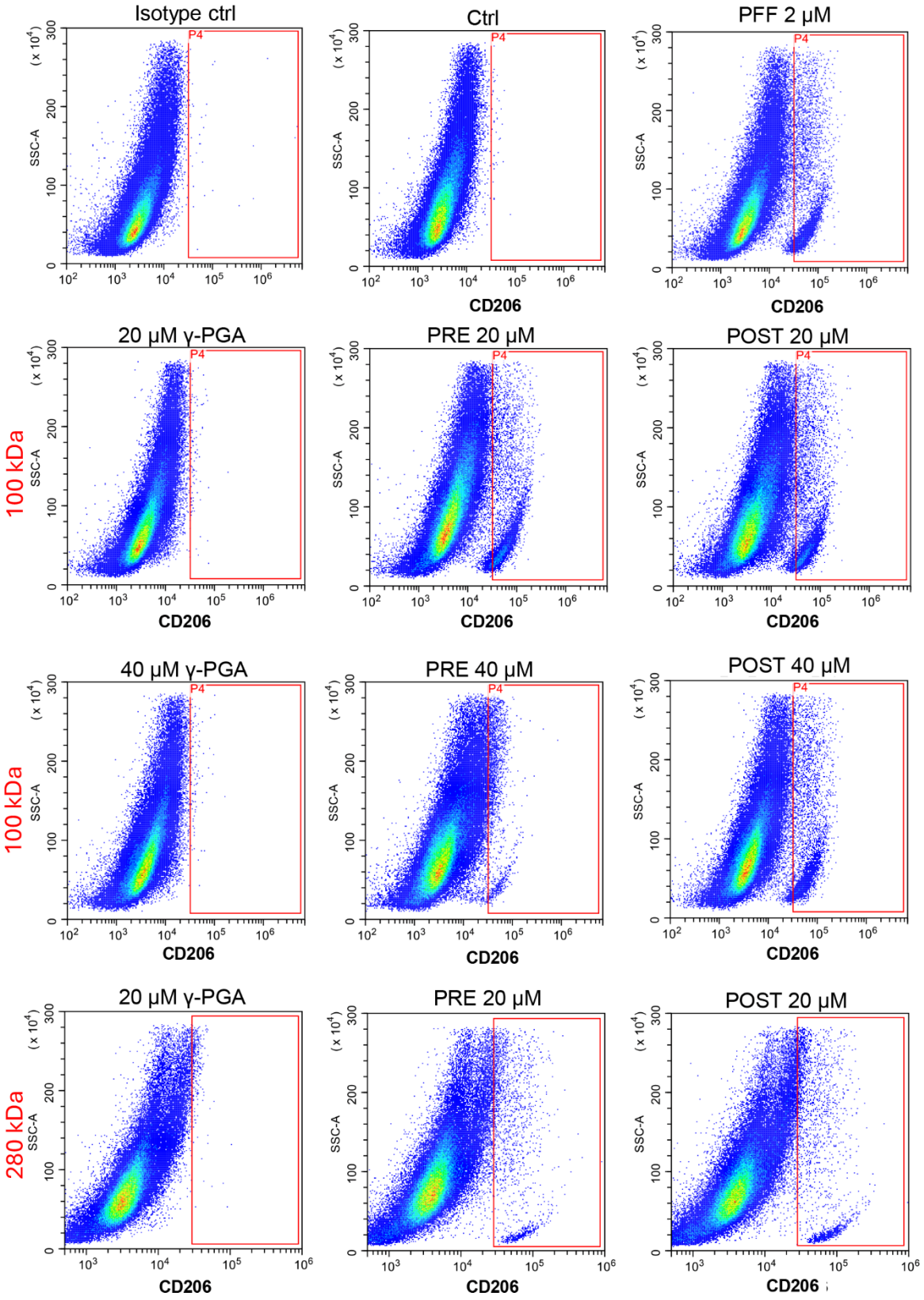

Figure I.4 CD206 marker expression in PFF and γ-PGA treated macrophages. *Representative flow cytometry dot plot showing the expression of CD86 in macrophages treated with PFFs, γ-PGA at 100 kDa and 280 kDa and in combination of PFFs and γ-PGA (PRE and POST treatment) compared to Ctrl. Positive populations are outlined in red gates made on the Isotype ctrl.*

Appendix II: published papers

International Journal of Biological Macromolecules 318 (2025) 145303

Contents lists available at ScienceDirect

International Journal of Biological Macromolecules

journal homepage: www.elsevier.com/locate/ijbiomac

Poly-γ-glutamic acid alleviates cytotoxicity and inflammation induced by pre-formed fibrils of α-synuclein in murine primary astrocytes

Claudia Novello [a,1], Mattia Parati [b,c,d,1], Samanta Mazzetti [a,e,2], Oriana Rampoldi [a], Huseyin Berkcan Isilgan [a], Milo Jarno Basellini [a], Chiara M.G. De Luca [f], Arianna Ciullini [f], Ilaria L. Dellarole [f], Alessandro Fantin [a], Isabella Russo [g], Brian L. Johnston [d,h], Moira Paroni [a], Chiara Rolando [a], Fabio Moda [i], Gianni Pezzoli [e], Iza K. Radecka [b], Graziella Cappelletti [a,*]

[a] Department of Biosciences, Università degli Studi di Milano, Milan, Italy
[b] Faculty of Science and Engineering, School of Life Sciences, University of Wolverhampton, United Kingdom
[c] FlexSea Ltd., London, United Kingdom
[d] iBiotech LTD., Wolverhampton, England, United Kingdom
[e] Fondazione Pezzoli per la Malattia di Parkinson, Milan, Italy
[f] Neurology 5, Neuropathology, Fondazione IRCSS Istituto Neurologico Carlo Besta, Milan, Italy
[g] Unit of Biology and Genetics, Department of Molecular and Translational Medicine, University of Brescia, Brescia, Italy
[h] School of Pharmacy, University of Wolverhampton, Wolverhampton, United Kingdom
[i] SSD Laboratory Medicine, Fondazione IRCSS Istituto Neurologico Carlo Besta, Milan, Italy

ARTICLE INFO

Keywords:
Poly-γ-glutamic acid (γ-PGA)
α-Synuclein
Parkinson's disease
Astrocytes
Fibrils
Inflammation

ABSTRACT

Poly-γ-glutamic acid (γ-PGA) is a bacterial-derived natural biopolymer that has gathered significant interest due to its antioxidant, anti-inflammatory, and neuroprotective properties. These characteristics make γ-PGA a potential candidate for the treatment of neurodegenerative diseases. In Parkinson's disease (PD), whose key pathological feature is the accumulation of neuronal α-synuclein aggregates, astrocytes, in addition to microglia, play a crucial role in clearing these aggregates; however, their capacity is limited. Overwhelmed astrocytes trigger an inflammatory response that exacerbates neurodegeneration. Therefore, strategies aimed at regulating the uptake of extracellular α-synuclein aggregates by astrocytes and mitigating inflammation could hold therapeutic promise. This work aimed to investigate the potential of γ-PGA in preventing or reversing the toxicity and inflammatory response induced by pre-formed α-synuclein fibrils (PFFs) in murine cortical astrocytes. Cell viability assays demonstrated that γ-PGA can counteract the toxicity induced by α-synuclein PFFs. Confocal microscopy and 3D reconstruction analyses revealed that γ-PGA colocalizes with PFFs, leading to a reduction in the uptake of these aggregates by astrocytes and a subsequent decrease in their inflammatory response. Consequently, γ-PGA emerges as a promising candidate for further investigation in the therapeutic management of PD.

1. Introduction

Poly-γ-glutamic acid (γ-PGA) is a biodegradable, non-toxic, eco-friendly, and non-immunogenic biopolymer whose interest in biomedicine has seen recent development. γ-PGA consists of glutamic acid monomers that are coupled to each other *via* amide bonds between α- or γ-carboxylic groups [1]. Unlike conventional proteins, γ-PGA is synthesized through the Poly-γ-Glutamate Synthetase intermembrane complex that allows the producer to form γ-peptidic bonds and adjust the molar mass [2]. Among its peculiar features, γ-PGA has

Abbreviations: FITC, Fluorescein-5-isothiocyanate; HBSS, Hanks' balanced salt solution; MTT, 3-(4,5-dimethylthiazol-2-yl)-2,5-diphenyl tetrazolium bromide; PD, Parkinson's disease; PFFs, pre-formed α-synuclein fibrils; RT, room temperature; ThT, Thioflavin T; TLR4, Toll-like receptor 4; γ-PGA, Poly-γ-glutamic acid.

* Corresponding author at: Department of Biosciences, Università degli Studi di Milano, 20133 Milano, Italy.
E-mail address: graziella.cappelletti@unimi.it (G. Cappelletti).

[1] Contributed equally.

[2] Present addresses: Department of Clinical Neurosciences, Parkinson and Movement Disorders Unit, Fondazione IRCCS Istituto Neurologico Carlo Besta, Milano, Italy.

https://doi.org/10.1016/j.ijbiomac.2025.145303
Received 18 December 2024; Received in revised form 29 May 2025; Accepted 14 June 2025
Available online 16 June 2025

demonstrated anti-inflammatory and antioxidative properties and has been shown to alleviate neuronal cell death and memory deficits [3–6], highlighting its potential therapeutic value in neurodegenerative diseases.

Parkinson's disease (PD) is the most common neurodegenerative movement disorder [7,8], pathologically associated with neuronal cell death in certain brain regions, and with the presence of aggregated α-synuclein-rich intraneuronal inclusions, known as Lewy bodies and Lewy neurites [9]. The α-synuclein aggregation process is known to result in the formation of various pathological species, culminating in the appearance of fibrils, the main component of such inclusions [10]. Current evidence also suggests that aggregates of α-synuclein may be transmitted from cell to cell, contributing to disease progression [11]. Several studies in cellular models support the idea that such transfer could occur through different pathways, including tunneling nanotubes, endocytosis, and exosomes [12–14]. Moreover, it is known that α-synuclein aggregates can be secreted from neurons during stress or their degeneration, resulting in an increased concentration of aggregates in the extracellular environment [15,16]. Extracellular α-synuclein aggregates not only could be taken up by neurons but could also affect the phenotype and behaviour of other cell types such as astrocytes [17–19]. Indeed, astrocytes are involved in the clearance of extracellular aggregated α-synuclein species released from neurons by internalizing and degrading them through the endo-lysosomal pathway, thus playing a protective role for neurons. However, their capacity is limited, and excessive uptake can overwhelm astrocytes, leading to cellular toxicity [20]. Moreover, high concentrations of α-synuclein in the extracellular environment activate the innate immune-dependent inflammatory pathway that induces the acquisition by astrocytes of a reactive inflammatory phenotype (A1 type). This feature could contribute to the progression of the pathology as astrocytes lose the ability to promote neuronal survival, synaptogenesis, outgrowth, and phagocytosis, and release pro-inflammatory molecules that trigger neuronal cell death [21,22]. Thus, approaches that can regulate extracellular α-synuclein aggregates and act on neuroinflammation might be beneficial.

Here we aim to explore the biological effect of γ-PGA, produced through fermentation from generally recognized as safe (GRAS) organism *Bacillus subtilis* natto, in murine primary astrocytes exposed to α-synuclein pre-formed fibrils (PFFs), a recognized cellular model used to recapitulate astrocyte pathological hallmarks in PD [23,24]. We investigated the protective effect of γ-PGA on cell viability and cell inflammation, focusing our attention on the interplay between γ-PGA and α-synuclein PFFs. To this end, we tested two types of conditions through administration of γ-PGA before or after the treatment with α-synuclein PFFs. From these investigations, we observed that γ-PGA reverses PFF cytotoxic effect by acting on the amount of their internalization and cellular inflammation. Interestingly, *in vitro* data indicate that γ-PGA could potentially affect α-synuclein aggregation. Collectively, our data suggest that γ-PGA should be further explored as a novel therapeutic compound in the context of α-synuclein pathology and its treatment.

2. Material and methods

2.1. α-Synuclein pre-formed fibrils (PFFs) preparation

Human α-synuclein was produced by *E. coli* (BL21(BE3)) and purified as previously described [25]. Lyophilized α-synuclein was resuspended in sterile PBS, and ultracentrifuged at 220,000*g* for 45 min at 4 °C. Then, the obtained supernatant was collected and placed in the thermomixer for 14 days at 1000 rpm. Enriched-PFFs, isolated by the soluble part of the preparation by centrifugation at 16,100*g* for 15 min, were then quantified relative to the initial concentration of monomer before fibrillation and resuspended in sterile PBS at the concentration of 5 mg/ml [26]. α-Synuclein PFFs' fibrillation and structure were verified by Thioflavin T (ThT) assay and electron microscopy (Fig. S1). For ThT assay, 10 μM α-synuclein PFFs and supernatant containing monomer were added to 25 μM of ThT in PBS, mixed and incubated for 15 min at RT. 25 μM of ThT in PBS was used as a control measurement. Fluorescence emission spectra were recorded at 482 nm upon excitation at 440 nm confirming the increased fluorescence of α-synuclein PFFs, containing amyloid-like fibrils, compared to monomers (Fig. S1, A). For electron microscopy, 7 μl of 25 μM protein sample was applied to glow discharged carbon formvar copper grids and allowed to air-dry. Then, negative staining was performed with 1 % uranyl acetate, applied twice to the grids for 15 s. Electron microscopy images were captured using a Talos L120C microscopy (Fig. S1, B).

pHrodo α-synuclein PFFs were generated by using pHrodo™ iFL Green Microscale Protein Labeling kit (Thermo Fisher Scientific, P36015). In detail, α-synuclein PFFs, resuspended at a concentration of 1 mg/ml in PBS with 100 mM sodium bicarbonate, were incubated with pHrodo, dissolved in 50 μl of DMSO for 90 min in the dark. pHRodo α-synuclein PFFs, isolated by centrifugation at 16,100*g* for 15 min, were washed with PBS twice to remove the unconjugated pHrodo and resuspended in sterile PBS at the desired concentration.

2.2. γ-PGA preparation

Lyophilized γ-PGA (Natto, Japan) of 193 kDa molecular weight was resuspended in sterile PBS to obtain a 2 mM stock solution. Then, the initial pH of 5.5 was adjusted to 7.4.

For the visualization in immunofluorescence, γ-PGA was conjugated with Fluorescein-5-isothiocyanate (FITC) (Merck, 3326-32-7) as previously described [27]. In detail, γ-PGA was incubated with FITC with a 1:0.01 ratio in the dark at RT. After 90 min, the solution was eluted in a PD Spintrap™ G-25 column using sterile PBS (Merck, GE28–9180-04), to remove the unconjugated FITC.

2.3. Cortical primary astrocyte culture

Primary astrocytic cultures were derived from the spare cortex of postnatal days 1–3 (P1-P3) C57BL/6J WT mice, as previously described [28]. Animal procedures were carried out in accordance with the guidelines of the care and use of laboratory animals established by Italian and European Directives (D. Lgs n° 2014/26, 2010/63/UE). Cerebral cortices were dissociated in cold Hanks' balanced salt solution (HBSS, Euroclone) with 1 % Penicillin/Streptomycin (Euroclone). After enzymatic and mechanical dissociation, the cell suspension was centrifuged twice for 5 min at 200*g*. Successively, cells were resuspended in complete astrocytes medium containing DMEM high glucose, 10 % Fetal Bovine Serum (FBS, Euroclone), 1 % Penicillin/ Streptomycin. Cell suspension was plated in a T75 or T25 flask previously coated with poly-L-Lysine 10 μg/ml and maintained in culture at 37 °C with 5 % CO_2. The following day, the flasks were washed with PBS to remove any residual tissue. The culture was maintained until confluence, at which point cells were shaken at 200 rpm for 2 h to remove microglia and oligodendrocytes, obtaining a pure astrocyte culture.

2.4. Cell treatment

Cells were cultured onto poly-L-Lysine (10 μg/ml)-coated coverslips in a 24-well plate, in a poly-L-Lysine (10 μg/ml)-coated 48-well plate or 6-well plate at a density of $2.1 \times 10^4/cm^2$ for 24 h. Then, cells were treated with 2 μM PFFs and 27.5 μM γ-PGA in two conditions: *i*) the PRE treatment, in which γ-PGA is added before PFFs, and *ii*) the POST treatment, in which cells are first exposed to PFFs and then to γ-PGA. In both cases, PFFs treatment was carried out for 18 h while γ-PGA is added 2 h before or after PFFs.

2.5. Cell viability assay

3-(4,5-Dimethylthiazol-2-yl)-2,5-diphenyl tetrazolium bromide

(MTT) assay was performed to evaluate the cytotoxic effect of γ-PGA and PFFs. Cells were seeded in a poly-L-Lysine-coated 48 well plate, cultured for 24 h and treated with 2 μM PFFs, γ-PGA at different concentrations (0.275, 2.75, 27.5 μM) or a combination of the two following PRE and POST treatment. At the end of the treatment, cells were incubated with 0.5 mg/ml MTT solution (Merck, code number: M2128) for 3 h at 37 °C. Formazan crystals that had formed were dissolved using a 0.1 M HCl, Triton X-100 in isopropanol solution. Then, optical density (OD) was recorded at 570 nm using an Ensight plate reader.

2.6. Immunofluorescence

Cells were fixed with 4 % paraformaldehyde for 10 min at RT and blocked with 1 % BSA diluted in PBS containing 0.3 % Triton X-100 for 1 h at RT. Primary antibodies were diluted in 1 % BSA, 0.1 % Triton X-100 in PBS; in detail, the following antibodies, incubated overnight at 4 °C, were used: mouse anti-α-synuclein 1:500 (Merck, code number: S5566), goat anti-Complement C3 1:500 (Life technologies, code number PA1-29715), chicken anti S100β 1:700 (Synaptic Systems, code number: 284006), and anti-LAMP1 1:500 (Abcam, code number ab24170). The following day, after three washes with PBS, cells were incubated for 45 min at RT with secondary antibodies diluted in 0.1 % BSA in PBS. The secondary antibodies used were: donkey anti-mouse Alexa 647 1:500 (Life technologies, code number: A32787), donkey anti-rabbit Alexa 488 (Life technologies, code number: A21206), donkey anti-goat Alexa 488 1:300, and donkey anti-chicken 568 1:300 (Jackson Immunoresearch, code numbers: 705-545-147, and 703-165-155, respectively). Later, after 3 washes with PBS, nuclei were stained using Hoechst 33342 1:5000 in PBS for 10 min at RT and mounted using Mowiol®, DABCO®. Images were acquired with a 20× objective, an oil-immersion 60× objective or a silicon-immersion 100× objective, using a Nikon spinning disk confocal microscope, equipped with CSI–W1 confocal scanner unit, and a Nikon A1 laser scanning confocal microscope.

2.7. 3D reconstruction

For 3D visualization, images were imported into arivis Vision4D® 3.6.0 software (Zeiss Company). The region of interest (ROI) from 100× acquisitions was created using the "Transformation gallery > Crop" tool. The "Intensity threshold segmentation" pipeline was applied to reconstruct α-synuclein PFFs, S100β, and nuclei continuous staining. γ-PGA staining, which shows a punctate distribution, was reconstructed using the "blob finder" pipeline.

2.8. Western blotting

Primary astrocytes, seeded in a 6-well plate, were lysed in Laemmli buffer. Equal amounts of protein (20 μg) were separated by SDS-PAGE and transferred overnight to a PVDF membrane (Immobilon®-P transfer membrane, Merck, code number IPFL00005). Membranes were blocked with 5 % BSA diluted in Tris-buffered saline (TBS: 20 mM Tris, 150 mM NaCl, pH 7.6) for 1 h at RT and incubated overnight at 4 °C with the following primary antibodies diluted in TBS containing 0.1 % Tween-20 (TBST): LC3 1:1000 (SIGMA-Aldrich, code number: L8918), p62 1:2000 (SIGMA-Aldrich, code number P0067), GAPDH 1:5000 (SIGMA-Aldrich, code number: G8795). Then, membranes were washed with TBST for 3 times and incubated with secondary antibody donkey anti-rabbit Alexa 488 1:4000 (Invitrogen, code number A21206) for 1 h at RT. After 3 washes, blots were visualized using iBright™ FL1500 (Life technologies) and band intensities were quantified using ImageJ software.

2.9. Enzyme linked immunosorbent assay (ELISA)

Supernatants of 200,000 cells were collected after 18 h of treatment as previously described, and analyzed for IL-6 (BioLegend, code number 431301), TNF-α (BioLegend, code number 430901), CXCL10 (Bio-Techne, code number DY466-05), and IL-1β (BioLegend, code number 432601) by ELISA according to the manufacturer's instructions. ELISA plates were read on microplate reader (SAFAS MP96), and data were analyzed with Prism software.

2.10. α-Synuclein aggregation studies

In vitro studies were performed to evaluate the potential effect of γ-PGA on α-synuclein aggregation. The experiments were performed using a black 384-well optical flat bottom plate (Life technologies). Each well was filled with the reaction mix composed of 170 mM NaCl, 40 mM PBS, pH 8, 10 μM Thioflavin-T (ThT), 7 μM α-synuclein with or without the presence of γ-PGA at three different concentrations (2.75 μM, 27.5 μM and 275 μM), reaching a final reaction volume of 50 μl. Two silica beads (0.8 mm) were added to each well to sustain α-synuclein aggregation. The capacity of γ-PGA to undergo self-assembly was evaluated. Finally, 7 μM PFFs were pre-incubated with 275 μM γ-PGA for 2 h at 37 °C to assess the effect of γ-PGA treated PFFs on α-synuclein aggregation compared to untreated PFFs. Each experimental condition was analyzed in quadruplicate to ensure reliability. The plates were inserted into a FLUOstar CLARIOSTAR microplate reader (BMG Labtech) and subjected to alternating cycles of shaking (1 min, 600 rpm, single orbital), and incubation (14 min at 42 °C). Fluorescence readings (480 nm) were taken every 15 min (30 flashes per well at 450 nm). The mean fluorescence values obtained from the four replicates of each sample were plotted on a graph against time.

Following the aggregation kinetics, samples were analyzed with transmission electron microscopy as described in Section 2.1.

2.11. Statistical analyses

Statistical analyses were conducted using GraphPad Prism 8 software (San Diego, CA, USA). All quantitative data are expressed as mean ± SEM and represent at least four independent sets of experiments. Depending on whether the data fitted a normal distribution, parametric or non-parametric One-way ANOVA was used for multiple comparisons of data. Significance was established at p value <0.05.

3. Results

3.1. γ-PGA rescues α-synuclein PFF induced cytotoxicity on murine primary astrocytes

γ-PGA is a well-characterized, non-toxic, and non-immunogenic biomacromolecule [1] but its effect on murine primary astrocytes has yet to be investigated. Thus, to examine the potential cytotoxic effects of γ-PGA on astrocytes, cells were incubated with increasing concentrations of γ-PGA for 24 h and viability was evaluated using MTT assay. As expected, we observed that γ-PGA had no cytotoxic effect on primary astrocytes at any of the tested concentrations (0.275, 2.75, and 27.5 μM). Surprisingly, we observed a dose-dependent increase in cell viability, with the 27.5 μM concentration significantly improving primary astrocytes viability compared to the control and the 0.275 μM concentration (Fig. 1A). Therefore, 27.5 μM concentration was selected to test the protective or recovery effect of γ-PGA on PFF-treated primary astrocytes, a widely used model to recapitulate the pathological features of astrocytes in PD [23,29]. For this purpose, we used a treatment approach of either adding γ-PGA before (PRE treatment) or after (POST treatment) PFFs administration. As expected, the addition of PFFs to astrocytes decreased cell survival. Interestingly, cell survival was significantly rescued with the POST treatment of γ-PGA (Fig. 1B).

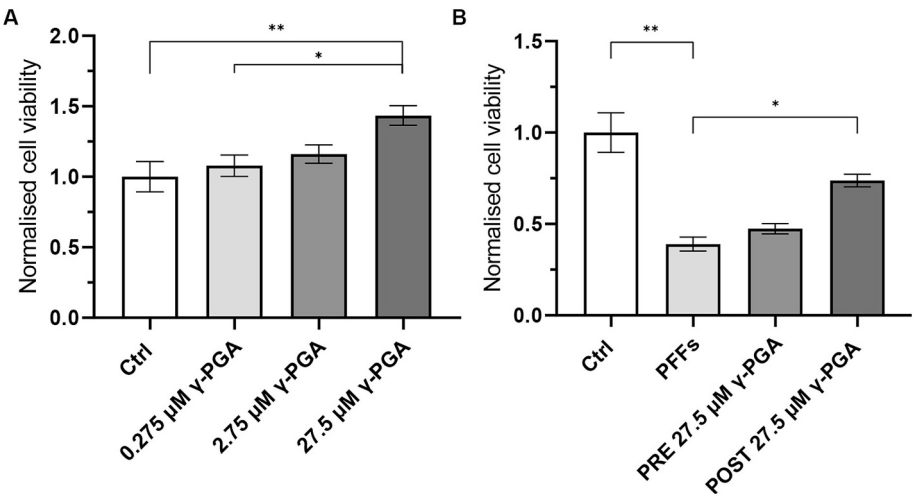

Fig. 1. γ-PGA rescues α-synuclein PFF-induced toxicity in primary astrocytes. A) Cell viability of primary astrocytes treated with increasing concentrations of γ-PGA (0.275, 2.75, 27.5 μM). Data are expressed as mean ± SEM, normalized to control and analyzed by ordinary one-way ANOVA with Tukey's *post hoc* test ($n = 5$). B) Cell viability of primary astrocytes treated with α-synuclein PFFs alone and in co-treatment with γ-PGA added before (PRE) or after PFFs (POST). Data are expressed as mean ± SEM, normalized to control and analyzed by Kruskal-Wallis test with Dunn's correction (n = 5), $^{**}p < 0.01$, $^{*}p < 0.05$.

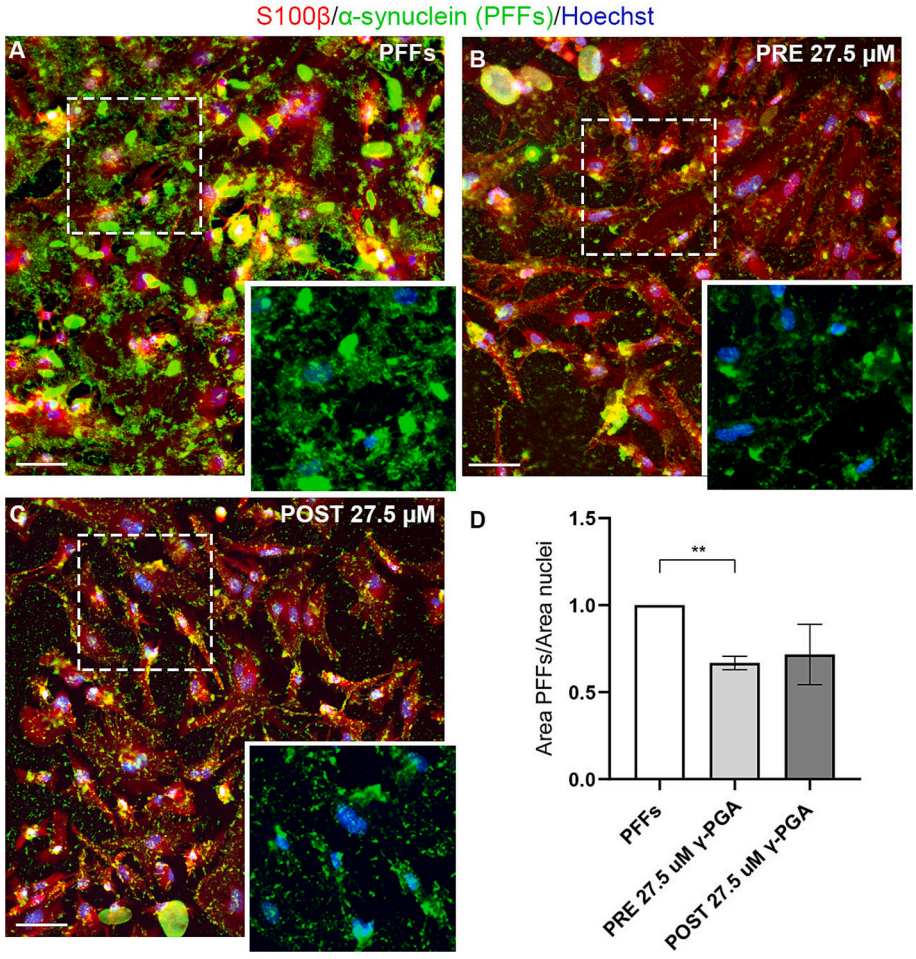

Fig. 2. γ-PGA limits the extent of α-synuclein PFFs in primary astrocytes. Spinning disk confocal microscopy images showing α-synuclein PFFs distribution in primary astrocytes, labeled with S100β (A) and treated with γ-PGA before (B) or after (C) the addition of PFFs. Nuclei were counterstained with Hoechst. Scale bar, 50 μm (D). The graph shows the total area of PFFs normalized on the area of nuclei. Data are expressed as fold change of control ± SEM and analyzed by One sample *t*-test ($n = 4$), $^{**}p < 0.01$.

3.2. γ-PGA impacts on the distribution of α-synuclein PFFs in primary astrocyte culture

We explored whether the impact of γ-PGA on astrocyte viability could be attributed to its capacity to modulate or interfere with α-synuclein PFFs. Hence, with the same experimental design, we initially analyzed, by immunofluorescence and using an antibody against total α-synuclein, the total area of α-synuclein PFFs (Fig. 2). By adding γ-PGA either before or after PFFs, the extent of α-synuclein aggregates was reduced compared to PFF treatment alone (Fig. 2A, B, C). Notably, the PRE treatment significantly decreased the total area of PFFs compared to PFF treatment alone (Fig. 2D). To further assess how γ-PGA distributes relative to α-synuclein PFFs in astrocytes cell culture, we labeled γ-PGA with FITC and investigated its localization by means of immunofluorescence assay. We observed that when astrocytes were treated with γ-PGA only, γ-PGA distributed mainly inside the cells (Fig. 3A, white arrowheads), as shown by the orthogonal view of the image (Fig. 3A', A"), and by 3D reconstruction with arivis Vision4D® 3.6.0 software (Fig. 3B, B'; white arrowheads; Supplementary Movie 1). When astrocytes were treated with α-synuclein PFFs only, we also observed their intra and extracellular distribution (Fig. 3B, white arrowheads and arrow, respectively). Z-axis orthogonal projections of confocal multiplane images revealed the internalization of α-synuclein PFFs within astrocytes (Fig. 3C-C"), further confirmed by the 3D reconstruction with arivis Vision4D® 3.6.0 software (Fig. 3D', white arrowheads; Supplementary Video 2). Lastly, when γ-PGA was co-administered with

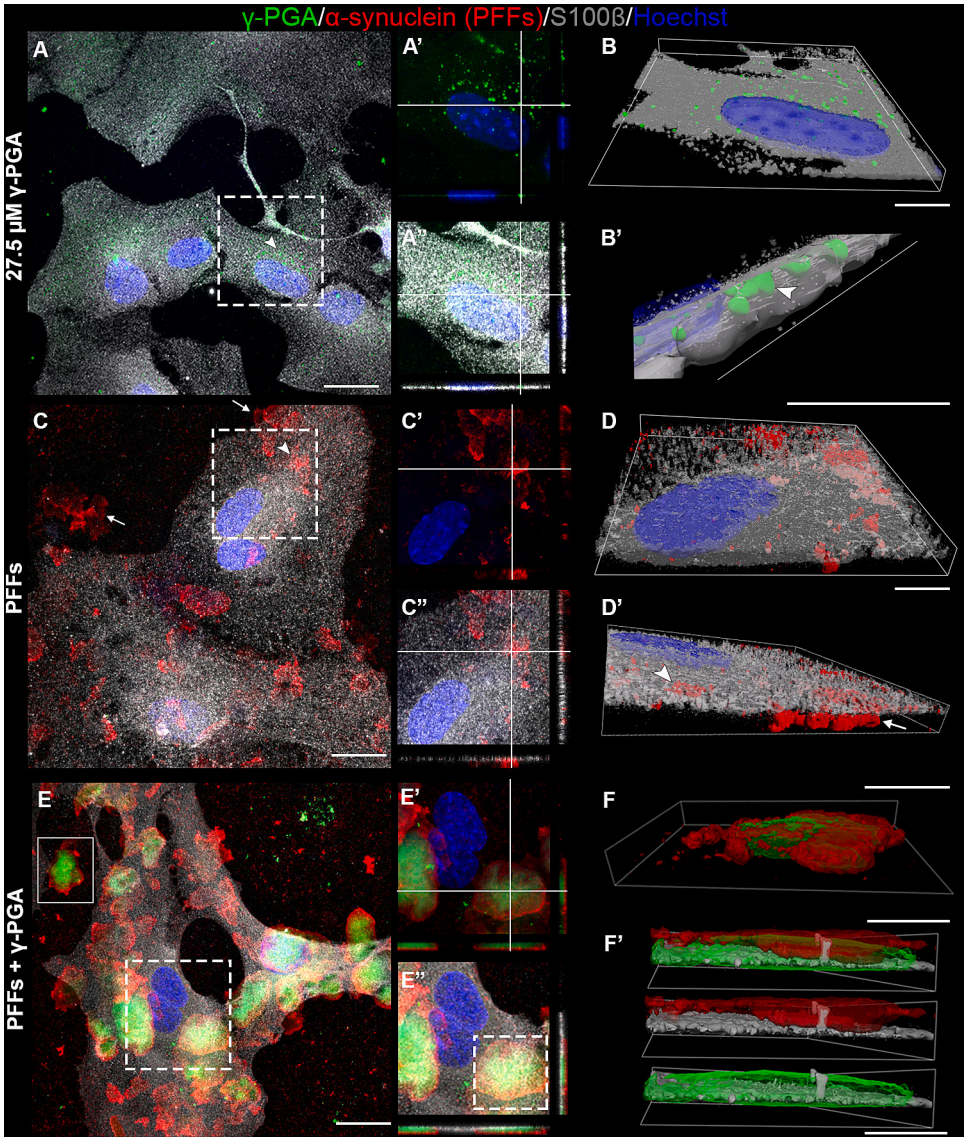

Fig. 3. The interplay between γ-PGA and α-synuclein PFFs in primary astrocytes. **A)** Spinning disk confocal images showing the distribution of γ-PGA in murine primary astrocytes. A' and A" show the magnification of the dashed rectangle in A and the orthogonal projections that represent the XZ (bottom) and YZ (right) planes and highlight the presence of γ-PGA inside the cell. B and B′ show the top and side view of the 3D reconstructions obtained with arivis Vision4D® 3.6.0 software of A". C) Spinning disk confocal images showing α-synuclein PFFs distribution in astrocytes. C′ and C″ show the magnification of the dashed rectangle in C and the *Z*-axis projection. D and D′ show the top and side view of the 3D reconstructions obtained with arivis Vision4D® 3.6.0 software of C. E) Representative spinning disk confocal image of PRE treatment with γ-PGA of primary astrocytes. E' and E" show the magnification of the dashed rectangle in E and orthogonal view showing the distribution of γ-PGA relative to α-synuclein PFFs. F represents the 3D reconstruction by arivis Vision4D® 3.6.0 software of the rectangle in E showing γ-PGA and α-synuclein PFF colocalization in the extracellular environment. F′ illustrates the lateral view of 3D reconstruction of the dashed rectangle in E"; the split channels highlight the disposition of γ-PGA and α-synuclein PFFs when compared to S100β labeled astrocytes. Nuclei were counterstained with Hoechst. White arrows and white arrowheads in A, B′, C and D′ show the intracellular and extracellular localization, respectively, of either y-PGA or PFFs. A, A', A", C, C′, C″, E, E', E": scale bar, 20 µm. B, B′, D, D′, F, F′: scale bar, 5 µm.

α-synuclein PFFs to primary astrocytes, we observed that γ-PGA colocalized with α-synuclein PFFs in both PRE treatment (Fig. 3E, F, Supplementary Movie 3) and POST treatment (data not shown). Moreover, upon observing their arrangement relative to the cell, γ-PGA clearly localized between α-synuclein PFFs and S100β-labeled astrocytes, as shown in the orthogonal projection (Fig. 3E, E") and 3D reconstruction (Fig. 3F').

3.3. γ-PGA limits the internalization of α-synuclein PFFs by primary astrocytes

The amount of α-synuclein PFFs within astrocytes is a key factor, which affects their ability to clear it, whereby excessive accumulation could impair the protein's degradation pathway [30]. Thus, we explored whether γ-PGA could have any impact on the internalization of PFFs by astrocytes. To evaluate this hypothesis, we labeled α-synuclein PFFs with a pH-sensitive dye (pHrodo-PFFs) that becomes fluorescent when the pH of the surrounding environment increases in acidity, such as late endosomes and lysosomes. We noted that fluorescence area and intensity of pHrodo-PFFs were significantly lower following both γ-PGA treatments (Fig. 4B, C) compared to pHrodo-PFFs alone (Fig. 4A). Notably, γ-PGA PRE-treatment was the most effective in reducing α-synuclein PFF internalization (Fig. 4D). In parallel, we explored whether γ-PGA may affect the degradation of PFFs by analyzing the autophagic and lysosomal pathways involved in their clearance [31,32]. To assess the effect of γ-PGA treatment on autophagy, we examined LC3 and p62 levels by Western blotting. Treatment with α-synuclein PFFs led to a significant increase of LC3-II/LC3-I ratio (Fig. 4E, F) and accumulation of p62 (Fig. 4E, G), suggesting an impairment in the autophagic flux. Although no differences were observed with PRE-treatment of γ-PGA, POST treatment resulted in a mild decrease in p62 levels (Fig. 4E, G). With respect to the lysosomal pathway, we employed LAMP1 as a marker of autophagy-related lysosomal organelles [33], and found an increase in LAMP1 fluorescence area and intensity with PFF treatment, that was not altered by γ-PGA treatment (Fig. S2). These results suggest that γ-PGA mainly exerts its effect by limiting PFF internalization in primary astrocytes.

3.4. γ-PGA prevents and recovers PFF-induced inflammation in primary astrocytes

It is widely recognized that astrocytes play a key role in the inflammatory response during PD pathogenesis [17]. Several studies have shown that α-synuclein aggregates can activate the astrocytic inflammatory response inducing the acquisition of a reactive phenotype that exacerbates the pathological condition [29,34]. Thus, given the anti-inflammatory properties of γ-PGA [4,5], we tested whether this biomacromolecule could prevent or alleviate astrocytes inflammation induced by α-synuclein PFFs. Immunofluorescence assay was employed to evaluate Complement C3 protein, a marker of A1 reactive astrocytes [21] (Fig. 5). As expected, γ-PGA alone had no effect on C3 protein in terms of both fluorescence area and intensity (Fig. S3) whereas treatment with α-synuclein PFFs increased C3 deposition compared to the control (Fig. 5A, B). Both PRE and POST treatment with γ-PGA significantly reduced fluorescence area and intensity of C3 staining compared to PFFs (Fig. 5C, D, E, F). Notably, we did not observe any significant difference in γ-PGA anti-inflammatory properties between PRE and POST treatment (Fig. 5E, F).

To further investigate the inflammatory response, we measured the levels of pro-inflammatory cytokines released by treated astrocytes, including TNF-α, IL-1β, IL-6, and the chemokine CXCL10, which have previously been reported to be elevated in PFF treated astrocytes [24,35]. In both control and γ-PGA-treated astrocytes, we detected very low levels of CXCL10 and IL-1β release (Fig. 5G, H), while no detectable levels of TNF-α and IL-6 were observed (Fig. 5I, J). As expected, PFF treatment led to a significant increase in the release of CXCL10, IL-1β and TNF-α, which was significantly attenuated following POST treatment with γ-PGA (Fig. 5G, H, I). Moreover, no differences were found between control and POST treatment. Regarding IL-6, γ-PGA POST treatment showed a trend toward reduced release in PFF treated cells (Fig. 5J). Collectively, these findings support the role of γ-PGA in attenuating the inflammatory response induced by α-synuclein PFFs.

3.5. γ-PGA affects α-synuclein aggregation in vitro

To thoroughly investigate whether γ-PGA interferes with α-synuclein aggregation *per se*, we performed *in vitro* studies and showed the biopolymer's capacity to delay the aggregation of α-synuclein in a dose-dependent manner (Fig. 6A). In particular, the green curve shows the aggregation kinetics of α-synuclein in the absence of γ-PGA. The pink, blue and red curves refer to the experimental conditions with increasing concentrations of γ-PGA at 2.75 μM, 27.5 μM and 275 μM, respectively. Remarkably, the 27.5 μM and the 275 μM concentrations were the most effective in inhibiting the aggregation of α-synuclein. Notably, at the concentration of 275 μM, aggregation did not occur even after 40 h. The gray curves in the graph refer to γ-PGA alone (at the different concentrations tested: 2.75 μM, 27.5 μM, and 275 μM) and none of them show any propensity to undergo self-assembly.

Samples collected following incubation with 27.5 μM of γ-PGA, were analyzed by electron microscopy to better characterize the effect of the polymer on the presence and the structure of α-synuclein aggregates. Following γ-PGA incubation with monomeric α-synuclein, no fibrils were observed, while oligomer-like structures were detected (Fig. S4). This strengthens the role of γ-PGA in interfering with α-synuclein aggregation.

The highest concentration of γ-PGA (275 μM) was used to treat PFFs before testing their ability to trigger the aggregation of α-synuclein (Fig. 6B). Both treated and untreated PFFs (purple and orange curves, respectively) were able to accelerate the aggregation kinetics of α-synuclein (green curve). Interestingly, a trend toward attenuation of PFF effect is observed when preincubated with γ-PGA.

4. Discussion

γ-PGA is an innovative, non-toxic, non-immunogenic biopolymer whose biosynthetic pathway allows the producer to create γ-peptidic bonds with variations in both molar mass and crystallinity [2]. This unique feature has led to growing interest in γ-PGA, owing to its diverse properties that make it suitable for a variety of research areas, including biomedicine [36,37]. Among its features, the antioxidant, anti-inflammatory, and neuronal cell death-attenuation properties are remarkable [3–6]. This study explored, for the first time, the biological effect of γ-PGA in the field of PD. γ-PGA can be synthesized naturally by *Bacillus subtilis* during the fermentation of Natto beans. These traditional soybean fermented foods are highly consumed in Japan where, interestingly, the relative PD incidence rate is reported to be significantly lower than in Europe [38]. Given the properties of γ-PGA, we investigated its biological effect on murine primary astrocytes treated with α-synuclein PFFs as a model of PD for the study of cytotoxicity, neuroinflammation, and protein clearance. Indeed, astrocytes play a crucial role in PD pathogenesis by regulating both the clearance of extracellular aggregated α-synuclein and the modulation of neuroinflammatory responses [20,39]. We chose two types of treatment by either administering γ-PGA before or after α-synuclein PFFs to explore its protective or rescue effect on murine primary astrocytes. The major finding of our study is that γ-PGA reverses the cytotoxic effects of α-synuclein PFFs, acts on the ability of astrocytes to internalize them and decreases cellular inflammation, as summarized by the proposed model in Fig. 7.

Given that one of the main challenges in the neurodegeneration field is to design protective strategies based on chemical or biological drugs, our work aims to tackle this by exploring the properties of γ-PGA.

Emerging research has demonstrated the non-toxic and excellent

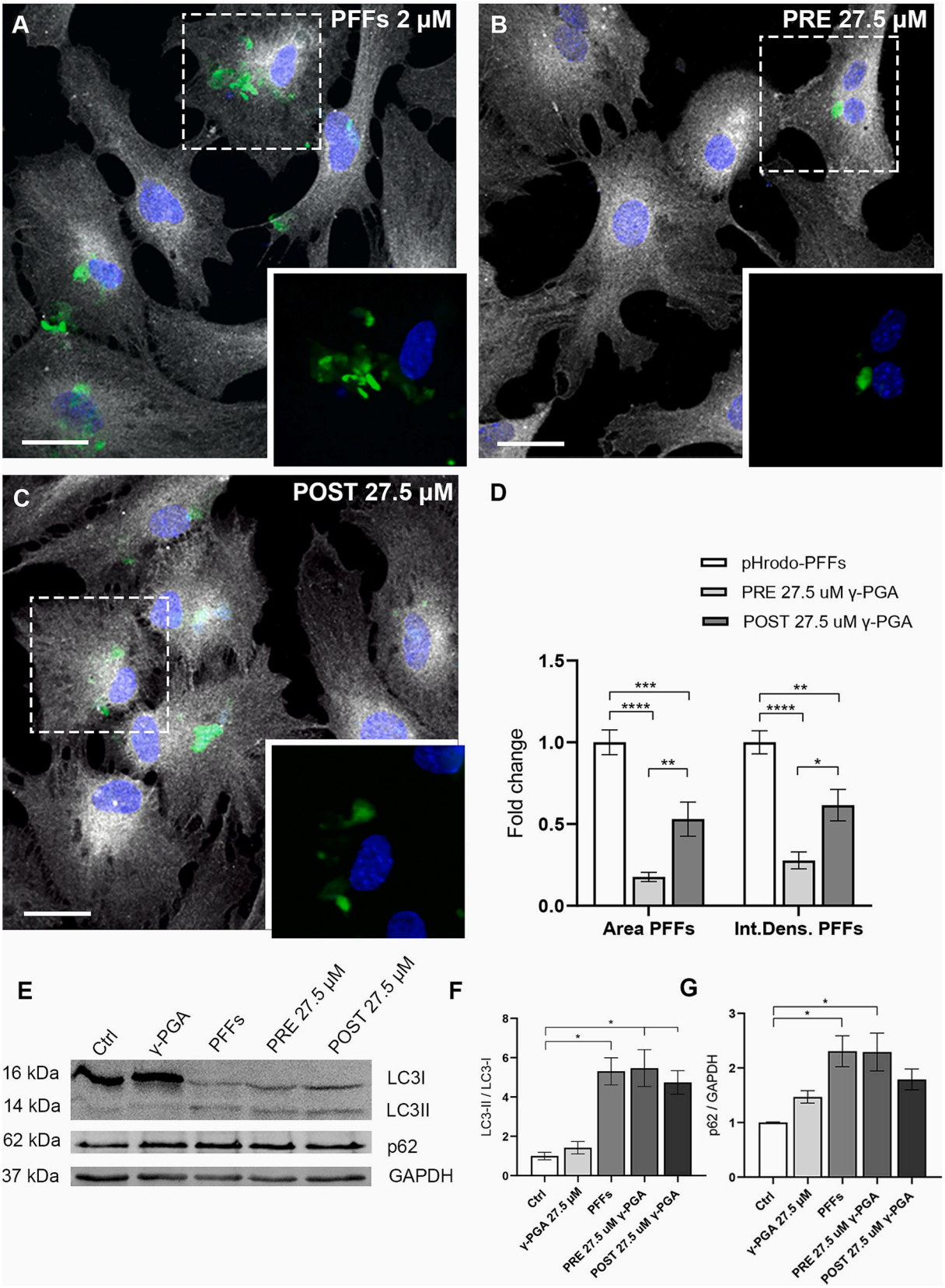

Fig. 4. γ-PGA administration decreases PFFs internalization by primary astrocytes. Maximum intensity Z-projection confocal images of primary astrocytes labeled with S100β and treated with pHrodo-PFFs (A) and with γ-PGA added before (B) or after (C) PFFs. Nuclei were counterstained using Hoechst. Scale bar, 20 μm. D) The graph shows the area covered by pHrodo-PFFs and pHrodo-PFF fluorescence intensity (Integrated Density) both normalized on the area of nuclei. E) Representative immunoblots for LC3 (LC3I, 16 kDa; LC3II, 14 kDa), p62 (62 kDa) and GAPDH (37 kDa). G) and H) graphs show LC3-II/LC3-I ratio and quantification of p62 normalized over GAPDH. Data are reported as mean ± SEM, normalized to control and analyzed by ordinary one-way ANOVA with Tukey's *post hoc* test ($n = 4$), $^{*}p < 0.05$, $^{**}p < 0.01$, $^{***}p < 0.001$, $^{****}p < 0.0001$.

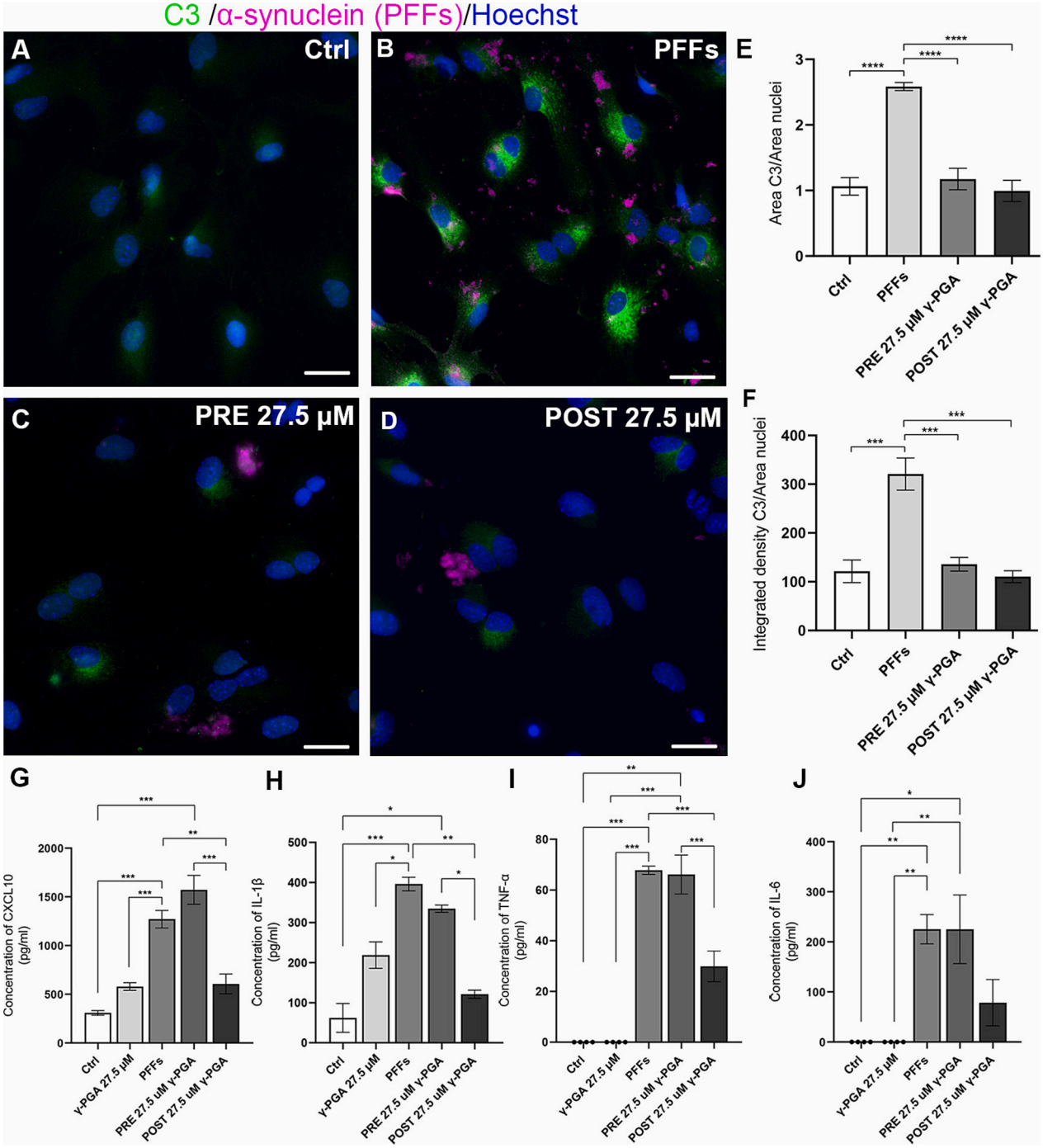

Fig. 5. γ-PGA administration decreases PFF-induced inflammation in primary astrocytes. Representative confocal images showing complement C3 staining in primary astrocytes in control condition (A), treated with PFFs (B) and with γ-PGA added before (C) or after (D) the addition of PFFs. Nuclei were counterstained using Hoechst. Scale bar, 20 μm. The Graphs show area (E) and fluorescence intensity (Integrated density) (F) of C3 protein normalized on the area of nuclei. Graphs G, H, I and J respectively show CXCL10, IL-1β, TNF-α, and IL-6 release by primary astrocytes alone or in the presence of γ-PGA, PFFs or the combination of the two, quantified by ELISA. Data are reported as mean ± SEM and analyzed by ordinary one-way ANOVA with Tukey's *post hoc* test (n = 4), *p < 0.05, **p < 0.01, ***p < 0.001, ****p < 0.0001.

safety profile of γ-PGA in diverse experimental settings [2,6]. Here, we tested whether γ-PGA could affect primary murine astrocyte survival and reported that, it increased cell viability in a dose-dependent manner. In the context of α-synuclein PFFs, multiple evidence suggests that aggregated α-synuclein species induce toxicity [40]. However, the mechanisms are still debated. Some studies hypothesize that the interaction of aggregated α-synuclein with cellular membranes induces their disruption, activation of inflammatory pathways, autophagic and lysosomal processes, and cell death through apoptosis [24,41]. We report that α-synuclein PFFs decrease astrocyte viability and that γ-PGA, can counteract PFF-induced toxicity, suggesting that the polymer may have cell-protective effects. Our results could be explained in two possible ways. First, cell protection could be due to the potent antioxidant properties of γ-PGA that can act as ion chelator, free radical scavenger, and inhibitor of lipid peroxidation [6]. Indeed, we demonstrated, for the first time, that γ-PGA is readily internalized by astrocytes, with

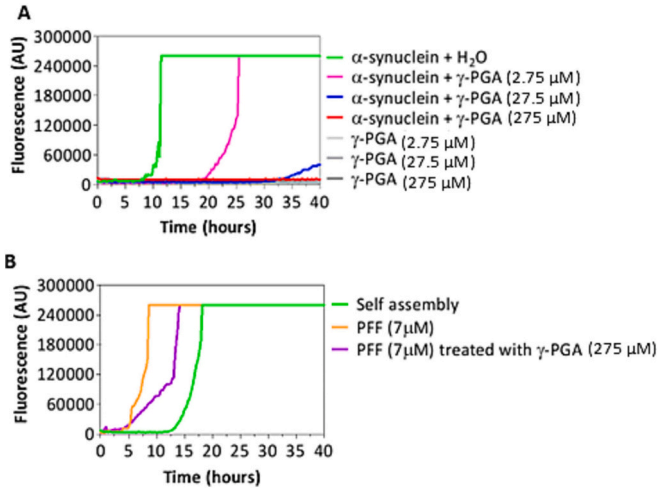

Fig. 6. γ-PGA affects α-synuclein aggregate formation *in vitro*. A) Aggregation kinetics of monomeric α-synuclein supplemented with different concentrations of γ-PGA: 2.75 μM (pink curve), 27.5 μM (blue curve) and 275 μM (red curve). The gray lines refer to γ-PGA alone (2.75, 27.5, 275 μM). B) Aggregation kinetics of monomeric α-synuclein in the presence of PFFs either treated with 275 μM of γ-PGA (purple curve) or untreated (orange curve). The graphs show the average fluorescence intensity of the four replicates for each curve plotted against time.

diffuse, punctate cytoplasmatic localization. Secondly, γ-PGA may exert a direct buffering effect on α-synuclein PFFs thereby reducing their toxicity.

Looking at the interplay between γ-PGA and α-synuclein, our data gathered from *in vitro* α-synuclein aggregation assay suggest that γ-PGA could interfere with the aggregation process in a dose-dependent manner, with a trend toward attenuation of PFF assembly even when incubated with pre-formed aggregates. Moreover, incubation with γ-PGA seems to reduce the presence of fibrils, along with the appearance of small α-synuclein oligomer-like structure, suggesting that γ-PGA may influence α-synuclein aggregation in a cell-free system. Nevertheless, the polydispersity of α-synuclein PFFs should be considered when interpreting this type of *in vitro* assays, as the impact of γ-PGA could only involve certain subtypes of fibrils, size or morphology dependent. Further analyses in this direction may be needed to unveil the exact nature of the interaction.

In addition, we showed that the two proteins colocalize in both extracellular and intracellular environments, and that both POST and PRE treatments with γ-PGA are effective in reducing α-synuclein PFF burden. This might suggest that γ-PGA may, at least to some extent, disrupt α-synuclein aggregates or, alternatively, reduce their interaction with astrocytes, potentially affecting their internalization. Indeed, the internalization of extracellular α-synuclein aggregates by astrocytes is a key aspect in neurodegenerative processes, as astrocytes are known to be actively involved in their clearance [20,26,42]. Nevertheless, the amount of α-synuclein uptake is critical for astrocyte homeostasis as excessive accumulation could overwhelm protein degradation processes leading to cellular stress [20,42]. Several mechanisms may be involved in the entry of PFFs into the cells, such as direct membrane penetration [43], caveolae-mediated [44] and clathrin-dependent endocytosis [45]. In addition, one study showed that PFF uptake by astrocytes could be mediated by dynamin-mediated endocytosis as dynamin facilitates the budding of endocytic vesicles from the plasma membrane [26].

Here, we found that γ-PGA has a marked inhibitory effect on astrocyte ability to internalize α-synuclein PFFs (Fig. 7B, a). Interestingly, the PRE treatment reduced both the size and the intensity of internalized α-synuclein PFFs to a greater extent, compared to POST treatment. In respect to the mechanisms by which γ-PGA limits α-synuclein PFF internalization, we propose two hypotheses. Firstly, γ-PGA could compete for cellular uptake pathways employed by α-synuclein aggregates. This hypothesis is supported by our findings on both the presence of γ-PGA within astrocytes (Fig. 7B, b), and its localization between the cell and α-synuclein PFFs (Fig. 7B, c). The second hypothesis builds upon our results on the colocalization of the two molecules, suggesting that γ-PGA may have a buffering effect and retain PFFs, preventing their internalization (Fig. 7B, d). Moreover, we investigated the lysosomal and autophagic pathway which is responsible for clearing cytosolic aggregated proteins such as fibrillar α-synuclein [31]. We observed that treatment with PFFs impairs autophagy-lysosome pathways, as suggested by the increase of LC3-II/LC3-I ratio, the accumulation of p62, and the increase of LAMP1-labeled lysosomes, as previously demonstrated [31,32]. Interestingly, POST treatment with γ-PGA led to a mild decrease of p62 accumulation, which might suggest a partial role in modulating autophagy. However, our results support the hypothesis that γ-PGA primarily exerts its effect by limiting PFF internalization in astrocytes. Despite we also observed a reduction in the overall extent of extracellular aggregates, further studies are required to better

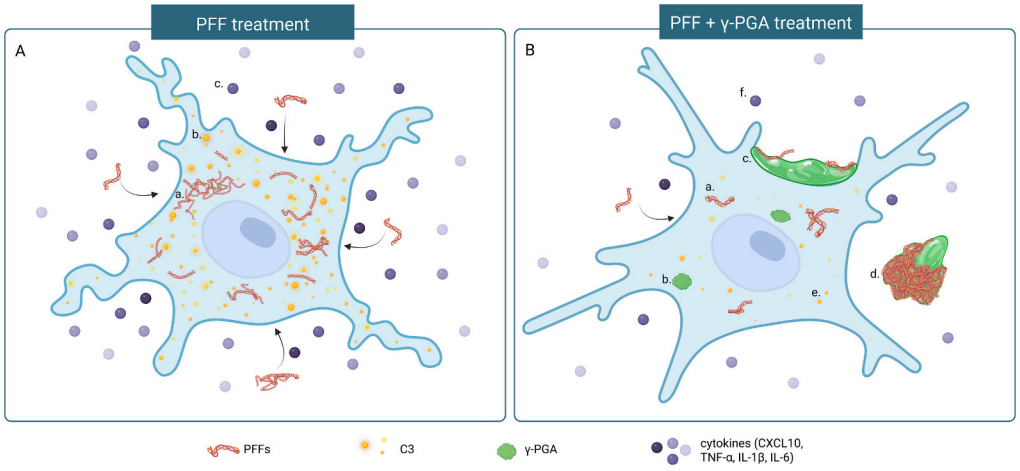

Fig. 7. Schematic illustration of γ-PGA effect on PFF-treated primary astrocytes. A) In primary astrocytes that are treated with PFFs, the fibrils are internalized by the cell (a), and an inflammatory response is observed, as shown by C3 staining (b), and by the release of pro-inflammatory cytokines (c); this results in cell toxicity. B) In primary astrocytes co-treated with γ-PGA, a reduction in PFF internalization is observed (a). γ-PGA localizes inside the cell (b), on its surface (c), and colocalizes with PFFs in the extracellular space (d). A decrease in C3 inflammation and pro-inflammatory cytokines release is also observed (e, f), leading to reduced cellular toxicity. Created in BioRender. Cappelletti, G. (2025) https://BioRender.com/bbanupg.

investigate the buffering capacity of γ-PGA in limiting α-synuclein spreading and its effect on neurons.

A relevant feature of astrocytes is that they are active players in neuroinflammation, and their response may be beneficial or detrimental, depending on the kind of stimuli they encounter [39]. Previous studies have demonstrated that extracellular α-synuclein aggregates, such as α-synuclein fibrils, induce innate immune pathway activation such as Toll-like receptor 4-mediated pathways, causing inflammatory responses in astrocytes [46]. However, although it is still debated whether adult astrocytes express TLR4 *in vivo* [21,47,48], it has been stated that innate Complement component 3 (C3) is one of the most distinctive and highly upregulated genes in neurotoxic and pro-inflammatory astrocytes, namely A1 astrocytes [21,49]. Indeed, *in situ* hybridization and qPCR assays for C3 on *post-mortem* human brain of PD patients have revealed that $C3^{+}$ astrocytes abundance is significantly increased compared to controls [21]. Therefore, we investigated γ~~-PGA~~ the effect of γ-PGA on α-synuclein PFF-induced inflammation of astrocytes by evaluating C3 as an inflammatory marker. Our results suggest, in accordance with what has been previously shown [50], that α-synuclein PFFs increases C3 deposition in astrocytes (Fig. 7A, b) and that γ-PGA can both prevent and recover astrocytes inflammation (Fig. 7B, e). Given that C3 expression in α-synuclein PFF-treated astrocytes has been reported to induce neuronal cell death [50], a molecule capable of mitigating complement activation in astrocytes holds significant promise as a therapeutic strategy for PD. Moreover, we observed a pro-inflammatory profile in α-synuclein PFF-treated astrocytes, characterized by increased release of TNF-α, IL-1β, IL-6 and CXCL10 (Fig. 7, c). High levels of TNF-α, IL-1β and IL-6 can promote glial reactivity, contribute to chronic inflammation and neuronal dysfunction, while CXCL10 can lead to sustained neuroinflammation and immune cell infiltration, ultimately disrupting neural homeostasis [51]. In our study, we found that POST treatment with γ-PGA led to a mild decrease in IL-6 release, while significantly reduced TNF-α, IL-1β and CXCL10 levels in astrocytes treated with PFFs (Fig. 7, f). Thus, even though the PRE treatment may provide a greater reduction in α-synuclein PFF internalization, our results on the autophagic pathway and on astrocyte inflammation indicate POST treatment as the most promising therapeutic strategy.

5. Conclusions

Overall, these data provide a "proof of concept" that bacterial-derived γ-PGA may be considered a promising candidate for mitigating α-synuclein pathology. Adding γ-PGA after PFF exposure seems to be more effective than preventive treatment and this is essential for any therapeutic approach targeting PD, where neuroinflammation is already ongoing and α-synuclein aggregates already exist and need to be effectively 'inactivated' or removed.

Nevertheless, many aspects remain to be elucidated including the molecular mechanisms underlying its biological effect shown here, its ability to interfere with other aggregate species, including α-synuclein oligomers, and its potential beneficial effect on neurons. Interestingly, γ-PGA is a well-characterized prebiotic able to increase the species associated with a healthy microbiome; this feature is promising given the microbiota dysbiosis, the high level of inflammation, and the presence of α-synuclein aggregates described in the gut of PD patients.

We supplied a file as Supporting information that includes complementary data (PDF). This file includes the characterization of α-synuclein PFFs, LAMP1 quantification, the effect of γ-PGA on astrocyte inflammation (C3 staining), and electron microscopy analyses of α-synuclein and γ-PGA after *in vitro* aggregation assay. Next, we supplied 3 videos (.mp4): Supplementary Video 1 (the movie refers to the 3D reconstructions obtained with arivis Vision4D® 3.6.0 software of Fig. 3B); Supplementary Video 2 (the movie refers to the 3D reconstructions obtained with arivis Vision4D® 3.6.0 software of Fig. 3D); Supplementary Video 3 (the movie refers to the 3D reconstructions obtained with arivis Vision4D® 3.6.0 software of Fig. 3E). Supplementary data to this article can be found online at https://doi.org/10.1016/j.ijbiomac.2025.145303.

CRediT authorship contribution statement

Claudia Novello: Writing – review & editing, Writing – original draft, Investigation, Formal analysis, Conceptualization. **Mattia Parati:** Writing – review & editing, Writing – original draft, Investigation, Formal analysis, Conceptualization. **Samanta Mazzetti:** Writing – review & editing, Writing – original draft, Investigation, Formal analysis, Conceptualization. **Oriana Rampoldi:** Investigation, Formal analysis. **Huseyin Berkcan Isilgan:** Investigation, Formal analysis. **Milo Jarno Basellini:** Investigation, Formal analysis. **Chiara M.G. De Luca:** Investigation, Formal analysis. **Arianna Ciullini:** Investigation, Formal analysis. **Ilaria L. Dellarole:** Investigation, Formal analysis. **Alessandro Fantin:** Investigation, Formal analysis. **Isabella Russo:** Writing – review & editing. **Brian L. Johnston:** Writing – review & editing. **Moira Paroni:** Formal analysis, Writing – original draft, Writing – review & editing. **Chiara Rolando:** Writing – review & editing, Writing – original draft, Investigation, Formal analysis, Conceptualization. **Fabio Moda:** Writing – review & editing, Investigation, Formal analysis. **Gianni Pezzoli:** Writing – review & editing. **Iza K. Radecka:** Writing – review & editing. **Graziella Cappelletti:** Writing – review & editing, Writing – original draft, Investigation, Formal analysis, Conceptualization.

Funding sources

This work was partially supported by iBiotech LTD, the University of Wolverhampton Research Investment Fund (RIF4); by the ERDF Science in Industry Research Centre (SIRC 01R19P03464) project. This research was partially funded by Italian "5 × 1000" funding to "Fondazione Pezzoli per la malattia di Parkinson" (GC) and by the Italian Ministry of Health (GR-2021-12372019, PNRR-MAD-2022-12376035, 5M-2018-23680266 and RC) to FM.

Declaration of competing interest

The authors declare no competing financial interest.

Acknowledgment

The authors thank "Fondazione Pezzoli per la malattia di Parkinson" (Milan, Italy) for SM salary and for long-lasting support to GC. We would like to thank David Townrow and Diane Spencer from the Faculty of Science and Engineering, University of Wolverhampton, as well as Dr. Barbara Mendreck from Centre of Polymer and Carbon Materials, Polish Academy of Sciences, for their technical support on material analysis. Part of this work was carried out at UNITECH NOLIMITS, an advanced imaging facility established by the Università degli Studi di Milano.

Data availability

The authors confirm that the data supporting the findings of this study are available within the article and Supplementary materials.

References

[1] D. Li, L. Hou, Y. Gao, Z. Tian, B. Fan, F. Wang, S. Li, Recent advances in microbial synthesis of poly-γ-glutamic acid: a review, Foods 11 (2022), https://doi.org/10.3390/foods11050739.
[2] M. Parati, I. Khalil, F. Tchuenbou-Magaia, G. Adamus, B. Mendrek, R. Hill, I. Radecka, Building a circular economy around poly(D/L-γ-glutamic acid)- a smart microbial biopolymer, Biotechnol. Adv. 61 (2022), https://doi.org/10.1016/j.biotechadv.2022.108049.
[3] T. Zhang, M.S. Ryu, X. Wu, H.J. Yang, S.J. Jeong, J.W. Seo, D.Y. Jeong, S. Park, Alleviation of neuronal cell death and memory deficit with chungkookjang made with Bacillus amyloliquefaciens and Bacillus subtilis potentially through promoting

gut–brain axis in artery-occluded gerbils, Foods 10 (2021), https://doi.org/10.3390/foods10112697.
[4] H. Ahn, S.G. Kang, S. Il Yoon, P.H. Kim, D. Kim, G.S. Lee, Poly-gamma-glutamic acid from Bacillus subtilis upregulates pro-inflammatory cytokines while inhibiting NLRP3, NLRC4 and AIM2 inflammasome activation, Cell. Mol. Immunol. 15 (2018) 111–119, https://doi.org/10.1038/cmi.2016.13.
[5] D.Y. Jeong, M.S. Ryu, H.J. Yang, S. Park, γ-PGA-Rich Chungkookjang, short-term fermented soybeans: prevents memory impairment by modulating brain insulin sensitivity, neuro-inflammation, and the gut–microbiome–brain axis, Foods 10 (2021), https://doi.org/10.3390/foods10020221.
[6] J.M. Lee, W.J. Jang, S.H. Park, I.S. Kong, Antioxidant and gastrointestinal cytoprotective effect of edible polypeptide poly-γ-glutamic acid, Int. J. Biol. Macromol. 153 (2020) 616–624, https://doi.org/10.1016/j.ijbiomac.2020.03.050.
[7] N. Panicker, P. Ge, V.L. Dawson, T.M. Dawson, The cell biology of Parkinson's disease, J. Cell Biol. 220 (2021), https://doi.org/10.1083/JCB.202012095.
[8] R. Balestrino, A.H.V. Schapira, Parkinson disease, Eur. J. Neurol. 27 (2020) 27–42, https://doi.org/10.1111/ENE.14108.
[9] M.G. Spillantini, M.L. Schmidt, V.M.-Y. Lee, J.Q. Trojanowski, R. Jakes, M. Goedert, α-Synuclein in Lewy bodies, Nature 388 (1997) 839–840, https://doi.org/10.1038/42166.
[10] L. Gadhe, A. Sakunthala, S. Mukherjee, N. Gahlot, R. Bera, A.S. Sawner, P. Kadu, S. K. Maji, Intermediates of α-synuclein aggregation: implications in Parkinson's disease pathogenesis, Biophys. Chem. 281 (2022) 106736, https://doi.org/10.1016/J.BPC.2021.106736.
[11] D. Valdinocci, R. Radford, S. Siow, R. Chung, D. Pountney, Potential modes of intercellular α-synuclein transmission, Int. J. Mol. Sci. 18 (2017) 469, https://doi.org/10.3390/ijms18020469.
[12] S. Abounit, L. Bousset, F. Loria, S. Zhu, F. de Chaumont, L. Pieri, J. Olivo-Marin, R. Melki, C. Zurzolo, Tunneling nanotubes spread fibrillar α-synuclein by intercellular trafficking of lysosomes, EMBO J. 35 (2016) 2120–2138, https://doi.org/10.15252/EMBJ.201593411.
[13] X. Mao, M.T. Ou, S.S. Karuppagounder, T.I. Kam, X. Yin, Y. Xiong, P. Ge, G. E. Umanah, S. Brahmachari, J.H. Shin, H.C. Kang, J. Zhang, J. Xu, R. Chen, H. Park, S.A. Andrabi, S.U. Kang, R.A. Gonçalves, Y. Liang, S. Zhang, C. Qi, S. Lam, J. A. Keiler, J. Tyson, D. Kim, N. Panicker, S.P. Yun, C.J. Workman, D.A.A. Vignali, V. L. Dawson, H.S. Ko, T.M. Dawson, Pathological α-synuclein transmission initiated by binding lymphocyte-activation gene 3, Science 353 (2016), https://doi.org/10.1126/SCIENCE.AAH3374.
[14] G. Bieri, A.D. Gitler, M. Brahic, Internalization, axonal transport and release of fibrillar forms of alpha-synuclein, Neurobiol. Dis. 109 (2018) 219–225, https://doi.org/10.1016/J.NBD.2017.03.007.
[15] K.M. Danzer, W.P. Ruf, P. Putcha, D. Joyner, T. Hashimoto, C. Glabe, B.T. Hyman, P.J. McLean, Heat-shock protein 70 modulates toxic extracellular α-synuclein oligomers and rescues trans-synaptic toxicity, FASEB J. 25 (2011) 326–336, https://doi.org/10.1096/FJ.10-164624.
[16] C. Kim, D.H. Ho, J.E. Suk, S. You, S. Michael, J. Kang, S.J. Lee, E. Masliah, D. Hwang, H.J. Lee, S.J. Lee, Neuron-released oligomeric α-synuclein is an endogenous agonist of TLR2 for paracrine activation of microglia, Nature Communications 4 (2013) 1–12, https://doi.org/10.1038/ncomms2534, 2013 4:1.
[17] H.D.E. Booth, W.D. Hirst, R. Wade-Martins, The role of astrocyte dysfunction in Parkinson's disease pathogenesis, Trends Neurosci. 40 (2017) 358–370, https://doi.org/10.1016/j.tins.2017.04.001.
[18] F. Loria, J.Y. Vargas, L. Bousset, S. Syan, A. Salles, R. Melki, C. Zurzolo, α-Synuclein transfer between neurons and astrocytes indicates that astrocytes play a role in degradation rather than in spreading, Acta Neuropathol. 134 (2017) 789–808, https://doi.org/10.1007/S00401-017-1746-2.
[19] V. Lindström, G. Gustafsson, L.H. Sanders, E.H. Howlett, J. Sigvardson, A. Kasrayan, M. Ingelsson, J. Bergström, A. Erlandsson, Extensive uptake of α-synuclein oligomers in astrocytes results in sustained intracellular deposits and mitochondrial damage, Mol. Cell. Neurosci. 82 (2017) 143–156, https://doi.org/10.1016/J.MCN.2017.04.009.
[20] V. Giusti, G. Kaur, E. Giusto, L. Civiero, Brain clearance of protein aggregates: a close-up on astrocytes, Mol Neurodegener 19 (2024), https://doi.org/10.1186/s13024-024-00703-1.
[21] S.A. Liddelow, K.A. Guttenplan, L.E. Clarke, F.C. Bennett, C.J. Bohlen, L. Schirmer, M.L. Bennett, A.E. Münch, W.S. Chung, T.C. Peterson, D.K. Wilton, A. Frouin, B. A. Napier, N. Panicker, M. Kumar, M.S. Buckwalter, D.H. Rowitch, V.L. Dawson, T. M. Dawson, B. Stevens, B.A. Barres, Neurotoxic reactive astrocytes are induced by activated microglia, Nature 541 (2017) 481–487, https://doi.org/10.1038/nature21029.
[22] R. Patani, G.E. Hardingham, S.A. Liddelow, Functional roles of reactive astrocytes in neuroinflammation and neurodegeneration, Nat. Rev. Neurol. 19 (2023) 395–409, https://doi.org/10.1038/S41582-023-00822-1.
[23] A. Filippini, V. Mutti, G. Faustini, F. Longhena, I. Ramazzina, F. Rizzi, A. Kaganovich, D.A. Roosen, N. Landeck, M. Duffy, I. Tessari, F. Bono, C. Fiorentini, E. Greggio, L. Bubacco, A. Bellucci, M. Missale, M.R. Cookson, M. Gennarelli, I. Russo, Extracellular clusterin limits the uptake of α-synuclein fibrils by murine and human astrocytes, Glia 69 (2021) 681, https://doi.org/10.1002/GLIA.23920.
[24] T.W. Chou, N.P. Chang, M. Krishnagiri, A.P. Patel, M. Lindman, J.P. Angel, P. L. Kung, C. Atkins, B.P. Daniels, Fibrillar α-synuclein induces neurotoxic astrocyte activation via RIP kinase signaling and NF-κB, Cell Death & Disease 12 (2021) 1–11, https://doi.org/10.1038/s41419-021-04049-0, 2021 12:8.
[25] P. Baden, M.J. Perez, H. Raji, F. Bertoli, S. Kalb, M. Illescas, F. Spanos, C. Giuliano, A.M. Calogero, M. Oldrati, H. Hebestreit, G. Cappelletti, K. Brockmann, T. Gasser, A.H.V. Schapira, C. Ugalde, M. Deleidi, Glucocerebrosidase is imported into mitochondria and preserves complex I integrity and energy metabolism, Nat. Commun. 14 (2023), https://doi.org/10.1038/s41467-023-37454-4.
[26] A. Filippini, V. Mutti, G. Faustini, F. Longhena, I. Ramazzina, F. Rizzi, A. Kaganovich, D.A. Roosen, N. Landeck, M. Duffy, I. Tessari, F. Bono, C. Fiorentini, E. Greggio, L. Bubacco, A. Bellucci, M. Missale, M.R. Cookson, M. Gennarelli, I. Russo, Extracellular clusterin limits the uptake of α-synuclein fibrils by murine and human astrocytes, Glia 69 (2021) 681–696, https://doi.org/10.1002/GLIA.23920.
[27] I.R. Khalil, M.P. Khechara, S. Kurusamy, A.L. Armesilla, A. Gupta, B. Mendrek, T. Khalaf, M. Scandola, M.L. Focarete, M. Kowalczuk, I. Radecka, Poly-gamma-glutamic acid (-PGA)-based encapsulation of adenovirus to evade neutralizing antibodies, Molecules 23 (2018), https://doi.org/10.3390/molecules23102565.
[28] M. Boccazzi, C. Rolando, M.P. Abbracchio, A. Buffo, S. Ceruti, Purines regulate adult brain subventricular zone cell functions: contribution of reactive astrocytes, Glia 62 (2014) 428–439, https://doi.org/10.1002/glia.22614.
[29] T.W. Chou, N.P. Chang, M. Krishnagiri, A.P. Patel, M. Lindman, J.P. Angel, P. L. Kung, C. Atkins, B.P. Daniels, Fibrillar α-synuclein induces neurotoxic astrocyte activation via RIP kinase signaling and NF-κB, Cell Death & Disease 12 (2021) 1–11, https://doi.org/10.1038/s41419-021-04049-0, 2021 12:8.
[30] V. Giusti, G. Kaur, E. Giusto, L. Civiero, Brain clearance of protein aggregates: a close-up on astrocytes, Molecular Neurodegeneration 19 (2024) 1–18, https://doi.org/10.1186/S13024-024-00703-1, 2024 19:1.
[31] M. Pantazopoulou, V. Brembati, A. Kanellidi, L. Bousset, R. Melki, L. Stefanis, Distinct alpha-synuclein species induced by seeding are selectively cleared by the lysosome or the proteasome in neuronally differentiated SH-SY5Y cells, J. Neurochem. 156 (2021) 880–896, https://doi.org/10.1111/JNC.15174;WGROUP:STRING:PUBLICATION.
[32] J. Gao, G. Perera, M. Bhadbhade, G.M. Halliday, N. Dzamko, Autophagy activation promotes clearance of α-synuclein inclusions in fibril-seeded human neural cells, J. Biol. Chem. 294 (2019) 14241–14256, https://doi.org/10.1074/jbc.RA119.008733.
[33] X.T. Cheng, Y.X. Xie, B. Zhou, N. Huang, T. Farfel-Becker, Z.H. Sheng, Revisiting LAMP1 as a marker for degradative autophagy-lysosomal organelles in the nervous system, Autophagy 14 (2018) 1472–1474, https://doi.org/10.1080/15548627.2018.1482147.
[34] H. Hindeya Gebreyesus, T. Gebrehiwot Gebremichael, The potential role of astrocytes in Parkinson's disease (PD), Med Sci (Basel) 8 (2020), https://doi.org/10.3390/medsci8010007.
[35] A. Raj, R. Banerjee, V. Holla, N. Kamble, R. Yadav, P.K. Pal, I. Datta, Dysregulation of protein degradation and alteration of secretome in α-synuclein-exposed astrocytes: implications for dopaminergic neuronal dysfunction, Cell Communication and Signaling 22 (2024), https://doi.org/10.1186/S12964-024-01928-9.
[36] L. Wang, S. Chen, B. Yu, Poly-γ-glutamic acid: recent achievements, diverse applications and future perspectives, Trends Food Sci. Technol. 119 (2022) 1–12, https://doi.org/10.1016/j.tifs.2021.11.009.
[37] P. Nair, G.R. Navale, M.S. Dharne, Poly-gamma-glutamic acid biopolymer: a sleeping giant with diverse applications and unique opportunities for commercialization, Biomass Convers. Biorefinery 13 (2023) 4555–4573, https://doi.org/10.1007/s13399-021-01467-0.
[38] Y. Kanaya, K. Kume, H. Morino, R. Ohsawa, T. Kurashige, M. Kamada, T. Torii, Y. Izumi, H. Maruyama, H. Kawakami, Analysis of genetic risk factors in Japanese patients with Parkinson's disease, Journal of Human Genetics 66 (2021) 957–964, https://doi.org/10.1038/S10038-021-00910-4, 2021 66:10.
[39] E. Colombo, C. Farina, Astrocytes: key regulators of neuroinflammation, Trends Immunol. 37 (2016) 608–620, https://doi.org/10.1016/J.IT.2016.06.006.
[40] P. Alam, L. Bousset, R. Melki, D.E. Otzen, α-Synuclein oligomers and fibrils: a spectrum of species, a spectrum of toxicities, J. Neurochem. 150 (2019) 522–534, https://doi.org/10.1111/jnc.14808.
[41] S.J. Guiney, P.A. Adlard, P. Lei, C.H. Mawal, A.I. Bush, D.I. Finkelstein, S. Ayton, Fibrillar α-synuclein toxicity depends on functional lysosomes, J. Biol. Chem. 295 (2020) 17497, https://doi.org/10.1074/JBC.RA120.013428.
[42] A. Filippini, M. Gennarelli, I. Russo, α-Synuclein and glia in Parkinson's disease: a beneficial or a detrimental duet for the endo-lysosomal system? Cell. Mol. Neurobiol. 39 (2019) 161–168, https://doi.org/10.1007/S10571-019-00649-9.
[43] B.V. Dieriks, T.I.H. Park, C. Fourie, R.L.M. Faull, M. Dragunow, M.A. Curtis, α-Synuclein transfer through tunneling nanotubes occurs in SH-SY5Y cells and primary brain pericytes from Parkinson's disease patients, Scientific Reports 7 (2017) 1–11, https://doi.org/10.1038/srep42984, 2017 7:1.
[44] A. Madeira, J. Yang, X. Zhang, E. Vikeved, A. Nilsson, P.E. Andrén, P. Svenningsson, Caveolin-1 interacts with alpha-synuclein and mediates toxic actions of cellular alpha-synuclein overexpression, Neurochem. Int. 59 (2011) 280–289, https://doi.org/10.1016/J.NEUINT.2011.05.017.
[45] L. Rodriguez, M.M. Marano, A. Tandon, Import and export of misfolded α-synuclein, Front. Neurosci. 12 (2018) 358041, https://doi.org/10.3389/FNINS.2018.00344/BIBTEX.
[46] E.H. Rannikko, S.S. Weber, P.J. Kahle, Exogenous α-synuclein induces toll-like receptor 4 dependent inflammatory responses in astrocytes, BMC Neurosci. 16 (2015), https://doi.org/10.1186/S12868-015-0192-0.
[47] Y. Zhang, S.A. Sloan, L.E. Clarke, C. Caneda, C.A. Plaza, P.D. Blumenthal, H. Vogel, G.K. Steinberg, M.S.B. Edwards, G. Li, J.A. Duncan, S.H. Cheshier, L.M. Shuer, E. F. Chang, G.A. Grant, M.G.H. Gephart, B.A. Barres, Purification and characterization of progenitor and mature human astrocytes reveals transcriptional and functional differences with mouse, Neuron 89 (2016) 37–53, https://doi.org/10.1016/J.NEURON.2015.11.013.

[48] E. Gregersen, C. Betzer, W.S. Kim, G. Kovacs, L. Reimer, G.M. Halliday, S. Thiel, P. H. Jensen, Alpha-synuclein activates the classical complement pathway and mediates complement-dependent cell toxicity, J. Neuroinflammation 18 (2021), https://doi.org/10.1186/S12974-021-02225-9.

[49] J.M. Lawrence, K. Schardien, B. Wigdahl, M.R. Nonnemacher, Roles of neuropathology-associated reactive astrocytes: a systematic review, Acta Neuropathologica Communications 11 (2023) 1–28, https://doi.org/10.1186/S40478-023-01526-9, 2023 11:1.

[50] S.X. Ma, B.A. Seo, D. Kim, Y. Xiong, S.H. Kwon, S. Brahmachari, S. Kim, T.I. Kam, R.S. Nirujogi, S.H. Kwon, V.L. Dawson, T.M. Dawson, A. Pandey, C.H. Na, H.S. Ko, Complement and coagulation cascades are potentially involved in dopaminergic neurodegeneration in α-synuclein-based mouse models of Parkinson's disease, J. Proteome Res. 20 (2021) 3428–3443, https://doi.org/10.1021/ACS.JPROTEOME.0C01002.

[51] T.M. Fisher, S.A. Liddelow, Emerging roles of astrocytes as immune effectors in the central nervous system, Trends Immunol. 45 (2024) 824–836, https://doi.org/10.1016/J.IT.2024.08.008.

Side projects

PARylation in Parkinson's disease: a bridge between Lewy body formation and neuronal cell death

pre-print doi: https://doi.org/10.1101/2025.03.12.642849

Under review, in Nature cell death and disease

Claudia Novello[1], Federica Giampietro[1], Alessandra Maria Calogero[1,2], Giorgio Giaccone[3], Michele Salemi[4], Manuela Bramerio[5], Emanuela Bonoldi[5], Daniela Calandrella[2,5], Elena Contaldi[6], Ioannis Ugo Isaias[6,7], Chiara Rolando[1], Gianni Pezzoli[2,#], Graziella Cappelletti[1,#,*], Samanta Mazzetti[2,8,#,*]

[1] Department of Biosciences, Università degli Studi di Milano, Milan, Italy
[2] Fondazione Pezzoli per la Malattia di Parkinson, Milan, Italy
[3] Unit of Neuropathology and Neurology, Fondazione IRCCS Istituto Neurologico Carlo Besta, Milan, Italy
[4] Oasi Research Institute-IRCCS, Troina (EN), Italy
[5] Niguarda_ Department of Hematology, Oncolgy and Molecular Medicine, Grande Ospedale Metropolitano Niguarda, Milan, Italy
[6] Parkinson Institute, ASST G. Pini-CTO, Milan, Milan, Italy
[7] Department of Neurology, University Hospital of Würzburg and the Julius Maximilian University of Würzburg, 97080 Würzburg, Germany
[8] Unit of Movement Disorders, Fondazione IRCCS Istituto Neurologico Carlo Besta

[#] These authors contributed equally to this work
[*] Corresponding authors

Abstract

Poly-ADP-ribosylation (PARylation), catalyzed by the enzyme PARP1, involves the addition of poly-ADP-ribose polymers (PAR) and has been associated with α-synuclein aggregation in Parkinson's disease (PD) models. This study aimed to unravel the role of PARylation in α-synuclein aggregation and neuronal cell death in the complex environment of post-mortem human PD brains. Using high-resolution imaging and 3D reconstruction analysis, we observed that PAR accumulate in the cytoplasm in regions affected by PD pathology, preceding the formation of α-synuclein oligomers. Additionally, we found that PAR and stress granules contribute to the formation of Lewy bodies. Increased colocalization of PAR with mitochondria in the substantia nigra of PD patients, along with the presence of PAR-positive condensed DNA, further suggests a role in neuronal cell death. Collectively, our findings reveal a critical involvement of PARylation in the pathological mechanisms underlying neurodegeneration in PD and position PARylation as a potential therapeutic target.

Keywords: PARylation, α-Synuclein, oligomers, stress granules, Lewy body morphogenesis, Parthanatos, Parkinson's disease.

1 Introduction

Parkinson's disease (PD) is the most common neurodegenerative movement disorder associated with the loss of *substantia nigra* dopaminergic neurons and the presence of intraneuronal inclusions known as Lewy bodies (LBs) and Lewy neurites[1,2], which are enriched in α-synuclein protein[3]. Many aspects of PD pathogenesis remain unclear, particularly the mechanisms driving α-synuclein aggregation and neuronal death[4].

Special attention is paid to the role of post-translational modifications (PTMs) in neurodegeneration, as they are crucial in influencing structure, function, and biochemical properties of proteins[5]. Interestingly, *in vitro* and in mouse model evidence revealed that pathological accumulation of α-synuclein could be driven by PARP1-mediated Poly-ADP-ribosylation (PARylation)[6], a PTM consisting in the covalent addition of poly-ADP-ribose units to the carboxyl group of acidic residues on target proteins. Poly-ADP-ribose polymers (PAR) formation is catalysed by the nuclear enzyme PARP1[7,8], that consists of three domains: *i)* N-terminal DNA-binding domain, *ii)* central auto-modification domain, and *iii)* C-terminal catalytic domain (CAT)[7,8]. Physiologically, PARP1-mediated PARylation is fundamental for several cellular pathways such as protein stability[9–11], gene expression[12], inflammation[13], and autophagy[14], but it is particularly known for its dual function in regulating cellular response to oxidative stress[15,16], which is reported to be elevated in PD[17]. In *in vitro* stressed cell models, cytoplasmic PAR increase determines the formation of stress granules[18] through the PARylation of stress granules proteins, such as Ras-GTPase-activating protein (GAP)-binding protein 1 (G3BP1)[19]. While these findings are highly informative, there is a lack of evidence demonstrating PAR's role in the human PD brain and how it regulates various stress-related cellular processes, including stress granule formation and cell death, *in vivo*.

PARP1 plays a pivotal role in regulating cell function and survival. It is essential for DNA damage repair[16,20]; but its overactivation in response to severe DNA damage can lead to Parthanatos pathway[21]. Parthanatos is a caspase-independent cell death mechanism characterized by PAR overproduction and accumulation into the cytoplasm. This process is linked to mitochondrial release of apoptosis-inducing factor (AIF), followed by the nuclear translocation of the AIF/macrophage migration inhibitory factor (MIF) complex, which leads to MIF-mediated DNA fragmentation[22,23].

Emerging evidence links PARP1 overactivation to α-synuclein aggregation and Parthanatos pathway activation in a PD mouse model[6,24]. These data are supported by the observation of an increase in PAR levels, concomitantly with a α-synuclein decrease, in the cerebrospinal fluid of PD patients compared with control subjects[6,25,26]. In addition, in *post-mortem* human brain obtained from PD patients, PARP1 translocates from the nucleus to the cytoplasm of the *substantia nigra* dopaminergic neurons where it colocalizes with α-synuclein and accumulates into LBs[27]. Lastly, PAR

were found to colocalize with phosphorylated α-synuclein[28]. These studies suggest a key role for PARylation of α-synuclein in neurodegeneration but its involvement in the early stages of aggregation is still unexplored, leading us to investigate this process in *post-mortem* human brain from PD patients. In the complexity of human brain, we aimed to disentangle: *i)* the interplay of PARylation and α-synuclein aggregation from the initial appearance of α-synuclein oligomers to mature LB; *ii)* the impact of PARylation in the response to cellular stresses, specifically the formation of stress granules; *iii)* the role of PARylation in neuronal cell death, focusing on PARylation of both mitochondria and condensed DNA, specifically involved in Parthanatos pathway. We found cytoplasmic accumulation of PAR in the brain regions mirroring previously reported PARP1 activity in PD human brain[27]. We also linked cytoplasmic PARylation with LB formation, including α-synuclein oligomers, which are the earliest aggregates[29] providing crucial evidence that PARylation drives α-synuclein aggregation[6] in the human brain. Furthermore, our analysis of G3BP1 and TIA1-related proteins (TIAR), which are markers of stress granule proteins, revealed their redistribution during LB formation[18]. Finally, we pointed out an increase of PARylation within mitochondria and the presence of condensed DNA, suggesting the activation of Parthanatos pathway that could be responsible for dopaminergic neurons cell death in PD human brain. All together these data added important pieces to understand how α-synuclein can be involved in neurodegeneration and contribute to the emerging view that PARylation could be a promising future therapeutic target.

2 Results

2.1 PAR neuronal redistribution is linked to α-synuclein aggregation in brain of PD patients

In vitro studies and genetic mouse model showed that PARP1 and PAR are involved in PD pathogenesis, including the conversion of α-synuclein to a more toxic species and neuron death[6,25,27]. In the present study we aimed to investigate whether PARylation, an index for PARP enzymatic activity, may be altered in human PD brain and how it can influence disease pathophysiology. First, we analysed whether PARP1 redistribution from the nucleus to the cytoplasm of neurons and astrocytes that we previously found in PD patients[27] also affects the localization of PAR. For this purpose, we performed immunoenzymatic assay for PAR. In control subjects, PAR was predominantly localised in the nuclei of neurons (Fig. 1a, black arrowheads). However, in PD patients, we observed a redistribution of PAR from the nucleus to the cytoplasm, consistent with the previously reported pattern for PARP1 (Fig. 1b, black arrows). We quantified the number of PAR-positive nuclei and found a significant reduction in PD patients compared to controls in the frontal cortex, entorhinal cortex, and cingulate cortex (Fig. 1c-e). In contrast, no significant differences were found between controls and PD subjects in the percentage of PAR-positive nuclei in cortical

astrocytes, where PAR remained predominantly localised in the nucleus with little to no presence in their cellular body (Supplementary Fig. 1c). We also investigated PAR redistribution in astrocytes and neurons in the *substantia nigra*. As for frontal cortex, we reported no differences in PAR positive nuclei of astrocytes between controls and PD subjects (Supplementary Fig. 1a-b", d). Regarding neuronal PAR redistribution (Fig.1 f, g), while most PD patients exhibited a reduction in PAR-positive nuclei compared to controls, this decrease was not statistically significant (Fig. 1h).

We further investigated the relationship between PAR and α-synuclein in the *substantia nigra*. Thus, we conducted immunofluorescence for PAR, TH, and α-synuclein. As expected, in neurons of control subjects, PAR staining was confined to the nuclei, while we observed the classical α-synuclein dot-like signal primarily localized in the synaptic compartment (Fig. 1i-i"). In PD samples, we observed both neurons with PAR-positive nuclei (Fig. 1l, white arrow) and PAR-negative nuclei (Fig. 1l, dashed rectangle). In both cases, PAR was also clearly detectable in the neuronal cytoplasm, indicating its translocation from the nucleus (Fig. 1l). α-Synuclein began to accumulate in the cell body (Fig. 1l, l"), where PAR was also distributed (Fig. 1l-l'). Notably, among the neurons with PAR-positive nuclei, a significant proportion (76%) also exhibited diffuse or aggregated α-synuclein in the cytoplasm (Fig. 1m). To further explore these findings, we investigated PAR positivity in the nucleus alongside the presence of undefined (Fig. 1n-n") or ring-shaped (Fig. 1o-o") α-synuclein aggregates, which represents different stages of aggregate maturation [30,31]. Interestingly, the percentage of neurons containing ring-shaped α-synuclein aggregates was higher in presence of PAR-positive nuclei (95%) compared to PAR-negative nuclei (56%) (Fig. 1p). Collectively, these data indicate that the redistribution of PAR from the nucleus to the cytoplasm occurs exclusively in neurons and appears to be associated to α-synuclein aggregation. Moreover, a second step of redistribution was observed, in which PAR distributes again in the nucleus with the appearance of ring-shaped α-synuclein aggregates in the cytoplasm. These data provide additional insights into the crucial steps of LB formation, advancing our understanding from the earlier stages involving undefined aggregates to the development of the characteristic ring-shaped structure[31–33].

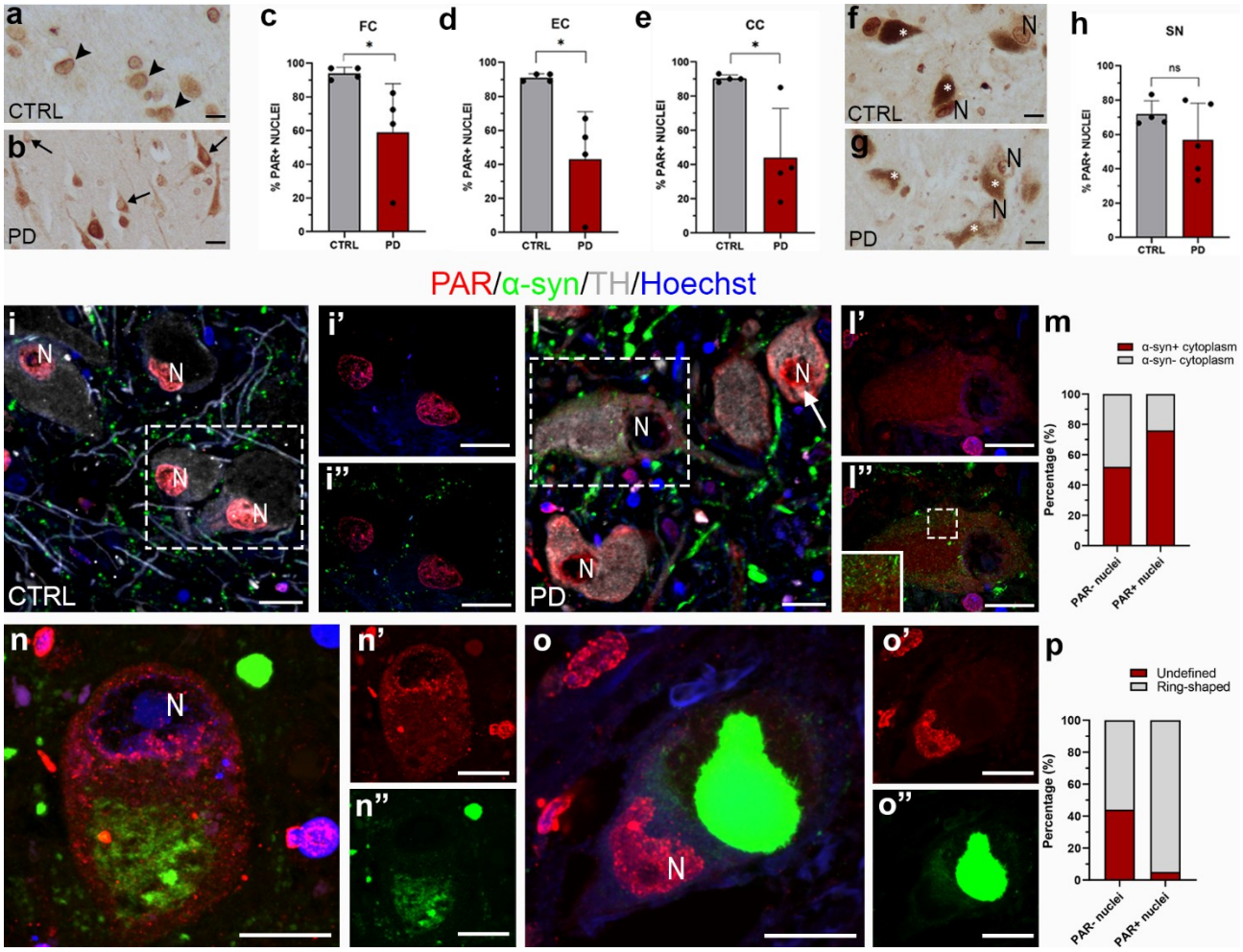

Fig. 1 PAR distribution changes in post-mortem human brain in PD patients compared to control subjects. *(**a, b**) representative image of PAR distribution in human frontal cortex. In control samples, PAR is localized in the nuclei of neurons (black arrowheads), while in PD patients a redistribution from nucleus to cytoplasm can be observed (black arrows). (**c, e**) the graphs show the percentage of PAR positive neuronal nuclei (**c**, FC: CTRL, 493 neurons, n = 4 vs PD, 418 neurons, n = 4; **d**, EC: CTRL, 224 neurons, n = 4 vs PD, 373 neurons, n = 4; **e**, CC: CTRL, 233 neurons, n = 4 vs PD, 247 neurons, n = 4). Data in graphs are reported as mean ± standard deviation. Mann-Whitney test, *p < 0.05. (**f, g**) PAR distribution in substantia nigra of control subjects and PD patients. The graph in **h** shows the percentage of PAR positive neuronal nuclei in substantia nigra (CTRL, 120 neurons, n = 4 vs PD, 150 neurons, n = 5). Data are reported as mean ± standard deviation. Mann-Whitney test, ns. (**i-l"**) show PAR and α-synuclein distribution in substantia nigra of control and PD patients. In control subjects, neuronal PAR staining is restricted to the nuclei (**i-i'**), and α-synuclein presents a dot-like signal within the synaptic compartment (**i,i"**). On the contrary, in PD, both neurons with PAR positive nucleus (**l**, white arrow) and neurons with PAR negative nucleus (**l**, dashed rectangle) are observed; in both cases, PAR is clearly detectable also in the neuronal cellular body, indicating a redistribution from the nucleus. α-Synuclein begins to accumulate in the neuronal cell body, colocalizing with PAR (**l"**). The graph in **m** shows the percentage of cells with PAR negative or positive nucleus (PAR$^-$ and PAR$^+$ nuclei, respectively) and with or without diffused or aggregated α-synuclein in the cytoplasm (a-syn$^+$ and a-syn$^-$ cytoplasm, respectively) of substantia nigra dopaminergic neurons (54 neurons, n=4 PD). (**n-o"**) show PAR distribution in neurons with*

*undefined (n-n") and ring-shaped (**o-o"**) α-synuclein aggregates. The graph in **p** shows the percentage of cells with PAR positive or negative nucleus presenting undefined (25 neurons, n=4 PD) or ring-shaped (19 neurons, n=4 PD) α-synuclein aggregates. Nuclei are counterstained using Hoechst. Scale bar, 20 µm. CC = cingulate cortex; CTRL = control; EC = entorhinal cortex; FC = frontal cortex; N = nucleus; ns = non-significant; SN = substantia nigra; white asterisks = neuromelanin.*

2.2 PARylation and stress granules co-work in α-synuclein aggregation during LB formation

We investigated in more detail the interplay between α-synuclein and PAR in undefined and ring-shaped aggregates, in dopaminergic neurons of substantia nigra (Fig. 2 a-b"). Interestingly, we observed that the fraction of α-synuclein that colocalizes with PAR significantly decreases from the undefined aggregate (Fig. 2a-a", c), when the inclusion starts to form in the neuronal cytoplasm, to the ring-shaped aggregate, once α-synuclein is compacted to form a ring-like structure (Fig. 2b-b", c). Since G3BP1 PARylation in the cytoplasm triggers stress granule assembly in cell models[15,18,19], that can act as seed for pathological aggregation[34,35], we investigated the presence of two key stress granule components, the RNA binding protein G3BP1 and TIAR, in LB formation. Analysing the distribution of G3BP1 and TIAR, the typical staining of small, roundish granules was observed in the neuronal cell bodies (Fig. 2d', white arrowheads; Supplementary Fig. 2 a'). G3BP1 and TIAR colocalize with α-synuclein aggregates in both undefined aggregates (Fig. 2d, d', Supplementary Fig. 2a, a') and in the ring-shaped structure (Fig. 2e, e', Supplementary Fig. 2b, b'). In contrast to PAR, quantitative analyses show a significant increase of G3BP1 in mature aggregates compared to undefined aggregates (Fig. 2f). We also observed an increase, although non-significant, for TIAR (Supplementary Fig. 2c). Moreover, we revealed a significant increase in the nuclear staining for both G3BP1 and TIAR in PD patients compared to controls (Fig. 2g-l).

All together these data indicate that PARylation and enrichment in stress granules are present in PD dopaminergic neurons and differently mark α-synuclein aggregates during LB formation.

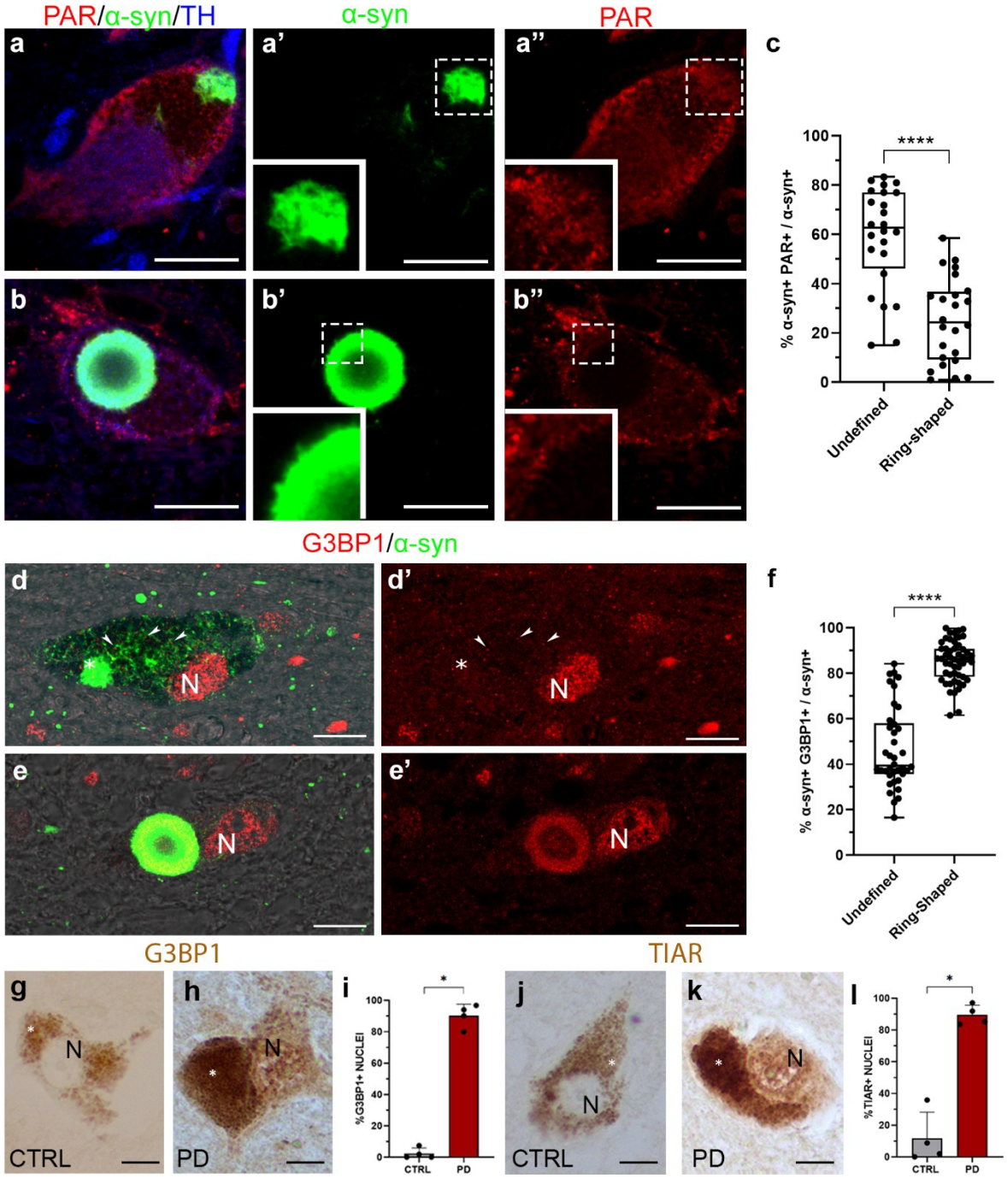

Fig. 2 PAR and stress granules mutual involvement in α-synuclein aggregation in PD patients. *(**a, b**) PAR translocate into the cell bodies of substantia nigra dopaminergic neurons and partially colocalize with α-synuclein aggregates. Colocalization is higher in the undefined stage (**a-a"**) compared with the ring-shaped structures (**b-b"**), where PAR localize in the peripheral region (**b"**). Scale bar, 20 μm. The graph in **c** (24 undefined aggregates, n = 4 PD; 24 ring-shaped aggregates, n= 4 PD) indicates the percentage of α-synuclein colocalizing with PAR expressed by Mander's coefficient (M1). Data are reported as mean ± standard deviation. Mann-Whitney test, **** $p < 0.0001$. (**d** and **e**) show colocalization between α-synuclein and G3BP1, a marker of early stress granules. G3BP is present within the nucleus and shows a point-like signal in the cytoplasm (**d, d'**, arrowheads); stress granules are observed between the α-synuclein network (d', arrowheads),*

*evident in the cell body, and neuromelanin granules, visible with phase contrast. Colocalization increases from the undefined aggregate (**d, d'**, white asterisks) to the ring-shaped structure, where G3BP1 is located in the outer layer (**e-e'**). Scale bar, 20 µm. The graph in **f** (38 undefined aggregates, n = 5 PD; 51 ring-shaped aggregates, n = 5 PD) indicates the percentage of α-synuclein colocalizing with G3BP1 expressed by Mander's coefficient (M1). Data are reported as mean ± standard deviation. Mann-Whitney test, **** p < 0.0001. (**g-l**) immunoenzymatic assay showing the distribution of G3BP1 and TIAR in substantia nigra dopaminergic neurons. In CTRL samples, nuclei are negative for both (**g, j**) while in PD patients, G3BP1 and TIAR localize within the nuclei (**h, k**). White asterisks indicate neuromelanin. Scale bar, 20 µm. The percentage of G3BP1 (CTRL, n = 4, 268 neurons vs PD, n = 4, 285 neurons) and TIAR (CTRL, n = 4, 229 neurons vs PD, n = 4, 274 neurons) positive nuclei are shown in **i** and **l**, respectively. Data in graphs are reported as mean ± standard deviation. Mann-Whitney test, *p < 0.05; CTRL = control; N = Nucleus. Inset in a', a", b', b": 2,5x.*

2.3 PARylation involvement in early α-synuclein aggregation

Given the higher colocalization of PAR and α-synuclein in undefined α-synuclein aggregates (Fig. 2c), we hypothesized that PAR may play a key role in the early stages of protein aggregation. To investigate this, we explored the interplay between PARylation and α-synuclein oligomers, which are considered the earliest form of α-synuclein aggregates[29,36,37]. We used Proximity Ligation Assay (PLA) to detect α-synuclein oligomers alongside immunofluorescence in *substantia nigra* of PD patients. As expected, PAR was localised in the cell bodies of TH-positive neurons (Fig. 3a, a', b, b', c, c'), where α-synuclein oligomers were also present (Fig. 3a, a', b, b', c, c'). In detail, these oligomers, found throughout the cytoplasm in early aggregation stages (Fig. 3a'), as well as more aggregated forms (Fig. 3b'), and ring-shaped structure (Fig. 3c'), colocalized with cytoplasmatic PAR.

To further analyze the interaction between PARylation and α-synuclein oligomers, we used high-resolution imaging and 3D reconstruction, and quantified α-synuclein oligomers and PAR interactions (Fig. 3a", b", c", Supplementary video 1-3). Through this approach, we confirmed that α-synuclein oligomers colocalize with PAR (Fig. 3d) and quantified the percentage of PAR-positive oligomers. The percentage increased during the early and intermediate stages of aggregation (32% and 50% respectively) and decreased when ring-shaped structures formed (15%). Notably, the ring-shaped structure showed an onion-like structure with PAR distributed both in the center, where they colocalize with Hoechst, and in the periphery, where they colocalize with α-synuclein oligomers, surrounded by TH signal (Fig. 3 e, f). Moreover, a detailed examination of brain sections revealed the presence of some α-synuclein oligomers-positive structures (Fig. 3g, g'; n=2), that resemble the so-called tunnelling nanotube, recently described in human brain[31]. In detail, the neuron to which the

227 tunnelling nanotube connects, is decorated with cytoplasmic PAR staining that colocalize with α-
228 synuclein oligomers (Fig. 3g"), indicating a possible involvement of PARylation in the spreading of
229 oligomers.
230 Finally, we examined the relationship between stress granule proteins G3BP1, TIAR, and α-synuclein
231 oligomers, revealing that G3BP1 and TIAR-positive stress granules accumulate alongside α synuclein
232 oligomers (Supplementary Fig. 3).
233 Collectively, these data support a pivotal involvement of PARylation in the earliest stages of α-
234 synuclein aggregation.

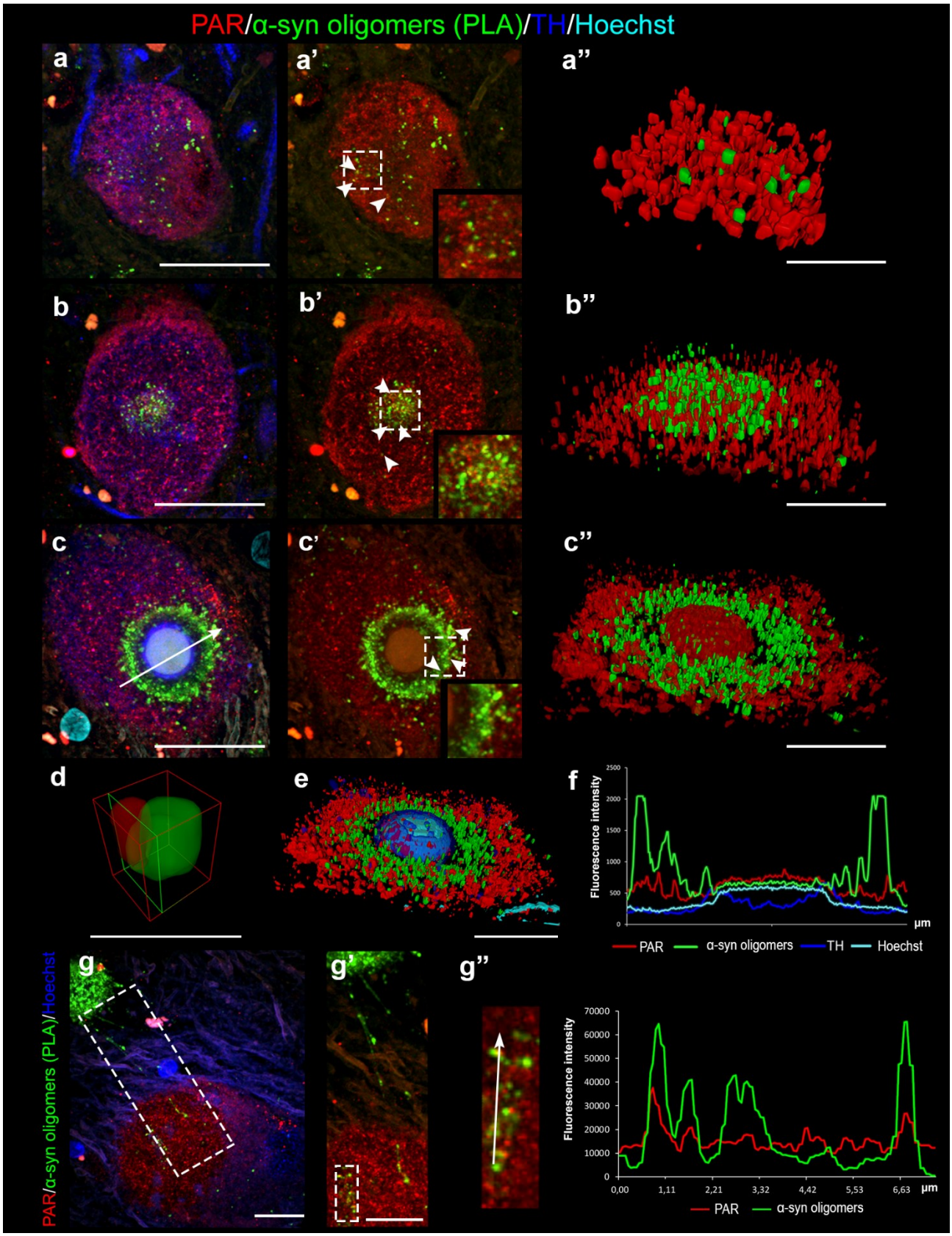

Fig. 3 PAR colocalizes with α-synuclein oligomers during the aggregation process in PD patients. *In substantia nigra dopaminergic neurons (**a-c'**), colocalization between PAR and α-synuclein oligomers in neuronal cell bodies, starting from the earliest stage, when α-synuclein oligomers are*

*scattered in the cytoplasm (**a'**, white arrowheads), but also in undefined aggregate (**b'**, white arrowheads), and in the ring-shaped structure where colocalization is limited at the peripheral region (**c'**, white arrowheads). (**a"**, **b"** and **c"**) show 3D reconstruction obtained with arivis Vision4D 3.6.0 software of confocal images. (**d**) Example of PARylation of α-synuclein oligomer obtained with 3D reconstruction. (**e-f**) 3D reconstruction by arivis Vision4D 3.6.0 of **c** and the intensity profile graph for PAR, α-synuclein oligomer, TH and Hoechst signals along the line intersecting the ring-shaped aggregate in **c**. Nuclei are counterstained using Hoechst. (**g-g"**) α-synuclein oligomers outline a structure resembling a tunnelling nanotube (white dashed rectangle, 1,5x magnified in **g'**), which connects a cytoplasmic PAR-rich neuron and an α-synuclein aggregate. **g''** shows the 2.5x magnification of a small portion of the tunnelling nanotube in **g'** (white dashed rectangle) and the intensity profile that shows partial overlapping peaks, indicating that also in this structure some oligomers are PARylated. **a, a'**, **b, b'**, **c**, **c'**: scale bar, 20 µm. **a''**, **b''**, **c''**, **e**: scale bar, 5 µm. **d**: scale bar, 1 µm. **g**, **g'**: scale bar, 10 µm. Inset in a', b', c': 1,5x.*

2.4 PARylation is involved in Parthanatos and α-synuclein spreading in *substantia nigra* of PD patients

PAR accumulation in the cell body has been previously described as indicative of severe cellular stress[38]. Indeed, AIF PARylation induces its release from the mitochondria and, consequently, the activation of Parthanatos leading to cell death[23]. Evidence for the involvement of Parthanatos pathway in PD pathology has primarily been derived from *in vitro* studies and mouse models[6,39]. Therefore, in this work, we aimed to investigate whether PAR could localize into mitochondria in human PD brains and could be responsible for neuronal cell death of *substantia nigra* dopaminergic neurons. Triple immunofluorescence analysis revealed that mitochondria, marked by Voltage-dependent anion channel 1 (VDAC1), are widely distributed throughout the cytoplasm of dopaminergic neurons in both control (Fig. 4a, a') and PD samples (Fig. 4b, b'). In control neurons, PAR predominantly localizes to the nucleus (Fig. 4a, a''). However, in PD neurons, PAR accumulation to the cytoplasm (Fig. 4b, b''), as previously demonstrated, and colocalizes with VDAC1 (Fig. 4b), as further confirmed by high-resolution 3D imaging (Fig. 4e). Interestingly, we observed that PAR also colocalize with mitochondria surrounding α-synuclein-labelled LB (Fig. 4c-c'').

Quantitative analysis showed a significant increase in the colocalization between PAR and mitochondria in the cytoplasm of *substantia nigra* dopaminergic neurons in PD patients compared to control (Fig. 4d). Moreover, 3D reconstruction provided the first evidence of PAR localization within mitochondria (Fig. 4f, g), suggesting its involvement in activating the Parthanatos cell death pathway in human PD brain.

Since Parthanatos pathway is known to trigger DNA condensation[22,23], we further investigated this phenomenon. We revealed that condensed DNA was present inside *substantia nigra* neurons and that the condensed DNA is also PAR positive and localized in neurons showing mature LB (Fig. 5a-a'''). All together, these findings suggest that PAR plays a critical role in mediating neuronal cell death in substantia nigra dopaminergic neurons in PD patients.

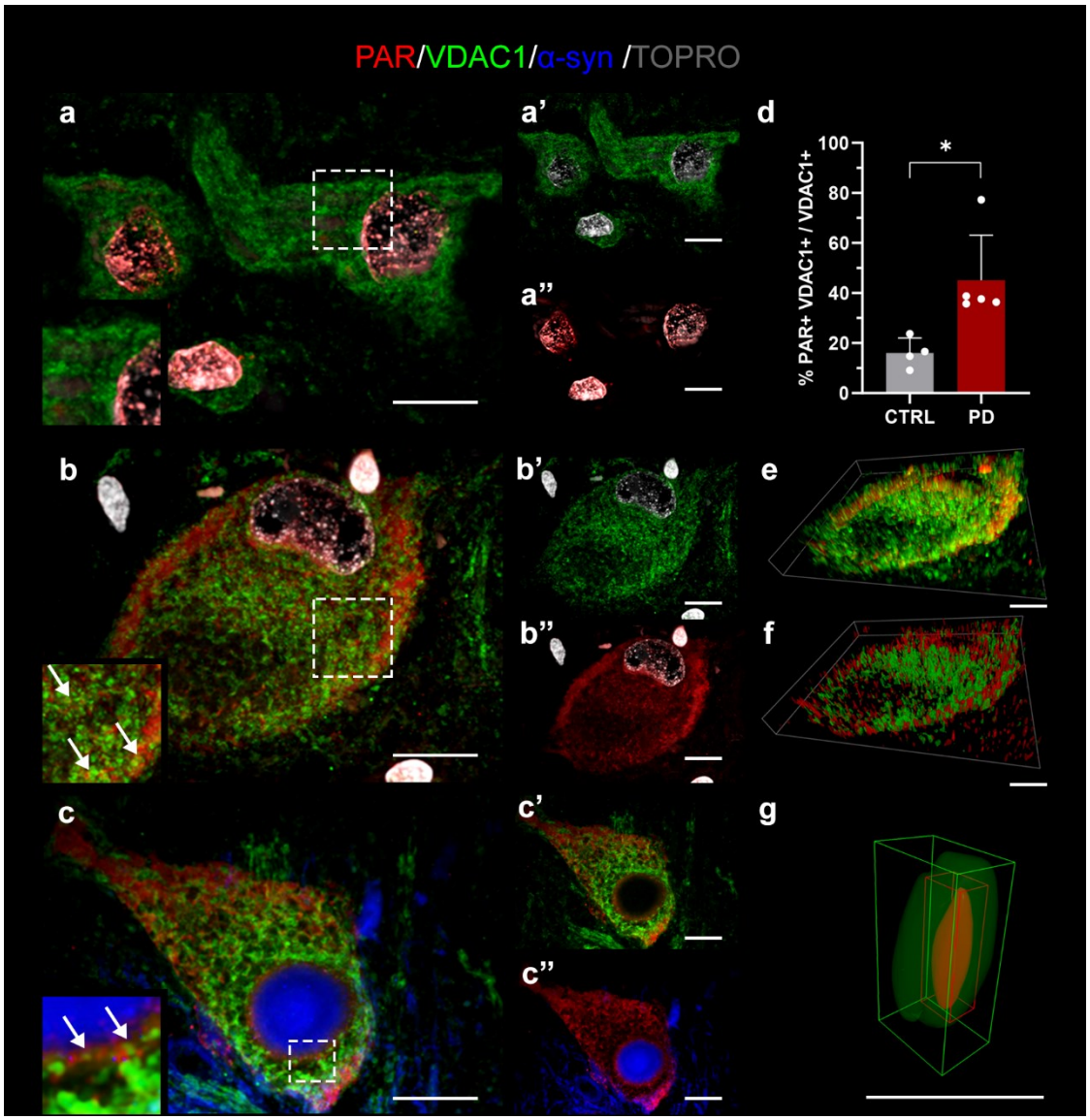

Fig. 4 Mitochondria PARylation in substantia nigra dopaminergic neurons of PD patients. *In control subjects, PAR are distributed in neurons nuclei (**a, a"**) while VDAC1-labeled mitochondria localize into the cytoplasm, as expected (**a, a'**). In PD samples, cytoplasmic PAR (**b, b"**) partially colocalize with mitochondria (**b,** white arrows in the inset). PAR also colocalize with mitochondria that surround α-synuclein labeled LB (white arrows in the inset of **c,** 3x magnified). The graph in **d** (CTRL, n= 4, 88 neurons vs PD, n= 5, 133 neurons) indicates the percentage of mitochondria staining colocalizing with PAR expressed by Mander's coefficient (M1). Data are reported as mean ± standard deviation. Mann-Whitney test, *p < 0.05. **e** and **f** show the 3D reconstruction obtained*

with Nis Elements software and with arivis Vision4D 3.6.0 software, respectively, of image ***b****. (****g****) 3D reconstruction of a mitochondrion of substantia nigra dopaminergic neuron showing PAR inside it. Nuclei are counterstained using TOPRO****. a-a'', b-b'', c-c'', e, f****: scale bar, 20 µm.* ***g****: scale bar, 3 µm.*

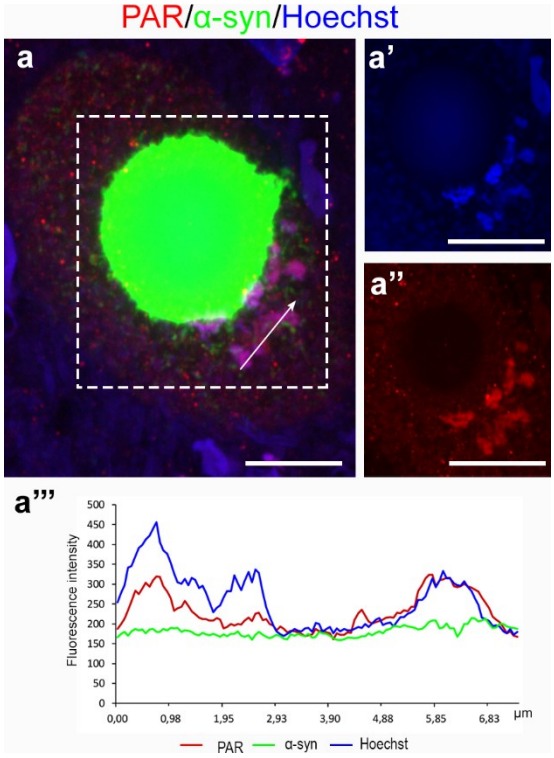

Fig. 5 Interplay among α-synuclein aggregates, DNA condensation, and PARylation. *Substantia nigra dopaminergic neuron with a mature LB* ***(a)*** *shows condensed DNA, marked with Hoechst* ***(a')****, that colocalizes with PAR* ***(a")****.* ***(a"')*** *Intensity profile graph that highlights the overlapping signals of Hoechst and PAR along the arrow shown in* ***a****. Scale bar, 10 µm.*

3 Discussion

PARP1-mediated PARylation has emerged as an important player in PD pathology, and, particularly, in exacerbating α-synuclein aggregation[6,28]. This key finding is supported by studies of cell and mouse models as well as in the CSF of PD patients[6,25]. Building on this, we investigated PARylation in *post-mortem* human PD brain to explore its potential link with α-synuclein aggregation and neuronal cell death. Our results led us to the proposed model illustrated in (Fig. 6). Briefly, in PD PAR polymers usually found in the nucleus (Fig. 6a) accumulate into the cytoplasm of neurons (Fig. 6b), where they colocalize with different forms of α-synuclein aggregates (Fig. 6c-f), mainly with the earliest form (Fig. 6c), and also in the periphery of LB (Fig. 6d, e) suggesting that PARylation may act as a trigger for α-synuclein aggregation. α-Synuclein aggregates colocalize also with stress granule proteins, though this occurs after the aggregates become PAR-positive (Fig. 6c-e), suggesting a role of PARylation in stress granules formation in PD human brain, as previously demonstrated in cellular and animal models[40,41]. Finally, PAR polymers colocalize with mitochondria having the potential to activate Parthanatos cell death pathway (Fig. 6e), as strongly suggested by the presence of condensed PARylated DNA (Fig. 6f). Studying *post-mortem* human PD brains provides valuable

insight into the molecular events driving LB formation, complementing the knowledge gained from *in vitro* and animal models[30]. Our findings indicate a significant role for PAR in the neurodegenerative process of PD. This advances our understanding of the molecular events underlying LB formation, their propagation, and the mechanisms leading to neuronal cell death in PD patients.

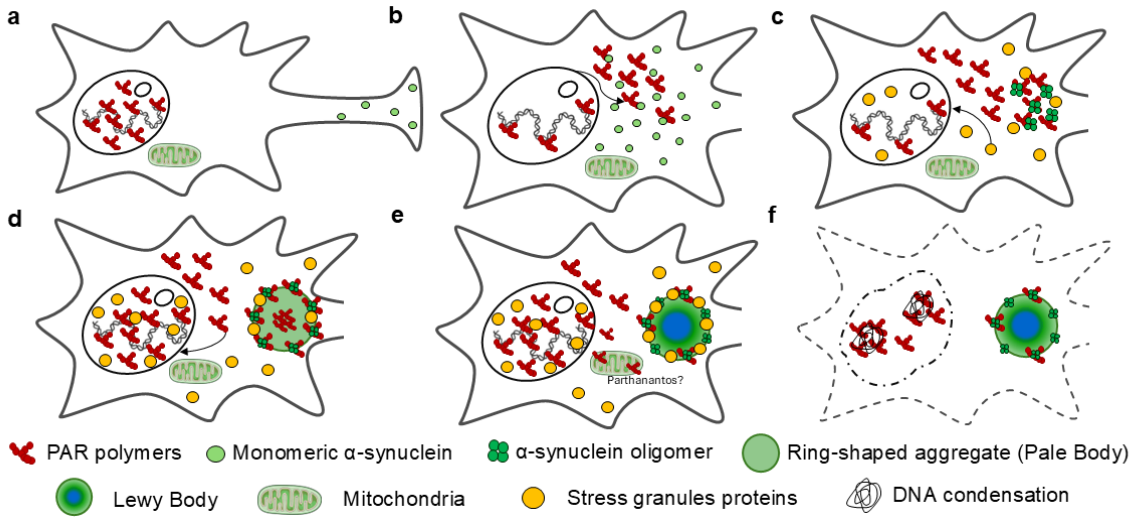

Fig. 6 PAR redistribution and α-synuclein aggregation during Lewy body formation and neuronal cell death. *Schematic model showing the sequences of events in LB formation concurrently with the redistribution of PAR and stress granules. (**a**) In controls, PAR are located in the nuclei, where they carry out their physiological function in repairing DNA, while α-synuclein mainly localizes in the synaptic compartment. (**b**) In PD, both PAR and α-synuclein start to accumulate in the neuronal cell body. (**c**) α-synuclein oligomers are present in undefined aggregates where colocalize with PAR and stress granules proteins (Supplementary Fig. 3). Stress granules partially translocate within the nucleus. (**d**) With the formation of aggregates with ring-shaped structure, both PAR and stress granule proteins localize within the nucleus; notably PAR are arranged both in the center and in the periphery of the ring-shaped structure (Pale Body), where they co-localize with α-synuclein oligomers. (**e**) PAR polymers co-localize with mitochondria, which is the first step in activating the Parthanatos cell death pathway; in the mature LB, PAR and stress granule proteins can be identified in the peripheral region; Hoechst staining (blue) is detectable in the core of these aggregates. (**f**) Neurons that show a mature LB and, also show PARylated and condensed DNA.*

Although alterations of PARP1-mediated PARylation have been extensively described in many pathological conditions such as cancer, autoimmune, and cardiovascular diseases[13], its role in neurodegenerative diseases including PD, Alzheimer's disease, Huntington's disease, and multiple sclerosis is emerging only in these last years[42]. PARP1 is primarily localized in the nucleus, where it plays a protective role in repairing DNA single and double strand breaks. However, prolonged

activation of PARP1 can lead to cell death through NAD^+ depletion, impaired cellular function, and DNA fragmentation[7]. Thus, PARP1 overactivation, observed in PD, suggests that PAR overproduction may be a key pathological process[13,15]. In this study, we observed a decrease of PAR in the neuronal nuclei of PD patients compared to control in cortical areas affected by α-synuclein pathology and a strong translocation from the nucleus to neuronal cytoplasm, in both the cortex and *substantia nigra*. This cytoplasmic redistribution aligns with the nuclear depletion and cytoplasmic relocation of the PARP1 previously reported in dopaminergic neurons from *post-mortem* PD brains[27] as well as the increased PAR levels detected in the CSF of PD patients[6].

In this study, we found that PAR in the soma of *substantia nigra* dopaminergic neurons colocalize with cytoplasmic α-synuclein and with the different forms of α-synuclein inclusions during LB morphogenesis. Over the years, many efforts have been made to identify the different components of LB and understand the mechanisms leading to their formation[30,31]. Furthermore, the higher colocalization of PAR with the early stages of α-synuclein aggregation, together with the presence of PAR-positive α-synuclein oligomers, highlights a potential role for PARylation in triggering α-synuclein aggregation, and supports prior hypotheses that PARP1-mediated PARylation is involved in this process. PARylation may drive aggregation through direct interaction between PAR and α-synuclein, likely via electrostatic forces involving the positively charged lysine residues of α-synuclein[28]. Alternatively, PARylation may indirectly affect α-synuclein aggregation through its regulation of autophagy which is impaired in PD[43]. Overactivation of PARP1 and an overproduction of PAR, as reported in the present work, could result in PARylation of autophagy-related proteins and NAD^+ depletion that induce SIRT1 inactivation[44,45]. This could impair autophagy and increase the susceptibility of neurons to aggregated α-synuclein, damaged organelles, and oxidative stress. Additionally, PAR elevation in the cytoplasm has been shown to promote stress granule formation in cell models[18], with PARylation promoting granule biogenesis[19]. For the first time, we observed the presence of stress granule proteins in *substantia nigra* dopaminergic neurons of PD human brain, particularly in mature LB and, to a lesser extent, in undefined aggregates. The higher presence of stress granules in LB compared to earlier forms, suggest that stress granules assembly may occur later, while PAR, plays a more pivotal role in the early steps of PD pathology.

G3BP1 ADP-ribosylation has previously been described in cell models as a key actor in stress granules formation[18] under both acute and chronic stress conditions[46], and is also implicated in the nuclear translocation of G3BP1[19]. In our study, alongside stress granule formation, we observed the increase in the nuclear staining for both G3BP1 and TIAR in PD patients compared to controls, indicating a nucleocytoplasmic shuttling for these two proteins. This phenomenon may reflect the chronic stress characteristics of PD. Indeed, the role of PARylation in the nucleocytoplasmic shuttling

has been already demonstrated for another stress granule protein, the adenylateuridylate-rich element (ARE)-binding protein embryonic lethal abnormal vision-like 1 (Elavl1)/human antigen R (HuR), a mechanism to regulate gene expression at the post-transcriptional level in an *in vitro* model[47]. The observed nuclear-cytoplasmic dynamics of G3BP1 and TIAR in PD may, therefore, indicate a broader role for PARylation in modulating cellular stress responses and gene expression. This supports the hypothesis that chronic PARP1 activation in PD may contribute to the pathological aggregation of α-synuclein and stress granule formation through these nucleocytoplasmic transport mechanisms.

The role of α-synuclein neurodegeneration in PD via the Parthanatos death cascade was first described following *in vivo* and *in vitro* administration of α-synuclein pre-formed fibrils (PFFs) that increases nitric oxide formation and activates PARP1[6]. This was later confirmed by studies showing that genetic and pharmacological manipulation of the pathway prevents neurodegeneration in PD mouse models and primary neuronal cultures[39]. In *post-mortem* human brain, we observed a marked increase in PAR colocalization with mitochondria in *substantia nigra* dopaminergic neurons of PD patients compared to controls. Moreover, through 3D reconstruction we identified PAR polymers within mitochondria.

Given that endogenous AIF, one of the effectors of Parthanatos pathway, is located both at the outer mitochondrial membrane on the cytosolic side and attached to the inner membrane facing the intermembrane space [48], and binds PAR with high affinity [49], our findings suggest that the increased mitochondria PARylation in dopaminergic neurons of PD patients, may indicate Parthanatos pathway activation. Additionally, we also observed PAR colocalization with mitochondria adjacent to a mature LB. This might indicate that a link exists between α-synuclein, LBs, and neuronal cell death. Neurons with mature LBs also displayed PARylated condensed DNA, further supporting this connection.

In light of these results and emerging data from the literature, it is clear that PARylation could represent an attractive therapeutic target to act on in PD pathology[38]. Two main approaches could be pursued: *i)* the direct inhibition of PARP1 and *ii)* the inhibition of PARP1 effectors in the Parthanatos pathway. The first approach could be based on the inhibition of PARP1 enzyme to counteract the production of excessive PAR polymers that could exacerbate α-synuclein aggregation[25]. Several inhibitors are commercially available and currently used to treat different types of cancer, acting as a PARP1 active site binder or as trapping compound on DNA. Among them, olaparib and veliparib, used in the treatment of ovarian and breast cancer, were also found to be protective in different *in vitro* and *in vivo* PD and neurodegenerative models[25,50] . Moreover, administration of PARP1 indirect inhibitors (nilotinib) has been attempted in a clinical trial, in PD patients, but did not provide the expected results[51] (ClinicalTrial.gov: NCT03205488). This is understandable since patients enrolled

were in the late stage of the disease, when PARP1 has already exerted its action and, probably, contributed to α-synuclein aggregation and neuronal cell death via Parthanatos pathway. Therefore, it might be an option to consider PARP1 as an early target to act on in the early stages of neurodegeneration. Nevertheless, it cannot be excluded that lack of effect is due to the inhibitor used that may not acts directly on PARP1. However, some issues need to be considered; among these, the selectivity is fundamental, since some of the inhibitors act not only on PARP1 but also on PARP2 and other PARP isoforms. Moreover, the administration could have to be chronic, and, given PARP1 plays many biological functions, this may be associated with a risk of various side effects such as genotoxicity[50]. Recently, another compound, called 10e, was tested *in vitro* and emerged as a potential inhibitor to be further investigated in PD animal models. Indeed, it is a structural analogue of FDA-approved olaparib, with higher PARP1 affinity, selectivity, and lower toxicity[52]. Since it appears that the death of *substantia nigra* dopaminergic neurons is mediated by the PARP1-based cell death called Parthanatos pathway, the second approach that could be pursued is to inhibit the effectors of this pathway such as the flavoprotein AIF and the nuclease MIF. Thus, the strategies of controlling the level of intracellular PAR targeting Poly (ADP-ribose) glycohydrolase (PARG) enzyme, which is responsible of its degradation[24], might be considered.

In conclusion, this study points out the role of PARP1-mediated PARylation in PD pathology. The study of molecular events occurring in *post-mortem* human brain integrated with the experimental studies on cell and mouse models, indicate a role of PAR in stress granule assembly and LB formation, their propagation and, ultimately neuronal cell death. The involvement of PARylation in triggering α-synuclein aggregation, which is supported by the identification of PARylated α-synuclein oligomers, and in triggering Parthanatos cell death pathway in *substantia nigra* dopaminergic neurons, suggests that it could be a therapeutic target in an early stage on the disease. Finally, a question arises: what can cause chronic stress, inducing PAR overactivation and stress granules formation, as observed in PD patients? Some studies reported a possible involvement of viral infection in PD[53] and viral infectious has been demonstrated to be able to activate stress granules[54,55].

4 Methods

4.1 Patients

All patients were enrolled and followed during the course of the disease at the Parkinson's Centre ASST G. Pini-CTO of Milan. The clinical diagnosis of PD was carried out according to the UK Brain Bank criteria[56,57] and confirmed by neuropathological assessment performed by two

experienced neurologists in movement disorders, GG and MB, in compliance with current BrainNet Europe Consortium guidelines[58].

Post-mortem human brains obtained from PD patients (N=8) and from age-matched control subjects (N= 6) clinically free from neurological diseases were used (Supplementary Table 1). Written informed consent was obtained from all subjects in agreement with relevant laws and institutional guidelines and approved by the appropriate institutional committees. The study procedures were approved by the Ethics Committee of the University of Milan (protocol code 66/21).

Brains were fixed in 10% buffered formalin for at least 21 days at 20°C. Selected areas were paraffine embedded and cut at the microtome (MR2258, Histoline) to obtain 5 mm thick sections of mesencephalon, entorhinal, cingulate and the frontal cortex, processed for the following analysis.

4.2 Immunohistochemistry

After deparaffination and rehydration, tissue sections were sequentially incubated with: *i)* 80% formic acid solution for 20 min for antigen retrieval, *ii)* 3% H_2O_2 for 20 min for endogenous peroxidases inactivation; *iii)* 1% BSA in 0.01 M phosphate saline buffer (PBS) containing 0.1% Triton X-100 for 20 min (BSAT); *iv)* the primary antibody, mouse anti-PAR (the PAR chain length used as immunogen ranges from 2 to 50 monomers; 1:200), mouse anti-G3BP (1:250) or mouse anti-TIAR (1:100), diluted in BSAT and incubated overnight at room temperature (RT) (Supplementary Table 2). To visualize the antigen-antibody binding the EnVision anti-mouse secondary antibody (Agilent 1 h, RT) and 3,3′-Diaminobenzidine as chromogen (DAB, Agilent kit) were used (Supplementary Table 2). Tissue sections were mounted with permanent mounting medium (Eukitt). Images were acquired with the optical microscope Zeiss at 10X and 20X magnification.

4.3 Immunofluorescence and Proximity Ligation Assay (PLA)

For the immunofluorescence staining, sections containing *substantia nigra* and frontal cortex were incubated with either 80% formic acid solution for 20 min or high pH antigen retrieval solution 50X (Agilent, S2367; diluted 1:50 in PBS) at 90°C for 20 min plus 10 min at RT and 5 min in PBS. Then, incubation with BSAT for 20 min at RT followed by a mix of anti-PAR with different primary antibodies (S100 calcium-binding protein B (S100β), Tyrosine Hydroxylase (TH), Voltage-dependent anion channel 1 (VDAC1), and α-synuclein), or by a mix of G3BP1/TIAR and α-synuclein antibodies was carried out overnight at RT (Table 2). Tissue sections were then incubated with specific fluorescent secondary antibodies (Table 2) for 2 h at RT in the dark.

PLA was used to detect α-synuclein oligomers[36], accordingly to protocols previously described[59]. Briefly, sections were incubated with a mixture containing α-synuclein S3062-MINUS

and α-synuclein S3062-PLUS probes, anti-PAR and anti-TH antibody diluted in Duolink® Antibody Diluent for 1 h at 37°C and then overnight at RT. To carry out the amplification reaction, tissue sections were treated as follows: *i)* Duolink® ligase (1:40) in Duolink® ligation solution (1:5) (diluted in milliQ water at 37°C for 1 h, *ii)* Polymerase (1:80) in Duolink® Amplification Reagent Green (1:5 in milliQ water) for 2 h at 37 °C, to which donkey anti-mouse secondary antibody conjugated to Alexa Fluor® 568 and donkey anti-goat secondary antibody conjugated to Alexa Fluor® 647 were added to the polymerase step to detect double immunofluorescence. Nuclei were stained using either Hoechst 33342 (1:5000) or TO-PRO®-3 (1:1000), 10 min at RT. Sections were mounted using Mowiol® + DABCO® and finally, examined with Nikon spinning disk confocal microscope, equipped with CSI–W1 confocal scanner unit using a water-immersion 40X and silicon-immersion 100X objectives.

4.4 3D reconstruction

For 3D visualization, arivis Vision4D® 3.6.0 software (Zeiss Company), a powerful tool that guarantees precise and reproducible quantitative morphometric analyses to visualize small and complex structure[60,61], was used. In detail, images were imported into the software and transformed into the 12-pixel format. The region of interest (ROI) of deconvolved 100X acquisitions was created using the "Transformation gallery > Crop" tool. After gamma correction to enhance faint objects and denoising to remove residual noise, different pipelines were used to 3D reconstruction. The "Intensity threshold segmentation" pipeline was used for both TH and nuclei continuous staining. PLA puncta, PAR and VDAC1 staining, which show a point like distribution, are reconstructed using "blob finder" pipeline, selecting a suitable range of exposure using the "preview" tool.[35,36]

4.5 Image and statistical analysis

Images were analyzed using Fiji software (NIH). In detail, counting of PAR positive nuclei of neurons and astrocytes in the corresponding anatomic regions was performed using cell counter tool, while JACOP plug-in was selected for colocalization analysis calculating Mander's coefficient[62]. Statistical analysis was performed using GraphPad™ 8.0 software. Un-paired non-parametric Mann-Whitney test was carried out to compare groups considering a *p-value* <0.05 as statistically significant.

References

1. Balestrino, R. & Schapira, A. H. V. Parkinson disease. Eur J Neurol 27, 27–42 (2020).
2. Panicker, N., Ge, P., Dawson, V. L. & Dawson, T. M. The cell biology of Parkinson's disease. J Cell Biol 220, (2021).
3. Spillantini, M. G. et al. α-Synuclein in Lewy bodies. Nature 388, 839–840 (1997).

4. Brás, I. C., Xylaki, M. & Outeiro, T. F. Mechanisms of alpha-synuclein toxicity: An update and outlook. Progress in Brain Research vol. 252 91–129 Preprint at https://doi.org/10.1016/bs.pbr.2019.10.005 (2020).
5. Schaffert, L. N. & Carter, W. G. Do post-translational modifications influence protein aggregation in neurodegenerative diseases: A systematic review. Brain Sciences vol. 10 Preprint at https://doi.org/10.3390/brainsci10040232 (2020).
6. Kam, T. I. et al. Poly(ADP-ribose) drives pathologic a-synuclein neurodegeneration in Parkinson's disease. Science (1979) 362, (2018).
7. Amé, J. C., Spenlehauer, C. & De Murcia, G. The PARP superfamily. Bioessays 26, 882–893 (2004).
8. Kurosaki, T. et al. Primary structure of human poly(ADP-ribose) synthetase as deduced from cDNA sequence. Journal of Biological Chemistry 262, 15990–15997 (1987).
9. Andrabi, S. A. et al. Iduna protects the brain from glutamate excitotoxicity and stroke by interfering with poly(ADP-ribose) polymer-induced cell death. Nat Med 17, 692–699 (2011).
10. Kang, H. C. et al. Iduna is a poly(ADP-ribose) (PAR)-dependent E3 ubiquitin ligase that regulates DNA damage. Proc Natl Acad Sci U S A 108, 14103–14108 (2011).
11. Zhang, Y. et al. RNF146 is a poly(ADP-ribose)-directed E3 ligase that regulates axin degradation and Wnt signalling. Nat Cell Biol 13, 623–629 (2011).
12. Beneke, S. Regulation of chromatin structure by poly(ADP-ribosyl)ation. Front Genet 3, (2012).
13. Ke, Y. et al. The Role of PARPs in Inflammation-and Metabolic-Related Diseases: Molecular Mechanisms and Beyond. Cells 8, 1–22 (2019).
14. Mao, K. et al. Poly (ADP-ribose) polymerase 1 inhibition prevents neurodegeneration and promotes α-synuclein degradation via transcription factor EB-dependent autophagy in mutant α-synucleinA53T model of Parkinson's disease. Aging Cell 19, (2020).
15. Krietsch, J. et al. Reprogramming cellular events by poly(ADP-ribose)-binding proteins. Molecular Aspects of Medicine vol. 34 1066–1087 Preprint at https://doi.org/10.1016/j.mam.2012.12.005 (2013).
16. Wei, H. & Yu, X. Functions of PARylation in DNA Damage Repair Pathways. Genomics, Proteomics and Bioinformatics vol. 14 131–139 Preprint at https://doi.org/10.1016/j.gpb.2016.05.001 (2016).
17. Hijaz, B. A. & Volpicelli-Daley, L. A. Initiation and propagation of α-synuclein aggregation in the nervous system. Molecular Neurodegeneration vol. 15 Preprint at https://doi.org/10.1186/s13024-020-00368-6 (2020).
18. Leung, A. K. L. et al. Poly(ADP-Ribose) Regulates Stress Responses and MicroRNA Activity in the Cytoplasm. Mol Cell 42, 489–499 (2011).
19. Isabelle, M., Gagné, J. P., Gallouzi, I. E. & Poirier, G. G. Quantitative proteomics and dynamic imaging reveal that G3BP-mediated stress granule assembly is poly(ADP-ribose)-dependent following exposure to MNNG-induced DNA alkylation. J Cell Sci 125, 4555–4566 (2012).
20. Palazzo, L., Mikolčević, P., Mikoč, A. & Ahel, I. ADP-ribosylation signalling and human disease. Open Biol 9, 190041 (2019).
21. David, K. K., Andrabi, S. A., Dawson, T. M. & Dawson, V. L. Parthanatos, A messenger of death. Frontiers in Bioscience 14, 1116–1128 (2009).
22. Wang, Y. et al. Poly(ADP-ribose) (PAR) binding to apoptosis-inducing factor is critical for PAR polymerase-1-dependent cell death (parthanatos). Sci Signal 4, (2011).
23. Liu, L. et al. The key players of parthanatos: opportunities for targeting multiple levels in the therapy of parthanatos-based pathogenesis. Cell Mol Life Sci 79, (2022).

24. Pan, B. & Petersson, E. J. A PARP-1 Feed-Forward Mechanism to Accelerate α-Synuclein Toxicity in Parkinson's Disease. Biochemistry 58, 859–860 (2019).
25. Olsen, A. L. & Feany, M. B. PARP Inhibitors and Parkinson's Disease. New England Journal of Medicine 380, 492–494 (2019).
26. Sako, W., Murakami, N., Izumi, Y. & Kaji, R. Reduced alpha-synuclein in cerebrospinal fluid in synucleinopathies: Evidence from a meta-analysis. Movement Disorders 29, 1599–1605 (2014).
27. Salemi, M. et al. Poly (ADP-ribose) polymerase 1 and Parkinson's disease: A study in post-mortem human brain. Neurochem Int 144, (2021).
28. Puentes, L. N. et al. Poly (ADP-ribose) Interacts With Phosphorylated α-Synuclein in Post Mortem PD Samples. Front Aging Neurosci 13, (2021).
29. Verma, M., Vats, A. & Taneja, V. Toxic species in amyloid disorders: Oligomers or mature fibrils. Annals of Indian Academy of Neurology vol. 18 138–145 Preprint at https://doi.org/10.4103/0972-2327.144284 (2015).
30. Fares, M. B., Jagannath, S. & Lashuel, H. A. Reverse engineering Lewy bodies: how far have we come and how far can we go? Nat Rev Neurosci 22, 111–131 (2021).
31. Mazzetti, S. et al. Linking acetylated α-Tubulin redistribution to α-Synuclein pathology in brain of Parkinson's disease patients. NPJ Parkinsons Dis 10, (2024).
32. Moors, T. E. et al. The subcellular arrangement of alpha-synuclein proteoforms in the Parkinson's disease brain as revealed by multicolor STED microscopy. Acta Neuropathol 142, 423–448 (2021).
33. Takahashi, H. & Wakabayashi, K. The cellular pathology of Parkinson's disease. Neuropathology 21, 315–322 (2001).
34. Lumpkin, C. J. et al. Broad proteomics analysis of seeding-induced aggregation of α-synuclein in M83 neurons reveals remodeling of proteostasis mechanisms that might contribute to Parkinson's disease pathogenesis. Mol Brain 17, 1–16 (2024).
35. Baradaran-Heravi, Y., Van Broeckhoven, C. & van der Zee, J. Stress granule mediated protein aggregation and underlying gene defects in the FTD-ALS spectrum. Neurobiol Dis 134, (2020).
36. Bengoa-Vergniory, N., Roberts, R. F., Wade-Martins, R. & Alegre-Abarrategui, J. Alpha-synuclein oligomers: a new hope. Acta Neuropathol 134, 819–838 (2017).
37. Du, X. Y., Xie, X. X. & Liu, R. T. The Role of α-Synuclein Oligomers in Parkinson's Disease. Int J Mol Sci 21, 1–17 (2020).
38. Yang, L., Guttman, L., Dawson, V. L. & Dawson, T. M. Parthanatos: Mechanisms, modulation, and therapeutic prospects in neurodegenerative disease and stroke. Biochem Pharmacol 116174 (2024) doi:10.1016/J.BCP.2024.116174.
39. Park, H. et al. PAAN/MIF nuclease inhibition prevents neurodegeneration in Parkinson's disease. Cell 185, 1943-1959.e21 (2022).
40. Duan, Y. et al. PARylation regulates stress granule dynamics, phase separation, and neurotoxicity of disease-related RNA-binding proteins. Cell Res 29, 233–247 (2019).
41. McGurk, L. et al. Poly(ADP-Ribose) Prevents Pathological Phase Separation of TDP-43 by Promoting Liquid Demixing and Stress Granule Localization. Mol Cell 71, 703-717.e9 (2018).
42. Mao, K. & Zhang, G. The role of PARP1 in neurodegenerative diseases and aging. FEBS J 289, 2013–2024 (2022).

43. Wu, Y.-C. et al. The Critical Role of SIRT1 in Parkinson's Disease: Mechanism and Therapeutic Considerations. (2020) doi:10.14336/AD.2020.0216.
44. Brady, P. N., Goel, A. & Johnson, M. A. Poly(ADP-Ribose) Polymerases in Host-Pathogen Interactions, Inflammation, and Immunity. Microbiology and Molecular Biology Reviews 83, (2019).
45. Bai, P. et al. PARP-1 Inhibition Increases Mitochondrial Metabolism through SIRT1 Activation. Cell Metab 13, 461–468 (2011).
46. Reineke, L. C. & Neilson, J. R. Differences between acute and chronic stress granules, and how these differences may impact function in human disease. Biochem Pharmacol 162, 123–131 (2019).
47. Ke, Y. et al. PARP1 promotes gene expression at the post-transcriptional level by modulating the RNA-binding protein HuR. Nature Communications 2017 8:1 8, 1–16 (2017).
48. Yu, S.-W. et al. Outer mitochondrial membrane localization of apoptosis-inducing factor: mechanistic implications for release. ASN Neuro 1, AN20090046 (2009).
49. Wang, Y. et al. A nuclease that mediates cell death induced by DNA damage and poly(ADP-ribose) polymerase-1. Science 354, (2016).
50. Berger, N. A. et al. Opportunities for the repurposing of PARP inhibitors for the therapy of non-oncological diseases. Br J Pharmacol 175, 192–222 (2018).
51. Simuni, T. et al. Efficacy of Nilotinib in Patients With Moderately Advanced Parkinson Disease: A Randomized Clinical Trial. JAMA Neurol 78, 312–320 (2021).
52. Puentes, L. N., Lengyel-Zhand, Z., Reilly, S. W. & Mach, R. H. Evaluation of a Low-Toxicity PARP Inhibitor as a Neuroprotective Agent for Parkinson's Disease. Mol Neurobiol 58, 3641–3652 (2021).
53. Leta, V. et al. Viruses, parkinsonism and Parkinson's disease: the past, present and future. Journal of Neural Transmission 2022 129:9 129, 1119–1132 (2022).
54. Panas, M. D. et al. Sequestration of G3BP coupled with efficient translation inhibits stress granules in Semliki Forest virus infection. Mol Biol Cell 23, 4701–4712 (2012).
55. Lindquist, M. E., Lifland, A. W., Utley, T. J., Santangelo, P. J. & Crowe, J. E. Respiratory Syncytial Virus Induces Host RNA Stress Granules To Facilitate Viral Replication. J Virol 84, 12274–12284 (2010).
56. Hughes, A. J., Daniel, S. E. & Lees, A. J. Improved accuracy of clinical diagnosis of Lewy body Parkinson's disease. Neurology 57, 1497–1499 (2001).
57. Hughes, A. J., Daniel, S. E., Kilford, L. & Lees, A. J. Accuracy of clinical diagnosis of idiopathic Parkinson's disease: a clinico-pathological study of 100 cases. J Neurol Neurosurg Psychiatry 55, 181–184 (1992).
58. Alafuzoff, I. et al. Staging/typing of Lewy body related α-synuclein pathology: a study of the BrainNet Europe Consortium. Acta Neuropathol 117, 635–652 (2009).
59. Mazzetti, S. et al. α-Synuclein oligomers in skin biopsy of idiopathic and monozygotic twin patients with Parkinson's disease. Brain 143, 920–931 (2020).
60. Fricker, M., Runions, J. & Moore, I. Quantitative fluorescence microscopy: from art to science. Annu Rev Plant Biol 57, 79–107 (2006).
61. Eliceiri, K. W. et al. Biological imaging software tools. Nat Methods 9, 697–710 (2012).
62. Bolte, S. & Cordelières, F. P. A guided tour into subcellular colocalization analysis in light microscopy. J Microsc 224, 213–232 (2006).

GRAPHICAL ABSTRACT

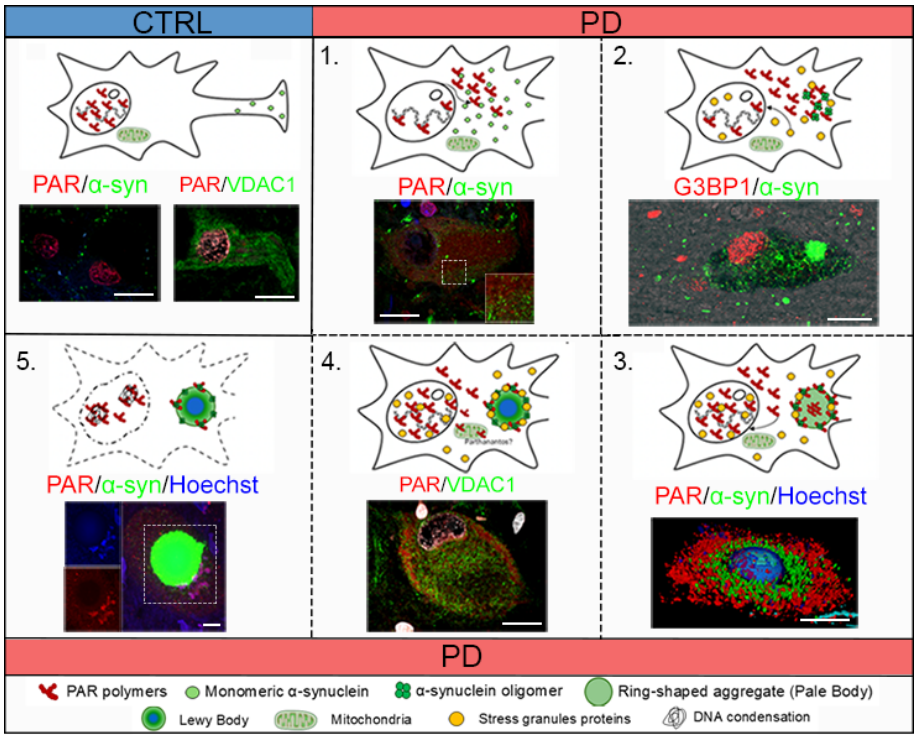

ACKNOWLEDGEMENTS

The authors thank all patients and families for their contribution, “Fondazione Pezzoli per la Malattia di Parkinson” (Milan-Italy) for SM, FG and AMC salary and for long-lasting support to GC.

CONFLICT OF INTEREST STATEMENT

The authors declare they have no conflict of interest.

AUTHOR CONTRIBUTIONS STATEMENT

All authors contributed to the study conception. MB, EB, GG, SM, FG processed human samples. CN and FG performed immunohistochemistry and multiple labelling experiments. CN, SM and FG performed confocal and super resolution imaging, as well as processing and analysis of images, also using arivis Vision 4D software. SM, CN, FG, AMC, CR and GC performed data analysis. GC, GP, SM, CN, FG, GG, IUI, AMC, DC, EC and CR designed research, analysed and interpreted the data, and contributed to writing the manuscript.

ETHICS STATEMENT

The study was conducted according to the guidelines of the Declaration of Helsinki and approved by the Ethics Committee of the University of Milan (protocol code 66/21, 15 June 2021).

FUNDINGS

This research was funded by Italian "5×1000" funding to "Fondazione Grigioni per il Morbo di Parkinson". Part of this work was carried out at UNITECH NOLIMITS, an advanced imaging facility established by the Università degli Studi di Milano.

DATA AVAILABILITY

The datasets generated and/or analyzed during the current study are available upon request from the corresponding authors.

MATERIALS AND CORRESPONDENCE

Correspondence and requests for materials should be addressed to Graziella Cappelletti and Samanta Mazzetti

SUPPLEMENTARY FIGURES 1-3

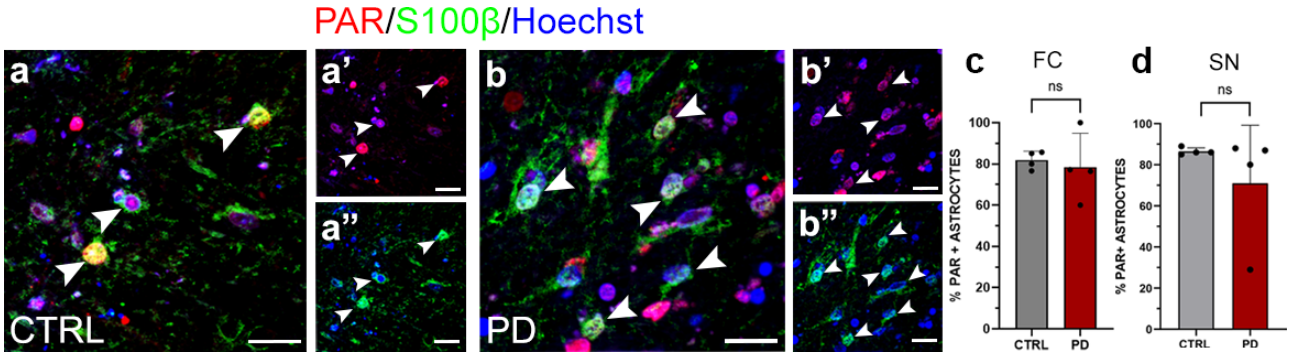

Supplementary Figure 1. *Confocal analysis of PAR in astrocytes. (**a-b"**) representative image showing PAR nuclear distribution (white arrowheads) in astrocytes of substantia nigra of control subjects (**a-a"**) and PD patients (**b-b"**). Scale bar, 20 µm. The graphs show the percentage of PAR positive astrocytes nuclei in frontal cortex (**c**, FC: CTRL, 132 astrocytes, n = 4 vs PD, 171 astrocytes, n = 4) and substantia nigra (**d**, SN: CTRL, 141 astrocytes, n = 4 vs PD, 150 astrocytes n = 4). Data are reported as mean ± standard deviation. Mann-Whitney test, p>0.05; ns. CTRL = control; FC = frontal cortex; N = nucleus; ns = non-significant; SN = substantia nigra.*

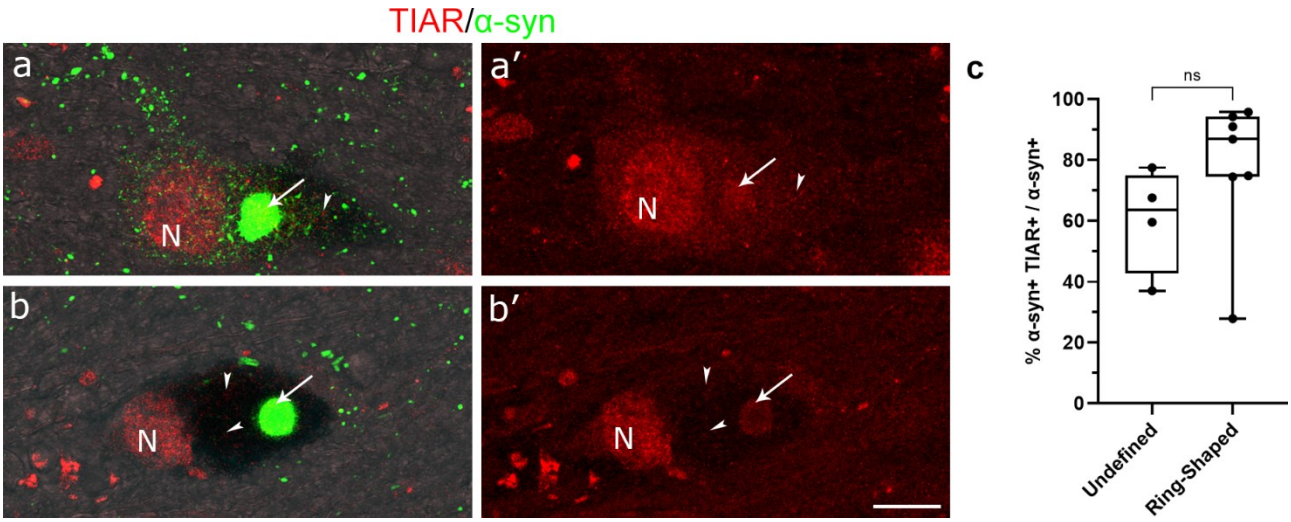

Supplementary Figure 2. *Confocal analyses of TIAR and α-synuclein during Lewy body morphogenesis in PD patients. (**a, a'**) TIAR localizes in the nuclei and shows a point-like signal in the cytoplasm (white arrowhead) between the α-synuclein network and neuromelanin granules, visible with phase contrast, and colocalizing with α-synuclein undefined aggregate (white arrow). (**b, b'**) When the ring-shaped structure is formed TIAR is present in both the nucleus and cytoplasm (white arrowheads) where it colocalizes with α-synuclein (white arrow). Colocalization increases from the undefined to the ring-shaped aggregate. Scale bar, 20 µm. The graph in **c** (n= 1 PD, undefined = 4; ring-shaped = 7) indicates the percentage of α-synuclein colocalizing with TIAR expressed by Mander's coefficient (M1). Data are reported as mean ± standard deviation. Mann-Whitney test, ns. N = Nucleus. ns = non-significant.*

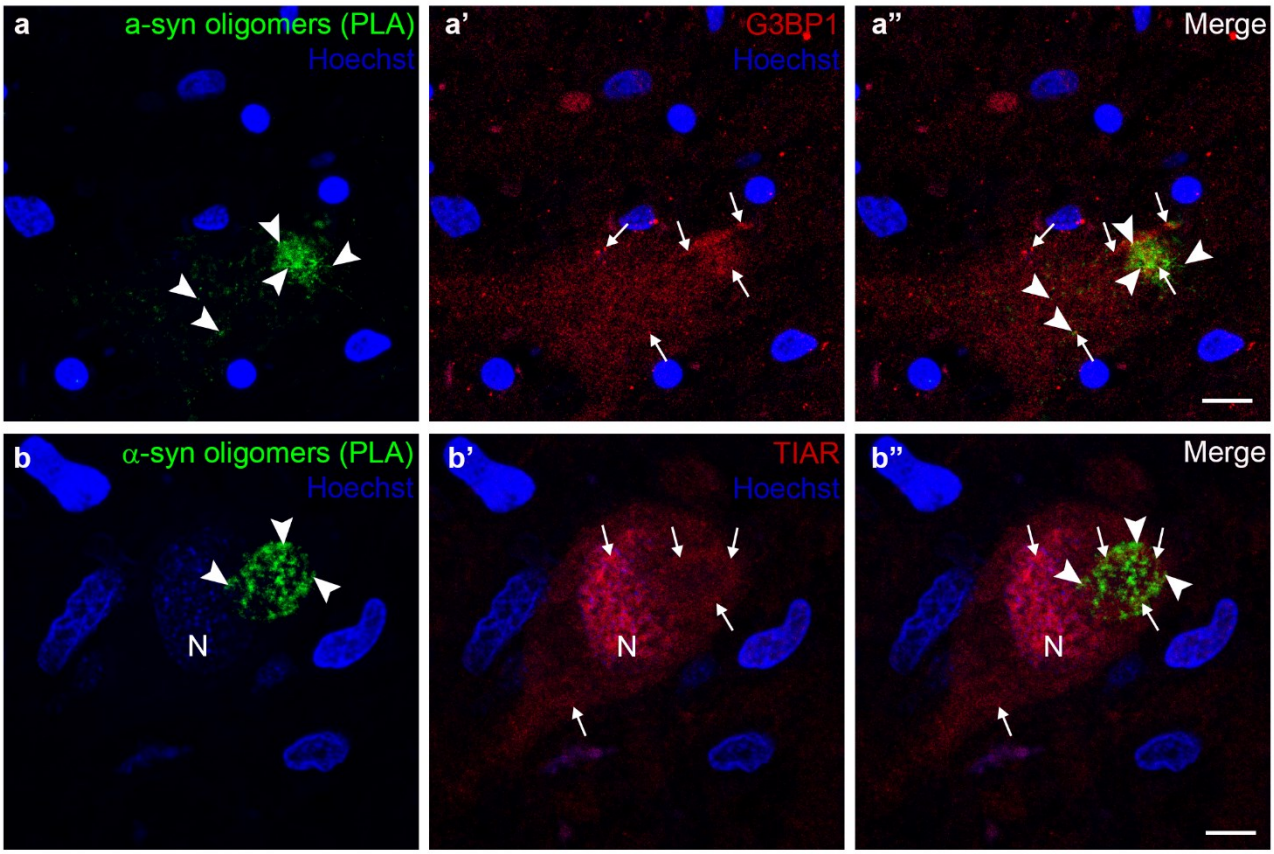

Supplementary Figure 3. *Stress granules and α-synuclein oligomers. α-Synuclein oligomers are diffused in the cytoplasm and form an undefined aggregate (**a, b**; arrowheads); G3BP1 (**a'**) and TIAR (**b'**), showing a point-like signal (arrows) both in the cytoplasm and in the neuronal nucleus, partially colocalize with α-synuclein oligomers (**a", b"**). Nuclei are counterstained using Hoechst. Scale bar, 20 µm. N = Nucleus*

SUPPLEMENTARY TABLES 1-2

Clinical Diagnosis	Gender	Age of onset	Age of death	Disease duration (years)
CTRL#1	M	/	71	/
CTRL#2	F	/	93	/
CTRL#3	F	/	82	/
CTRL#4	F	/	64	/
CTRL#5	F	/	84	/
CTRL#6	F	/	64	/
PD#1	M	62	80	18
PD#2	M	59	87	28
PD#3	F	65	84	19
PD#4	F	53	91	38
PD#5	F	59	79	20
PD#6	M	57	71	14
PD#7	M	57	75	18
PD#8	M	59	75	16

Supplementary Table 1. Demographic and clinical characteristics of the subjects included in this study.

Antigen	Code	Host	Dilution
Primary antibodies			
G3BP (Human G3BP1 aa 200-350)	Ab56574 Abcam	Mouse	1:250
Poly-ADP ribose (PAR)	MABC547 Merck	Mouse	1:100
S-100β (Rat S100β aa 1 to 92)	2874006 Synaptic Systems	Chicken	1:500
TIAR (Human TIAR aa 161-365)	610352 BD Transduction Laboratories™	Mouse	1:100
Tyrosine Hydroxylase (TH) (synthetic peptide sequence, VQDELDTLAHAL, corresponding to C-terminus)	PA518372 Thermo Fisher Scientific	Goat	1:200
VDAC1 (the immunogen used is proprietary information)	ab15895 Abcam	Rabbit	1:200
α-synuclein (human aa 111-132, corresponding to C-terminus)	S3062 Merck	Rabbit	1:2000
α-synuclein (human synthetic peptide aa 100 to C-terminus)	Ab21976 Abcam	Sheep	1:100
Secondary antibodies			
Alexa Fluor® 568 anti-mouse	A10037 Thermo Fisher Scientific	Donkey	1:200

Alexa Fluor® brilliant violet 421 anti-chicken	703-675-155 Jackson Immunoresearch	Donkey	1:300
Alexa Fluor® 647 anti-goat	705-615-147 Jackson Immunoresearch	Donkey	1:300
Alexa Fluor® 488 anti-rabbit	A21206 Thermo Fisher Scientific	Donkey	1:200
Alexa Fluor® 647 anti-rabbit	A32795 Thermo Fisher Scientific	Donkey	1:200
Alexa Fluor® brilliant violet 421 anti-sheep	713-675-147 Jackson Immunoresearch	Donkey	1:300
Probes, kit and stains			
Duolink® in situ probe marker MINUS	DUO920101KT Merck	-	-
Duolink® in situ probe marker PLUS	DUO920091KT Merck	-	-
Duolink® In Situ Detection Reagents green	DUO92014 Merck	-	-
EnVision FLEX DAB + Substrate Chromogen System	K3468 Agilent	-	-
Hoescht 33342	62249 Thermo Fisher Scientific	-	1:5000
TO-PRO®-3	629661 Thermo Fisher Scientific	-	1:1000

Supplementary Table 2. Primary and secondary antibodies included in this study.

Supplementary movies

Movie 1: The movie refers to arivis 4D software 3D reconstruction of figure 3a’’’.

Movie 2: The movie refers to arivis 4D software 3D reconstruction of figure 3b’’’.

Movie 3: The movie refers to arivis 4D software 3D reconstruction of figure 3c’’’.

Received: 30 December 2023 | Accepted: 21 June 2024

DOI: 10.1111/bpa.13284

RESEARCH ARTICLE

Brain Pathology

Comparing *GBA1*-Parkinson's disease and idiopathic Parkinson's disease: α-Synuclein oligomers and synaptic density as biomarkers in the skin biopsy

Samanta Mazzetti[1,2] | **Elena Contaldi**[3] | **Milo Jarno Basellini**[1] | **Claudia Novello**[1] | **Alessandra Maria Calogero**[1,2] | **Letizia Straniero**[4,5] | **Federica Garrì**[2] | **Valentina Ferri**[2,3] | **Daniela Calandrella**[2,3] | **Francesca Del Sorbo**[3] | **Rosanna Asselta**[4,5] | **Emanuele Cereda**[6] | **Graziella Cappelletti**[1,7] | **Ioannis Ugo Isaias**[3,8] | **Gianni Pezzoli**[2,3]

[1]Department of Biosciences, Università degli Studi di Milano, Milan, Italy

[2]Fondazione Grigioni per il Morbo di Parkinson, Milan, Italy

[3]Parkinson Institute, ASST "G.Pini-CTO", Milan, Italy

[4]Department of Biomedical Sciences, Humanitas University, Milan, Italy

[5]IRCCS Humanitas Research Hospital, Milan, Italy

[6]Clinical Nutrition and Dietetics Unit, Fondazione IRCCS Policlinico San Matteo, Pavia, Italy

[7]Center of Excellence on Neurodegenerative Diseases, Università degli Studi di Milano, Milan, Italy

[8]Department of Neurology, University Hospital of Würzburg and Julius Maximilian University of Würzburg, Würzburg, Germany

Correspondence
Samanta Mazzetti and Graziella Cappelletti, Department of Biosciences, Università degli Studi di Milano, via Celoria 26, Milano 20133, Italy.
Email: samanta.mazzetti@gmail.com and graziella.cappelletti@unimi.it

Funding information
Fondazione Grigioni per il Morbo di Parkinson, Grant/Award Number: "5 × 1000"; MUR, Programmi di Ricerca Scientifica di Rilevante Interesse Nazionale, Grant/Award Number: 2017228L3J; Fondazione Regionale per la Ricerca Biomedica, Grant/Award Number: ERAPerMed2022-212

Abstract

The main genetic risk factors for Parkinson's disease (PD) are presently represented by variants in *GBA1* gene encoding for the β-glucocerebrosidase (GCase). Searching for a peripheral biomarker that can be used for selecting and monitoring patients in clinical trials targeting *GBA1*-associated PD (*GBA1*-PD) is a current challenge. We previously demonstrated that α-synuclein oligomers expressed as proximity ligation assay (PLA) score in synaptic terminals of skin biopsy are a reliable biomarker for distinguishing idiopathic PD (iPD) from healthy controls (HC). This cross-sectional study investigates an unexplored cohort of *GBA1*-PD ($n = 27$) compared to 28 HC, and 36 iPD cases to (i) analyze α-synuclein oligomers and quantify them throughout PLA score, (ii) investigate GCase expression in brain and synaptic terminals targeting the sweat gland, (iii) unravel indicators that could differentiate patients with specific *GBA1* mutations. PLA score discriminates *GBA1*-PD from HC with sensitivity = 88.9% (95% CI 70.84–97.65), specificity = 88.5% (95% CI 69.85–97.55), and PPV = 88.9% (95% CI 73.24–95.90), AUC value = 0.927 (95% CI 0.859–0.996). No difference was found between *GBA1*-PD patients and iPD, suggesting a common pathological

Samanta Mazzetti and Elena Contaldi are co-first authors.

Graziella Cappelletti, Ioannis Ugo Isaias, and Gianni Pezzoli are co-last authors.

pathway based on α-synuclein oligomers. GCase score did not differ in *GBA1*-PD, iPD, and HC in the synaptic terminals, whereas a positive correlation was found between PLA score and GCase score. Moreover, a significant increase in synaptic density was observed in *GBA1*-PD compared to iPD and HC ($P < 0.0001$). Employing ROC curve to discriminate *GBA1*-PD from iPD, we found an AUC value for synaptic density = 0.855 (95% CI 0.749–0.961) with sensitivity = 85.2% (95% CI 66.27%–95.81%), specificity = 77.1% (95% CI 59.86%–89.58%), and PPV = 74.19% (60.53%–84.35%). The highest synaptic density values were observed in p.N409S patients. This work points out to the value of both PLA score and synaptic density in distinguishing *GBA1*-PD from iPD and to their potential to stratify and monitor patients in the context of new pathway-specific therapeutic options.

KEYWORDS
autonomic nervous system, biomarker, *GBA1*, Parkinson's disease, skin biopsy, α-synuclein

1 | INTRODUCTION

Parkinson's disease (PD) is a multisystem and multifactorial disorder caused by a combination of genetic and environmental agents [1] and characterized by aberrant accumulations of the protein α-synuclein, a major constituent of histopathological lesions in PD [2]. Genetic variants range from common alleles with low penetrance to rarer highly penetrant ones [3]. Because of this multifactorial pathogenesis, PD is clinically heterogeneous and characterized by high variability in the presentation of motor and nonmotor symptoms [4].

The main genetic risk factors for PD are represented by variants in the Glucosylceramidase beta 1 gene (*GBA1*), which are associated with an increased risk in a range between 5- and 8-fold [5, 6]. *GBA1* encodes the β-glucocerebrosidase (GCase), a lysosomal enzyme involved in glycosphingolipid metabolism, regulating processes ranging from membrane properties modification to autophagy [6]. Approximately, 300 *GBA1* mutations have been described in Gaucher's disease (GD, a lysosomal storage disorder characterized by biallelic mutations in *GBA1*), many of which are also found in PD [7]. Furthermore, some variants (p.N409S and p.L483P; legacy names p.N370S and p.L444P, respectively) have high allelic frequencies among PD patients. Other variants (p.E365K and p.T408M; legacy names p.E326K and p.T369M, respectively), even if not pathogenic for GD, have been associated with an increased risk for PD [8, 9]. As for genotype–phenotype correlations, multivariable analysis adjusted for sex, age at onset, and disease duration indicated that mutations causing a more severe GD phenotype (e.g., p.L483P-related) were associated with a 3-fold greater risk for dementia in PD patients, but similar mortality risk when compared to less severe mutations [10–13]. Interestingly, α-synuclein aggregation and GCase reduction are mutually linked as revealed by studies performed in different experimental models both in the central and peripheral nervous system [14–16]. Functional loss of GD-linked GCase in neuronal cell models compromises lysosomal protein degradation, affects α-synuclein clearance, and causes its accumulation, thus exacerbating cell stress [16]. On the other hand, α-synuclein aggregates inhibit the normal GCase activity in idiopathic PD (iPD) brain, suggesting that GCase depletion may also contribute to the pathogenesis of iPD [16].

Recently, the search for a reliable biomarker on peripherally collected material (plasma and peripheral blood mononuclear cells) provided evidence that glucosylceramide levels in plasma could be used as a biomarker for selecting and monitoring patients in clinical trials targeting *GBA1*-associated PD (*GBA1*-PD; [17]). Furthermore, the α-synuclein seed amplification assay for analyzing cerebrospinal fluid (CSF) was able to classify both iPD and *GBA1*-PD with high sensitivity and specificity [18]. Besides blood and CSF, the peripheral nervous system could represent an accessible and valuable source for the discovery of novel biomarkers and for better unraveling pathogenic mechanisms involved in PD [19]. We recently identified α-synuclein oligomers in skin biopsy and demonstrated that these aggregates are a reliable biomarker for distinguishing iPD from healthy controls (HC) [20].

In the present study, we focused on a cohort of *GBA1*-PD patients aiming to: (i) understand if α-synuclein oligomer accumulation is a common feature also in PD patients with a strong genetic component, (ii) investigate whether GCase expression changes in synaptic terminals of autonomic structures in skin biopsies, and (iii) unravel indicators that could differentiate patients with specific *GBA1* mutations.

2 | METHODS

2.1 | Subjects

The population of the present cross-sectional study was composed of 91 subjects: 28 HC, 36 iPD patients, and

27 PD carriers of *GBA1* gene variants (see Table 1 for details on demographic and clinical data). All subjects were consecutively enrolled from March 2014 to March 2022 at the Parkinson Institute (Milan, Italy) by neurologists experienced in movement disorders and contributing to the Parkinson Institute Biobank [21]. The diagnosis of PD was made according to the UK Brain Bank criteria [22]. As exclusion criteria, we considered a history of diseases or other conditions potentially leading to peripheral neuropathy or general contraindications for performing a skin biopsy. Genetic analysis was performed as previously described: DNA was extracted from peripheral blood using a Chemagic Star workstation (Hamilton, ON, Canada), and the genetic analysis on the *GBA1* gene was performed with a combination of different technologies, ranging from allele-specific PCR [23] to exome sequencing [24]. To ensure the homogeneous assessment of skin biomarkers among the most common *GBA1* variants, specific subgroups were also identified, that is, p.N409S ($n = 7$) and p.L483P ($n = 12$). The remaining 8 patients carried heterogeneous mutations (biallelic mutation p.N409S/p.E365K, $n = 1$; biallelic mutation p.N409S/p.N409S, $n = 1$; p.Q401X, $n = 1$; c.73delC, $n = 1$; p.S38X, $n = 1$; RecNcil, $n = 1$; p.D448H, $n = 1$; p.E388K, $n = 1$). In iPD patients, mutations in *GBA1* and other PD-related genes were excluded. Patients and HC were balanced for age and sex. The following clinical data were collected for all patients: age at PD onset, disease duration, and levodopa equivalent daily dose (LEDD, calculated according to [25]). The Unified Parkinson's Disease Rating Scale (UPDRS) [26] was administered, and the severity of motor symptoms and disease staging were assessed in the medication off state by movement disorder specialists using the UPDRS part III and the Hoehn and Yahr (HY) scale [27]. Other relevant data, including the presence of hyposmia according to medical reports, probable REM sleep behavior disorder (pRBD) according to a cut-off score ≥6 in the RBD Screening Questionnaire (RBDSQ) [28], and constipation (following Rome III criteria [29]) were collected. The presence of orthostatic hypotension (OH) was confirmed based on specific prescription patterns and/or the detection during clinical examination of a fall of at least 20 mmHg in systolic blood pressure (30 mmHg in patients with supine hypertension) and/or 10 mmHg in diastolic blood pressure within 3 min of standing [30]. Autonomic functions were further investigated using the Composite Autonomic Symptom Score 31 (COMPASS-31) [31], a self-administered questionnaire addressing several autonomic domains (orthostatic intolerance, vasomotor, secretomotor, gastrointestinal, bladder, and pupillomotor). Cognitive functions were examined using the Mini-Mental State Examination (MMSE) [32], the Frontal Assessment Battery (FAB) [33], and the Montreal Cognitive Assessment (MoCA) [34].

2.2 | Skin biopsy

Forearm skin biopsies were fixed in Zamboni solution for 24 h at 4°C, then paraffin-embedded and sliced in 3-μm thick serial sections using a microtome (MR2258, Histo-Line Laboratories, Milan, Italy), as previously described [20]. Each sample was processed as follows: (i) one section was stained with hematoxylin and eosin to verify sweat glands presence; (ii) three sections underwent proximity ligation assay (PLA) procedure to localize α-synuclein oligomers and immunofluorescence staining for synaptophysin and (iii) three sections underwent the GCase tyramide signal amplification and synaptophysin staining.

2.3 | Proximity ligation assay and immunofluorescence

α-Synuclein oligomers were detected by a PLA commercial Duolink kit (Sigma-Aldrich, St Louis, Missouri, USA) according to the manufacturer's instructions as previously described [20, 35]. In detail, PLUS and MINUS probes were directly conjugated to the rabbit anti α-synuclein antibody S3062 (polyclonal antibody directed against a synthetic peptide within aa 111–132 of human α-Synuclein, Sigma-Aldrich) to obtain α-synuclein-PLUS and α-synuclein-MINUS probes [20, 36, 37]. Once obtained, these were used in the PLA procedure carried out together with classical immunofluorescence as described in details in [20]. Briefly, after deparaffinization and rehydration, sections were pretreated with 10% formic acid (10 min). After a 20-min blocking step with 1% bovine serum albumin (BSA) in 0.01 M phosphate-buffered saline (PBS) plus 0.1% Triton X-100, sections were incubated with α-synuclein-PLUS and α-synuclein-MINUS probes (1:100 in PLA diluent) and mouse anti-synaptophysin (clone DakSynap, 1:100; Agilent, Santa Clara, USA) for 2 h at 37°C. The amplification reaction was accomplished and samples were counterstained with Hoechst 33342 (1:1000; Life Technologies, MA, USA) for 10 min and mounted using Mowiol-DABCO. Positive and negative controls were performed as previously described [20]. The polyclonal anti α-synuclein antibody used for probe conjugation is a well characterized α-synuclein antibody able to recognize monomeric α-synuclein in immunofluorescence assay. Indeed, its high specificity was previously verified performing both the staining in a OlaHsd mice, a substrain of C57BL/6J mice carrying a spontaneous deletion of the *SNCA* gene [38], and the preadsorbtion assay [36]. Furthermore, it exhibits also high sensibility as revealed by its typical synaptic pattern in controls and PD patients when used in immunofluorescence assay, while the same antibody used in the PLA assay does not recognize physiological synaptic α-synuclein, but it marks the oligomeric forms in the immediate

TABLE 1 Demographic, clinical, and skin biopsy data of *GBA1*-PD, iPD, and HC.

Variables	*GBA1*-PD (*N* = 27)	iPD (*N* = 36)	HC (*N* = 28)	*P*-value
Age at skin biopsy, years, mean (SD)	56.96 (10.15)	61.94 (9.68)	60.25 (11.03)	0.165[a]
				0.052[b]
Sex (male), *n* (%)	15 (55.6%)	21 (58.3%)	12 (42.9%)	0.208[e]
				1.0[f]
Age at PD onset, years, mean (SD)	45.85 (9.32)	54.39 (9.86)	—	**0.001**[b]
Disease duration, years, median (IQR)	10 (10)	6 (11.25)	—	**0.019**[c]
LEDD, median (IQR)	707 (550)	555.16 (618.75)	—	0.232[c]
HY scale				
1–2, 5, *n* (%)	19 (70.4%)	23 (63.9%)	—	0.563[f]
3–4, *n* (%)	8 (29.6%)	9 (25%)		
UPDRS I score, median (IQR)	2 (4)	0.5 (3)	—	0.051[c]
UPDRS II score, mean (SD)	12.14 (8.07)	7.10 (5.94)	—	**0.013**[b]
UPDRS III score (off), mean (SD)	26.54 (13.06)	25.52 (16.41)	—	0.818[b]
UPDRS IV score, median (IQR)	4 (4)	3 (4)	—	0.178[c]
pRBD, *n* (%)	15 (55.5%)	13 (36.1%)	—	0.136[f]
Hyposmia, *n* (%)	8 (29.6%)	12 (33.3%)	—	0.561[f]
Constipation, *n* (%)	16 (59.2%)	28 (77.8%)	—	0.134[f]
Orthostatic hypotension, *n* (%)	14 (51.8%)	13 (36.1%)	—	**0.003**[f]
COMPASS-31, orthostatic intolerance, mean (SD)	15.52 (9.45)	3.61 (7.50)	0 (0)	**<0.0001**[d]
				<0.0001[c]
COMPASS-31, vasomotor, mean (SD)	0.44 (0.85)	0.58 (1.13)	0.07 (0.38)	0.081[d]
				0.774[c]
COMPASS-31, secretomotor, mean (SD)	3.37 (3.70)	2.75 (3.81)	1.64 (2.04)	0.376[d]
				0.488[c]
COMPASS-31, gastrointestinal, mean (SD)	5.25 (4.47)	3.89 (4.07)	3.29 (3.52)	0.147[d]
				0.184[c]
COMPASS-31, bladder, mean (SD)	2.30 (1.68)	1.36 (1.44)	0.75 (1.27)	**0.001**[d]
				0.024[c]
COMPASS-31, pupillomotor, mean (SD)	0.70 (0.87)	1.36 (1.31)	0.64 (0.83)	**0.049**[d]
				0.048[c]
COMPASS-31, total, mean (SD)	28.81 (11.76)	14.97 (11.75)	6.39 (5.37)	**<0.0001**[d]
				<0.0001[c]
MMSE score, median (IQR)	27.60 (4.29)	26 (3.01)	—	0.605[c]
FAB score, median (IQR)	14.20 (7.50)	13.90 (2.40)	—	0.682[c]
MoCA score, mean (SD)	16.13 (5.73)	19.53 (4.60)	—	0.073[b]
PLA score, median (IQR)	259 (394)	213.82 (256.04)	27.78 (75.81)	**<0.0001**[d]
				0.429[c]
Synaptic density, median (IQR)	0.048 (0.05)	0.018 (0.01)	0.017 (0.02)	**<0.0001**[d]
				<0.0001[c]

Note: Significant *P*-values ($P < 0.05$) are highlighted in bold.
Abbreviations: COMPASS-31, Composite Autonomic Symptom Score 31; FAB, frontal assessment battery; HC, healthy controls; HY, Hoehn & Yahr scale; iPD, idiopathic Parkinson's disease; LEDD, levodopa equivalent daily dose; MMSE, Mini-Mental State Examination; MoCA, Montreal Cognitive Assessment; PLA, proximation ligation assay; pRBD, probable REM sleep behavior disorder; UPDRS, Unified Parkinson's Disease Rating Scale.
[a]ANOVA analysis *GBA1*-PD versus iPD versus HC.
[b]Independent samples *t*-test *GBA1*-PD versus iPD.
[c]Mann–Whitney test *GBA1*-PD versus iPD.
[d]Kruskal–Wallis test *GBA1*-PD versus iPD versus HC.
[e]Fisher's exact test *GBA1*-PD versus iPD versus HC.
[f]Fisher's exact test *GBA1*-PD versus iPD.

vicinity of pale bodies in *post-mortem* human brains [20, 37].

To detect GCase (Rab Mab EPR5142, KO validated, directed against a synthetic peptide within human GCase aa 50–150; Abcam, Milan, Italy) we used the tyramide signal amplification system, as described in the supplementary materials.

Images were collected at 60× magnification (1024 × 1024). The sections were analyzed with a Nikon spinning disk confocal microscope using a silicon-immersion 40× objective. In addition, we used a spinning disk super-resolution by optical pixel reassignment (SoRa) technique using the silicon-immersion 100× objective plus a resolution improvement of 2.8×. PLA score was calculated as previously described [20]: the area of PLA signal within synapses (synaptophysin-positive) was normalized for synaptic density (synaptophysin-positive area/total area of the sweat gland). Similarly, the GCase score was calculated as follows: GCase staining was measured inside synapses (synaptophysin-positive) and normalized for synaptic density (synaptophysin-positive area/total area of the sweat gland).

2.4 | Statistical analysis

Based on our previous work [20], we considered the difference in PLA score between PD and HC as the primary outcome measure to calculate the sample size. Expecting an effect size (Cohen's *d*) of 1.18, a two-tailed type I error = 5% and power = 90%, we estimated a sample size of at least 17 patients in each group ("pwr" package, RStudio 2022.07.2 + 576).

Variables were expressed as counts (percentages) when categorical and as mean (standard deviation, SD) or median (interquartile range, IQR) when continuous according to the normality of distribution. The normality of data was assessed using the Shapiro–Wilk test. Differences between groups were analyzed by ANOVA (multiple groups) adjusting for relevant covariates and the independent samples *t*-test (two groups) or the non-parametric equivalents (Kruskal-Wallis and Mann–Whitney tests, respectively). Based on the assumption of equal or unequal variances, Bonferroni or Games-Howell post hoc corrections for multiple testing were respectively applied. Comparison of categorical variables was assessed using Fisher's exact test. To explore biomarkers' discriminatory power, a receiver operating characteristic (ROC) curve analysis was performed, obtaining the area under the curve (AUC) and significance values. AUC interpretation was determined according to Mandrekar and colleagues [39]. Optimal cut-off values were established by coordinate tracing of the ROC curve according to Youden's index analysis. Sensitivity, specificity, positive and negative predictive values (PPV, NPV), were obtained. Correlations between biomarkers and clinical data were investigated using Pearson's or Spearman's analysis as appropriate. Finally, non-collinear independent variables associated with clinical symptoms were investigated using multivariable linear (continuous variables on either a normal or log-transformed scale) and logistic (dichotomous) regression analysis. All tests were two-tailed, and the significance level was set to $P < 0.05$. Analyses were performed using SPSS version 25 (IBM Corporation, Armonk, USA), GraphPad Prism version 8 (GraphPad Software Inc., San Diego, USA), and RStudio 2022.07.2 + 576.

3 | RESULTS

3.1 | PLA score as a biomarker to distinguish *GBA1*-PD

In agreement with previous results [20], α-synuclein oligomers were increased inside synapses surrounding sweat glands using high-resolution microscopy in iPD (Figure 1A–A″) compared to HC (Figure 1C–C″). Here, we revealed the presence of α-synuclein oligomers also in *GBA1*-PD (Figure 1B–B″). The median values of PLA scores were significantly higher in the *GBA1*-PD than in HC ($P < 0.0001$; Table 1). This finding was confirmed in univariate analysis (with log-transformed PLA score used as dependent variable) and after controlling for the effect of age and sex (adjusted *P*-value 0.00027; Figure 1D). Notably, no difference was found between *GBA1*-PD patients and iPD cases. Looking at the subpopulations of *GBA1*-PD, we did not observe any significant difference in mean PLA score between patients carrying different mutations (Figure 1E). These results were confirmed even when considering p.L483P versus p.N409S mutations alone ($P = 0.627$). ROC curve analysis, used to discriminate *GBA1*-PD from HC, showed an AUC value = 0.927 (95% CI 0.859–0.996, $P < 0.0001$; see Figure 1F). Using a cut-off ≥98.64, the sensitivity was = 88.9% (95% CI 70.84–97.65), specificity = 88.5% (95% CI 69.85–97.55), PPV = 88.9% (95% CI 73.24–95.90), and NPV = 88.5% (95% CI 72.33–95.74). This cut-off allowed the stratification of our cohort into two groups: subjects with positive PLA score (PLA^+ ≥98.64) and negative PLA staining (PLA^- <98.64). No significant correlation was found between PLA score and continuous clinical variables (age at PD onset, UPDRS I-II-III-IV, LEDD, disease duration, COMPASS-31, MMSE, FAB, and MoCA scores). In the whole PD cohort, no difference was observed in categorical variables (presence of pRBD, hyposmia, constipation, OH, and HY staging) between PLA^+ versus PLA^- patients. In the iPD subgroup, all pRBD patients ($N = 13$) were PLA^+, whereas among those without pRBD, 7 (30.4%) were PLA^- ($P = 0.034$). However, multivariable logistic regression analysis using age, sex, disease duration, PLA, and genetic status as independent variables revealed that the

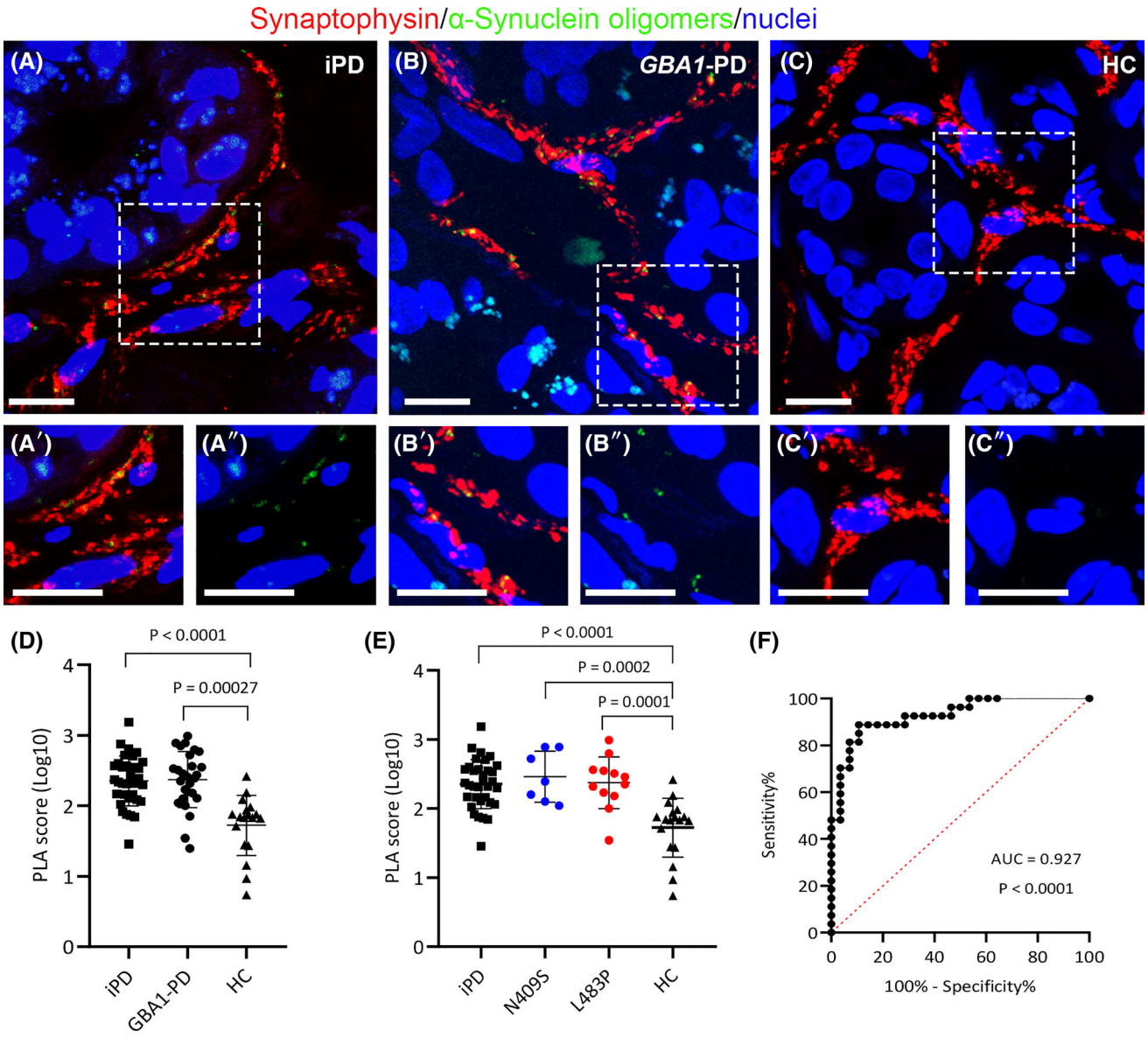

FIGURE 1 α-Synuclein oligomers in skin biopsies of *GBA1*-PD. (A–C″) Confocal images of sweat glands show α-Synuclein oligomers (PLA signal, green, A, A″, B, B″, C, C″), synapses (synaptophysin staining, red, A, A′, B, B′, C, C′), and nuclei (Hoechst, blue, A–C″) in idiopathic PD (iPD, A–A″), *GBA1*-PD (B–B″), and healthy controls (HC, C–C″). Squared insets in (A, B, C) are 2× magnified in A′, A″, B′, B″, C′, C″ (high resolution image obtained by SoRa). Scale bar, 10 μm. (D) Univariate analysis to compare mean PLA score values between *GBA1*-PD, idiopathic PD (iPD), and healthy controls (HC). Significant *P*-values (after Bonferroni post hoc correction and adjusted for age and sex) are shown. (E) PLA score (log-transformed) in *GBA1*-PD subgroups. Significant *P*-values (ANOVA analysis with Games-Howell post hoc test) are shown. (F) ROC curve of PLA score to discriminate between *GBA1*-PD and HC.

presence of pRBD was mostly associated with disease duration ($P = 0.054$) and not with PLA staining.

3.2 | GCase and PLA score correlate in PD

Given the strict bidirectional pathogenic loop that involves α-synuclein aggregation and GCase reduction in cellular and mouse models [16], we wondered whether GCase expression changes in synaptic terminals of autonomic structures in skin biopsies of *GBA1*-PD where we detected the specific increase of α-synuclein oligomers. We first checked for GCase staining in *post-mortem* human brains (Supplementary Figure S1) and found that it decreased in iPD patients compared to controls, as previously reported [40], and localized also at the synapses. Moving to skin biopsies, we found that GCase mostly localizes between the epidermis and the Stratum Corneum, in accordance with what has already been reported [41]. To date, GCase expression within the peripheral nervous system has not been investigated. Here, in a subgroup of 35 PD patients (23 *GBA1*-PD,

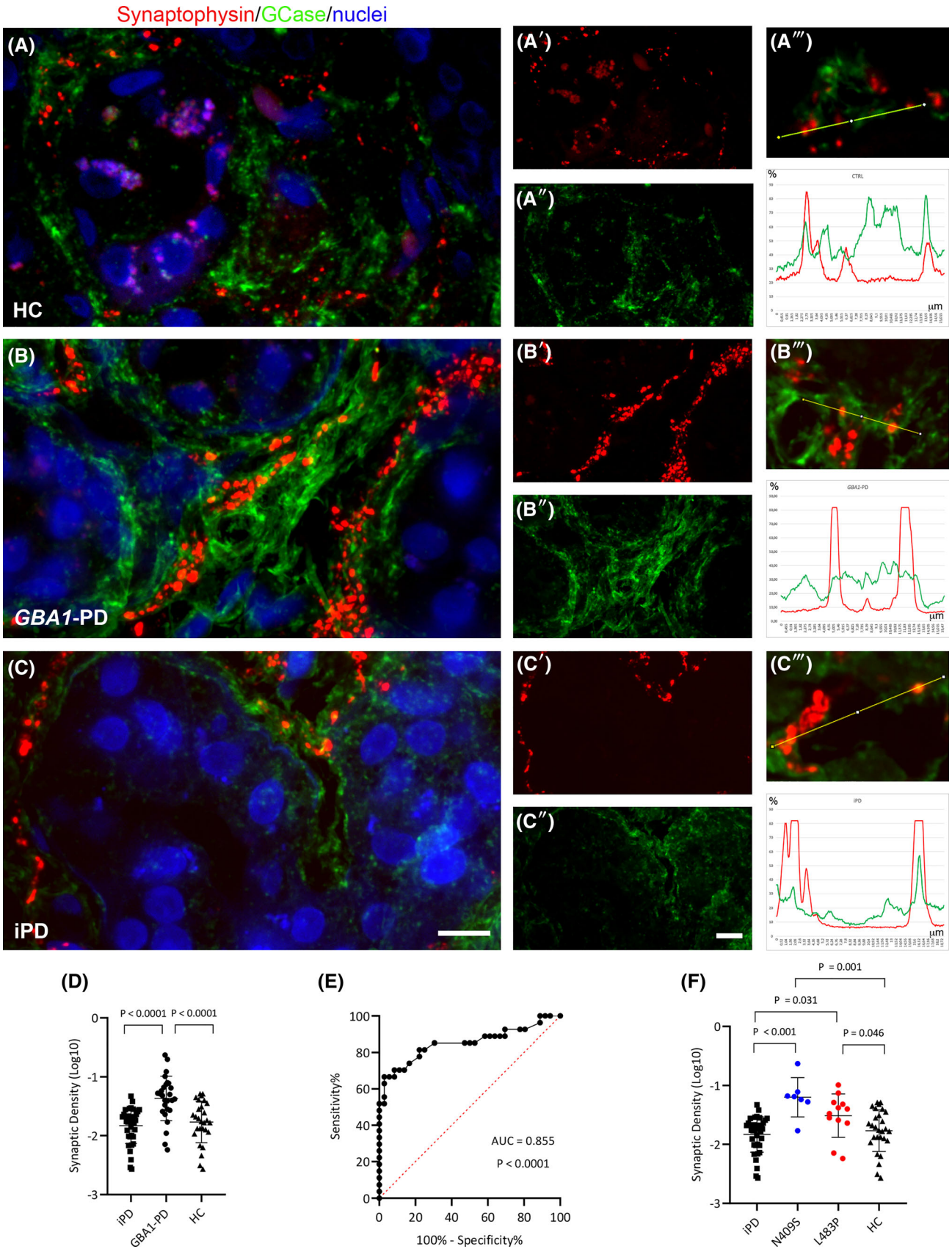

FIGURE 2 Legend on next page.

12 iPD) and 11 HC, we looked at GCase staining in the synaptic terminals surrounding the secretory coils of sweat glands and observed a diffuse and punctate pattern in all analyzed groups. Interestingly, the GCase signal seemed to be increased in *GBA1*-PD when compared to both control subjects and iPD (Figure 2A–C; A″, B″, C″). Thus, we focused on the synaptic compartment, and we observed that some synaptic terminals contained GCase, as clearly visible using the intensity profile (Figure 2A‴, B‴, C‴). We performed the quantitative analysis of the GCase expression inside synapses and normalized for synaptic density to obtain the GCase score and found no significant difference in GCase score between controls, *GBA1*-PD, and iPD (Supplementary Figure S2). This result was confirmed when considering all PD patients versus HC ($P = 0.277$). Interestingly, when analyzing the whole PD population ($N = 35$), we found a direct correlation between PLA score and GCase score ($r = 0.390$, $P = 0.025$), which was mostly driven by the *GBA1*-PD subgroup ($r = 0.479$, $P = 0.021$). This correlation was not confirmed in iPD ($r = 0.073$, $P = 0.832$) and HC ($r = -0.385$, $P = 0.242$). Finally, we performed in the PD group multivariable regression analysis using log-transformed PLA score as the dependent variable and age, disease duration, genetic status, and log-transformed GCase score as independent non-collinear variables. We found that the GCase score was the only variable significantly associated with PLA score ($\beta = 0.364$, $P = 0.044$; Supplementary Figure S3). No significant difference was detected when stratifying the analysis according to different *GBA1*-PD mutations.

To explore a possible relation between GCase and α-synuclein species other than oligomers, we performed additional stainings for total, phosphorylated, and aggregated, β-sheet containing α-synuclein. Looking at total α-synuclein inside the synapses (Supplementary Figure S5A–A″), we observed no differences among HC, iPD, and *GBA1*-PD (Supplementary Figure S5B). We then analysed phosphorylated and aggregated species of α-synuclein using the following specific antibodies and dye: anti-S129 phosphorylated α-synuclein antibody; conformational 5G4 antibody that recognizes α-synuclein aggregates including β-sheet conformation; and Thioflavin-S that stains amyloid fibrils (Supplementary Figure S6). As expected, both phosphorylated and aggregated species of α-synuclein were clearly detected inside Lewy bodies in *post-mortem* PD human brain (Supplementary Figure S6A,C,E). However, skin biopsies from HC, iPD, and *GBA1*-PD did not show any staining for phosphorylated α-synuclein (Supplementary Figure S6B–B″), β-sheet containing aggregated α-synuclein (Supplementary Figure S6D–D″), and amyloid fibrils (Supplementary Figure S6F–F″) inside the synapses.

3.3 | The increase in synaptic density identifies *GBA1*-PD but not iPD

Although the GCase score resulted unmodified in *GBA1*-PD, the increase of GCase signal prompted us to investigate whether this finding could be caused by changes in synaptic density. Indeed, a rough increase in synaptophysin staining was observed in *GBA1*-PD (Figure 2A″, B″, C″). Synaptic density was increased as well in *GBA1*-PD compared to both iPD patients and HC (Figure 2D; $P < 0.0001$; Table 1). This statistically significant difference was confirmed in univariate analysis (with log-transformed synaptic density used as the dependent variable) and after controlling for disease duration and age at PD onset (adjusted $P < 0.0001$). ROC curve analysis was employed to discriminate *GBA1*-PD from iPD, and we found an AUC value for synaptic density = 0.855 (95% CI 0.749–0.961, $P = 0.000002$; Figure 2E). A cut-off ≥0.023 showed a sensitivity = 85.2% (95% CI 66.27%–95.81%), a specificity = 77.1% (95% CI 59.86%–89.58%), a PPV = 74.19% (60.53%–84.35%), and a NPV = 87.10% (72.85%–94.44%) in detecting *GBA1*-PD. Notably, looking at synaptic density in subpopulations of *GBA1*-PD, we observed the highest values in p.N409S patients (Figure 2F), the mild form of *GBA1*-PD.

The increase in synaptic density observed in *GBA1*-PD could rely on a variety of mechanisms including compensatory synaptogenesis in a context of synaptic dysfunction and loss. We addressed this issue by using a well-known marker of sprouting, namely growth associated protein 43 (GAP43) and looking at its distribution at the synapse. The relative amount of GAP43 signal within the synapses (Supplementary Figure S7A–A″) was not significantly different among HC, iPD, and *GBA1*-PD (Supplementary Figure S7B). Interestingly, the analysis of the correlation between synaptic GAP43 and synaptic density revealed an inverse correlation in HC ($r = -0.76$; $P = 0.012$) and iPD ($r = -0.36$; $P = 0.30$), while a positive correlation was a specific feature of the *GBA1*-PD subpopulation ($r = 0.51$; $P = 0.13$; Supplementary Figure S7C).

FIGURE 2 Synaptophysin and GCase in skin biopsies. Confocal images showing synaptophysin (red), GCase staining (green) and nuclei (Hoechst, blue) in sweat glands of controls (A–A‴), *GBA1*-PD (B–B‴), and iPD. Scale bar, 15 μm. Intensity profiles show the superimposition of some peaks in a single *z*-plane along the designed line in A‴, B‴, C‴. (D) Univariate analysis to compare mean synaptic density values between *GBA1*-PD, idiopathic PD (iPD), and healthy controls (HC). Significant *P*-values (after Bonferroni post hoc correction and adjusted for age and sex) are shown. (E) ROC curve analysis of synaptic density values suitably allowed the discrimination of *GBA1*-PD from iPD. (F) PLA score (log-transformed) in *GBA1*-PD subgroups. Significant *P*-values (ANOVA analysis with Games-Howell post hoc test) are shown.

Finally, we decided to explore the association between synaptic density and clinical variables in the overall PD population, and we observed a significant correlation with the orthostatic intolerance subitem ($r = 0.509$, $P < 0.001$; Supplementary Figure S4A) and the total score of the COMPASS-31 ($r = 0.415$, $P = 0.001$; Supplementary Figure S4B). Besides, patients with OH were most likely to have a synaptic density ≥0.023 (73.1%, $P = 0.02$). Finally, we run multivariable linear regression analyses using age, sex and disease duration as adjusting variables and synaptic density and genetic status as alternate independent predictors. Synaptic density in the overall PD population and genetic status were both associated with both the orthostatic intolerance subitem and the total score of the COMPASS-31. Nonetheless, the analyses showed that the goodness of fit (using the Akaike information criterion as a measure of the relative quality of a model for a given set of data) of the models including synaptic density or genetic status were substantially comparable for both clinical outcomes.

4 | DISCUSSION

This study has a twofold importance. First, our results reinforce the concept that α-synuclein oligomers could be a reliable biomarker for distinguishing iPD from control subjects [20] and show that the sensitivity is even higher in the discrimination of *GBA1*-PD patients (88.9%). Second, we added new information to the pathological pathways characterizing different subpopulations of PD throughout the analysis of synaptic terminals targeting the sweat gland. Here, we observe a positive correlation between α-synuclein oligomers (PLA score) and GCase expression (GCase score) in *GBA1*-PD cohort and report that the *GBA1*-PD cohort exhibits an increase in synaptic density compared to iPD. Notably, the highest values were attributed to variant p.N409S, which is associated with a mild form of *GBA1*-PD. Next, synaptic density displays a moderate correlation with clinical assessment of autonomic dysfunction in the overall PD population.

The increase of α-synuclein oligomers in *GBA1*-PD skin biopsies was expected given that almost all the *post-mortem* brains obtained from *GBA1*-PD present Lewy bodies pathology [42]. Thus, the study of the peripheral nervous system likely reflects what happens in the central nervous system [19]. The common pathway of α-synuclein aggregation in iPD and *GBA1*-PD has been supported also by a very recent analysis of the CSF using the α-synuclein seed amplification assay, which gave similar results, obtaining the highest sensitivity in *GBA1*-PD [18].

Focusing on the role of GCase in PD, evidence exists that α-synuclein aggregation and GCase reduction are mutually linked [16]. Previous studies in human brains described a combination of reduced protein levels and catalytic activity, mainly in the *substantia nigra* [15]. On this basis, we expected a decrease in GCase protein levels in the skin and in the synaptic terminals of the *GBA1*-PD and iPD patients. Surprisingly, we observed an overall increase of the GCase signal in the skin of *GBA1*-PD. Given that GCase is a lysosomal ubiquitous enzyme that plays important functions in regulating membrane properties but also extracellular roles beyond the lysosome [41], we may speculate that a compensatory mechanism leads to GCase overexpression in the tissue for counteracting its loss of enzymatic activity. Indeed, *GBA1* mutations affect the endosomal-lysosomal pathway and lead to the accumulation of crowded membranes and dysmorphic organelles, that have already been described in Lewy Bodies [43]. Interestingly, the GCase staining observes in skin biopsy seems to resemble the typical pattern of organelles such as lysosomes. However, we did not see any significant difference in the GCase expression in the synaptic terminals targeting the sweat gland. This discrepancy could be linked to the compensatory sprouting leading to an enrichment of newly formed fibers and, in turn, of GCase in the periphery. To address this point, we evaluated the correlation between synaptic density and GAP43, a sprouting marker. In particular, the inverse correlation in HC suggests that the sprouting decreases in case of high levels of synaptic density, on the contrary, in *GBA1*-PD the sprouting increases with the increase of synaptic density. This phenomenon could be caused by dysfunctional synaptic terminals in *GBA1*-PD patients, probably caused by the described vicious circle that links GCase reduced activity and α-synuclein aggregation [16]. In fact, a direct correlation was found in the *GBA1*-PD subgroup between the GCase score and the PLA score, a finding that supports the presence of a pathogenetic loop involving GCase and α-synuclein aggregation in the periphery. Indeed, a previous study in cell and animal models [16] demonstrated that GCase mutation leads to enzymatic deficiency, that directly induces α-synuclein aggregation by stabilizing soluble oligomers. The α-synuclein aggregates exert an inhibitory effect on GCase activity engendering a vicious circle. This self-propagating positive feedback process proceeds until a pathogenic threshold is surpassed, resulting in neurodegeneration. Given that, GCase could be an attractive target for PD therapy, in order to reduce α-synuclein aggregation also in the peripheral nervous system of *GBA1*-PD.

Since α-synuclein aggregation is a complex process that implies a spectrum of species [44], to get an insight into the correlation of GCase with the process of aggregation of α-synuclein in skin biopsies, we moved beyond α-synuclein oligomers and studied other α-synuclein species, from the monomeric to the aggregated ones. Interestingly, we did not detect any difference in monomeric α-synuclein among HC, iPD, and *GBA1*-PD, indicating that it does not discriminate between patients and controls. Furthermore, we did not observe the presence of

aggregated β-sheet-containing forms, neither with conformational antibody neither with specific dye. In addition, we detect no phosphorylated α-synuclein in our samples. If fibrils and greater assemblies are a later step in the aggregation process, phosphorylation of α-synuclein has also been suggested to feature more advanced stages compared to α-synuclein oligomerization [45, 46], which have been described as an early event in the pathology [35, 47]. This could suggest that in our samples the aggregation process of α-synuclein is at an early stage, or that the intrinsic signal amplification of the PLA technique lets us to unravel the presence of very low amount of oligomers that are not detectable by classical immunofluorescence. Not observing phosphorylated α-synuclein in our samples might appear to contradict previous literature [48]. We cannot rule out the hypothesis that the absence of phospho-synuclein staining in our specimens may be explained by the selection of the forearm as the biopsy site, together with the lower intra-patient sampling in our procedure compared to other studies, as already suggested [49, 50].

Interestingly, we observed that synaptic density, related to the sweat gland secretory coil, in the overall PD population shows a moderate correlation with clinical assessment of autonomic dysfunction, particularly with the total score of the COMPASS-31 and the orthostatic intolerance subitem. This could be explained by the frequent coexistence of excessive sweating and orthostatic hypotension reported in the prodromal phase of PD [51] and by the evidence that sweating is regulated by vasodilation of the vessels surrounding the sweat glands secretory coils [52]. Our results agree with a higher dysautonomic burden in *GBA1*-PD compared to iPD [53], even though the two groups could not be balanced for age at onset and disease duration and these confounders must be taken into account when interpreting our results. However, the increase of synaptic density in the overall *GBA1*-PD is unexpected. In fact, we previously reported sweat gland denervation in a higher percentage of iPD subjects compared to HC [20] and others described in iPD patients intraepidermal nerve fiber denervation and loss of autonomic nerves to sweat glands and blood vessels [54]. Furthermore, the deposition of phosphorylated α-synuclein in autonomic fibers was greater in PD patients with autonomic failure [55]. The involvement of the autonomic nervous system is often affecting the cardiac and skin branches in parallel, as proved by the high concordance between ^{123}I-metaiodobenzylguanidine (^{123}I-MIBG) myocardial scintigraphy and skin biopsy data [56]. Focusing on *GBA1*-PD, ^{123}I-MIBG has been reported to be worse than in iPD [57], whilst other studies showed similar uptakes [58]. This discrepancy can be caused by the heterogeneity of the *GBA1*-PD variants analyzed. The peculiar profile of autonomic dysfunction in *GBA1*-PD has been further explored in recent research [59], which confirmed through autonomic testing greater cardiovascular and sudomotor dysautonomia in *GBA1*-PD compared with matched PD control subjects.

The relationship between α-synuclein, skin denervation, and clinical features has yielded conflicting results so far. On the one hand, higher ratios of α-synuclein were found to be correlated with reduced sudomotor nerve fiber and both HY scores and sympathetic/parasympathetic function [60]. On the other, some works reported no correlation with age, disease duration, or severity of PD [61], as well as a uniform distribution of phosphorylated α-synuclein not following the side with greater motor impairment [62]. Indeed, in line with the present results, we previously showed [20] high PLA scores both in PD patients with and without autonomic dysfunction and no significant association between PLA and disease duration or the severity of motor features. Several factors could explain these discrepancies in the available literature. First, the moderate association between autonomic symptoms and skin biopsy measures is likely influenced by the use of questionnaires, which may increase the bias of subjective reporting. Previous research observed considerable discordance between overall self-reported scores and electrophysiological test abnormalities [63], as also confirmed in a recent study [59]. Additionally, the prevalence of underrecognized dysautonomia in PD is close to 50% [64]. Last, synaptic density and PLA score may reflect dynamic measures with variable patterns over time and in relation to disease progression. Indeed, synaptic remodeling (pruning and/or sprouting processes) could take place in the sudomotor fibers and compensate for nerve degeneration. Notably, the regeneration property of peripheral nervous system fibers, including both sensory and autonomic skin fibers, has been extensively described [65] and a study by Jeziorska et al. used growth-associated protein 43 (GAP43) to assess altered nerve fiber regeneration in patients with PD [66]. Therefore, it could be argued that compensatory synaptic remodeling may have prevented the elucidation of the exact relationship between peripheral denervation measures and the severity of autonomic symptoms.

This study has indeed some drawbacks, that is, (i) the cross-sectional design which did not allow us to explore a cause-effect relationship between skin biopsy measures and clinical features; (ii) the lack of an instrumental assessment of autonomic symptoms; and (iii) the presence of unbalanced clinical and demographic characteristics in iPD and *GBA1*-PD subgroups. Concerning the last, we have partially addressed the effect of confounders in multivariable analysis.

5 | CONCLUSION

Collectively, our research suggests that the assessment of α-synuclein oligomers and synaptic density in the skin has the potential to provide a reliable, accessible, and

accurate biomarker in iPD and *GBA1*-PD. Our findings may carry preliminary implications for the understanding of peripheral pathophysiological mechanisms underlying nonmotor burden in *GBA1*-PD. A deeper understanding of such mechanisms both in the prodromal and manifest phase of *GBA1*-PD is of paramount importance to address key questions about treatment response in the expanding scenario of pathway-specific therapeutic options, as well as to inform future strategies for more precise patient stratification. In conclusion, we reported the quantitative analysis of α-synuclein oligomers and synaptic density in the skin as a biomarker of iPD and *GBA1*-associated PD.

AUTHOR CONTRIBUTIONS

Design: SM, ECo, DC, EC, GC, GP, IUI. Execution: SM, ECo, EC, FG, CN, AMC, MJB, FD, LS, VF. Analysis: SM, ECo, EC. Writing: SM, ECo. Editing of final version of the manuscript: EC, RA, GC, GP, IUI.

ACKNOWLEDGMENTS

The authors thank all patients and families for their contribution and the Fondazione Grigioni per il Morbo di Parkinson (Milan-Italy) for long-lasting support to CG and AR. Part of this work was carried out at UNITECH NOLIMITS, an advanced imaging facility established by the Università degli Studi di Milano. The graphical abstract was created in part using and modifying images from Servier Medical Art (smart.servier.com) licensed under CC BY 4.0 (creativecommons.org/licenses/by/4.0/).

FUNDING INFORMATION

This work was supported by Italian "5 × 1000" funding to the "Fondazione Grigioni per il Morbo di Parkinson," Milan, Italy, MUR-PRIN (Programmi di Ricerca Scientifica di Rilevante Interesse Nazionale, Grant n. 2017228L3J), and Fondazione Regionale per la Ricerca Biomedica (FRRB, Milano) under the frame of ERA PerMed 2022 (2022-212, DEEPEN-iRBD). IUI received grants, speaking and consultant honoraria from Medtronic, Newronika, and the Fondazione Grigioni per il Morbo di Parkinson and speaking honoraria from AbbVie. LS was supported by a fellowship from the "Fondazione Grigioni per il Morbo di Parkinson."

CONFLICT OF INTEREST STATEMENT

The authors declare no conflicts of interest.

DATA AVAILABILITY STATEMENT

Source data used for analyses presented in this study are available from the authors upon request.

ETHICS STATEMENT

This research was carried out in agreement with the principles of the Declaration of Helsinki. All patients gave their written informed consent. Concerning skin biopsy, study procedures were approved by the local Ethics Committee (protocol code 483/18). Human brain samples were obtained from the Nervous Tissue Bank of Milan and the study was approved by the Ethics Committee of the University of Milan (protocol code 66/21).

ORCID

Samanta Mazzetti https://orcid.org/0000-0002-2944-8357
Elena Contaldi https://orcid.org/0000-0002-0218-5251
Milo Jarno Basellini https://orcid.org/0000-0002-4568-216X
Claudia Novello https://orcid.org/0009-0007-6658-7595
Alessandra Maria Calogero https://orcid.org/0000-0003-2262-4992
Letizia Straniero https://orcid.org/0000-0002-1733-7561
Federica Garrì https://orcid.org/0000-0002-3555-3882
Daniela Calandrella https://orcid.org/0000-0002-4803-0490
Francesca Del Sorbo https://orcid.org/0000-0002-5021-3624
Rosanna Asselta https://orcid.org/0000-0001-5351-0619
Emanuele Cereda https://orcid.org/0000-0002-0747-1951
Graziella Cappelletti https://orcid.org/0000-0003-0903-5392
Ioannis Ugo Isaias https://orcid.org/0000-0002-3552-5144
Gianni Pezzoli https://orcid.org/0000-0003-4665-6710

REFERENCES

1. Ascherio A, Schwarzschild MA. The epidemiology of Parkinson's disease: risk factors and prevention. Lancet Neurol. 2016;15(12):1257–72.
2. Spillantini MG, Schmidt ML, Lee VMY, Trojanowski JQ, Jakes R, Goedert M. α-Synuclein in Lewy bodies. Nature. 1997;388(6645):839–40.
3. Nalls MA, Blauwendraat C, Vallerga CL, Heilbron K, Bandres-Ciga S, Chang D, et al. Identification of novel risk loci, causal insights, and heritable risk for Parkinson's disease: a meta-analysis of genome-wide association studies. Lancet Neurol. 2019;18(12):1091–102.
4. Thenganatt MA, Jankovic J. Parkinson disease subtypes. JAMA Neurol. 2014;71(4):499–504.
5. Sidransky E, Nalls MA, Aasly JO, Aharon-Peretz J, Annesi G, Barbosa ER, et al. Multicenter analysis of glucocerebrosidase mutations in Parkinson's disease. N Engl J Med. 2009;361(17):1651–61.
6. Blumenreich S, Nehushtan T, Barav OB, Saville JT, Dingjan T, Hardy J, et al. Elevation of gangliosides in four brain regions from Parkinson's disease patients with a GBA mutation. NPJ Parkinsons Dis. 2022;8(1):99.
7. Giraldo P, Alfonso P, Irún P, Gort L, Chabás A, Vilageliu L, et al. Mapping the genetic and clinical characteristics of Gaucher disease in the Iberian Peninsula. Orphanet J Rare Dis. 2012;19(7):17.
8. Duran R, Mencacci NE, Angeli AV, Shoai M, Deas E, Houlden H, et al. The glucocerobrosidase E326K variant predisposes to Parkinson's disease, but does not cause Gaucher's disease: GBA E326K predisposes to PD. Mov Disord. 2013;28(2):232–6.

9. Riboldi GM, Di Fonzo AB. GBA, Gaucher disease, and Parkinson's disease: from genetic to clinic to new therapeutic approaches. Cells. 2019;8(4):364.
10. Cilia R, Tunesi S, Marotta G, Cereda E, Siri C, Tesei S, et al. Survival and dementia in GBA-associated Parkinson's disease: the mutation matters. Ann Neurol. 2016;80(5):662–73.
11. Mata IF, Samii A, Schneer SH, Roberts JW, Griffith A, Leis BC, et al. Glucocerebrosidase gene mutations: a risk factor for Lewy body disorders. Arch Neurol. 2008;65(3):379–382. https://doi.org/10.1001/archneurol.2007.68
12. Neumann J, Bras J, Deas E, O'Sullivan SS, Parkkinen L, Lachmann RH, et al. Glucocerebrosidase mutations in clinical and pathologically proven Parkinson's disease. Brain. 2009;132(7):1783–94.
13. Gan-Or Z, Amshalom I, Kilarski LL, Bar-Shira A, Gana-Weisz M, Mirelman A, et al. Differential effects of severe vs mild GBA mutations on Parkinson disease. Neurology. 2015;84(9):880–7.
14. Fishbein I, Kuo YM, Giasson BI, Nussbaum RL. Augmentation of phenotype in a transgenic Parkinson mouse heterozygous for a Gaucher mutation. Brain. 2014;137(12):3235–47.
15. Gegg ME, Burke D, Heales SJR, Cooper JM, Hardy J, Wood NW, et al. Glucocerebrosidase deficiency in substantia nigra of parkinson disease brains. Ann Neurol. 2012;72(3):455–63.
16. Mazzulli JR, Xu YH, Sun Y, Knight AL, McLean PJ, Caldwell GA, et al. Gaucher disease glucocerebrosidase and α-synuclein form a bidirectional pathogenic loop in synucleinopathies. Cell. 2011;146(1):37–52.
17. den Heijer JM, Cullen VC, Pereira DR, Yavuz Y, de Kam ML, Grievink HW, et al. A biomarker study in patients with GBA1-Parkinson's disease and healthy controls. Mov Disord. 2023;38:783–95.
18. Siderowf A, Concha-Marambio L, Lafontant DE, Farris CM, Ma Y, Urenia PA, et al. Assessment of heterogeneity among participants in the Parkinson's progression markers initiative cohort using α-synuclein seed amplification: a cross-sectional study. Lancet Neurol. 2023;22(5):407–17.
19. Basellini MJ, Kothuis JM, Comincini A, Pezzoli G, Cappelletti G, Mazzetti S. Pathological pathways and alpha-synuclein in Parkinson's disease: a view from the periphery. Front Biosci. 2023;28(2):33.
20. Mazzetti S, Basellini MJ, Ferri V, Cassani E, Cereda E, Paolini M, et al. α-Synuclein oligomers in skin biopsy of idiopathic and monozygotic twin patients with Parkinson's disease. Brain. 2020;143(3):920–31.
21. Filocamo M, Baldo C, Goldwurm S, Renieri A, Angelini C, Moggio M, et al. Telethon network of genetic biobanks: a key service for diagnosis and research on rare diseases. Orphanet J Rare Dis. 2013;8(1):129.
22. Hughes AJ, Daniel SE, Kilford L, Lees AJ. Accuracy of clinical diagnosis of idiopathic Parkinson's disease: a clinico-pathological study of 100 cases. J Neurol Neurosurg Psychiatry. 1992;55(3):181–4.
23. Straniero L, Rimoldi V, Melistaccio G, Di Fonzo A, Pezzoli G, Duga S, et al. A rapid and low-cost test for screening the most common Parkinson's disease-related GBA variants. Parkinsonism Relat Disord. 2020;80:138–41.
24. Straniero L, Rimoldi V, Monfrini E, Bonvegna S, Melistaccio G, Lake J, et al. Role of lysosomal gene variants in modulating GBA -associated Parkinson's disease risk. Mov Disord. 2022;37(6):1202–10.
25. Tomlinson CL, Stowe R, Patel S, Rick C, Gray R, Clarke CE. Systematic review of levodopa dose equivalency reporting in Parkinson's disease. Mov Disord. 2010;25(15):2649–53.
26. Goetz CG, Tilley BC, Shaftman SR, Stebbins GT, Fahn S, Martinez-Martin P, et al. Movement Disorder Society-sponsored revision of the unified Parkinson's disease rating scale (MDS-UPDRS): scale presentation and clinimetric testing results. Mov Disord. 2008;23(15):2129–70.
27. Goetz CG, Poewe W, Rascol O, Sampaio C, Stebbins GT, Counsell C, et al. Movement Disorder Society task force report on the Hoehn and Yahr staging scale: status and recommendations. Mov Disord. 2004;19(9):1020–8.
28. Nomura T, Inoue Y, Kagimura T, Uemura Y, Nakashima K. Utility of the REM sleep behavior disorder screening questionnaire (RBDSQ) in Parkinson's disease patients. Sleep Med. 2011;12(7):711–3.
29. Barichella M, Cereda E, Cassani E, Frazzitta G, Pezzoli G. A focus on Rome III criteria for the assessment of constipation in Parkinson's disease. Mov Disord. 2017;32(4):630.
30. Freeman R, Wieling W, Axelrod FB, Benditt DG, Benarroch E, Biaggioni I, et al. Consensus statement on the definition of orthostatic hypotension, neurally mediated syncope and the postural tachycardia syndrome. Clin Auton Res. 2011;21(2):69–72.
31. Pierangeli G, Turrini A, Giannini G, Del Sorbo F, Calandra-Buonaura G, Guaraldi P, et al. Translation and linguistic validation of the composite autonomic symptom score COMPASS 31. Neurol Sci. 2015;36(10):1897–902.
32. Folstein MF, Folstein SE, McHugh PR. "Mini-mental state". A practical method for grading the cognitive state of patients for the clinician. J Psychiatr Res. 1975;12(3):189–98.
33. Lima CF, Meireles LP, Fonseca R, Castro SL, Garrett C. The frontal assessment battery (FAB) in Parkinson's disease and correlations with formal measures of executive functioning. J Neurol. 2008;255(11):1756–61.
34. Nasreddine ZS, Phillips NA, Bédirian V, Charbonneau S, Whitehead V, Collin I, et al. The Montreal Cognitive Assessment, MoCA: a brief screening tool for mild cognitive impairment. J Am Geriatr Soc. 2005;53(4):695–9.
35. Roberts RF, Wade-Martins R, Alegre-Abarrategui J. Direct visualization of alpha-synuclein oligomers reveals previously undetected pathology in Parkinson's disease brain. Brain. 2015;138(6):1642–57.
36. Calogero AM, Basellini MJ, Isilgan HB, Longhena F, Bellucci A, Mazzetti S, et al. Acetylated α-tubulin and α-synuclein: physiological interplay and contribution to α-synuclein oligomerization. Int J Mol Sci. 2023;24(15):12287.
37. Mazzetti S, Giampietro F, Calogero AM, Isilgan HB, Gagliardi G, Rolando C, et al. Linking acetylated α-tubulin redistribution to α-synuclein pathology in brain of Parkinson's disease patients. NPJ Parkinsons Dis. 2024;10(1):2.
38. Amadeo A, Pizzi S, Comincini A, Modena D, Calogero AM, Madaschi L, et al. The association between α-synuclein and α-tubulin in brain synapses. Int J Mol Sci. 2021;22(17):9153.
39. Mandrekar JN. Receiver operating characteristic curve in diagnostic test assessment. J Thorac Oncol. 2010;5(9):1315–6.
40. Murphy KE, Gysbers AM, Abbott SK, Tayebi N, Kim WS, Sidransky E, et al. Reduced glucocerebrosidase is associated with increased α-synuclein in sporadic Parkinson's disease. Brain. 2014;137(3):834–48.
41. Boer DEC, van Smeden J, Bouwstra JA, Aerts JMFG. Glucocerebrosidase: functions in and beyond the lysosome. JCM. 2020;9(3):736.
42. Schneider SA, Alcalay RN. Neuropathology of genetic synucleinopathies with parkinsonism: review of the literature: neuropathology of genetic Parkinson's disease. Mov Disord. 2017;32(11):1504–23.
43. Shahmoradian SH, Lewis AJ, Genoud C, Hench J, Moors TE, Navarro PP, et al. Lewy pathology in Parkinson's disease consists of crowded organelles and lipid membranes. Nat Neurosci. 2019;22(7):1099–109.
44. Alam P, Bousset L, Melki R, Otzen DE. α-Synuclein oligomers and fibrils: a spectrum of species, a spectrum of toxicities. J Neurochem. 2019;150(5):522–34.

45. Zhou J, Broe M, Huang Y, Anderson JP, Gai WP, Milward EA, et al. Changes in the solubility and phosphorylation of α-synuclein over the course of Parkinson's disease. Acta Neuropathol. 2011; 121(6):695–704.
46. Oueslati A. Implication of alpha-synuclein phosphorylation at S129 in synucleinopathies: what have we learned in the last decade? JPD. 2016;6(1):39–51.
47. Bengoa-Vergniory N, Roberts RF, Wade-Martins R, Alegre-Abarrategui J. Alpha-synuclein oligomers: a new hope. Acta Neuropathol. 2017;134(6):819–38.
48. Gibbons CH, Levine T, Adler C, Bellaire B, Wang N, Stohl J, et al. Skin biopsy detection of phosphorylated α-synuclein in patients with synucleinopathies. JAMA. 2024;331(15):1298–306.
49. Liu X, Yang J, Yuan Y, He Q, Gao Y, Jiang C, et al. Optimization of the detection method for phosphorylated α-synuclein in Parkinson disease by skin biopsy. Front Neurol. 2020;30(11): 569446.
50. Doppler K. Detection of dermal alpha-synuclein deposits as a biomarker for Parkinson's disease. JPD. 2021;11(3):937–47.
51. Seppi K, Ray Chaudhuri K, Coelho M, Fox SH, Katzenschlager R, Perez Lloret S, et al. Update on treatments for nonmotor symptoms of Parkinson's disease-an evidence-based medicine review. Mov Disord. 2019;34(2):180–98.
52. Wang N, Gibbons CH, Freeman R. Novel immunohistochemical techniques using discrete signal amplification systems for human cutaneous peripheral nerve fiber imaging. J Histochem Cytochem. 2011;59(4):382–90.
53. Blandini F, Cilia R, Cerri S, Pezzoli G, Schapira AHV, Mullin S, et al. Glucocerebrosidase mutations and synucleinopathies: toward a model of precision medicine. Mov Disord. 2019;34(1):9–21.
54. Nolano M, Provitera V, Manganelli F, Iodice R, Stancanelli A, Caporaso G, et al. Loss of cutaneous large and small fibers in naive and l-dopa–treated PD patients. Neurology. 2017;89(8): 776–84.
55. Donadio V. Skin nerve α-synuclein deposits in Parkinson's disease and other synucleinopathies: a review. Clin Auton Res. 2019;29(6): 577–85.
56. Giannoccaro MP, Donadio V, Incensi A, Pizza F, Cason E, Di Stasi V, et al. Skin biopsy and I-123 MIBG scintigraphy findings in idiopathic Parkinson's disease and parkinsonism: a comparative study: skin biopsy and I-123 MIBG scintigraphy findings in PD. Mov Disord. 2015;30(7):986–9.
57. Kim MS, Park DG, An Y, Yoon JH. Dual-phase ^{18}F-FP-CIT positron emission tomography and cardiac ^{123}I-MIBG scintigraphy of Parkinson's disease patients with GBA mutations: evidence of the body-first type? Eur J Neurol. 2023;30(2):344–52.
58. Oeda T, Umemura A, Mori Y, Tomita S, Kohsaka M, Park K, et al. Impact of glucocerebrosidase mutations on motor and nonmotor complications in Parkinson's disease. Neurobiol Aging. 2015;36(12):3306–13.
59. Devigili G, Straccia G, Cereda E, Garavaglia B, Fedeli A, Elia AE, et al. Unraveling autonomic dysfunction in GBA -related Parkinson's disease. Movement Disord Clin Pract. 2023;10:1620–38.
60. Wang N, Gibbons CH, Lafo J, Freeman R. α-Synuclein in cutaneous autonomic nerves. Neurology. 2013;81(18):1604–10.
61. Gibbons CH, Wang N, Freeman R. Cutaneous alpha-synuclein from paraffin embedded autopsy specimens in Parkinson's disease. JPD. 2017;7(3):503–9.
62. Donadio V, Incensi A, Rizzo G, Scaglione C, Capellari S, Fileccia E, et al. Spine topographical distribution of skin α-synuclein deposits in idiopathic Parkinson disease. J Neuropathol Exp Neurol. 2017;76(5):384–9.
63. Papapetropoulos S, Argyriou AA, Chroni E. No correlation between the clinical severity of autonomic symptoms (SCOPA-AUT) and electrophysiological test abnormalities in advanced Parkinson's disease: letters to the editors. Mov Disord. 2006;21(3):430–1.
64. Merola A, Romagnolo A, Rosso M, Suri R, Berndt Z, Maule S, et al. Autonomic dysfunction in Parkinson's disease: a prospective cohort study: prospective PD autonomic function assessment. Mov Disord. 2018;33(3):391–7.
65. Holahan MR. A shift from a pivotal to supporting role for the growth-associated protein (GAP-43) in the coordination of axonal structural and functional plasticity. Front Cell Neurosci. 2017; 31(11):266.
66. Jeziorska M, Atkinson A, Kass-Iliyya L, Javed S, Kobylecki C, Gosal D, et al. Increased intraepidermal nerve fiber degeneration and impaired regeneration relate to symptoms and deficits in Parkinson's disease. Front Neurol. 2019;14(10):111.

SUPPORTING INFORMATION

Additional supporting information can be found online in the Supporting Information section at the end of this article.

How to cite this article: Mazzetti S, Contaldi E, Basellini MJ, Novello C, Calogero AM, Straniero L, et al. Comparing *GBA1*-Parkinson's disease and idiopathic Parkinson's disease: α-Synuclein oligomers and synaptic density as biomarkers in the skin biopsy. Brain Pathology. 2024. e13284. https://doi.org/10.1111/bpa.13284

SUPPLEMENTARY METHODS

Tyramide signal amplification

The sections were incubated with the following: (1) 3% hydrogen peroxide to inhibit endogenous peroxidase; (2) 1% BSA and 0.3% Triton™ X-100 diluted in TN (0.1 M Tris-HCl, 0.15 M NaCl); (3) GCase (1:2000) in 1% BSA and 0.3% Triton X-100 diluted in TN overnight (ON) at room temperature (RT); (4) HRP-conjugated secondary antibodies (donkey anti-rabbit, 1:5000) in TN for 2 h at RT; (5) Cy3-labeled tyramide (1:200) in Amplification Diluent for 5 min at RT. On the same sections, standard immunofluorescence was also performed. After a 20-min blocking step with 1% BSA and 0.1% Triton™ X-100 diluted in PBS, the sections were incubated with a mix of primary antibodies containing mouse anti-synaptophysin (1:100) and goat anti-tyrosine hydroxylase (1:200; Life Technologies) diluted in 0.1% BSA overnight at RT. Donkey anti-mouse conjugated to Alexa Fluor 647 (1:200; Life Technologies) and donkey anti-goat conjugated to Alexa Fluor 488 (1:600; Jackson ImmunoResearch Europe, Cambridgeshire, UK) were selected as secondary antibodies and incubated for 2 h at RT. Samples were counterstained with Hoechst 33342 (1:1000; Life Technologies) for 10 min and mounted using Mowiol + DABCO.

Immunofluorescence assay.

After deparaffination and rehydration, skin biopsy sections were pretreated with 10% Formic Acid for 10 min at RT, as indicated in "Methods" section, and then incubated with 1% BSA, 0.1% Triton X-100 in PBS 20 min at RT. After that, sections were incubated ON at RT with mixtures of primary antibodies containing either mouse anti-synaptophysin or guinea pig anti-synaptophysin 1(code no. 101 004, 1:100; Synaptic System) together with one of the following: rabbit anti monomeric α-synuclein (code no. S3062, 1:2000; Sigma-Aldrich), mouse anti aggregated α-synuclein 5G4 (clone 5G4, code no. MABN389, 1:250; Merck Millipore), rabbit anti Ser129 phosphorylated α-synuclein (clone EP1536Y, code no. ab51253, 1:500, Abcam), mouse anti-GAP43 (clone GAP-8A12, code no. NBP1-41337, 1:400; Novus Biologicals) antibodies. After three washes with PBS, the appropriate mixture of secondary antibodies was added for 2 h at RT in the dark. The secondary antibodies used were the following: Rhodamine Red™-X-conjugated AffiniPure Donkey anti-mouse (1:300, code no. 715-295-151, Jackson ImmunoResearch Europe LTD), donkey anti-rabbit Alexa Fluor™ 555 (1:200, code no. ab150070, Abcam), donkey anti-mouse Alexa Fluor™ 488 (1:300, code no. 715-545-151, Jackson ImmunoResearch Europe LTD), goat anti-guinea pig Alexa Fluor™ 488 (1:300; code no. A-11073, Invitrogen). To visualize nuclei, Hoechst 33342 was added, 10 min at RT in the dark, and, finally, tissue sections were mounted with Mowiol-DABCO.
Post-mortem human brains were used as positive controls for aggregated α-synuclein staining and assayed in parallel to skin biopsies. Briefly, sections were pretreated with 80% Formic Acid for 20 min at RT, incubated with 1% BSA, 0.1% Triton X-100, 20 min at RT, and with mouse anti aggregated α-synuclein 5G4 (1:500) or rabbit anti Ser129 phosphorylated α-synuclein (1:500).

Thioflavin S staining

To evaluate the presence of Thioflavin S positive fibrils, skin and *post-mortem* human brain slices were deparaffinated, rehydrated, and stained accordingly to (Defossez and Delacourte, 1987). Briefly, samples were incubated with filtered 1% Thioflavin S (Sigma-Aldrich) for 10 min at RT in the

dark. Subsequently, sections were washed twice with 80% ethanol for 3 min and with water for 10 min, then mounted with glycerol.

SUPPLEMENTARY REFERENCE

Défossez A, Delacourte A. Transformation of degenerating neurofibrils into amyloid substance in Alzheimer's disease: histochemical and immunohistochemical studies. J Neurol Sci. 1987 Oct;81(1):1-10. (doi: 10.1016/0022-510x(87)90179-1).

SUPPLEMENTARY FIGURES

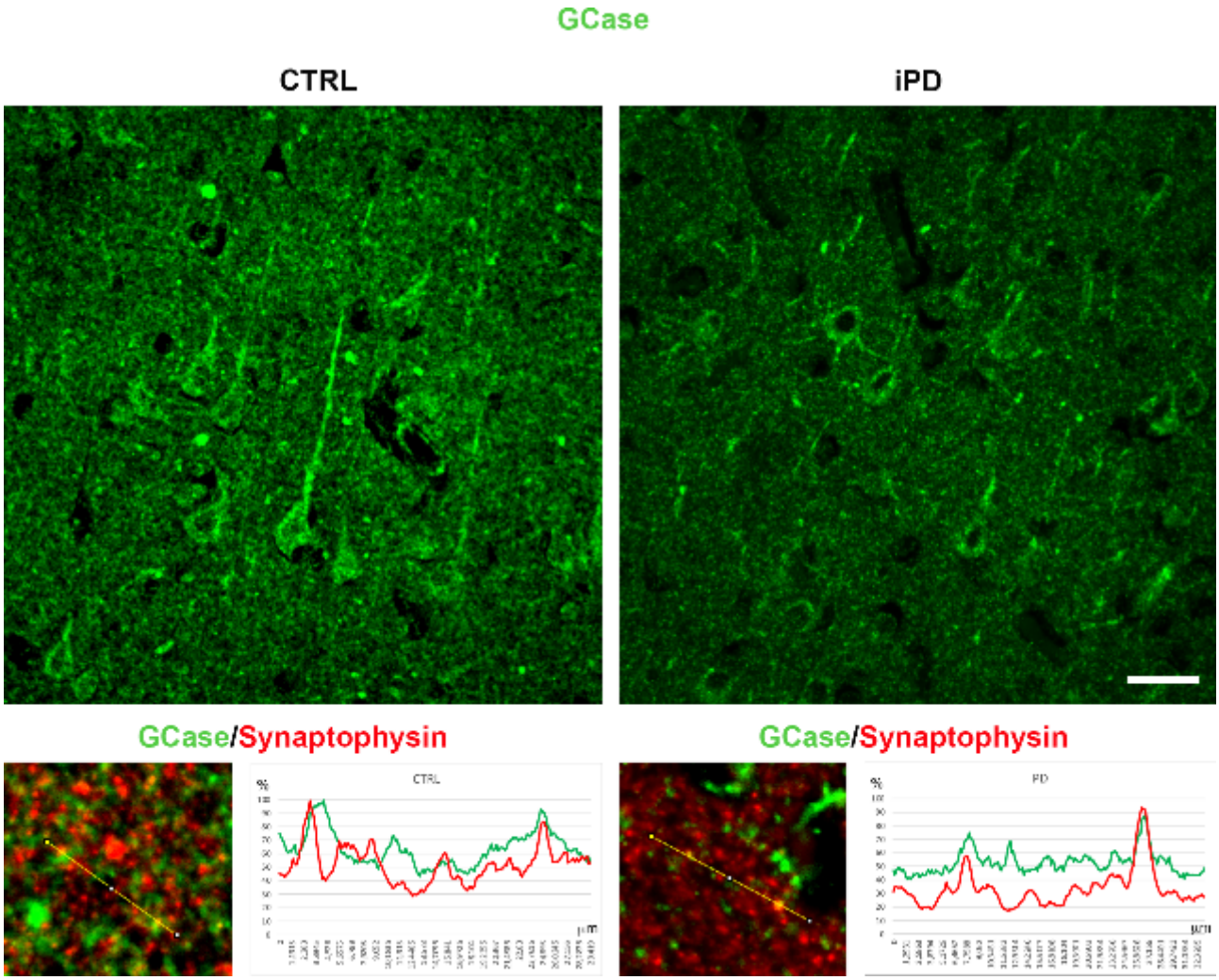

Supplementary Fig. 1 - **GCase staining in the entorhinal cortex obtained from control subjects and iPD patients.** GCase staining (green) appears to be decreased in iPD patients compared to controls (CTRL) and localizes also in some of the synaptophysin-positive synaptic terminals, as shown by the intensity profiles. Scale bar, 30 μm.

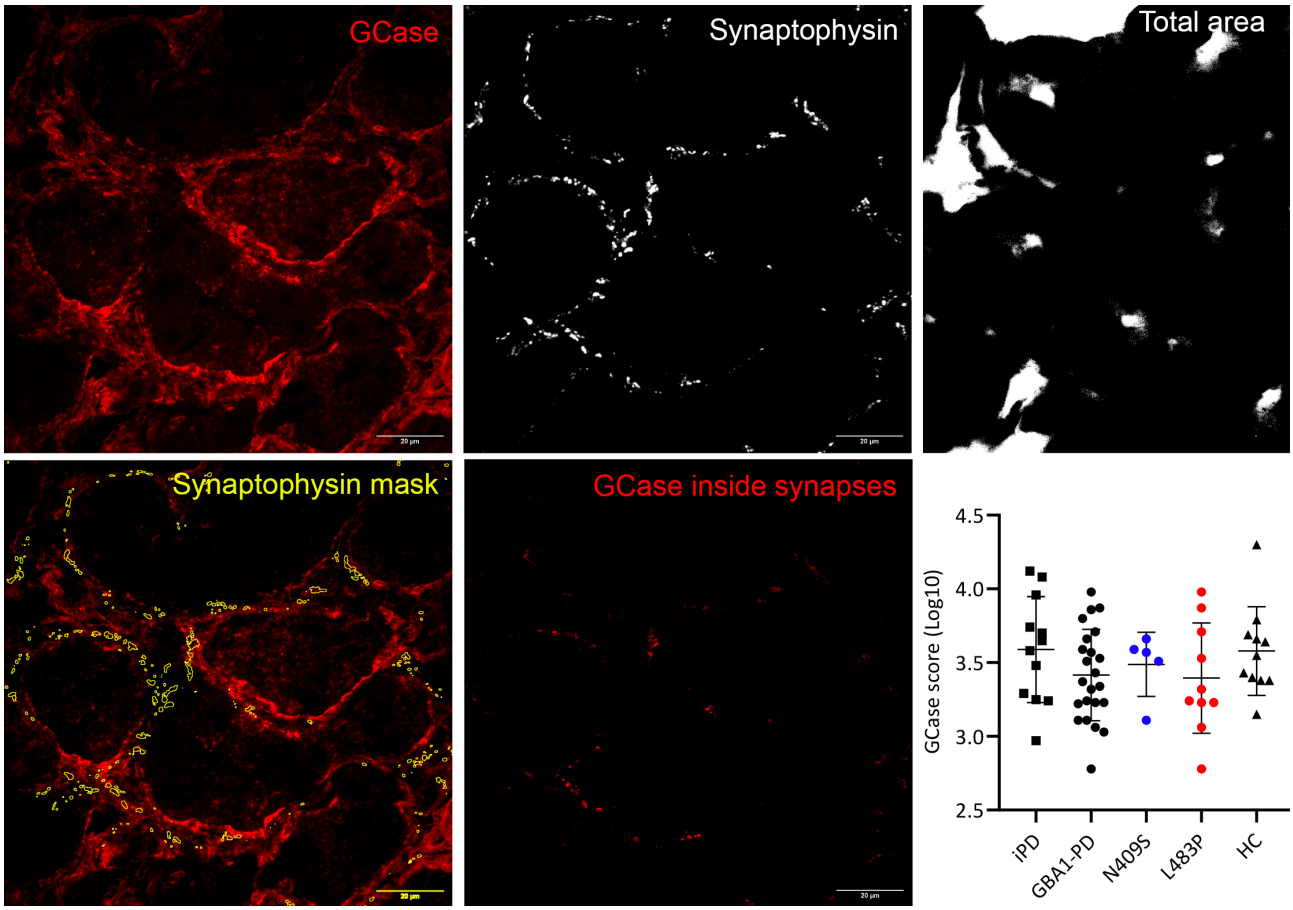

Supplementary Fig. 2 - GCase score. Mask of synaptophysin-positive signal (yellow) was superimposed to GCase staining (red). The area covered by GCase staining inside synapses was normalized on total sweat gland area (black). The graph represents univariate analysis to compare mean GCase score values (log-transformed) between idiopathic PD (iPD), total *GBA1*-PD, *GBA1*-PD subgroups, and healthy controls (HC). Scale bar, 20 μm.

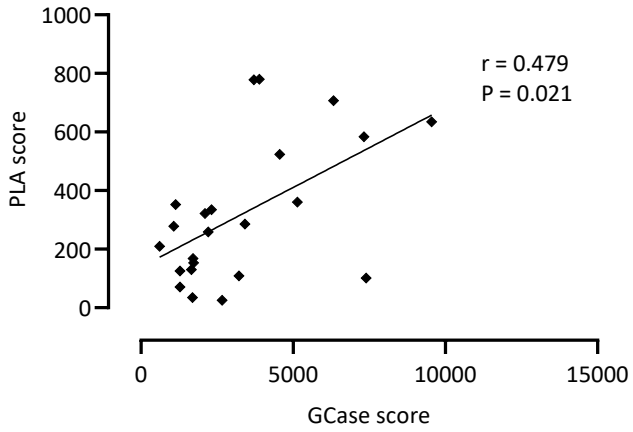

Supplementary Fig. 3 Correlation analysis in *GBA1*-PD between PLA score and GCase score.

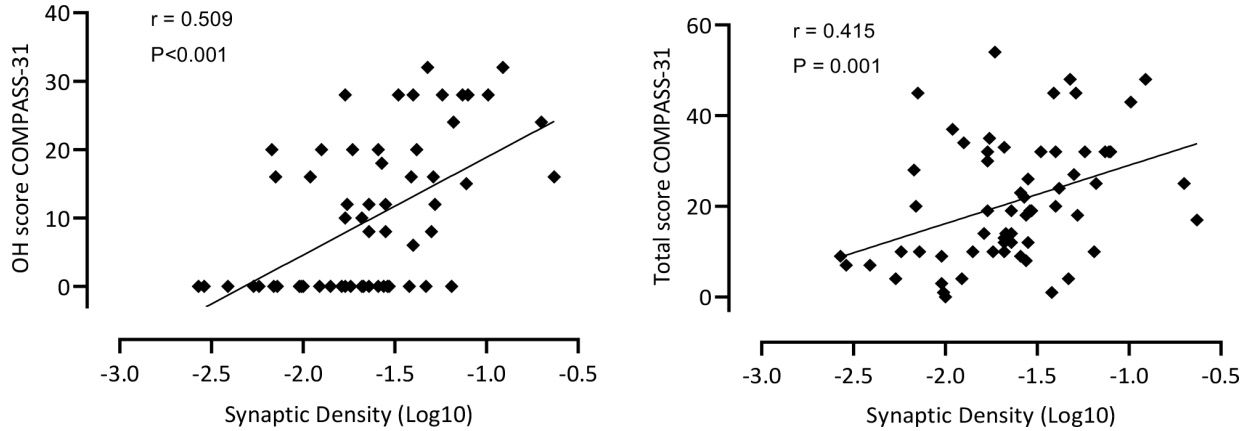

Supplementary Fig. 4 Autonomic function and synaptic density in the total overall PD population. Pearson correlation analysis between synaptic density and the orthostatic intolerance subitem (OH score COMPASS-31) or the total score of the COMPASS-31.

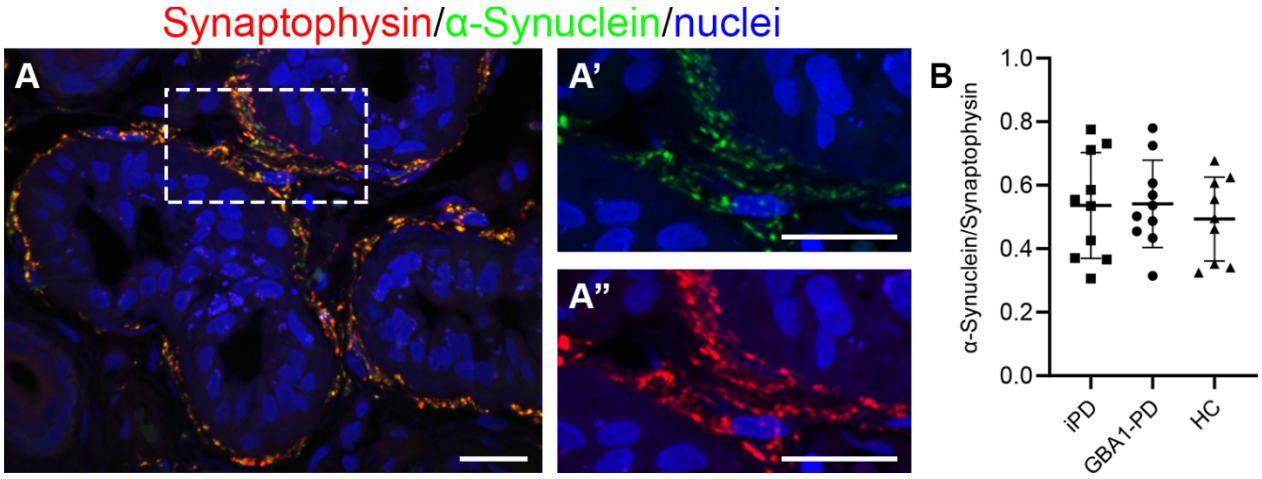

Supplementary Fig. 5 Monomeric α-Synuclein in skin biopsies. (A) Representative confocal images showing α-Synuclein (green), synapses (Synaptophysin, red), and nuclei (blue) in sweat glands. Magnifications of α-Synuclein (A') and Synaptophysin (A'') staining within the white square in image A are showed. Nuclei are counterstained with Hoechst. Scale bar, 20 µm. (B) Graph shows the mean values ofα-Synuclein in synapses normalized on Synaptophysin area (α-Synuclein/Synaptophysin) in idiopathic PD (iPD), *GBA1*-PD, and healthy control (HC). No differences are detectable (ANOVA analyses with Tukey's post hoc test)

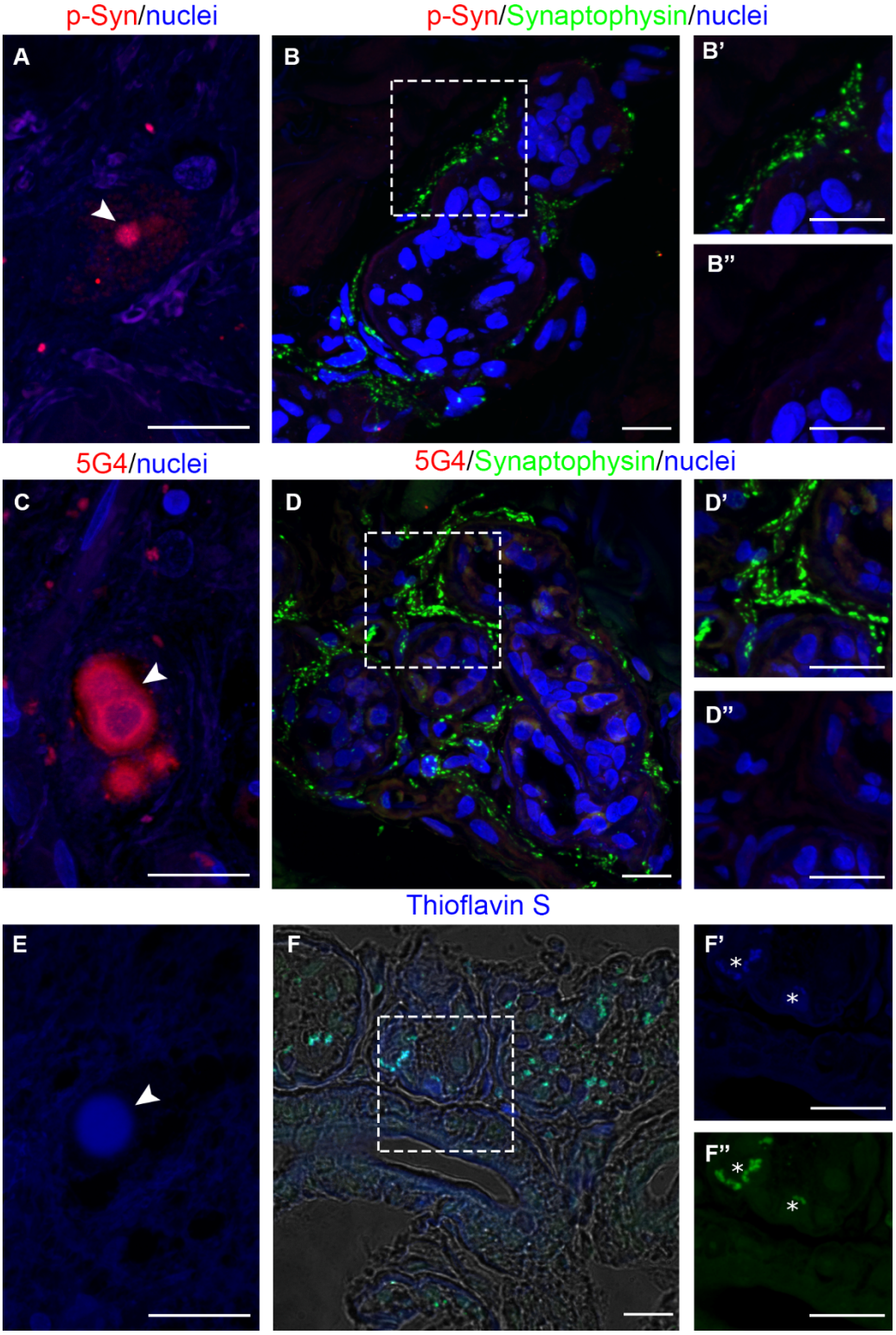

Supplementary Fig. 6. Analysis of phosphorylated and aggregated species of α-Synuclein in *substantia nigra* and skin biopsy. Representative images showing staining in *post-mortem* PD brains (A, C, E) and in skin biopsies (B-B'', D-D'', F-F''). Lewy Bodies (arrowheads) are stained for both phosphorylated (p-Syn, red in A) and aggregated α-Synuclein (5G4, red in C) in *substantia nigra* of *post-mortem* human brains. Phosphorylated and aggregated α-Synuclein staining (B-B'' and D-D'', respectively) are undetectable in sweat glands of skin biopsies. Squared areas in B and D are magnified in B'-B'' and D'-D''). The specific staining for Thioflavin S positive fibrils is detectable in the Lewy Body in brain tissue (E), but not in the skin biopsies (F). Contrast phase image was superimposed in F to

highlight anatomic structures. The squared area in F was magnified in F' and F''. Asterisks indicate tissue autofluorescence. Nuclei are counterstained with Hoechst (A-D''). Scale bar, 20 µm.

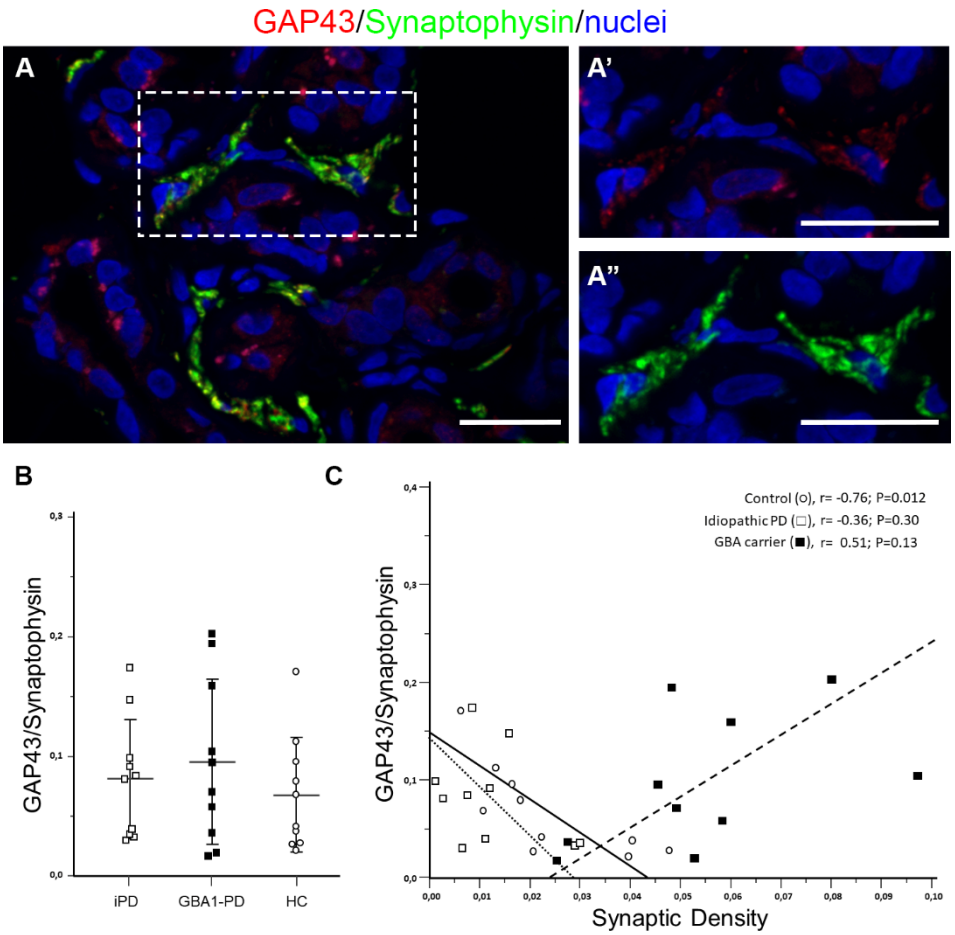

Supplementary Fig. 7. Analysis of GAP43 in the synapses of skin biopsies. (A) Representative confocal images of sweat glands showing growth associated protein 43 (GAP43, red), Synaptophysin (green), and nuclei (blue) staining. The squared area in A is magnified in (A', A''). Nuclei are counterstained with Hoechst. Scale bar, 20 µm. (B) Graph shows the mean values of GAP43 positive synapses area normalized on total Synaptophysin area (GAP43/Synaptophysin) in idiopathic PD (iPD), *GBA1*-PD and healthy controls (HC). No differences are detectable among them (ANOVA analyses with Tukey's post hoc test). (C) Pearson correlation analysis between GAP43 and Synaptic Density in the study population.